fermentation

Special Issue Reprint

Fermentation Processes

Modeling, Optimization and Control: 2nd Edition

Edited by
Ricardo Aguilar-López

mdpi.com/journal/fermentation

MDPI

Fermentation Processes: Modeling, Optimization and Control: 2nd Edition

Fermentation Processes: Modeling, Optimization and Control: 2nd Edition

Guest Editor

Ricardo Aguilar-López

MDPI

Basel • Beijing • Wuhan • Barcelona • Belgrade • Novi Sad • Cluj • Manchester

Guest Editor
Ricardo Aguilar-López
Biotechnology and
Bioengineering
Center of Research and
Advanced Studies
Mexico City
Mexico

Editorial Office
MDPI AG
Grosspeteranlage 5
4052 Basel, Switzerland

This is a reprint of the Special Issue, published open access by the journal *Fermentation* (ISSN 2311-5637), freely accessible at: https://www.mdpi.com/journal/fermentation/special_issues/GQJ40M3X96.

For citation purposes, cite each article independently as indicated on the article page online and as indicated below:

Lastname, A.A.; Lastname, B.B. Article Title. *Journal Name* **Year**, *Volume Number*, Page Range.

ISBN 978-3-7258-5111-9 (Hbk)
ISBN 978-3-7258-5112-6 (PDF)
https://doi.org/10.3390/books978-3-7258-5112-6

Contents

About the Editor

Ricardo Aguilar-López

Ricardo Aguilar-López holds the position of Investigador Titular "Cinvestav 3C" (Senior Researcher, Level 3, Cinvestav) in the Department of Biotechnology and Bioengineering at CINVESTAV-IPN. He earned his Sc.D. in Chemical Engineering from Universidad Autónoma Metropolitana in 1998, followed by a Sc.D. in Automatic Control from Cinvestav in 2003. Since joining Cinvestav in 2007, he has authored approximately 165 technical articles in international journals and around 80 contributions to specialized book chapters and conference proceedings. As a National Researcher, Level III (SNII), he has supervised 13 master's and 12 doctoral students. He leads his laboratory in topics related to dynamic analysis and control of bioprocesses, focusing on modeling and simulation of bioprocesses, dynamic analysis, design of nonlinear controllers, and estimation schemes. His research encompasses topics such as bioprocess intensification, continuous bioreactor control, soft sensors, and real-time monitoring—hallmarks of his recent publications.

Preface

This Reprint presents recent advances in the modeling, optimization, and control of fermentative processes. Integrating mathematical models, data-driven techniques, and advanced control strategies, it aims to enhance process efficiency, yield, and product quality. Designed for researchers and practitioners, it offers both theoretical foundations and practical applications, bridging the gap between bioprocess engineering and modern systems analysis.

Ricardo Aguilar-López
Guest Editor

fermentation

MDPI

Editorial

Fermentation Processes: Modeling, Optimization and Control: 2nd Edition

Ricardo Aguilar López

Department of Biotechnology and Bioengineering, Centro de Investigación y de Estudios Avanzados, México City 07360, Mexico; raguilar@cinvestav.mx; Tel.: +52-55-5747-3800

Fermentation is an important cornerstone of bioengineering, which plays a critical role in the production of a wide array of products including pharmaceuticals, biofuels, food additives, industrial chemicals and enzymes. As a biological process that involves the metabolic activity of microorganisms, fermentation is inherently complex, nonlinear, and dynamic. This complexity poses significant challenges to researchers and engineers who aim to optimize product yield and quality, and enhance process efficiency.

To address these challenges, significant attention has been devoted to the development of robust strategies for modeling, monitoring, and controlling fermentation processes. Accurate modeling provides a foundation for understanding the underlying biological and physicochemical phenomena that enable simulation, prediction, and process design in the fermentative production of target products. Meanwhile, real-time monitoring is essential for tracking key process variables such as biomass concentration, substrate consumption, and product formation, thereby offering insight into the state of the system. Lastly, advanced control techniques ensure that the process operates within optimal conditions, despite disturbances and uncertainties, to maximize productivity and ensure regulatory compliance.

The integration of these elements is vital for the transition from empirical, trial-and-error methods to data-driven and model-based approaches in modern bioprocessing. The synergy between these technologies, such as modern measurement devices, new algorithms for optimization and process control, and computational hardware, has profound implications for sustainability issues. Traditional fermentation processes can be resource-intensive, often requiring significant inputs of water, energy, and raw materials. Through AI-enhanced optimization, waste can be minimized, energy efficiency can be achieved, and the overall environmental impact can be significantly reduced. These initiatives not only improve productivity but also help forge pathways to a more sustainable industrial future.

Under this framework, this Special Issue features several contributions that are focused on novel tools applied to fermentative processes, such as machine learning for improved protein production, heuristic and theoretical optimization procedures based on control strategies, improved culture media or the use of nonconventional microorganisms and bioreactor designs and configurations to maximize specific bioproducts like organic acids, as well as online strategies for the estimation of key operational variables in fermentation (Contributions 1–10).

Funding: This research received no external funding.

Conflicts of Interest: The author declares no conflicts of interest.

List of Contributions::

1. Ergün, M.A.; Köktürk-Güzel, B.E.; Keskin-Gündoğdu, T. Optimizing Xylanase Production: Bridging Statistical Design and Machine Learning for Improved Protein Production. *Fermentation* **2025**, *11*, 319, https://doi.org/10.3390/fermentation11060319.
2. Gutiérrez, E.; Noriega, M.; Fernández, C.; Pantano, N.; Rodriguez, L.; Scaglia, G. Dynamic Optimization of Xylitol Production Using Legendre-Based Control Parameterization. *Fermentation* **2025**, *11*, 308, https://doi.org/10.3390/fermentation11060308.
3. Pedone, I.S.; Aquino, F.I.; Costa, E.d.S.M.; Macagnan, K.L.; Porto, J.d.R.; Ribeiro, A.S.; Alves, M.I.; Vendruscolo, C.T.; Moreira, A.d.S. Assessment of Alternative Media Viability for Cell Growth Phase in the Lab-Scale Xanthan Pruni Production—Part I. *Fermentation* **2025**, *11*, 191, https://doi.org/10.3390/fermentation11040191.
4. Prathumpai, W.; Pinruan, U.; Sommai, S.; Komwijit, S.; Malairuang, K. Exopolysaccharide (EPS) Production by Endophytic and Basidiomycete Fungi. *Fermentation* **2025**, *11*, 183, https://doi.org/10.3390/fermentation11040183.
5. Ma, T.; Xin, Y.; Chen, X.; Wen, X.; Wang, F.; Liu, H.; Zhu, L.; Li, X.; You, M.; Yan, Y. Effects of Compound Lactic Acid Bacteria Additives on the Quality of Oat and Common Vetch Silage in the Northwest Sichuan Plateau. *Fermentation* **2025**, *11*, 93, https://doi.org/10.3390/fermentation11020093.
6. Yaderets, V.V.; Karpova, N.V.; Glagoleva, E.V.; Shibaeva, A.S.; Dzhavakhiya, V.V. The Optimization of the Nutrient Medium Composition for the Submerged Cultivation of the Mycolicibacterium neoaurum Strain VKM Ac-3067D in a 100 L Bioreactor Under Controlled Conditions by Mathematical Planning. *Fermentation* **2025**, *11*, 82. https://doi.org/10.3390/fermentation11020082.
7. Moser, A.; Appl, C.; Pörtner, R.; Baganz, F.; Hass, V.C. A New Concept for the Rapid Development of Digital Twin Core Models for Bioprocesses in Various Reactor Designs. *Fermentation* **2024**, *10*, 463, https://doi.org/10.3390/fermentation10090463.
8. Long, L.; Ren, X.; Zhang, F.; Shi, A.; Zhai, Y.; Chen, W.; Duan, Y.; Shi, P.; Chen, L.; Li, D. Enhanced Fermentation Process for Production of High Docosahexaenoic Acid Content by *Schizochytrium* sp. GCD2032. *Fermentation* **2024**, *10*, 460, https://doi.org/10.3390/fermentation10090460.
9. Sayın, B.; Bozkurt, A.G.; Kaban, G. Assessing Waste Sunflower Oil as a Substrate for Citric Acid Production: The Inhibitory Effect of Triton X-100. *Fermentation* **2024**, *10*, 374, https://doi.org/10.3390/fermentation10070374.
10. Wei, Y.; Liu, K.; Li, Y.; Li, Z.; Zhao, T.; Zhao, P.; Qi, Y.; Li, M.; Wang, Z. Online Monitoring of the Temperature and Relative Humidity of Recycled Bedding for Dairy Cows on Dairy Farms. *Fermentation* **2024**, *10*, 346. https://doi.org/10.3390/fermentation10070346.

fermentation

MDPI

Article

Optimizing Xylanase Production: Bridging Statistical Design and Machine Learning for Improved Protein Production

Merve Aslı Ergün [1], Başak Esin Köktürk-Güzel [2] and Tuğba Keskin-Gündoğdu [1,3,*]

[1] Department of Operations Research, Graduate School of Natural and Applied Sciences, Izmir Demokrasi University, Izmir 35140, Türkiye; mervergun2603@gmail.com
[2] Department of Electrical and Electronics Engineering, Faculty of Engineering, Izmir Demokrasi University, Izmir 35140, Türkiye; basak.guzel@idu.edu.tr
[3] Department of Industrial Engineering, Faculty of Engineering, Izmir Demokrasi University, Izmir 35140, Türkiye
* Correspondence: tugba.keskingundogdu@idu.edu.tr

Abstract: Proteins are crucial for medicine, pharmaceuticals, food, and environmental applications since they are used in various fields such as synthesis of drugs, industrial enzyme production, biodegradable plastics, bioremediation processes, etc. Xylanase is an important and versatile enzyme with applications across various industries, including pulp and paper, biofuel production, food processing, textiles, laundry detergents, and animal feed. Key parameters in biotechnological protein production include temperature, pH, and working volumes and especially medium compositions where optimization is crucial for large-scale applications due to cost considerations. Machine learning methods have emerged as effective alternatives to traditional statistical approaches in optimization. This study focuses on optimizing xylanase production via bioprocesses by employing regression analysis on datasets from various studies. The extreme gradient boosting (XGBoost) regression model was applied to predict xylanase activity under different experimental conditions, accurately predicting xylanase activity and identifying the significance of each variable. This study utilized experimentally derived datasets from peer-reviewed publications, in which the corresponding laboratory experiments had already been conducted and validated. The results demonstrate that machine learning methods can effectively optimize protein production processes, offering a strong alternative to traditional statistical approaches.

Keywords: xylanase production; XGBoost regression; optimization; protein production; machine learning

1. Introduction

Protein production by bioprocesses has become essential in modern medicine, pharmaceuticals, food production, and environmental activities. These proteins can be utilized in several applications, including the synthesis of essential pharmaceuticals like insulin and monoclonal antibodies, as well as the production of industrial enzymes, biodegradable polymers, and bioremediation agents [1,2]. The effective and sustainable production of these proteins is essential for addressing global issues such as food security, illness prevention, and environmental sustainability [3,4].

Xylanase has emerged as a versatile and essential enzyme among biotechnologically produced proteins, with applications in various industries, including pulp and paper, biofuel production, food processing, textiles, and animal feed [5,6]. Due to its extensive

industrial utility, xylanase is regarded as a highly significant protein in both biotechnological and industrial applications [7]. Its typical applications span the food industry, animal feed, bioconversion, textiles, and the paper and pulp sectors [8]. Additionally, xylanase is used to improve the clarity of fruit juices and wine; assist in the extraction of vegetable oils, coffee, and starch; facilitate oligosaccharide synthesis; and enhance the nutritional value of animal feed [9]. This enzyme is synthesized by various microorganisms, including fungi and actinomycetes, and belongs to a crucial class of hydrolases with a global market valuation of approximately 500 million USD [10].

Numerous factors influence xylanase synthesis in all fermentation methods. The initial aspect refers to the origin of the microorganism. Efforts are being made to improve the production yields of bacteria, fungi, protozoa, algae, etc., which are frequently utilized in xylanase synthesis, by recombinant methodologies. Recombinant production of xylanase can improve the yields of enzyme activity [11,12]. Enhancing the capabilities of species through recombinant technologies is an efficient method; yet, it is labor-intensive and expensive.

The selection of the appropriate bioreactor configuration is another aspect influencing production efficiency in xylanase synthesis. The decision of the process type depends on the microorganism's origin [13]. Numerous studies in the literature address xylanase production using batch or continuous reactors [14]; however, the predominant methods in recent years are deep culture and solid state fermentations [15,16]. The growing interest in solid-state fermentations is driven by the need to minimize process costs. Agricultural waste materials serve as a substrate source in solid-state fermentations. Utilizing agricultural waste for xylanase production with the proper microorganism is a highly effective method for cost reduction [17]. Nonetheless, similar to other bioprocesses, scaling up solid-state fermentation suffers significant costs, and reductions in yields obtained at the laboratory size may occur during the scale-up stages. It is widely recognized that 30–40% of the production expenses for commercial enzymes are attributed to the cost of the nutritional medium [18]. The fermentation profile of an organism is affected by nutritional and physiological factors, notably carbon and nitrogen sources, along with pH, temperature, agitation, dissolved oxygen, and inoculum density. Consequently, in xylanase production, it is imperative to establish appropriate media and culture conditions to attain optimal enzyme yield. Optimizing these growth parameters is crucial for maximizing industrial enzyme production, as improper optimization results in lower enzyme yields [19,20]. Therefore, the optimization of xylanase production is a multifaceted endeavor that encompasses the selection of microbial strains, fermentation methods, nutrient media composition, and the application of statistical optimization techniques. The integration of these elements, coupled with a focus on sustainability and commercial viability, positions xylanase production as a promising area of research with significant industrial implications.

Statistical approaches, particularly design of experiments (DoE), have been widely used to optimize enzyme production by systematically analyzing the effects of multiple variables. DoE helps reduce the number of experimental trials while improving efficiency, making it a powerful tool in biotechnological optimization [21,22]. However, many DoE techniques, including advanced experimental design methodologies, often require specialized software or tools that come with significant costs, which can be a disadvantage for researchers with limited budgets. Among various experimental design methodologies, factorial design and response surface methodology (RSM) have been extensively applied for optimizing medium composition in xylanase production, Table 1.

Table 1. Statistical Optimization Methods for Different Microorganisms.

Data Set No:	Process	Microorganism	Method	Factors	Reference
1	Batch	*Escherichia coli DH5a*	*fractional factorial design*	Glucose (10–20 g/L) $(NH_4)_2HPO_4$ (2–10 g/L) K_2HPO_4 (5–18 g/L) KH_2PO_4 (1–6 g/L) $MgSO_4$ (0.5–3 g/L)	[3]
2	Batch	*Aspergillus niger B03*	2^{5-1} fractional factorial design	$(NH_4)_2HPO_4$ (2.6–5.4 g/L) Urea (0.9–2.1 g/L) Malt sprout (6–18 g/L) Corn cobs (12–24 g/L) Wheat bran (6–16 g/L)	[2]
3	Solid state	*Bacillus circulans*	3^3 factorial design	Xylan (5–10 g/L) pH (8–9) Cultivation time (24–72 h)	[4]
4	Batch	*Bacillus* sp.	2^3 full factorial design	Xylan (2.5–7.5 g/L) Casein (1–2 g/L) NH_4Cl (0.3–1.3 g/L)	[23]
5	Batch	*Escherichia coli DH5a*	RSM	$(NH_4)_2HPO_4$ (4–10 g/L) K_2HPO_4 (7–18 g/L) $MgSO_4$ (1.5–3 g/L)	[3]
6	Batch	*Aspergillus niger B03*	RSM	$(NH_4)_2HPO_4$ (2.0–4.2 g/L) Urea (0.3–0.9 g/L) Malt sprout (0.4–10 g/L)	[2]
7	Batch	*Bacillus* sp.	RSM	Xylan (2.5–3.5 g/L) Casein (1.8–2.0 g/L)	[23]

While DoE provides valuable insights, machine-learning-based regression models offer a more flexible and cost-effective alternative. Unlike DoE, which relies on controlled experiments, regression models utilize existing data to predict xylanase production under various conditions, minimizing the need for additional costly and time-consuming trials. Moreover, ML-based approaches, such as boosting techniques, can capture complex interactions between parameters more effectively than traditional statistical methods, ultimately enhancing accuracy and reducing prediction errors. Using machine learning, enzyme production processes can be optimized more efficiently, making these techniques a promising alternative to traditional statistical methods [21].

A significant study by Pensupa et al. [24] shows the effectiveness of machine learning models in optimizing biomass production through fermentation processes, revealing that the Matern 5/2 Gaussian process regression model achieved the lowest root mean squared error of 0.75 g/L and an R-squared value of 0.90. This highlights the power of complex statistical frameworks to examine complex datasets and augment predictive precision in fermentation processes, therefore enhancing the comprehension of ideal growing circumstances for microbial cultures, including xylanase producers.

Moreover, Wu et al. [25] highlighted the significance of machine learning in monitoring yeast fermentation by Raman spectroscopy, delivering real-time data that improve monitoring precision throughout fermentation activities. These strategies could similarly improve the monitoring of essential parameters in xylanase production, allowing dynamic modifications to optimize enzyme yield.

Jeong and Kim [26] integrated image processing into machine learning methodologies, concentrating on quantitative evaluations in fermentation processes. Their use of convolutional neural networks (CNNs) creates new opportunities for visually studying fermentation dynamics, which can be crucial in enhancing both the visual and operational sides of xylanase production by enabling real-time modifications based on measurable fermentation indicators.

Additionally, Bowler et al. [27] introduce a novel use of ultrasonic measurements integrated with machine learning to forecast alcohol content during beer fermentation. Their findings demonstrate that simple monitoring techniques can significantly improve fermentation control. The implementation of comparable simple measurement techniques in xylanase production may facilitate accurate adjustment of fermentation parameters, hence ensuring optimal conditions during the process.

A comparison between DoE and ML-based approaches highlights their respective advantages. In DoE methodologies, data collection typically occurs through controlled experiments, whereas ML approaches, particularly boosting techniques, can process datasets to improve accuracy and minimize prediction errors. While DoE relies on hypothesis-driven mathematical models, ML methods utilize iterative algorithms that continuously refine predictions. Beyond serving as a complement to DoE techniques, machine learning methods provide a significant advantage by optimizing processes without dependence on proprietary software, employing predictive capabilities directly from the acquired data.

This work evaluates the use of machine-learning-based predictive modeling on publicly available experimental datasets extracted from the literature. No new laboratory experiments were conducted. The aim is to explore the capability of ML models, particularly XGBoost, to replicate or improve upon the predictive patterns captured by DoE approaches.

This study focuses on predicting xylanase production using the XGBoost regressor. The model was trained on a dataset comprising various experimental conditions, including glucose, $(NH_4)HPO_4$, K_2HPO_4, KH_2PO_4, $MgSO_4$, $(NH_4)_2HPO_4$, urea, malt sprout, corn cobs, and wheat bran concentrations. The objective was to accurately predict xylanase activity and identify key factors influencing enzyme production. The results demonstrate that machine learning methods can effectively optimize protein production processes, providing a robust and scalable alternative to traditional statistical approaches. This study not only highlights the potential of machine learning in biotechnological optimization but also provides a foundation for future research in this rapidly developing field.

2. Materials and Methods

2.1. Dataset

The data from studies that optimized xylanase production through experimental design were analyzed in this study. Various factorial design levels and response surface methodology approaches (central composite design, Box–Behnken design, etc.) were used for media optimization in the assessed research. The independent variables and the levels that were utilized in these studies can be seen in Table 1.

All datasets used in this study were compiled from previously published experimental studies focused on xylanase production using various microorganisms and fermentation designs. These datasets represent secondary sources obtained through manual data extraction from the literature, and no original experiments or synthetic (simulated) data were produced.

Farliahati et al. [3] conducted a two-stage study to optimize the medium composition in xylanase production using *Escherichia coli DH5α*. In the first phase of this study, the most effective factors were determined using a factorial design with five factors. Within the scope of the study, the factors considered in 18 different experimental setups were glucose (10–20 g/L), $(NH_4)_2HPO_4$ (2–10 g/L), K_2HPO_4 (5–18 g/L), KH_2PO_4 (1–6 g/L), and $MgSO_4$ (0.5–3 g/L) (see Table A1). In the second part of the study, the concentration ranges of three effective factors, $(NH_4)_2HPO_4$ (1–13 g/L), K_2HPO_4 (1.5–23.5 g/L), and $MgSO_4$ (0.75–3.75 g/L), were altered, and optimization results were improved in 15 experimental sets using the response surface methodology. All the experiments were conducted in

250 mL baffled flasks with 50 mL working volume, and the pH was kept at 7.4. The incubation temperature was 37 °C, and all the flasks were agitated at 200 rpm for 18 h in an orbital shaker. The dataset is available in tabular form in Table A5.

In another study conducted by Dobrev et al. [2], an optimization study was carried out considering the cost advantage provided by using cheaper and more accessible types of waste instead of xylan. In the deep culture experiments conducted with *Aspergillus niger B03*, 26 different setups were used with $(NH_4)_2HPO_4$ (2.6–5.4 g/L), urea (0.9–2.1 g/L), malt sprout (6–18 g/L), corn cobs (12–24 g/L), and wheat bran (6–16 g/L) (Table A2). In the second part of the study, the concentrations required for the maximum xylanase amount were optimized in 14 different experimental setups using the important factors identified as $(NH_4)_2HPO_4$ (2.6–20.4 g/L), urea (0.3–0.9 g/L), and malt sprout (0.4–10 g/L). The biosynthesis reactors were 500 mL flasks with 50 mL working volume. All flasks were kept at 28 °C in an orbital shaker, agitated at 200 rpm for 18 h (Table A6).

A solid culture fermentation study by *Bacillus circulans* was conducted by Bocchini et al. [4] using a 3 × 3 factorial design to optimize xylan concentrations (5–10 g/L), pH levels (8–9), and incubation times (24–72 h) for enhanced xylanase production. The concentrations of these three significant components were optimized at 27 different levels in the conducted studies. Xylanase production was performed in 125 mL Erlenmeyer flasks with a working volume of 20 mL. All the flasks were incubated for 12 h at 45 °C and agitated at 150 rpm. The detailed dataset of the experiments and the xylanase production values are listed in Table A3.

Pham et al. [23] modified the amounts of xylan (2.5–7.5 g/L), casein (1–2 g/L), and NH_4Cl (0.3–1.3 g/L) in the culture medium for xylanase production from *Bacillus* sp. L-1018 using response surface techniques and used a two-stage optimization process. Initially, a full factorial design was applied to navigate toward the ideal region. The full factorial design technique simultaneously assesses the primary impacts of variables and their interactions (Table A4). Moreover, full factorial design effectively identifies the path of steepest ascent to reach within range of the optimal answer. It is thus especially suited for the preliminary phases. A 2 × 3 factorial design with three components at two levels necessitates eight experimental runs. In the second phase, 13 tests were conducted adopting response surface methodology to optimize concentrations of xylan (2.5–3.5 g/L) and casein (1.8–2.0 g/L) for maximum xylanase production. Xylanase production experiments were conducted in 250 mL Erlenmeyer flasks with 50 mL working volume. All the flasks were kept in a water bath, and agitation was supplied by a magnetic agitator at 250 rpm (Table A7).

For each dataset, the "DoE" values refer to reported predictions or interpolated outputs from factorial or response surface methods in the original publications, while the "XGBoost" values are generated by training a machine learning model on the same experimental input–output pairs. The XGBoost model was trained and tested independently from any statistical modeling carried out in the original study.

2.2. Regression Analysis for Xylanase Production Prediction

In this study, we used supervised machine learning regression techniques to predict xylanase production based on experimental input parameters such as nutrient concentrations, pH, and temperature. Among various regression algorithms, we selected **extreme gradient boosting (XGBoost)** due to its high accuracy, scalability, and robustness in modeling nonlinear interactions in structured datasets [28].

Figure 1 illustrates the workflow of building and applying a machine learning model for predicting xylanase activity based on experimental input variables. Initially, data

obtained from laboratory experiments—including features such as xylan, casein, and glucose concentrations—are used to train a predictive model. During the training phase (top row), these features are paired with experimentally determined xylanase activity values to construct a supervised learning model.Once the model is trained, it can then be applied to new data points (bottom row), where the same set of input features is fed into the model to generate predicted xylanase activity values. This approach allows for the estimation of enzymatic performance without conducting additional experiments, thereby facilitating process optimization and decision making in a data-driven manner.

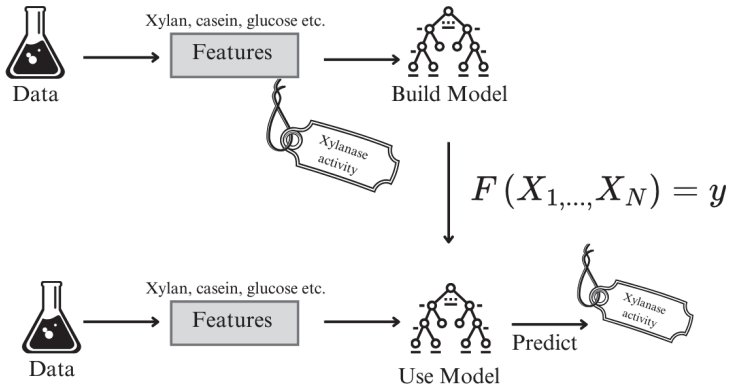

Figure 1. Blok Diagram of the Xylanase Production Prediction using XGBoost

Regression analysis aims to model the relationship between a set of input features $\mathbf{X} = (x_1, x_2, \ldots, x_p)$ and a continuous output variable y (xylanase activity in this case). Formally, it estimates a function $f : \mathbb{R}^p \to \mathbb{R}$ such that

$$y = f(\mathbf{X}) + \varepsilon \tag{1}$$

where ε represents random error or noise.

XGBoost is an open-source implementation of gradient boosted decision trees. It constructs an ensemble of regression trees where each new tree is trained to minimize the residual errors of the previous model [29]. The training process is guided by a regularized objective function:

$$\mathcal{L}(\theta) = \sum_{i=1}^{n} \ell(y_i, \hat{y}_i) + \sum_{t=1}^{T} \Omega(f_t) \tag{2}$$

Here, ℓ is typically the mean squared error (MSE):

$$\ell(y, \hat{y}) = \frac{1}{n} \sum_{i=1}^{n} (y_i - \hat{y}_i)^2 \tag{3}$$

and $\Omega(f_t)$ is a regularization term that penalizes overly complex models, thereby improving generalizability. At each iteration t, the model updates its prediction as

$$\hat{y}_i^{(t)} = \hat{y}_i^{(t-1)} + f_t(\mathbf{X}_i) \tag{4}$$

Figure 2 shows the block diagram of the XGBoost algorithm. In each booster iteration k, k = 1, 2, ..., T and T represent the total number of trees, the function $f_k(X, \theta_k)$ represents a regression tree trained to minimize the objective function θ_k, which consists of the loss of prediction and a regularization term. Here, θ_k denotes the set of parameters that define the structure of the regression tree f_k. These parameters include split decisions, feature

thresholds, leaf weights, and tree depth. They are used both for fitting the model and for computing the regularization term $\Omega(f_k)$, which penalizes overly complex trees to improve generalization. This objective ensures that each tree improves the model by fitting the residuals while controlling model complexity.

XGBoost has demonstrated superior performance in various domains, including bioinformatics [30,31], chemical engineering [32,33], and biotechnology [34], particularly when data are tabular and heterogeneous [35]. Furthermore, its built-in feature importance mechanism helps identify the most predictive variables in a given dataset, although this does not imply causality or biological significance.

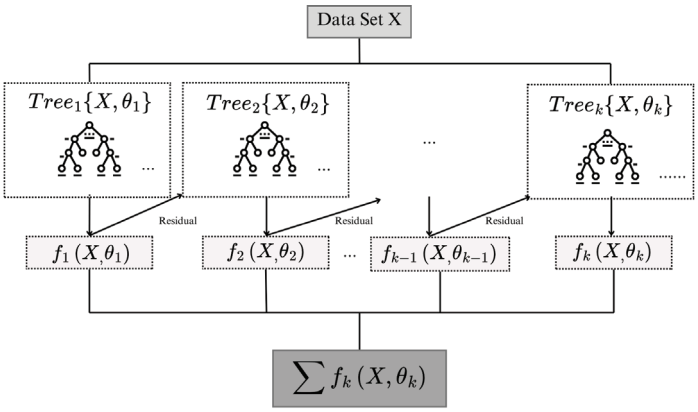

Figure 2. Block diagram of the XGBoost learning process. Adapted from [36]. In each boosting iteration (k), the function (f_k(X, θ_k)) represents a regression tree trained to minimize the objective function (θ_k).

In this study, XGBoost was trained using a diverse set of input variables collected from prior factorial and response surface experiments, allowing the model to capture complex interactions and generalize across different fermentation conditions.

2.3. Performance Evaluation

To assess the performance of the regression model, we used three common evaluation metrics: root mean squared error (RMSE), mean absolute percentage error (MAPE), and coefficient of determination (R^2). These metrics were selected to provide a comprehensive assessment of predictive accuracy from multiple perspectives. RMSE penalizes larger errors more heavily and is sensitive to outliers, which is important when high deviation points can influence process reliability. MAPE expresses the average prediction error as a percentage, allowing for easier interpretation across different output scales. Finally, R^2 measures how well the variation in the dependent variable is explained by the model, offering an overall goodness-of-fit evaluation.

By combining these three metrics, we aim to ensure a balanced and interpretable performance comparison between the XGBoost and DoE approaches.

RMSE measures the average error between the actual and predicted values. A lower RMSE indicates better model performance.

$$RMSE = \sqrt{\frac{1}{n}\sum_{i=1}^{n}(y_i - \hat{y}_i)^2} \tag{5}$$

MAPE calculates the average percentage error between actual and predicted values, making it useful for understanding relative error.

$$MAPE = \frac{100}{n}\sum_{i=1}^{n}\left|\frac{y_i - \hat{y}_i}{y_i}\right| \quad (6)$$

R^2 explains how well the model fits the data. A value closer to 1 indicates a better fit.

$$R^2 = 1 - \frac{\sum_{i=1}^{n}(y_i - \hat{y}_i)^2}{\sum_{i=1}^{n}(y_i - \bar{y})^2} \quad (7)$$

In this study, we analyzed these three metrics in detail to evaluate the model's performance comprehensively. We calculated RMSE, MAPE, and R^2 for both training and test datasets to compare how well the model generalizes. Additionally, we performed an evaluation using the predictions obtained from the design of experiments (DoE) approach, allowing us to assess the prediction accuracy of DoE-based models.

3. Results

In all regression experiments conducted within this study, the dataset was divided into training and testing sets using an 80–20% split. Performance metrics were calculated accordingly for both sets. It is important to note that while the XGBoost model was trained and evaluated on both training and test data, the design of experiments (DoE) approach does not involve a learning-based prediction process. Therefore, for DoE-based results, predictions on the training data were not derived from a model but rather interpolated or estimated through statistical fitting within the experimental design boundaries.

As a result, relatively higher error metrics for the training set in the DoE results—compared to XGBoost—are expected and do not indicate model underperformance. In contrast, performance on the test set provides a more objective and fair comparison between the two approaches, as it reflects the ability to generalize to unseen data. Accordingly, emphasis in the comparison of model effectiveness is placed primarily on the test set results throughout the following sections.

3.1. Regression for the Experiments Performed by Full Factorial Experimental Design

The figures below present the results of regression analyses performed using the XGBoost model on datasets generated through full factorial experimental designs. In each plot, the X-axis represents the experimentally observed xylanase activity, while the Y-axis shows the corresponding predicted values. Dots are the symbols for train values and stars are the symbols of test values. Blue dots indicate the predictions made by the XGBoost regression model, whereas red dots represent the estimations obtained via the design of experiments (DoE) approach. The black dashed diagonal line serves as a reference, illustrating the ideal case where predicted values perfectly match the experimental results.

Farliahati et al. [3] conducted a two-stage study using recombinant *Escherichia coli DH5α* to optimize xylanase production. In the first stage, five variables—glucose (10–20 g/L), $(NH_4)HPO_4$ (2–10 g/L), K_2HPO_4 (5–18 g/L), KH_2PO_4 (1–6 g/L), and $MgSO_4$ (0.5–3 g/L)—were investigated under 18 experimental conditions across 115 levels to maximize xylanase yield. As shown in Figure 3a, most data points lie close to the diagonal reference line, indicating strong agreement between the XGBoost model predictions and the experimental outcomes. However, a few discrepancies are observed, notably around the value of 2.2, which corresponds to a prediction from the DoE method. These deviations are likely due to experimental uncertainties rather than model inaccuracy. Such uncertainties may stem from factors common in bioprocess experiments, including variability in complex medium components (e.g., yeast extract), measurement errors in enzymatic activity assays (often due to sensitivity to time, temperature, or reagent stability), fluctuations in

environmental conditions during fermentation (such as pH or aeration), and biological variation among cultures (e.g., inoculum density or age). The variation observed along the primary line results from the wide range of data intervals in the experimental design. The chosen range of 5–18 g/L for K_2HPO_4 indicates that the experimental values deviate from the expected values. The detailed experimental data used in this analysis are provided in Table A5. Such significant variations in the quantities utilized in fermentation media can only be noticed for complex substrates. The research of Farliahati et al. [3] indicates that glucose's purity as a substrate permits a more limited operational range for K_2HPO_4. Within the parameters of the study, this phenomenon was also noted, resulting in a refinement of the outcome ranges and initiating the secondary optimization phase utilizing the RSM methodology (Table A5).

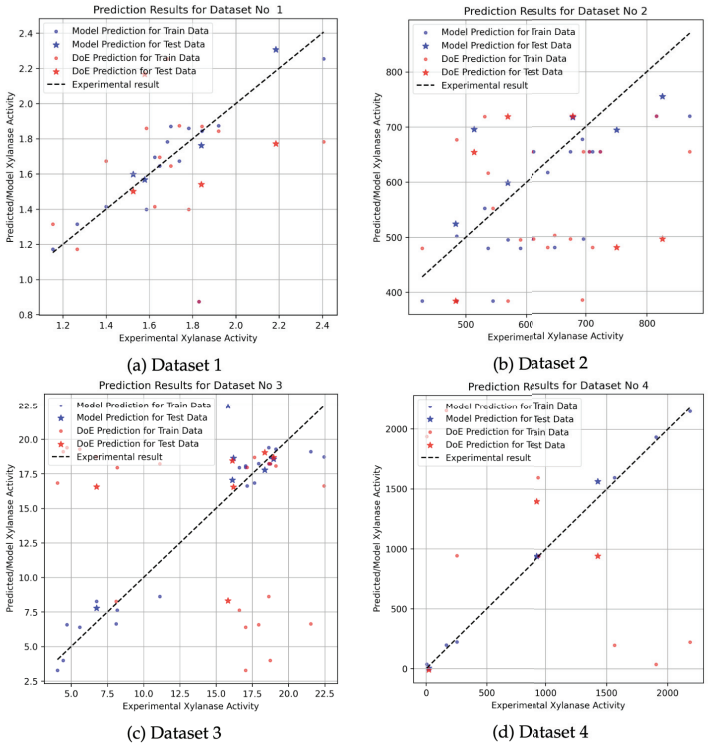

(a) Dataset 1 (b) Dataset 2

(c) Dataset 3 (d) Dataset 4

Figure 3. Prediction results for full-factorial datasets using XGBoost and DoE approaches. Blue dots indicate predictions made by the XGBoost model, and red dots represent estimations from the DoE approach. Dot symbols correspond to predictions on the training data, while star symbols indicate predictions on the test data. The black dashed line shows the ideal prediction line ($y = x$).

Dobrev et al. [2] conducted a study to optimize the nutrient medium for xylanase production using *Aspergillus niger B03* cultivated on agricultural wastes. The experimental design included a range of components such as $(NH_4)_2HPO_4$, urea, malt sprout, corn cobs, and wheat bran. Although the XGBoost regression model was trained on the same dataset (detailed in Table 2), the prediction performance was comparatively lower than that of other datasets. As shown in Figure 3b, the model predictions exhibit noticeable deviations from the reference line at several points, particularly at higher activity values. The factorial design employed in this study provides a broad range of variable combinations, which is beneficial for model training, but the observed deviations suggest that refined modeling with lower boundaries may be required to improve accuracy in such complex media formulations.

Table 2. XGBoost Results.

Data Set No	Train RMSE	Test RMSE	Train MAPE	Test MAPE	Train R^2	Test R^2
1	0.017	0.081	0.004	0.038	0.997	0.904
2	0.001	87.054	0.000	0.118	1.000	0.514
3	0.002	2.955	0.001	0.139	1.000	0.464
4	1.050	80.222	0.001	0.291	1.000	0.981
5	0.023	0.080	0.008	0.031	0.993	0.919
6	0.001	32.854	0.000	0.037	1.000	0.976
7	0.607	8.048	0.004	0.104	0.999	0.772

In another study, Bocchini et al. [4] optimized xylanase production by *Bacillus circulans D1* using a combination of full factorial design and Box–Behnken design (BBD). The optimization focused on three key variables: xylan concentration, pH, and cultivation time, across 27 experimental conditions (see Table A3). As shown in Figure 3c, the predictions obtained from the DoE and XGBoost models demonstrate a more pronounced divergence compared to other datasets. In particular, the DoE predictions show significant deviations from the experimental values, while the XGBoost regression model offers relatively closer estimates to the actual measurements. However, despite being more consistent than the DoE approach, the XGBoost model also exhibits variability and does not fully capture the experimental outcomes with high precision. These findings suggest that while the regression model performs better overall, the complexity of the underlying biological interactions in this dataset may require more advanced modeling strategies or a larger sample size to improve prediction accuracy.

The fermentation study conducted by Pham et al. [23] investigated xylanase production by *Bacillus* sp. I-1018 by optimizing three critical parameters: xylan, casein, and ammonium chloride concentrations. In Figure 3d, detailed in Table A7, the model prediction data are situated near the black dashed line, whereas the DOE predictions exhibit a wider dispersion. The increased frequency of the red points signifies a bigger variance in the predictions; however, a lower variance in the model's prediction data implies that the model produces successful outcomes.

3.2. Regression for the Experiments Performed by RSM

Figure 4a illustrates the results obtained from an optimization study conducted by Farliahati et al. [3] using response surface methodology (RSM) with three independent variables (dataset is available in Table A5). In this case, the predictions of the XGBoost model (represented by blue dots) exhibit greater stability from the reference line when compared to the predictions made by the DoE approach (red dots). The clustering of DoE predictions around the reference line indicates a high degree of accuracy and alignment with the experimental data, particularly in the mid-range xylanase activity levels. At higher activity values, both methods begin to diverge slightly, which may be attributed to experimental uncertainties or limitations in model generalizability. These findings suggest that although both models can track the general trend of the data, the XGBoost model provides more precise and stable predictions across the experimental range.

A similar evaluation was conducted on the dataset reported by Dobrev et al. [2] (see Table A6), who also utilized RSM for optimization purposes. As shown in the Figure 4b, both the XGBoost and DoE models show substantial correlation with the experimental values, especially at elevated xylanase activity levels. However, the XGBoost model exhibits noticeable variability in the mid-range activity region, where deviations from the reference line become more prominent. While predictions at lower activity values are largely consistent across both models, minor overestimations and underestimations occur in

the higher range. The XGBoosting model displays superior consistency, as evidenced by the denser clustering of blue points near the reference line. Overall, both methods successfully capture the general behavior of the process, but the XGBoosting model outperforms in terms of accuracy and robustness across all activity intervals.

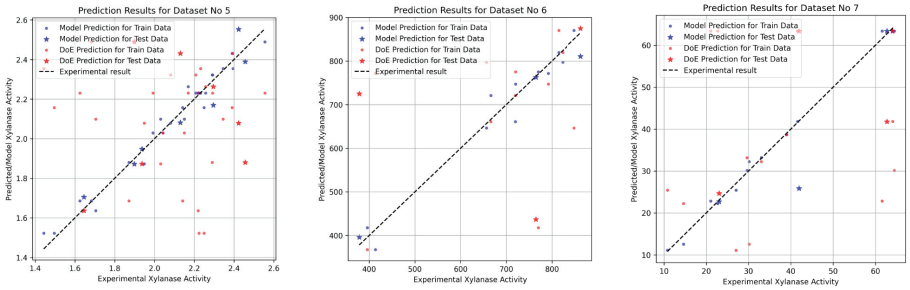

(a) Dataset 5 (b) Dataset 6 (c) Dataset 7

Figure 4. Prediction results for RSM-based datasets using XGBoost and DoE approaches. Blue dots represent predictions from the XGBoost model, while red dots correspond to the DoE estimations. Dot symbols indicate training data predictions; star symbols indicate test data predictions. The black dashed line represents the ideal prediction line ($y = x$).

Further evaluation was performed using the dataset derived from the work of Pham et al. [23] (see Table A7), which also employed an RSM-based experimental design. The scatter plot (Figure 4c) shows that the predicted values from both models closely align with the experimental xylanase activity measurements, indicating strong agreement with the reference line. Despite this overall alignment, more noticeable deviations are observed at the upper end of the activity spectrum, particularly for the DOE model. In contrast, the XGBoosting predictions maintain a more stable correspondence with the experimental data across the full range of activity levels. These results can be improved by further refinement of the ML-based model to enhance accuracy, particularly in boundary conditions or under extreme parameter settings.

The comparative analysis of experimental and predicted xylanase activity values across these three datasets offers valuable insights into the relative performance of machine learning and classical statistical approaches. While both methods capture the main trends in the data, the DoE approach demonstrates more stable performance, especially in the test datasets and at activity extremes. The results indicated variability in the performance of the XGBoost model across various datasets. Datasets with narrow experimental ranges, such as Dataset 4, demonstrated higher predictive accuracy, indicating that machine learning models are more effective within well-defined input spaces. In contrast, datasets characterized by broader or more heterogeneous parameter ranges (e.g., Dataset 2 and Dataset 3) demonstrated elevated prediction errors, likely related to increased complexity and noise that constrained the model's generalizability. The observations emphasize the significance of dataset characteristics, such as size, homogeneity, and noise levels, in influencing the performance of machine learning models.Therefore The XGBoost model, though promising, shows increased variability and may require further tuning, extended training datasets, or hybrid modeling strategies to improve prediction reliability.

Taken together, the results suggest that integrating the strengths of both methodologies—leveraging the predictive power of machine learning and the structural rigor of statistical design—may offer a more comprehensive and accurate framework for modeling and optimizing xylanase production processes (Table 3).

The feature importance values obtained from XGBoost for each dataset indicate the relative contribution of each input variable to the model's predictive performance. It is important to clarify that these importance scores do not imply any underlying biological or chemical significance. Instead, they reflect how frequently and effectively each feature is used by the XGBoost algorithm to reduce prediction error during training.

Table 3. DoE Results.

Sheet Name	Train RMSE	Test RMSE	Train MAPE	Test MAPE	Train R^2	Test R^2
1	0.271	0.042	0.070	0.021	0.134	0.975
2	96.690	71.850	0.127	0.101	0.216	0.669
3	1.405	1.179	0.105	0.077	0.947	0.915
4	26.672	26.554	0.771	0.478	0.999	0.998
5	0.047	0.043	0.018	0.018	0.972	0.976
6	32.215	41.323	0.043	0.073	0.953	0.961
7	1.239	0.940	0.038	0.024	0.995	0.997

For instance, in Dataset 1, the feature NH_4HPO_4 dominated the model with an importance score of 0.775, suggesting it played a major role in the decision paths constructed by the algorithm. Similarly, in Dataset 3, cultivation time (h) had a remarkably high importance of 0.964, indicating that XGBoost found this feature highly predictive within the context of the dataset.

Conversely, some features with known biochemical relevance may appear with low importance scores simply because they did not provide significant predictive value in the context of the model structure and available data. For example, in Dataset 4 features like X_2 (casein) g/L and X_3 (NH_4Cl) g/L had minimal contribution to the model outcome (0.008 and 0.001, respectively), not due to their irrelevance in a biological sense but rather due to their limited utility in reducing model error (Table 4).

Table 4. Feature contribution scores generated by XGBoost across six experimental datasets. The values reflect model-based importance, not causal or biological relationships.

Dataset	Feature	Importance
Dataset 1	$(NH_4)_2HPO_4$	0.775
	$MgSO_4$	0.084
	K_2HPO_4	0.060
	Glucose	0.055
	K_2HPO_4	0.025
Dataset 2	Corn cobs	0.718
	Wheat bran	0.210
	Urea	0.030
	$(NH_4)_2HPO_4$	0.025
	Malt sprout	0.018
Dataset 3	Cultivation time (h)	0.964
	pH	0.026
	Xylan (g/L)	0.009
Dataset 4	X_1 (Xylan) g/L	0.992
	X_2 (casein) g/L	0.008
	X_3 (NH_4Cl) g/L	0.001
Dataset 5	K_2HPO_4	0.498
	$(NH_4)_2HPO_4$	0.407
	$MgSO_4$	0.095
Dataset 6	Urea	0.499
	Malt sprout	0.460
	$(NH_4)_2HPO_4$	0.040

Overall, these results provide a data-driven insight into how XGBoost utilizes features within each specific dataset. They are valuable for model interpretation and optimization but should not be over-interpreted in terms of causal or mechanistic implications without further experimental validation.

4. Discussion

Recent research underscores the essential impact of machine learning techniques in optimizing xylanase production within the field of biotechnology. Xylanase is a multifunctional enzyme used in several industries including pulp and paper, biofuels, food processing, textiles, and animal feed. Due to the enzyme's extensive applications, effective production methods are essential, especially for industrial scale, where variables such as temperature, pH, and working volumes critically affect yield.

This work illustrates the potential benefits of machine learning (ML), specifically the XGBoost algorithm, in forecasting xylanase production utilizing datasets initially created through conventional design of experiments (DoE). In this study, XGBoost was selected as the machine learning model due to the characteristics of the available datasets. Specifically, the datasets contained a limited number of observations and were structured in a tabular format, making them less suitable for artificial neural networks (ANNs) or other conventional classifiers that typically require large volumes of data to perform effectively.

Prior to finalizing the modeling approach, we conducted preliminary experiments using artificial neural networks (ANN) and other conventional machine learning algorithms. However, these models showed suboptimal predictive performance, primarily attributed to overfitting on the relatively small and heterogeneous datasets [37,38]. While overfitting was a major concern, the decision to exclude these models was also informed by their limited generalization ability, sensitivity to small sample sizes, and inadequate capacity to capture complex nonlinear interactions effectively. In contrast, XGBoost was chosen for its well-documented robustness on small-to-medium-sized tabular datasets, its built-in regularization mechanisms, and its strong predictive performance observed in our initial evaluations.

Therefore, ANN and other conventional classifiers were not pursued further in the main analysis of this study. Our findings indicate that machine learning may match or even exceed traditional statistical methods in specific cases, particularly when the relationship between inputs and outputs is complex or nonlinear. Xylanase production processes often exhibit complex and nonlinear interactions among operational parameters such as pH, temperature, and substrate concentration. While DoE captures these interactions up to second-order polynomial levels, tree-based methods like XGBoost can flexibly partition the input space and approximate more intricate nonlinear patterns without predefining a functional form.

In the analyzed datasets, XGBoost demonstrated comparable or superior test set performance to DoE in several cases, particularly in datasets with complex or nonlinear relationships. While design of experiments (DoE) methodologies remain effective for structured experimental planning and hypothesis testing, their limited capacity to generalize beyond the training data can be restrictive in certain contexts. Conversely, machine learning models such as XGBoost offer increased flexibility by identifying hidden patterns in the data, which proved beneficial in our study. These findings are in line with the work of Zhai et al. [39], who applied ML models to predict volatile fatty acid concentrations in anaerobic sludge fermentation, achieving an R^2 of up to 0.949.

Our research aligns with the findings of Pensupa et al. [24], who employed Gaussian process regression to forecast biomass output from Yarrowia lipolytica fermentation and

identified 14 critical predictors. Our study demonstrates that the integration of data mining and machine learning can provide significant insights into fermentation performance, especially when utilizing secondary or heterogeneous datasets.

While XGBoost did not consistently outperform the DoE approach across all datasets, it demonstrated comparable or better performance in several cases, highlighting its potential as a robust, data-driven alternative for modeling bioprocess outcomes.

In summary, ML models like XGBoost provide a data-driven enhancement to traditional design of experiments, enabling improved generalization and predictive accuracy in complex fermentation systems. Subsequent efforts should incorporate feature interpretation methodologies such as SHAP, examine ensemble and hybrid models, and analyze time-series dynamics to enhance prediction and process optimization in biotechnological applications. Moreover, the incorporation of machine learning—especially via regression models and advanced data analysis methodologies—offers considerable potential for enhancing xylanase production. Assessing critical variables influencing enzyme activity might improve efficiency and cost-effectiveness, thereby matching with overreaching objectives in biotechnology including sustainability and food security.

5. Conclusions

This study highlights the effectiveness of XGBoost in predicting experimental outcomes compared to traditional DoE methods. The results show that machine learning models can significantly improve prediction accuracy and reduce error metrics, making them suitable for complex, data-driven experimental processes. However, the limitations of purely data-driven methods should not be overlooked, as they require extensive and high-quality datasets for optimal performance.

Although XGBoost demonstrated strong predictive capacity in several datasets, it did not consistently outperform DoE in all cases. The comparative advantage of each method appeared to depend on the dataset size, experimental design type, and variability in input parameters.

While DoE methods remain valuable for structured experimental design, incorporating machine learning techniques such as XGBoost can enhance predictive power and efficiency. Future research could explore hybrid approaches that leverage the strengths of both methods, ensuring a balance between statistical rigor and predictive accuracy. Additionally, expanding the dataset and implementing feature selection techniques could further improve model generalization and reliability in real-world applications.

By integrating advanced machine learning techniques with established statistical methods, researchers can achieve more precise and reliable experimental predictions, ultimately enhancing decision-making processes in various scientific and industrial applications.

Author Contributions: Conceptualization, T.K.-G.; methodology, B.E.K.-G.; software, B.E.K.-G.; validation, B.E.K.-G. and T.K.-G.; formal analysis, B.E.K.-G.; investigation, B.E.K.-G.; resources, M.A.E.; data curation, M.A.E.; writing—original draft preparation, M.A.E., B.E.K.-G. and T.K.-G.; writing—review and editing, T.K.-G.; visualization, M.A.E.; supervision, T.K.-G.; project administration, T.K.-G. All authors have read and agreed to the published version of the manuscript.

Funding: This study was supported by the Scientific Research Projects Coordination Unit of İzmir Demokrasi University. Project No: TEZ-MHF/2501.

Institutional Review Board Statement: Not applicable.

Informed Consent Statement: Not applicable.

Data Availability Statement: The Python code for the XGBoost-based regression analysis, along with sample data and result generation tools, is available at: https://github.com/basakesin/xylanase-model (accessed on 28 March 2025).

Acknowledgments: During the preparation of this manuscript, the authors used GPT-4o and Quillbot Premium for the purposes of language editing and text fluency. The authors have reviewed and edited the output and take full responsibility for the content of this publication.

Conflicts of Interest: The authors declare no conflicts of interest.

Abbreviations

The following abbreviations are used in this manuscript:

AI	Artificial intelligence
ANN	Artificial neural network
BBD	Box–Behnken design
CCD	Central composite design
CNN	Convolutional neural network
DoE	Design of experiments
GPR	Gaussian process regression
IU/mL	International units per milliliter
MAPE	Mean absolute percentage error
ML	Machine learning
MLR	Multiple linear regression
R^2	Coefficient of determination
RMSE	Root mean squared error
RSM	Response surface methodology
SHAP	Shapley additive explanations
SVR	Support vector regression
VFAs	Volatile fatty acids
XGBoost	Extreme gradient boosting

Appendix A

Table A1. Dataset No: 1.

Glucose (g/L)	$(NH_4)HPO_4$ (g/L)	K_2HPO_4 (g/L)	KH_2PO_4 (g/L)	$MgSO_4$ (g/L)	Experimental Xylanase Activity	Predicted Xylanase Activity
20	10	18	6	3	1.699	1.870
10	2	18	6	3	1.586	1.398
10	10	18	1	3	1.782	1.859
10	10	18	6	0.5	1.843	1.843
10	10	5	1	0.5	1.738	1.673
20	10	5	1	3	1.647	1.645
20	2	5	1	0.5	1.266	1.314
15	6	11.5	3.5	1.75	1.829	0.874
20	2	18	6	0.5	1.578	1.540
10	2	18	1	0.5	1.683	1.782
15	6	11.5	3.5	1.75	1.920	1.874
10	2	5	1	3	1.153	1.172
20	2	18	1	3	1.525	1.501
20	10	18	1	0.5	2.406	2.254
20	10	5	6	0.5	2.185	2.167
20	2	5	6	3	1.399	1.414
10	10	5	6	3	1.840	1.772
10	2	5	6	0.5	1.625	1.695

Table A2. Dataset No: 2.

$(NH_4)_2HPO_4$ (g/L)	Urea (g/L)	Malt Sprout (g/L)	Corn Cobs (g/L)	Wheat Bran (g/L)	Experimental Xylanase Activity	Predicted Xylanase Activity
2.6	0.9	6	12	16	428.12	384.32
5.4	0.9	6	12	6	568.79	479.86
2.6	2.1	6	12	6	649.09	479.86
5.4	2.1	6	12	16	544.56	384.32
2.6	0.9	18	12	6	589.81	479.86
5.4	0.9	18	12	16	483.24	384.32
2.6	2.1	18	12	16	484.91	384.32
5.4	2.1	18	12	6	536.66	479.86
2.6	0.9	6	24	6	569.31	495.54
5.4	0.9	6	24	16	750.47	718.72
2.6	2.1	6	24	16	869.88	718.72
5.4	2.1	6	24	6	513.49	495.54
2.6	0.9	18	24	16	825.29	718.72
5.4	0.9	18	24	6	695.87	495.54
2.6	2.1	18	24	6	611.15	495.54
5.4	2.1	18	24	16	815.58	718.72
5.4	1.5	12	18	11	723.41	654.25
2.6	1.5	12	18	11	678.61	654.25
4	2.1	12	18	11	674.75	654.25
4	0.9	12	18	11	614.37	654.25
4	1.5	18	18	11	710.87	654.25
4	1.5	6	18	11	705.62	654.25
4	1.5	12	24	11	694.44	677.02
4	1.5	12	12	11	484.97	501.98
4	1.5	12	18	16	637.56	616.27
4	1.5	12	18	6	531.08	552.45

Table A3. Dataset No: 3.

Xylan (g/L)	pH	Cultivation Time (h)	Experimental Xylanase Activity	Predicted Xylanase Activity
5	8	24	11.11	8.62
5	8	48	16.20	18.45
5	8	72	15.81	16.54
5	8.5	24	8.17	7.62
5	8.5	48	17.04	17.96
5	8.5	72	16.12	16.56
5	9	24	6.75	8.26
5	9	48	21.54	19.11
5	9	72	18.65	18.22
7.5	8	24	6.75	8.31
7.5	8	48	18.63	19.39
7.5	8	72	22.45	18.73
7.5	8.5	24	8.10	6.63
7.5	8.5	48	18.73	18.22
7.5	8.5	72	17.04	18.07
7.5	9	24	4.70	6.58
7.5	9	48	18.36	18.69
7.5	9	72	18.97	19.05
10	8	24	5.59	6.39
10	8	48	18.75	18.69
10	8	72	19.12	19.28
10	8.5	24	4.44	3.99
10	8.5	48	17.64	16.84
10	8.5	72	16.60	17.94
10	9	24	4.05	3.27
10	9	48	17.14	16.63
10	9	72	17.93	18.24

Table A4. Dataset No: 4.

X1 (Xylan) (g/L)	X2 (Casein) (g/L)	X3 (NH_4Cl) (g/L)	Observed XA (nkat/mL)	Predicted XA (nkat/mL)
2.5	1	0.3	1428.00	1397.80
7.5	1	0.3	5.30	36.10
2.5	2	0.3	1905.50	1936.34
7.5	2	0.3	253.70	222.86
2.5	1	1.3	1565.10	1595.94
7.5	1	1.3	22.10	−8.73
2.5	2	1.3	2184.90	2154.10
7.5	2	1.3	166.10	196.60
5.0	1.5	0.8	925.40	941.30
5.0	1.5	0.8	942.60	941.30
5.0	1.5	0.8	938.40	941.30

Table A5. Dataset No: 5.

$(NH_4)_2HPO_4$ (g/L)	K_2HPO_4 (g/L)	$MgSO_4$ (g/L)	Experimental Xylanase Activity	Predicted Xylanase Activity
10	7	3	1.871	1.880
10	7	3	1.898	1.880
10	18	1.5	2.423	2.489
10	18	3	2.292	2.322
1	12.5	2.25	1.443	1.523
7	12.5	0.75	2.456	2.431
7	12.5	2.25	2.219	2.230
7	12.5	2.25	2.219	2.230
10	18	3	2.290	2.322
10	7	1.5	2.296	2.263
7	12.5	3.75	1.992	2.029
4	7	3	1.705	1.636
7	12.5	2.25	2.257	2.230
4	7	3	1.645	1.636
13	12.5	2.25	2.141	2.157
10	7	1.5	2.169	2.263
7	1.5	2.25	1.625	1.686
7	1.5	2.25	1.683	1.686
7	23.5	2.25	2.345	2.354
7	12.5	3.75	2.042	2.029
4	18	3	2.130	2.079
4	7	1.5	1.937	1.873
7	23.5	2.25	2.395	2.354
4	18	3	2.081	2.079
4	18	1.5	2.031	2.099
1	12.5	2.25	1.496	1.523
7	12.5	0.75	2.390	2.431
10	18	1.5	2.555	2.489
4	7	1.5	1.948	1.873
4	18	1.5	2.150	2.099
7	12.5	2.25	2.207	2.230
7	12.5	2.25	2.232	2.230
13	12.5	2.25	2.249	2.157
7	12.5	2.25	2.224	2.230

Table A6. Dataset No: 6.

$(NH_4)_2HPO_4$ (g/L)	Urea (g/L)	Malt Sprout (g/L)	Experimental Xylanase Activity	Predicted Xylanase Activity
0.4	0.3	0.4	413.45	367.28
2.6	0.3	0.4	395.83	417.70
0.4	0.9	0.4	764.69	724.98
2.6	0.9	0.4	770.09	775.39
0.4	0.3	10	666.32	721.08
2.6	0.3	10	791.83	771.49
0.4	0.9	10	815.09	819.69
2.6	0.9	10	850.41	870.11
0.4	0.6	5.2	720.35	746.87
2.6	0.6	5.2	823.81	797.29
1.5	0.3	5.2	656.61	646.49
1.5	0.9	5.2	864.53	874.65
1.5	0.3	0.4	378.05	436.73
1.5	0.3	10	719.73	661.02

Table A7. Dataset No: 7.

A: Wheat Bran (g/L)	B: Yeast Extract + Peptone (g/L)	C: Temperature (°C)	Observed Xylanase Activity (IU/mL)	Predicted Xylanase Activity (IU/mL)
10	10	25	64.44	63.38
2	10	20	10.83	11.11
2	10	30	27.04	25.41
18	2	25	41.61	41.81
2	18	25	21.05	22.85
18	18	25	29.64	30.09
10	2	30	30.14	32.24
10	18	20	14.60	12.54
10	18	30	41.93	41.76
10	10	25	64.08	63.38
10	2	20	33.01	33.17
18	10	20	23.04	24.67
2	2	25	22.68	22.23
10	10	25	64.03	63.38
10	10	25	61.60	63.38
18	10	30	38.95	38.67
10	10	25	62.73	63.38

References

1. Collins, T.; Gerday, C.; Feller, G. Xylanases, xylanase families and extremophilic xylanases. *FEMS Microbiol. Rev.* **2005**, *29*, 3–23. [CrossRef] [PubMed]
2. Dobrev, G.T.; Pishtiyski, I.G.; Stanchev, V.S.; Mircheva, R. Optimization of nutrient medium containing agricultural wastes for xylanase production by *Aspergillus niger* B03 using optimal composite experimental design. *Bioresour. Technol.* **2007**, *98*, 2671–2678. [CrossRef] [PubMed]
3. Farliahati, M.R.; Ramanan, R.N.; Mohamad, R.; Puspaningsih, N.N.T.; Ariff, A.B. Enhanced production of xylanase by recombinant *Escherichia coli* DH5α through optimization of medium composition using response surface methodology. *Ann. Microbiol.* **2010**, *60*, 279–285. [CrossRef]
4. Bocchini, D.A.; Alves-Prado, H.F.; Baida, L.C.; Roberto, I.C.; Gomes, E.; Da Silva, R. Optimization of xylanase production by *Bacillus circulans* D1 in submerged fermentation using response surface methodology. *Process. Biochem.* **2002**, *38*, 727–731. [CrossRef]
5. Limkar, M.B.; Pawar, S.V.; Rathod, V.K. Statistical optimization of xylanase and alkaline protease co-production by *Bacillus* spp using Box-Behnken Design under submerged fermentation using wheat bran as a substrate. *Biocatal. Agric. Biotechnol.* **2019**, *17*, 455–464. [CrossRef]
6. Patel, K.; Dudhagara, P. Optimization of xylanase production by *Bacillus tequilensis* strain UD-3 using economical agricultural substrate and its application in rice straw pulp bleaching. *Biocatal. Agric. Biotechnol.* **2020**, *30*, 101846. [CrossRef]
7. Prade, R.A. Xylanases: From biology to biotechnology. *Biotechnol. Genet. Eng. Rev.* **1996**, *13*, 101–132. [CrossRef]
8. Sharma, D.; Sahu, S.; Singh, G.; Arya, S.K. An eco-friendly process for xylose production from waste of pulp and paper industry with xylanase catalyst. *Sustain. Chem. Environ.* **2023**, *3*, 100024. [CrossRef]

9. Garai, D.; Kumar, V. Response surface optimization for xylanase with high volumetric productivity by indigenous alkali tolerant *Aspergillus candidus* under submerged cultivation. *3 Biotech* **2013**, *3*, 127–136. [CrossRef]
10. Yıldırım, A.; İlhan Ayışığı, E.; Düzel, A.; Mayfield, S.P.; Sargın, S. Optimization of culture conditions for the production and activity of recombinant xylanase from microalgal platform. *Biochem. Eng. J.* **2023**, *197*, 108967. [CrossRef]
11. Bhardwaj, N.; Kumar, B.; Verma, P. A detailed overview of xylanases: An emerging biomolecule for current and future prospective. *Bioresour. Bioprocess.* **2019**, *6*, 40. [CrossRef]
12. Huang, K.; Chu, Y.; Qin, X.; Zhang, J.; Bai, Y.; Wang, Y.; Luo, H.; Huang, H.; Su, X. Recombinant production of two xylanase-somatostatin fusion proteins retaining somatostatin immunogenicity and xylanase activity in Pichia pastoris. *Appl. Microbiol. Biotechnol.* **2021**, *105*, 4167–4175. [CrossRef] [PubMed]
13. Kallel, F.; Driss, D.; Chaari, F.; Zouari-Ellouzi, S.; Chaabouni, M.; Ghorbel, R.; Chaabouni, S.E. Statistical optimization of low-cost production of an acidic xylanase by Bacillus mojavensis UEB-FK: Its potential applications. *Biocatal. Agric. Biotechnol.* **2016**, *5*, 1–10. [CrossRef]
14. Abdella, A.; Segato, F.; Wilkins, M.R. Optimization of process parameters and fermentation strategy for xylanase production in a stirred tank reactor using a mutant Aspergillus nidulans strain. *Biotechnol. Rep.* **2020**, *26*, e00457. [CrossRef]
15. Ajijolakewu, A.K.; Leh, C.P.; Abdullah, W.N.W.; Lee, C.K. Optimization of production conditions for xylanase production by newly isolated strain *Aspergillus niger* through solid state fermentation of oil palm empty fruit bunches. *Biocatal. Agric. Biotechnol.* **2017**, *11*, 239–247. [CrossRef]
16. Siwach, R.; Sharma, S.; Khan, A.A.; Kumar, A.; Agrawal, S. Optimization of xylanase production by *Bacillus* sp. MCC2212 under solid-state fermentation using response surface methodology. *Biocatal. Agric. Biotechnol.* **2024**, *57*, 103085. [CrossRef]
17. Liao, H.; Ying, W.; Li, X.; Zhu, J.; Xu, Y.; Zhang, J. Optimized production of xylooligosaccharides from poplar: A biorefinery strategy with sequential acetic acid/sodium acetate hydrolysis followed by xylanase hydrolysis. *Bioresour. Technol.* **2022**, *347*, 126683. [CrossRef]
18. Liu, C.; Sun, Z.T.; Du, J.H.; Wang, J. Response surface optimization of fermentation conditions for producing xylanase by *Aspergillus niger* SL-05. *J. Ind. Microbiol. Biotechnol.* **2008**, *35*, 703–711. [CrossRef]
19. Iram, A.; Cekmecelioglu, D.; Demirci, A. Optimization of the fermentation parameters to maximize the production of cellulases and xylanases using DDGS as the main feedstock in stirred tank bioreactors. *Biocatal. Agric. Biotechnol.* **2022**, *45*, 102514. [CrossRef]
20. Ezeilo, U.R.; Wahab, R.A.; Mahat, N.A. Optimization studies on cellulase and xylanase production by *Rhizopus oryzae* UC2 using raw oil palm frond leaves as substrate under solid state fermentation. *Renew. Energy* **2020**, *156*, 1301–1312. [CrossRef]
21. Uhoraningoga, A.; Kinsella, G.K.; Henehan, G.T.; Ryan, B.J. The goldilocks approach: A review of employing design of experiments in prokaryotic recombinant protein production. *Bioengineering* **2018**, *5*, 89. [CrossRef] [PubMed]
22. Adhyaru, D.N.; Bhatt, N.S.; Modi, H.A.; Divecha, J. Insight on xylanase from *Aspergillus tubingensis* FDHN1: Production, high yielding recovery optimization through statistical approach and application. *Biocatal. Agric. Biotechnol.* **2016**, *6*, 51–57. [CrossRef]
23. Pham, P.L.; Taillandier, P.; Delmas, M.; Strehaiano, P. Optimization of a culture medium for xylanase production by Bacillus sp. using statistical experimental designs. *World J. Microbiol. Biotechnol.* **1997**, *14*, 185–190. [CrossRef]
24. Pensupa, N.; Treebuppachartsakul, T.; Pechprasarn, S. Machine learning models using data mining for biomass production from Yarrowia lipolytica fermentation. *Fermentation* **2023**, *9*, 239. [CrossRef]
25. Wu, D.; Xu, Y.; Xu, F.; Shao, M.; Huang, M. Machine learning algorithms for in-line monitoring during yeast fermentations based on Raman spectroscopy. *Vib. Spectrosc.* **2024**, *132*, 103672. [CrossRef]
26. Jeong, J.; Kim, S. Application of machine learning for quantitative analysis of industrial fermentation using image processing. *Food Sci. Biotechnol.* **2025**, *34*, 373–381. [CrossRef]
27. Bowler, A.; Escrig, J.; Pound, M.; Watson, N. Predicting alcohol concentration during beer fermentation using ultrasonic measurements and machine learning. *Fermentation* **2021**, *7*, 34. [CrossRef]
28. Chen, T.; Guestrin, C. Xgboost: A scalable tree boosting system. In Proceedings of the 22nd Acm Sigkdd International Conference on Knowledge Discovery and Data Mining, San Francisco, CA, USA, 13–17 August 2016; pp. 785–794.
29. Nielsen, D. Tree Boosting with Xgboost-Why Does Xgboost Win "Every" Machine Learning Competition? Master's Thesis, NTNU, Taipei City, Taiwan, 2016.
30. Zhang, D.; Chen, H.D.; Zulfiqar, H.; Yuan, S.S.; Huang, Q.L.; Zhang, Z.Y.; Deng, K.J. iBLP: An XGBoost-Based Predictor for Identifying Bioluminescent Proteins. *Comput. Math. Methods Med.* **2021**, *2021*, 6664362. [CrossRef]
31. Dimitrakopoulos, G.N.; Vrahatis, A.G.; Plagianakos, V.; Sgarbas, K. Pathway analysis using XGBoost classification in Biomedical Data. In Proceedings of the 10th Hellenic Conference on Artificial Intelligence, Patras, Greece, 9–12 July 2018; pp. 1–6. [CrossRef]
32. Yang, A.; Sun, S.; Mi, H.; Wang, W.; Liu, J.; Kong, Z.Y. Interpretable feedforward neural network and XGBoost-based algorithms to predict CO_2 solubility in ionic liquids. *Ind. Eng. Chem. Res.* **2024**, *63*, 8293–8305. [CrossRef]

33. Al-Jamimi, H.A.; BinMakhashen, G.M.; Saleh, T.A. From data to clean water: XGBoost and Bayesian optimization for advanced wastewater treatment with ultrafiltration. *Neural Comput. Appl.* **2024**, *36*, 18863–18877. [CrossRef]
34. Xie, H.; Deng, Y.m.; Li, J.y.; Xie, K.h.; Tao, T.; Zhang, J.f. Predicting the risk of primary Sjögren's syndrome with key N7-methylguanosine-related genes: A novel XGBoost model. *Heliyon* **2024**, *10*, e31307. [CrossRef] [PubMed]
35. Shwartz-Ziv, R.; Armon, A. Tabular data: Deep learning is not all you need. *Inf. Fusion* **2022**, *81*, 84–90. [CrossRef]
36. Guo, R.; Zhao, Z.; Wang, T.; Liu, G.; Zhao, J.; Gao, D. Degradation state recognition of piston pump based on ICEEMDAN and XGBoost. *Appl. Sci.* **2020**, *10*, 6593. [CrossRef]
37. Grinsztajn, L.; Oyallon, E.; Varoquaux, G. Why do tree-based models still outperform deep learning on typical tabular data? *Adv. Neural Inf. Process. Syst.* **2022**, *35*, 507–520. [CrossRef]
38. Stevanović, S.; Dashti, H.; Milošević, M.; Al-Yakoob, S.; Stevanović, D. Comparison of ANN and XGBoost surrogate models trained on small numbers of building energy simulations. *PLoS ONE* **2024**, *19*, e0312573. [CrossRef]
39. Zhai, S.; Chen, K.; Yang, L.; Li, Z.; Yu, T.; Chen, L.; Zhu, H. Applying machine learning to anaerobic fermentation of waste sludge using two targeted modeling strategies. *Sci. Total Environ.* **2024**, *916*, 170232. [CrossRef]

fermentation

MDPI

Article

Dynamic Optimization of Xylitol Production Using Legendre-Based Control Parameterization

Eugenia Gutiérrez, Marianela Noriega, Cecilia Fernández *, Nadia Pantano, Leandro Rodriguez and Gustavo Scaglia

Instituto de Ingeniería Química, Universidad Nacional de San Juan (UNSJ), CONICET, Av. Libertador San Martín(O) 1109, San Juan J5400ARL, Argentina; meugegutierrez@gmail.com (E.G.); npantano@unsj.edu.ar (N.P.); lrodri@unsj.edu.ar (L.R.); gscaglia@unsj.edu.ar (G.S.)
* Correspondence: mcfernandez@unsj.edu.ar

Abstract: This paper presents an improved methodology for optimizing the fed-batch fermentation process of xylitol production, aiming to maximize the final concentration in a bioreactor co-fed with xylose and glucose. Xylitol is a valuable sugar alcohol widely used in the food and pharmaceutical industries, and its microbial production requires precise control over substrate feeding strategies. The proposed technique employs Legendre polynomials to parameterize two control actions (the feeding rates of glucose and xylose), and it uses a hybrid optimization algorithm combining Monte Carlo sampling with genetic algorithms for coefficient selection. Unlike traditional optimization approaches based on piecewise parameterization, which produce discontinuous control profiles and require post-processing, this method generates smooth profiles directly applicable to real systems. Additionally, it significantly reduces mathematical complexity compared to strategies that combine Fourier series with orthonormal polynomials while maintaining similar optimization results. The methodology achieves good results in xylitol production using only eight parameters, compared to at least twenty in other approaches. This dimensionality reduction improves the robustness of the optimization by decreasing the likelihood of convergence to local optima while also reducing the computational cost and enhancing feasibility for implementation. The results highlight the potential of this strategy as a practical and efficient tool for optimizing nonlinear multivariable bioprocesses.

Keywords: bioprocesses; Legendre polynomials; optimization; evolutionary algorithms; nonlinear system; genetic algorithm; ant colony

1. Introduction

Xylitol is a five-carbon sugar alcohol derived from xylose. Discovered in 1891, it has been widely used as a low-calorie sweetener due to its pleasant taste and beneficial properties. Since the 1960s, xylitol has been employed as a sweetening agent in various industries, including in food, pharmaceuticals, cosmetics, and oral hygiene products. Commercially, it is primarily obtained from plant sources, such as birch, other hardwood trees, and fibrous vegetation, through chemical processes that are both costly and environmentally demanding. Despite its natural occurrence in fruits and vegetables, large-scale production continues to rely on energy-intensive chemical methods that require high-pressure hydrogenation and expensive catalysts [1].

In response to these drawbacks, biotechnological production methods have gained significant attention due to their environmental sustainability and potential for cost reduction [2]. By harnessing microbial metabolism, xylitol can be obtained from renewable biomass through fermentation processes, avoiding harsh reaction conditions and reducing the dependency on fossil-derived chemicals. In particular, microbial fermentation using yeasts or bacteria allows for the selective conversion of xylose to xylitol under mild conditions, offering an attractive alternative to conventional synthesis. Additionally, these biological systems provide a framework for valorizing agro-industrial waste streams rich in hemicellulose, contributing to circular economy initiatives and the development of more sustainable value chains. Among the various fermentation strategies, fed-batch processes have proven especially effective for xylitol production [3]. In a fed-batch system, substrates are incrementally added to the bioreactor, enabling better control over nutrient availability, reducing inhibition effects, and maintaining favorable conditions for microbial activity. A common approach involves using glucose as the primary carbon source during the growth phase, followed by xylose feeding to enhance xylitol production. However, the design of optimal feeding profiles remains a complex task due to the nonlinear dynamics of microbial growth, substrate uptake, and product formation. Moreover, the metabolic behavior of microorganisms may vary significantly depending on factors such as oxygen availability, pH, temperature, or the presence of inhibitors, all of which add further layers of complexity to the optimization process.

Traditionally, the optimization of fed-batch fermentation relies on detailed first-principle models that describe biomass growth, substrate consumption, and product kinetics [4,5]. These models are essential for predicting system behavior and guiding process design. Nevertheless, their complexity often hinders their direct use in real-time control and optimization frameworks. Moreover, in practice, the accuracy of these models may be affected by parameter uncertainty, measurement noise, and biological variability, further complicating the implementation of optimal control strategies.

In industrial bioprocessing, mathematical optimization is a crucial tool to improve yield and efficiency [6]. A common technique involves parameterizing the control actions (typically the substrate feed rates) using piecewise constant or piecewise linear functions [7,8]. While conceptually simple, these strategies present several limitations. First, they require a large number of parameters to capture the desired feeding dynamics accurately, especially when finer time discretizations are used. Second, they often produce control profiles with discontinuities or abrupt changes between intervals. These non-smooth profiles can result in rapid variations in substrate concentration, leading to osmotic stress, metabolic imbalances, or even microbial inhibition.

Alternative approaches such as artificial neural networks [9], numerical search methods [10], and heuristic algorithms [11–14] have been proposed to address the challenges of dynamic optimization. These methods can be implemented either in offline or online frameworks, depending on the availability of real-time measurements and computational resources. While online strategies like Model Predictive Control continuously adjust control actions based on real-time process data [15], offline methods, such as the one employed in this study, compute optimal control trajectories in advance, without requiring real-time feedback. Furthermore, many existing approaches prioritize mathematical optimization without considering the physical or biological feasibility of the resulting control trajectories. In real systems, actuators such as pumps or valves cannot implement rapid setpoint changes, and microorganisms are sensitive to sudden environmental perturbations. Therefore, generating smooth feeding profiles is not only mathematically desirable but also essential for safe and effective bioprocess operation [16,17].

This work proposes an offline dynamic optimization methodology that uses process kinetics to pre-compute smooth feeding trajectories suitable for implementation in real systems. The focus is on offline optimization due to its lower computational burden and ease of implementation. The core of the methodology is a mathematical model that captures the key dynamics of biomass growth, substrate consumption, and xylitol production. Instead of discretizing the time domain into intervals with constant or linear values, the feeding rates are represented as continuous functions expanded in terms of orthogonal Legendre polynomials. Beyond bioprocesses, Legendre polynomials have been extensively applied in optimal control problems across various fields, including robotics, aerospace trajectory planning, and nonlinear dynamic systems, particularly through pseudospectral methods that exploit their orthogonality and numerical efficiency [18–21]. This orthonormal basis offers several advantages: it ensures smoothness and continuity, reduces the number of optimization parameters required, and allows for straightforward integration into gradient-free optimization frameworks, preventing abrupt variations that could lead to cell stress, inhibition, or even cell death [16].

As an enhancement over previous methods based on Fourier series and orthonormal polynomials [13,22–24], the use of Legendre polynomials reduces the mathematical complexity of the parameterization while preserving its flexibility. This leads to a more efficient formulation of the optimization problem, which can be solved with fewer degrees of freedom and improved numerical stability. In addition, a hybrid optimization algorithm is employed, combining the global exploration capabilities of Monte Carlo sampling with the convergence efficiency of genetic algorithms. This hybrid approach allows for a robust search of the optimal polynomial coefficients that define the feeding profiles.

The implementation of the proposed methodology is carried out in MATLAB® and Simulink®, and its effectiveness is demonstrated through numerical simulations of a fed-batch xylitol production process. The results are compared with a previously published optimal profile from [3], highlighting both the competitiveness of the xylitol yield and the simplicity of the resulting control trajectories. Importantly, the profiles obtained are immediately suitable for real application, as they require no post-processing or interpolation to ensure continuity.

In summary, this work presents a novel strategy for the optimization of substrate feeding in xylitol bioproduction processes. By integrating orthogonal polynomial parameterization with a hybrid optimization algorithm, the proposed approach addresses the key limitations of existing methods, offering an efficient, biologically consistent, and industrially viable solution. In addition, the reduction in the number of optimization parameters improves the robustness of the solution process by decreasing the likelihood of convergence to local optima, a frequent issue in high-dimensional heuristic optimization. Beyond its application to xylitol, the methodology is adaptable to a broad range of biotechnological systems where smooth control trajectories are required. The remainder of the manuscript is organized as follows: Section 2 presents the mathematical model of the xylitol production process. Section 3 introduces the proposed optimization strategy. Section 4 analyzes the simulation results. Finally, Section 5 summarizes the conclusions and outlines potential directions for future work.

2. Process of Mathematical Model

The mathematical model for xylitol production is formulated as a system of six differential equations. Originally proposed by Tochampa et al. [3], the model describes a bioreactor fed with two streams, namely, xylose and glucose, both at a concentration of 200 g/L. The state variables considered are the concentrations of biomass (C_x), xylose

(C_{xyl}), glucose (C_{glc}), extracellular xylitol (C_{xit}^{ex}), and intracellular xylitol (C_{xit}^{in}), as well as the operating volume (V_l):

$$\frac{dC_x}{dt} = -\frac{F_{glc} + F_{xyl}}{V_l} C_x + uC_x \tag{1}$$

$$\frac{dC_{xyl}}{dt} = -\frac{F_{xyl}}{V_l} C_{xyl}^f - \frac{F_{glc} + F_{xyl}}{V_l} C_{xyl} - q_{xyl} C_x \tag{2}$$

$$\frac{dC_{glc}}{dt} = \frac{F_{glc}}{V_l} C_{glc}^f - \frac{F_{glc} + F_{xyl}}{V_l} C_{glc} - q_{glc} C_x \tag{3}$$

$$\frac{dC_{xit}^{ex}}{dt} = -\frac{F_{glc} + F_{xyl}}{V_l} C_{xit}^{ex} - r'_{t,xit} C_x \tag{4}$$

$$\frac{dC_{xit}^{in}}{dt} = (r_{f,xit} - r_{u,xit} - r'_{t,xit})\rho_x - uC_{xit}^{in} \tag{5}$$

$$\frac{dV_l}{dt} = F_{glc} + F_{xyl} \tag{6}$$

where t denotes the time variable [h], defined over the fermentation horizon; F_{glc} and F_{xyl} are the volumetric flow rates of the glucose and xylose feed, respectively; u is the specific growth rate; C_{glc}^f and C_{xyl}^f are the concentrations of glucose and xylose in the feed; q_{xyl} and q_{glc} are the uptake rates of xylose and glucose; $r'_{t,xit}$ is the mass flow rate of xylitol on a dry weight basis; $r_{f,xit}$ is the specific xylitol formation rate; $r_{u,xit}$ is the specific intracellular xylitol consumption rate; and ρ_x is the cell density. Model parameters are listed in Table 1. The specific growth rate (u) depends on the glucose input and the xylitol produced, as shown in the following expression:

$$u = u_{glc}^{max} \frac{C_{glc}}{K_{s,glc} + C_{glc}} + u_{xit}^{max} \frac{C_{xit}^{in}}{K_{s,xit} + C_{xit}^{in}} \frac{K_r}{K_r + C_{glc}} \tag{7}$$

The specific uptake rates of xylose (q_{xyl}) and glucose (q_{glc}) are influenced by competitive inhibition between the substrates.

$$q_{glc} = q_{glc}^{max} \frac{C_{glc}}{K_{s,glc} + C_{glc}(1 + \frac{C_{xyl}}{K_{i,xyl}})} \tag{8}$$

$$q_{xyl} = q_{xyl}^{max} \frac{C_{xyl}}{K_{s,xyl} + C_{xyl}(1 + \frac{C_{glc}}{K_{i,glc}})} \tag{9}$$

The diffusive transport of xylitol from inside the cell to the outside ($r'_{t,xit}$), the specific intracellular formation rate of xylitol ($r_{f,xit}$), and the specific intracellular consumption rate of xylitol ($r_{u,xit}$) are described by

$$r'_{t,xit} = 3.6 \times 10^6 P_{xit} a_{cell} (C_{xit}^{in} - C_{xit}^{ex}) \tag{10}$$

$$r_{f,xit} = \frac{M_{xit}}{M_{xyl}} q_{xyl} \tag{11}$$

$$r_{u,xit} = \frac{u_{xit}}{Y_{x/xit}} \tag{12}$$

To simplify the model, the equation assumes that xylitol is only consumed for cell growth, as its consumption for cell maintenance is insignificant. The state variables' initial conditions for this process are as follows: $V_{l,0}$ = 2.5 L; $C_{x,0}$ = 6 g/L; $C_{gls,0}$ = 0 g/L; $C_{xyl,0}$ = 0 g/L; and $C_{xit,0}$ = 0 g/L. Additionally, the concentrations of glucose (C^f_{glc}) and xylose (C^f_{xyl}) in the feed are 200 g/L each.

Table 1. Description of model parameters.

Symbol	Description	Value	Unitis
u^{max}_{xit}	Max. specific growth rate with respect to xylitol.	0.189	h^{-1}
u^{max}_{glc}	Max. specific growth rate with respect to glucose.	0.662	h^{-1}
$K_{s,glc}$	Monod saturation constant for glucose.	9.998	$g_{gluc}L^{-1}$
$K_{s,xit}$	Monod saturation constant for xylitol.	16.068	$g_{xylitol}L^{-1}$
$K_{s,xyl}$	Monod saturation constant for xylose.	11.761	$g_{xyl}L^{-1}$
K_r	Repression constant for glucose.	0.100	$g_{gluc}L^{-1}$
q^{max}_{glc}	Max. specific uptake rate of glucose.	0.342	$g_{gluc}{}^{-1}h^{-1}$
q^{max}_{xyl}	Max. specific uptake rate of xylose.	3.276	$g_{xyl}{}^{-1}h^{-1}$
$K_{i,glc}$	Inhibition uptake constant of xylose by glucose.	0.100	$g_{gluc}L^{-1}$
$K_{i,xit}$	Inhibition uptake constant of glucose by xylose.	14.780	$g_{xyl}L^{-1}$
P_{xit}	Permeability coefficient of the cell membrane.	7.591×10^9	ms^{-1}
a_{cell}	Specific surface area of the cell.	7.6	m^2g^{-1}
M_{xit}	Molar mass of xylitol.	152	$gmol^{-1}$
M_{xyl}	Molar mass of xylose.	150	$gmol^{-1}$
$Y_{x/xit}$	Biomass yield on xylitol.	0.48	$g_{cell}g_{xylitol}{}^{-1}$

3. Optimization Strategy

The optimization strategy consists of three stages. First, the optimization problem is formulated by defining the objective and system constraints. Then, the control actions are parameterized to ensure a suitable and continuous representation. Finally, the parameters involved in parameterization are optimized to achieve a solution that enhances process performance.

3.1. Optimal Control Problem Statement

The optimal control problem is formulated to determine two control action profiles, the glucose and xylose feeding rates, that maximize xylitol production over a 20 h time horizon (t_f = 20 h). The objective function, constraints, and system dynamics are clearly defined to ensure feasibility and optimality. Specifically, the objective is to find the profiles of $F_{glc}(t)$ and $F_{xyl}(t)$ that maximize the concentration of xylitol at the final reaction time.

$$\max_{F_{glc}(t),\, F_{xyl}(t)} J = \max_{F_{glc}(t),\, F_{xyl}(t)} C^{ex}_{xit}(t_f) \tag{13}$$

This objective is subject to the equality constraints given by the mathematical model of the process (see Equations (1)–(6)), initial conditions (defined in [3]; see Equation (14)), and inequality constraints on the process variables (see Equation (15)).

$$[C_{x,0}; C_{glc,0}; C_{xyl,0}; C_{xit,0}] = [6; 0; 0; 0]\ \mathrm{g/L} \tag{14}$$

$$\begin{aligned} V_{l,0} &= 2.5\,\text{L}, \\ 2.5\,\text{L} \leq V_l(t_f) &\leq 4\,\text{L}, \\ 0\,\text{L/h} \leq F_{\text{glc}} &\leq 0.5\,\text{L/h}, \\ 0\,\text{L/h} \leq F_{\text{xyl}} &\leq 0.5\,\text{L/h}. \end{aligned} \tag{15}$$

3.2. Control Action Parameterization

The technique assumes the existence of an optimal control profile, represented as a function in the Hilbert space $L_2[0, t_f]$, where t_f denotes the known final reaction time. This choice ensures that the control function remains square-integrable, a desirable property in many optimization frameworks [25]. Given that the optimal control profile $F^*(t)$ is assumed to be continuous, it can be approximated using a truncated expansion in a set of orthonormal polynomials adapted to the interval $[0, t_f]$. These polynomials are derived from the classical Legendre basis defined on $[-1, 1]$, and they are mapped to the domain of interest through a change of variable detailed later (Equations (20)–(22)). The resulting approximate control profile is expressed as follows:

$$\tilde{F}(t) = a_0 P_0 + a_1 P_1 + a_2 P_2 + \ldots + a_i P_i + \ldots a_n P_n \tag{16}$$

Here, $\tilde{F}(t)$ is the approximated function, a_i represents the polynomial coefficients, and $P_i(t)$ represents the orthonormal polynomials defined on $[0, t_f]$. Consequently, solving the optimization problem involves determining the coefficients that yield smooth feeding control actions. The control actions for xylitol production are represented by the feeding rates of glucose, $\tilde{F}_{glc}$, and xylose, $\tilde{F}_{xyl}$, which are modeled using a second-(Equation (17)) or third-degree (Equation (18)) polynomial:

$$\tilde{F}_{glc} = c_0 P_0 + c_1 P_1 + c_2 P_2; \tilde{F}_{xyl} = b_0 P_0 + b_1 P_1 + b_2 P_2 \tag{17}$$

$$\tilde{F}_{glc} = c_0 P_0 + c_1 P_1 + c_2 P_2 + c_3 P_3; \tilde{F}_{xyl} = b_0 P_0 + b_1 P_1 + b_2 P_2 + b_3 P_3 \tag{18}$$

By optimizing the coefficients c_i and b_i of the Legendre polynomials, the optimal control vectors $\tilde{F}_{glc}$ and $\tilde{F}_{xyl}$ are obtained, maximizing the objective function (Equation (13)). Consequently, the system achieves optimal control policies.

The control action parameterization strategy is based on Legendre polynomials, a family of orthogonal polynomials that are well behaved within the interval $[-1, 1]$, facilitating the optimization process. These polynomials are redefined to fit the time interval $[0, t_f]$, ensuring their applicability to the problem's temporal domain. One of their key properties is orthogonality [26], meaning that the inner product of two Legendre polynomials of different degrees n and m in L_2 over this interval is zero when $n \neq m$. Since Legendre polynomials form a complete and orthogonal set, any square-integrable function within the interval can be approximated as a weighted sum of these polynomials. This property ensures flexibility in representing control action profiles while maintaining mathematical tractability [27].

Another fundamental property that supports the parameterization of the control action is Rodrigues' formula. This formula provides an explicit expression for generating Legendre polynomials of any degree, offering a systematic way to compute them efficiently [28].

$$Q_n(x) = \frac{1}{2^n n!} \frac{d^n}{dx^n} (x^2 - 1)^n \tag{19}$$

where Q_n are orthogonal polynomials in $L_2[-1, 1]$, and n is their degree [27].

To find an orthogonal basis in $L_2[0, t_f]$, the following transformation is required [27]:

$$x = 2\frac{t}{t_f} - 1 \tag{20}$$

Then,

$$Q_n(x) = Q_n(x(t)) = m_n(t) \tag{21}$$

where m_n are the orthogonal polynomials. Thus, to obtain an orthonormal basis in $L_2[0, t_f]$, the following is defined:

$$P_n = \frac{m_n(t)}{\|m_n(t)\|} \tag{22}$$

In this way, the orthonormal polynomials involved in Equations (17) and (18) are obtained. This transformation ensures that the polynomials remain well conditioned over the desired interval, enhancing numerical stability and computational efficiency.

3.3. Control Action Optimization

This parameter optimization technique aims to maximize the xylitol concentration at the process endpoint by determining the optimal control actions within a dual-substrate feeding strategy. To achieve this, a hybrid approach combining Monte Carlo simulation and a genetic algorithm is implemented to efficiently explore the optimization space. Initially, the Monte Carlo method, a probabilistic technique that relies on extensive random sampling, is employed to generate a diverse population of candidate solutions. Each candidate consists of a specific set of coefficients associated with the Legendre polynomials, which define the smooth substrate feeding profiles over the fermentation period. These candidates, also referred to as individuals, are evaluated by simulating the bioprocess dynamics, and their performance is assessed based on the resulting xylitol concentration at the end of the batch. This initial sampling phase allows for a broad exploration of the solution space, reducing the risk of premature convergence to suboptimal regions. Following this, the genetic algorithm takes over to further refine the most promising individuals. This evolutionary optimization technique imitates natural selection through genetic operations such as selection, crossover, and mutation, enabling the progressive improvement of the feeding profiles over successive generations. The combination of both methods leverages the global search capabilities of Monte Carlo and the local refinement strength of genetic algorithms, yielding high-quality solutions with reduced computational costs and enhanced robustness against local minima. Using a population matrix derived from the Monte Carlo-generated individuals, the genetic algorithm iteratively optimizes the control actions. The hybrid algorithm follows a structured sequence to optimize the control actions $\tilde{F}_{glc}$ and $\tilde{F}_{xyl}$, ensuring smooth profiles suitable for direct application. The steps are as follows:

1. Definition of the Individual and Parameter Scaling: Each individual represents a set of parameters to be optimized, defining the Legendre polynomial coefficients c_i and b_i. These parameters allow for the construction of the control action profiles, which are used to simulate the process and evaluate the objective function J. Each parameter a_i is determined using the following expression:

$$a_i = a_{i,\min} + \delta_i(a_{i,\max} - a_{i,\min}) \tag{23}$$

where δ is a weighting coefficient varying between 0 and 1, and $a_{i,\max}$ and $a_{i,\min}$ represent the upper and lower bounds of the parameter's variation range, respectively. A set of these coefficients uniquely defines each individual. The bounds for the optimization coefficients a_i are not fixed in advance. Instead, they are initially based on the expected range of the control actions and then progressively refined during the exploratory phase of the simulations. As improved solutions tend to cluster within certain value ranges, the bounds are empirically narrowed to focus the search on the most promising regions of the parameter space. This strategy is commonly used in heuristic optimization to enhance convergence efficiency without compromising solution diversity [29].

2. Initial Population Generation: A random initial population of $N = 5000$ individuals is generated using the Monte Carlo method. The objective function of each individual is evaluated based on the process simulation results (Equation (13)).
3. Selection: The best 20 individuals, based on their objective function value J, are selected using an elitist strategy.
4. Crossover: A one-point crossover operator is applied to the selected individuals, combining parameter sets to explore the search space and generate 20 additional individuals.
5. Mutation: By applying small perturbations to selected individuals, 40 new individuals are generated, where one randomly chosen parameter of each individual is modified within its variability range.
6. Exploration Mechanism: To prevent convergence to local extrema, an additional set of 20 randomly generated individuals is introduced in each generation, adapting their distribution based on the algorithm's evolution.

The process is repeated iteratively until convergence is reached or the predefined limit of $L = 50$ generations is met. Convergence is determined when the variation in J becomes minimal, typically before reaching 50 generations. The selection of the hyperparameters N and L follows the methodological criteria established in a previous study [30], where the influence of population size and the number of generations on convergence and solution quality was systematically analyzed. While the specific values used here are adjusted to suit the current case study, the selection process is based on the same reasoning and is therefore not repeated in full. It should be noted that all process constraints defined in Equation (15), including those on feeding rates and final volume, are strictly enforced during the candidate generation stage. These constraints originate from the reference model [3] and are based on the physical limitations of the bioreactor setup and the feeding equipment. In the implementation, a while-loop structure is used to verify the feasibility of each proposed control profile. If any of the constraints are violated, the profile is discarded, and a new one is generated. This ensures that only feasible individuals are passed on to the simulation and evaluation stages and that the optimization process remains confined to the admissible region of the solution space. Figure 1 outlines the steps taken to optimize the process control actions.

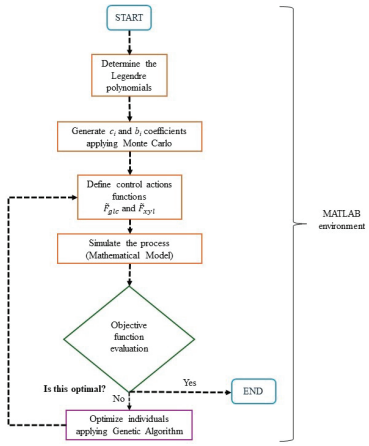

Figure 1. Overview of the optimization techniques implemented.

4. Results and Discussion

This section analyzes an alternative strategy for optimizing xylitol production through the parameterization of two control actions: the glucose and xylose feeding rates. The objective function is defined as the maximization of the xylitol concentration at the end of the process. To ensure a consistent and meaningful comparison, all simulations are carried out under the same operating conditions reported by Tochampa et al. [3]. While their method discretizes the time horizon into multiple intervals and optimizes each segment independently, the present approach employs continuous polynomial functions to represent the control profiles over the entire process duration. Specifically, second- and third-degree polynomials are considered to assess their ability to capture the system dynamics while maintaining a simple mathematical structure. Before introducing the results obtained with the proposed strategy, it is useful to examine in more detail the main limitations of the reference method.

In Tochampa's method, the feeding profiles are obtained through a piecewise constant parameterization optimized using genetic algorithms. While this approach provides flexibility within each time interval, it results in discontinuous control signals with abrupt transitions. These discontinuities require additional signal filtering before implementation in real systems, which introduces distortions and deviations from the original optimized profiles. Consequently, the control actions applied in practice differ from those derived during the optimization stage, leading to suboptimal performance in real applications. Furthermore, this methodology demands the optimization of ten independent parameters per control action, significantly increasing the dimensionality of the search space, the computational cost, and the risk of convergence to local minima. Under these conditions, Tochampa et al. [3] reported a maximum xylitol concentration of 20.06 g/L, which will serve as the benchmark for evaluating the effectiveness of the proposed continuous-parameter strategy.

As previously mentioned, this work explores the use of Legendre polynomials of the second and third degrees to parameterize the glucose and xylose feeding profiles in the xylitol production process. This strategy offers several advantages: it ensures smooth control actions, avoids the need for filtering before implementation in real systems, and reduces the mathematical complexity compared to other functional representations. Moreover, the use of orthogonal polynomials like Legendre allows for a compact and numerically stable formulation. To determine the optimal set of polynomial coefficients, a hybrid algorithm is employed. It combines the global search capabilities of Monte Carlo sampling with the local refinement offered by a genetic algorithm. This two-stage

optimization effectively balances exploration and exploitation, increasing the likelihood of efficiently reaching near-optimal solutions. The evolution of the optimization process is illustrated in Figure 2. Figure 2a shows the distribution of solutions obtained during the Monte Carlo phase, characterized by a broad and random search. Figure 2b reveals how the genetic algorithm progressively improves the objective function, demonstrating its capacity to fine-tune the results. These visualizations highlight the stochastic nature of the initial phase and the convergence trend achieved during the refinement stage.

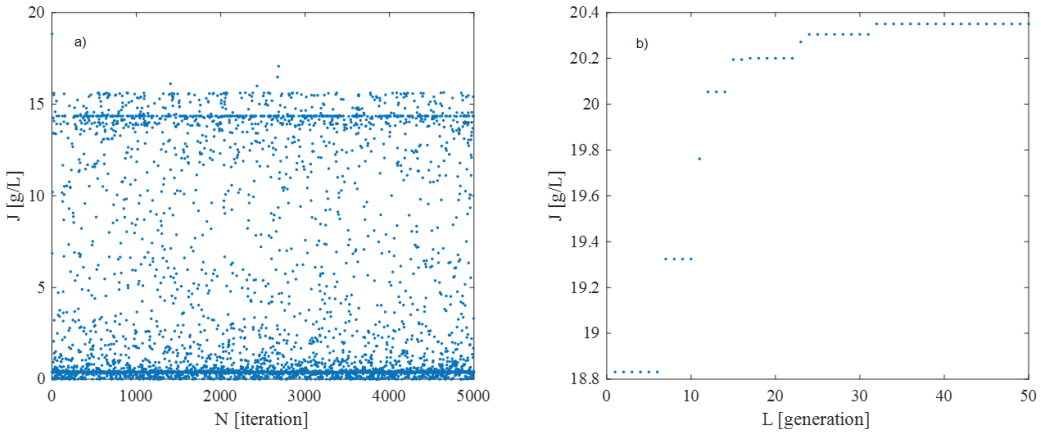

Figure 2. Evolution of the hybrid algorithm. (**a**) Monte Carlo, (**b**) genetic algorithm.

The resulting control profiles for each polynomial degree are represented in Equations (24) and (25), where the final form of the approximating polynomials is shown. The objective function values obtained in each case are 20.26 g/L and 20.35 g/L of xylitol, respectively. Although slight improvements are observed as the polynomial degree increases, the gains are not substantial enough to justify the added complexity and the increased number of parameters (considering the minimal improvement observed with the third-degree polynomials, higher-order expansions were not pursued to avoid overparameterization and to preserve the simplicity and implementability of the feeding profiles in real systems). The second-degree polynomial achieves a xylitol concentration comparable to that of the higher-degree cases and exceeds the 20.06 g/L reported by Tochampa et al. [3]. This suggests that the second-degree approximation strikes an effective balance between simplicity and performance, requiring fewer parameters while preserving smoothness and feasibility for implementation.

$$\tilde{F}_{glc} = 0.059 + 0.009t + 3.4 \times 10^{-4}t^2; \tilde{F}_{xyl} = 0.307 + 0.049t + 0.002t^2 \quad (24)$$

$$\tilde{F}_{glc} = 0.095 + 0.026t + 0.002t^2 + 5.6 \times 10^{-5}t^3; \tilde{F}_{xyl} = 0.26 + 0.005t + 0.009t^2 + 3.8 \times 10^{-4}t^3 \quad (25)$$

These results are further illustrated in Figure 3, which includes the feeding profiles obtained using the proposed methodology, alongside those reported by Tochampa et al. [3] The figure highlights the smoother nature of the proposed profiles, which avoid the abrupt changes and post-optimization filtering required by the piecewise constant strategy. This improvement is reflected in the concentration values and the qualitative behavior of the control profiles. The presence of slope discontinuities in the optimal feeding profiles may appear counterintuitive given the smoothness of Legendre polynomial expansions. However, this behavior is consistent with strategies reported in the literature, where optimal feeding policies often include non-feeding phases to avoid substrate or product inhibition. Such profiles effectively switch between fed-batch and batch operation depending on the system dynamics and constraints [31]. Compared to previous methodologies that use

Fourier series and orthonormal polynomials [13,22–24], this technique achieves equivalent optimization results with a considerably lower mathematical complexity. Figure 4 presents the evolution of the state variables during the process. Although the trajectories vary compared to the reference, the trend remains within the ranges reported in [3], with a smoother system evolution. This behavior is particularly beneficial for preventing microorganism stress, as abrupt changes in the feeding rate can negatively impact growth and metabolite production [16].

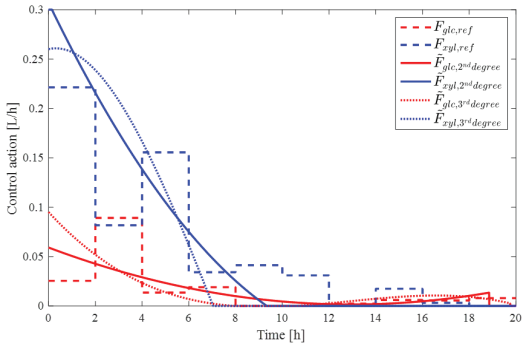

Figure 3. Optimal glucose and xylose feeding profiles.

A key advantage of the proposed methodology is that the resulting feeding profiles can be directly applied in a real system without further modification. In contrast, the stepped profiles used by Tochampa et al. [3] are not physically realizable, since instantaneous changes in feeding rates are impractical due to actuator response limitations. The smoothness of the proposed profiles avoids this issue and makes implementation feasible using standard control hardware. Although the reported increase in the xylitol concentration is modest, such improvements can yield substantial benefits in industrial settings, where improved productivity reduces the consumption of raw materials per unit of product, optimizes reactor utilization, and contributes to the overall profitability of the process.

Furthermore, although a formal robustness analysis is beyond the scope of this work, preliminary simulations indicate that the system is not highly sensitive to small variations in the polynomial coefficients or to minor perturbations in initial conditions. This inherent stability suggests that the proposed approach may retain performance even under realistic process uncertainties, which is particularly relevant in biological systems where exact conditions are difficult to maintain. Together, these results support the use of low-degree Legendre polynomials as a simple and implementation-ready strategy for the open-loop optimization of biological production processes.

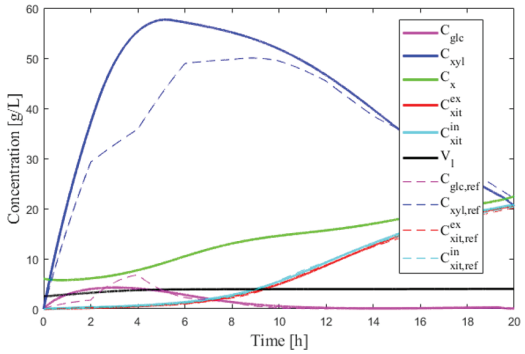

Figure 4. Optimal operation profiles for all state variables.

5. Conclusions

The proposed dynamic optimization strategy, based on low-degree Legendre polynomials, successfully parameterized the glucose and xylose feeding rates in a fed-batch xylitol production process. The resulting control profiles led to a 1.44% increase in the final xylitol concentration, from 20.06 g/L (reference) to 20.35 g/L, using only four parameters per control action. This improvement, though moderate in absolute terms, was achieved with a significantly simplified mathematical structure, resulting in reduced computational costs and enhanced implementation feasibility.

Beyond performance enhancement, the method ensures smooth control actions, avoiding the abrupt variations associated with piecewise constant strategies. This feature is particularly relevant for practical applications, where real systems cannot accommodate discontinuous profiles due to actuator limitations and biological sensitivity. The results confirm that a second-degree polynomial representation offers an effective balance between simplicity and accuracy, fulfilling the initial objective of achieving implementable and efficient optimal control strategies.

Given its compact formulation and favorable numerical properties, the proposed methodology constitutes a promising alternative for the open-loop optimization of nonlinear multivariable bioprocesses. Future work will focus on extending this approach to closed-loop control schemes and evaluating its performance under process uncertainties and experimental conditions.

Author Contributions: Conceptualization, E.G., C.F., M.N., and G.S.; methodology, E.G., C.F., M.N., N.P., and L.R.; software, E.G., C.F., M.N., and N.P.; formal analysis, E.G., C.F., M.N., and G.S.; investigation, E.G., M.N., and G.S.; writing—original draft preparation, E.G., C.F., and M.N.; writing—review and editing, E.G., C.F., M.N., N.P., L.R., and G.S.; supervision, G.S. All authors have read and agreed to the published version of the manuscript.

Funding: This article was financially supported by the National Scientific and Technical Research Council (CONICET) and the Institute of Chemical Engineering, Faculty of Engineering–National University of San Juan (IIQ-FI-UNSJ), Argentina.

Institutional Review Board Statement: Not applicable.

Informed Consent Statement: Not applicable.

Data Availability Statement: The original contributions presented in this study are included in the article. Further inquiries can be directed to the corresponding author.

Acknowledgments: We gratefully acknowledge the support of the National Council of Scientific and Technological Research (CONICET) and the Universidad Nacional de San Juan (UNSJ), whose funding and institutional support made this work possible. Their commitment to fostering research and innovation is fundamental in advancing scientific knowledge and technological development. We also thank the OpenAI AI language model, whose assistance was instrumental in refining the structure and clarity of this manuscript.

Conflicts of Interest: The authors declare no conflicts of interest.

References

1. Gasmi Benahmed, A.; Gasmi, A.; Arshad, M.; Shanaida, M.; Lysiuk, R.; Peana, M.; Pshyk-Titko, I.; Adamiv, S.; Shanaida, Y.; Bjørklund, G. Health benefits of xylitol. *Appl. Microbiol. Biotechnol.* **2020**, *104*, 7225–7237. [CrossRef] [PubMed]
2. de Albuquerque, T.L.; da Silva, I.J., Jr.; de Macedo, G.R.; Rocha, M.V.P. Biotechnological production of xylitol from lignocellulosic wastes: A review. *Process Biochem.* **2014**, *49*, 1779–1789. [CrossRef]
3. Tochampa, W.; Sirisansaneeyakul, S.; Vanichsriratana, W.; Srinophakun, P.; Bakker, H.H.; Wannawilai, S.; Chisti, Y. Optimal control of feeding in fed-batch production of xylitol. *Ind. Eng. Chem. Res.* **2015**, *54*, 1992–2000. [CrossRef]
4. Luus, R. Optimization of fed-batch fermentors by iterative dynamic programming. *Biotechnol. Bioeng.* **1993**, *41*, 599–602. [CrossRef]
5. Park, S.; Fred Ramirez, W. Optimal production of secreted protein in fed-batch reactors. *AIChE J.* **1988**, *34*, 1550–1558. [CrossRef]

6. Setoodeh, P.; Jahanmiri, A.; Eslamloueyan, R. Hybrid neural modeling framework for simulation and optimization of diauxie-involved fed-batch fermentative succinate production. *Chem. Eng. Sci.* **2012**, *81*, 57–76. [CrossRef]
7. Arpornwichanop, A.; Shomchoam, N. Studies on optimal control approach in a fed-batch fermentation. *Korean J. Chem. Eng.* **2007**, *24*, 11–15. [CrossRef]
8. Srinivasan, B.; Palanki, S.; Bonvin, D. Dynamic optimization of batch processes: I. Characterization of the nominal solution. *Comput. Chem. Eng.* **2003**, *27*, 1–26. [CrossRef]
9. Zhang, J. Developing robust neural network models by using both dynamic and static process operating data. *Ind. Eng. Chem. Res.* **2001**, *40*, 234–241. [CrossRef]
10. Luus, R. Application of dynamic programming to differential-algebraic process systems. *Comput. Chem. Eng.* **1993**, *17*, 373–377. [CrossRef]
11. Li, J.; Rhinehart, R.R. Heuristic random optimization. *Comput. Chem. Eng.* **1998**, *22*, 427–444. [CrossRef]
12. Pantano, M.N.; Fernández, M.C.; Amicarelli, A.; Scaglia, G.J. Evolutionary algorithms and orthogonal basis for dynamic optimization in L2 space for batch biodiesel production. *Chem. Eng. Res. Des.* **2022**, *177*, 354–364. [CrossRef]
13. Pantano, M.N.; Fernández, M.; Rodriguez, L.; Scaglia, G.J.E. *Optimización Dinámica Basada en Fourier: Aplicación al Proceso de Producción de Biodiesel*; Revista Iberoamericana de Automática e Informática Industrial: Valencia, Spain, 2020.
14. Banga, J.R.; Balsa-Canto, E.; Moles, C.G.; Alonso, A.A. Dynamic optimization of bioprocesses: Efficient and robust numerical strategies. *J. Biotechnol.* **2005**, *117*, 407–419. [CrossRef]
15. Camacho, E.F.; Bordons, C.; Camacho, E.F.; Bordons, C. *Constrained Model Predictive Control*; Springer: Berlin/Heidelberg, Germany, 2007.
16. Weegman, B.P.; Essawy, A.; Nash, P.; Carlson, A.L.; Voltzke, K.J.; Geng, Z.; Jahani, M.; Becker, B.B.; Papas, K.K.; Firpo, M.T. Nutrient regulation by continuous feeding for large-scale expansion of mammalian cells in spheroids. *J. Vis. Exp. JoVE* **2016**, 52224. [CrossRef]
17. Lee, S.J.; Song, H.; Lee, S.Y. Genome-based metabolic engineering of Mannheimia succiniciproducens for succinic acid production. *Appl. Environ. Microbiol.* **2006**, *72*, 1939–1948. [CrossRef] [PubMed]
18. Elnagar, G.N.; Kazemi, M.A.; Razzaghi, M. The pseudospectral Legendre method for discretizing optimal control problems. *IEEE Trans. Autom. Control* **1995**, *40*, 1793–1796. [CrossRef]
19. Gong, Q.; Fahroo, F.; Ross, I.M. A pseudospectral method for the optimal control of constrained feedback linearizable systems. *IEEE Trans. Autom. Control* **2006**, *51*, 1115–1129. [CrossRef]
20. Ross, I.M.; Fahroo, F. Pseudospectral methods for optimal motion planning of differentially flat systems. In Proceedings of the Proceedings of the 41st IEEE Conference on Decision and Control, Las Vegas, NV, USA, 10–13 December 2002; pp. 1135–1140. [CrossRef]
21. Trefethen, L.N. *Spectral Methods in MATLAB*; SIAM: Philadelphia, PA, USA, 2000. [CrossRef]
22. Pantano, M.N.; Fernández, M.C.; Ortiz, O.A.; Scaglia, G.J.; Vega, J.R. A Fourier-based control vector parameterization for the optimization of nonlinear dynamic processes with a finite terminal time. *Comput. Chem. Eng.* **2020**, *134*, 106721. [CrossRef]
23. Pantano, M.N.; Puchol, M.C.F.; Rossomando, F.G.; Scaglia, G.J. Open-Loop Dynamic Optimization for Nonlinear Multi-Input Systems. Application to Recombinant Protein Production. *IEEE Lat. Am. Trans.* **2021**, *19*, 1307–1314. [CrossRef]
24. Fernández, C.; Pantano, N.; Groff, C.; Gil, R.; Scaglia, G. Bioethanol production optimization by direct numerical methods and evolutionary algorithms. *IEEE Lat. Am. Trans.* **2024**, *22*, 259–265. [CrossRef]
25. Ito, K. Functional Analysis and Optimization. Lecture Monograph. 2016. Available online: https://kito.wordpress.ncsu.edu/files/2020/07/funa3-2.pdf (accessed on 30 March 2025).
26. Ramírez Rincón, W.A. Elementos de Polinomio de Legendre. Bachelor's Thesis, Universidad de Pamplona, Norte de Santander, Colombia, 2017.
27. Kreyszig, E. *Introductory Functional Analysis with Applications*; John Wiley & Sons: Hoboken, NJ, USA, 1991; Volume 17.
28. Arfken, G.B.; Weber, H.J. *Mathematical Methods for Physicists*, 6th ed.; Arfken, G.B., Weber, H.J., Eds.; Elsevier: Amsterdam, The Netherlands; Boston, MA, USA, 2005.
29. Kennedy, J.; Eberhart, R.C. A discrete binary version of the particle swarm algorithm. In Proceedings of the 1997 IEEE International Conference on Systems, Man, and Cybernetics, Computational Cybernetics and Simulation, Orlando, FL, USA, 12–15 October 1997; Volume 5, pp. 4104–4108.
30. Fernández, C.; Pantano, N.; Godoy, S.; Serrano, E.; Scaglia, G. Optimización de parámetros utilizando los métodos de Monte Carlo y Algoritmos Evolutivos. Aplicación a un controlador de seguimiento de trayectoria en sistemas no lineales. *Rev. Iberoam. Autom. Inform. Ind.* **2019**, *16*, 89–99. [CrossRef]
31. Hong, J. Optimal substrate feeding policy for a fed batch fermentation with substrate and product inhibition kinetics. *Biotechnol. Bioeng.* **1986**, *28*, 1421–1431. [CrossRef]

fermentation

MDPI

Article

Assessment of Alternative Media Viability for Cell Growth Phase in the Lab-Scale Xanthan Pruni Production—Part I

Isabel Santos Pedone [1], Fabíola Insaurriaga Aquino [1], Eduardo dos Santos Macedo Costa [2], Karine Laste Macagnan [2], Jéssica da Rosa Porto [3], Anderson Schwingel Ribeiro [3], Mariane Igansi Alves [1], Claire Tondo Vendruscolo [4] and Angelita da Silveira Moreira [1,2,*]

[1] Department of Agroindustrial Science and Technology, Federal University of Pelotas, Capão do Leão 96010-900, Brazil; isabeltecalimentos@gmail.com (I.S.P.); fabiolaiaquino@gmail.com (F.I.A.); marianeigansialves@hotmail.com (M.I.A.)
[2] Technological Development Center, Biotechnology Center, Federal University of Pelotas, Capão do Leão 96010-900, Brazil; eduardodossantosmacedocosta@gmail.com (E.d.S.M.C.); karinemacagnan@hotmail.com (K.L.M.)
[3] Program in Chemistry, Chemical Metrology Laboratory (LabMeQui), Federal University of Pelotas, Capão do Leão 96010-900, Brazil; jporto8.jp@gmail.com (J.d.R.P.); andersonsch@hotmail.com (A.S.R.)
[4] Biopolix Tecnological Materials, Ribeirão Preto 14056-680, Brazil; clairevendruscolo@gmail.com
* Correspondence: angelitadasilveiramoreira@gmail.com; Tel.: +55-(53)-981193979

Abstract: Xanthan is a highly relevant commercial microbial biopolymer. Its production occurs in two steps: the bacterium is cultivated in a nitrogen-rich medium for cell multiplication, and the obtained biomass is used as an inoculum for the polymer production phase. Different media compositions for cell growth were investigated, seeking to reduce or replace the peptone used in the standard medium. Peptone (P), yeast extract (YE), and rice parboiling water (RPW) concentration combinations were tested in cultivating *Xanthomonas arboricola* pv. pruni 101. A CRD 2^3 design, performed in a shaker, was used to assess the effects of independent variables on xanthan pruni microbial growth, N consumption, yield, viscosity, pseudoplasticity, and xanthan mineral content. After 24 h an increase in N was observed, without any significant impact on cell growth. Xanthan yield increased as a result of the alternative treatments, with P and YE influencing positively. However, T1, with the lowest levels of P, YE, and RPW increased viscosity and pseudoplasticity of xanthan pruni. RPW increased phosphorus, silicon, calcium, and magnesium, and P and YE increased potassium. These results indicate that partial replacement of P by RPW and YE is an economically viable and sustainable approach for the xanthan pruni production.

Keywords: *Xanthomonas*; alternative medium; rice parboilization water; cell growth; xanthan gum

1. Introduction

The properties of natural polymers such as biocompatibility, biodegradability, and renewability are attracting growing attention to these products. Among these polymers, xanthan, an extracellular biopolymer produced by bacteria of the *Xanthomonas* gender is highlighted. Due to its rheological and structural properties, xanthan is widely employed in the food, pharmaceutical, cosmetic, paintings, and petroleum industries [1]. The global demand for this product is registering constant growth. According to Global Market Insights, the xanthan gum market could reach USD 1.2b by 2030, at a composite annual

growth rate (CAGR) of 5.71%. Brazil also exhibits impressive consumption, attaining 30 thousand tons a year, supplied exclusively by international industries [2,3].

For the *Xanthomonas* cultivation and production, carbon sources are used as substrates, while sources of nitrogen and minerals are employed as nutrients [4]. The high costs associated with substrates constitute a process limitation. To minimize such costs, agro-industrial wastes are being studied as alternative substrate sources, such as water obtained from oil production [5], pineapple wastes [6], rice hulls [7], rice hulls [8], beet molasses [9], bread wastes [10], orange peels [11], and wine industry waste [12]. The development of sustainable, low-cost solutions for obtaining xanthan can significantly increase market opportunities [6].

Rice (*Oryza sativa* L.) is one of the most consumed staple foods, parboiled rice being one of its most consumed forms in Brazil. The rice parboiling process involves a hydrothermal treatment in which the hulled grain is immersed in drinking water to soak at temperatures above 58 °C, followed by partial or total gelatinization and further drying [13]. In the rice parboiling process, the grain's outer mineral layers, especially in the bran and aleurone layer, migrate towards the interior of the grain, and a portion of these RPW minerals are primarily determined by process parameters temperature, time, and operating conditions [14]. At the end of the process, the wastewater generated, containing high phosphorus and nitrogen, causes high biochemical oxygen demand, requiring suitable treatment before disposal. The composition of this nutrient-rich water represents a significant challenge for the rice industries, especially in view of the complexity of phosphorus and nitrogen management, which can cause environmental harm if not duly mitigated [15,16].

Until now, no strategies have been identified aiming at redirecting RPW waste to other industries, adding value to another product. RPW study was pioneered by our research group in the *X. arboricola* pv. pruni *(ex X. campestris* pv. pruni) production phase for obtaining xanthan, directly influencing the characteristics of the obtained gum [17]. Besides minimizing the environmental impacts, the use of this waste as substrate could contribute to xanthan cost reduction, making viable domestic production. Investment in xanthan domestic production brings economic benefits, such as a reduction in dependence on imports and job creation, in addition to promoting environmental sustainability by reducing impact through the use of industrial effluents as substrate [4]. Therefore, the scientific and technological advancement in xanthan production in Brazil is crucial for the development of this industry in our country, rendering it competitive in the global biopolymers market.

Xanthan pruni, a polymer analogous to xanthan and produced by *X. arboricola* pv. pruni, differs from commercial xanthan in its chemical composition. Studies have demonstrated that xanthan pruni contains rhamnose in its structure, likely incorporated in the side chains, which distinguishes it from conventional xanthan [18]. Studies on *X. arboricola* pv. pruni remain limited, and there is a lack of information regarding the impact of various alternative media on the production of xanthan pruni. Perez et al. (2020) [19] evaluated the supplementation of the medium with yeast extracts and observed a significant increase in biopolymer production. In the study by Moreira (2023) [20], culture media containing different minerals were used to produce xanthan pruni. Among the components, the use of RPW stood out, as well as carbon sources such as sucrose and cellulose, and nitrogen sources such as peptone and mineral salts. Given the scarcity of studies addressing different medium formulations to produce xanthan pruni, this work aims to contribute to the advancement of this topic by evaluating the feasibility of using alternative nutrient sources and their impacts on the production and characteristics of the biopolymer.

The aim of this study was to investigate the effects of rice parboiling water (RPW) use combined with peptone and yeast extract as N sources in culture media for *Xanthomonas arboricola* pv. pruni cell growth (the 101 strain being used as a model) and the production of its biopolymer, referred to in this study as xanthan pruni. The viability of these alternative media was examined by comparing cell growth, xanthan pruni yield, and its rheological properties with those obtained from conventional culture media. Besides, the main compounds present in parboiling water were identified to check if they influence xanthan synthesis. This is meant to contribute to the development of more sustainable, economically viable processes, by exploring alternative sources of substrates and assessing the effectiveness of different culture media components.

2. Materials and Methods

2.1. Rice Parboiling Wastewater Characterization

RPW was collected from the Nelson Wendt company in Pelotas, RS, Brazil, from the outlet tube during the discharge process into the effluent collection tank. The rice immersed in the tanks was a varietal mixture (2022 harvest). After collection, RPW samples were stored in plastic bottles and frozen at −18 °C for further characterization and utilization. The pH value [21], reducing sugars [22], and nitrogen content (Urea kit CE ref. 27—Labtest®, Delta, BC, Canada) were determined. Mineral characterization was performed with the aid of a MIP OES (Agilent Technologies, model Agilent 4200, Melbourne, Australia) spectrometer [23] (Table 1).

Table 1. Rice parboiling process wastewater characterization.

Parameters	
pH	4.6 ± 0.2
Reducing Sugars	3.40 ± 0.16
Nitrogen (mg/dL)	140.00 ± 1.12
Phosphorus (mg/L)	304.96 ± 9.90
Zinc (mg/L)	1.53 ± 0.05
Iron (mg/L)	9.36 ± 0.33
Silicon (mg/L)	39.43 ± 10.26
Calcium (mg/L)	32.80 ± 0.41
Potassium (mg/L)	4411.96 ± 196.21
Magnesium (mg/L)	169.23 ± 8.37
Manganese (mg/L)	43.17 ± 1.37
Sodium (mg/L)	21.86 ± 1.88

2.2. Inoculum Preparation

The *X. arboricola* pv. pruni 101 bacterium was kept in agar SPA [24] and cultivated in a liquid medium with different peptone (Himedia®, Kennett Square, PA, USA) concentrations, yeast extract (Procelys by Lesaffre®, Marcq-en-Barœul, France), and RPW, according to a central composite design 2^3 [24]. Factors were codified in three levels: low (−1), medium (0), and high (+1), with the central point representing the repetitions [25] (Table 2).

All the treatments were diluted in a solution of (g/L): 20 sucrose, 0.5 dibasic potassium phosphate, and 0.25 heptahydrate magnesium sulfate (Synth®, Diadema, Brazil). SPA standard medium [24] was utilized as a positive control, the composition of which is in (g/L): 5 of peptone, added to the previous solution. Cultivation was conducted in a 250 mL Erlenmeyer flask containing 40 mL of cultivation medium and 10 mL of bacterium suspension (9.14 UFC/mL), in SPA medium, incubated at 28 °C, 150 rpm for 24 h in an orbital shaker (B. Braun Biotech, Certomat BS-1, Melsungen, Germany). Initial and final

bacterial concentrations were assessed by means of serial dilutions and plating in agar SPA medium, the colonies counting being expressed in UFC/mL.

Table 2. Matrix of the complete factorial design 2^3, with 3 central points for defining the peptone, yeast extract, and RPW concentrations for *X. arboricola* pv. pruni 101 inocula production.

Treat.	Codified Levels			Real Levels		
	x1	**x2**	**x3**	**x1**	**x2**	**x3**
1	−1	−1	−1	1	1	20
2	+1	−1	−1	5	1	20
3	−1	+1	−1	1	5	20
4	+1	+1	−1	5	5	20
5	−1	−1	+1	1	1	80
6	+1	−1	+1	5	1	80
7	−1	+1	+1	1	5	80
8	+1	+1	+1	5	5	80
9	0	0	0	3	3	50
10	0	0	0	3	3	50
11	0	0	0	3	3	50

x1 = peptone (g/L), x2 = yeast extract (g/L), and x3 = RPW (%); Treat. = treatment.

2.3. Xanthan Pruni Production

The bioprocess occurred in 250 mL Erlenmeyers flasks containing 45 mL of MPII production medium [17] and 5 mL inoculum (Section 2.2) in an orbital shaker (B. Braun Biotech, Certomat BS-1, Melsungen, Germany) at 28 °C and 200 rpm for 72 h. Biopolymer recovery was performed with ethyl alcohol 96° GL (4:1 v/v), followed by oven-drying (CE-220-81, Cielenlab, Campinas, Brazil) at 56 °C to constant weight. The yield was determined by gravimetry and expressed in g/L.

2.4. Nitrogen

Residual nitrogen content (mg/L) was quantified in two steps with the aid of the Urea Kit CE (Labtest®, Richmond, BC, Canada, ref. 27). Broth samples were collected at the 0 and 24 h times, centrifuged at 10,000 rpm x for 10 min at 4 °C in a refrigerated centrifuge (Electron Corporation®, Sorvall-Thermo, EUA, Tokyo, Japan). The supernatant was analyzed in a UV-Vis spectrophotometer (Shimadzu, UV-1900i, Kyoto, Japan) at 500 nm. Nitrogen content calculation followed the standard method (urea 70 mg/L and sodium azide 7.7 mmol/L), according to Equation (1):

$$\text{Residual Nitrogen } (\text{mg/L}) = \frac{Absorbance\ of\ Sample}{Absorbance\ of\ Standard} \times 70 \times 10 \quad (1)$$

2.5. Viscosity

Rheological properties of xanthan aqueous solutions were assessed with the aid of a rheometer (RheoStress 600, model RS150, Haake®, Vreden, Germany). 1% (m/v) Xanthan aqueous solutions were prepared, agitated for 2 h, and stored at 4 °C for 24 h. Rheometric analysis was performed at 25 °C, with a cone and plate geometry (C60/2° Ti sensor; 0.105 mm interval).

2.6. Minerals

Mineral analysis was performed according to the method described by Rosa et al. (2016) [26]. At first, xanthan gum samples were treated by acidic digestion with the aid of an open system in a digesting block. Approximately 100 mg of the samples were weighed

and transferred to glass digesting tubes, to which 5 mL of concentrated nitric acid (HNO_3) was added. The mixture was heated in a digester at 220 °C under reflux for 3 h. The resulting solutions were diluted in ultrapure water and analyzed in triplicate with the aid of a microwave-induced plasma optical emission spectrometer (MIP OES) (Agilent Technologies, model Agilent 4200, Mulgrave, Australia).

2.7. Statistics

Experiments were performed in triplicate, and the results were expressed in averages and standard deviations. A *t*-test was performed to observe significance at the $p \leq 0.05$ level using RStudio software (2023.06.2+524). The effects of independent variables were determined using ANOVA with Statistica 10.0® software, with $p \leq 0.05$ considered significant.

3. Results and Discussion

3.1. Cell Growth

X. arboricola pv. pruni cell concentration in the examined alternative cell growth media and in standard SPA medium is listed in Table 3. In spite of the fact that the results show significant variations statistically in cell growth among the treatments and the SPA medium as seen by the *t*-test, the differences are relatively small. The SPA medium led to a 10.04 UFC/mL cell concentration, while in the remaining treatments, the concentration varied between 9.69 and 9.98 UFC/mL.

Table 3. *X. arboricola* pv. pruni strain 101 cell growth in media containing different peptone, yeast extract, and RPW concentrations.

Treat.	x1	x2	x3	Cell Growth (UFC/mL)
1	−1 (1)	−1 (1)	−1 (20)	9.93 ± 0.01 *
2	+1 (5)	−1 (1)	−1 (20)	9.87 ± 0.04 *
3	−1 (1)	+1 (5)	−1 (20)	9.94 ± 0.04 *
4	+1 (5)	+1 (5)	−1 (20)	9.98 ± 0.04 *
5	−1 (1)	−1 (1)	+1 (80)	9.92 ± 0.04 *
6	+1 (5)	−1 (1)	+1 (80)	9.69 ± 0.01 *
7	−1 (1)	+1 (5)	+1 (80)	9.83 ± 0.01 *
8	+1 (5)	+1 (5)	+1 (80)	9.81 ± 0.01 *
9	0 (3)	0 (3)	0 (50)	9.85 ± 0.03 *
10	0 (3)	0 (3)	0 (50)	9.78 ± 0.01 *
11	0 (3)	0 (3)	0 (50)	9.82 ± 0.01 *
SPA	5	-	-	10.04 ± 0.01

x1 = peptone (g/L), x2 = yeast extract ($g \cdot L^{-1}$), and x3 = RPW (%). Samples' asterisks (*) point to significant differences as compared to the standard ($p < 0.05$), according to the *t*-test.

Treatment 6, with 80% (v/v) RPW, led to a slightly lower result (9.69 ± 0.01 UFC/mL) as compared to treatments containing 20% (v/v) RPW (9.87 to 9.98 ± 0.04 UFC/mL). The results illustrated in Figure 1 evidence this trend. The negative signal of the RPW coefficient means that cell growth increased with a reduction in the mentioned parameter value, which may be associated with inhibitory compounds or high mineral levels in the water, especially silicon [14]. This phenomenon suggests that increased RPW concentration can have an inhibitory effect on *X. arboricola* pv. pruni growth.

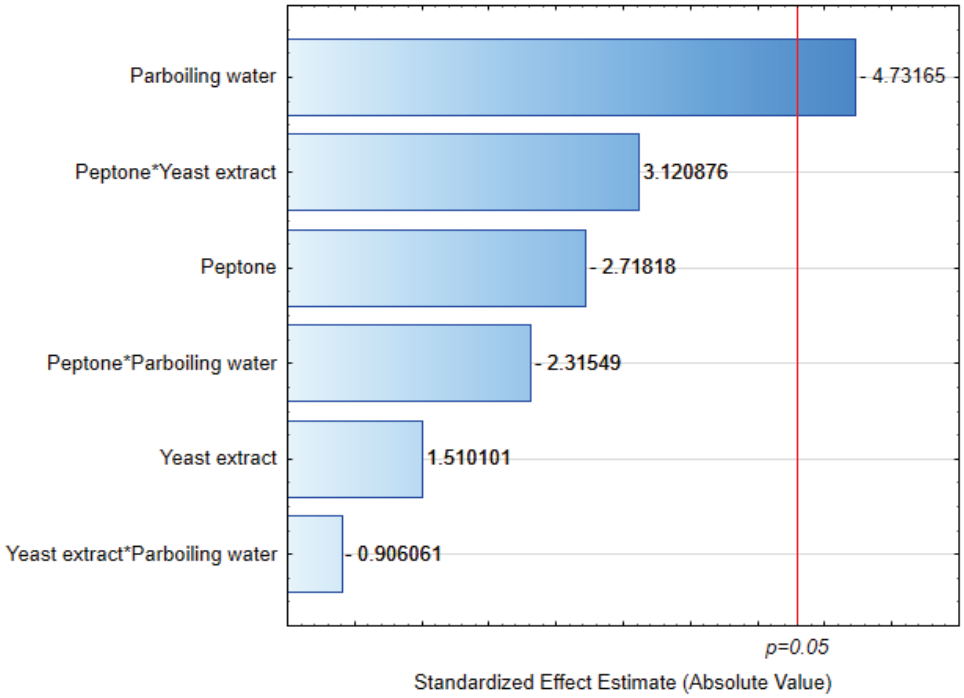

Figure 1. Effects of the independent variables (peptone, yeast extract, and RPW) on cell growth. Asterisks (*) represents interactions between variables.

3.2. Yield

Xanthan yield varied among treatments, with values between 7.0 and 8.9 g/L, while the standard SPA medium exhibited a yield of 6.8 g/L (Table 4). Exception made to treatment 5, all the remaining treatments resulted in significantly higher yields than those of the SPA standard medium. From a comparison among cell growth results, it can be seen that in this case, the cell concentration in the examined range was not a determining factor for yield. This suggests that although the SPA medium results in higher bacterial growth (Table 3), other factors related to medium composition, such as Fe, Zn, and Mn micromineral concentrations, could play an important role in yield increase.

Table 4. Yield of xanthan produced by *X. arboricola* pv. pruni strain 101 in media containing different peptone, yeast extract, and RPW concentrations.

Treat.	x1	x2	x3	Yield (g/L)
1	−1 (1)	−1 (1)	−1(20)	7.233 ± 0.20 *
2	+1 (5)	−1 (1)	−1 (20)	7.393 ± 0.42 *
3	−1 (1)	+1 (5)	−1 (20)	7.123 ± 0.51 *
4	+1 (5)	+1 (5)	−1 (20)	7.333 ± 0.22 *
5	−1 (1)	−1 (1)	+1 (80)	7.020 ± 0.32
6	+1 (5)	−1 (1)	+1 (80)	7.533 ± 0.26 *
7	−1 (1)	+1 (5)	+1 (80)	7.343 ± 0.35 *
8	+1 (5)	+1 (5)	+1 (80)	8.943 ± 0.63 *
9	0 (3)	0 (3)	0 (50)	7.610 ± 0.46 *
10	0 (3)	0 (3)	0 (50)	7.683 ± 0.40 *
11	0 (3)	0 (3)	0 (50)	7.393 ± 0.73 *
SPA	5	-	-	6.770 ± 0.65

x1 = peptone (g/L), x2 = yeast extract (g/L), and x3 = RPW (%). Asterisks (*) on the samples point to significant differences as compared to the standard ($p < 0.05$), according to the *t*-test.

The nitrogen source plays an essential role in the growth and production of xanthans by bacteria of the *Xanthomonas* gender [27]. According to the Pareto plot for xanthan yield (Figure 2), peptone was the most influential independent variable in the observed response, followed by yeast extract and RPW, in addition to the isolated RPW effect and the peptone–RPW combination. These results point out that peptone and yeast extract, when used by themselves, are able to provide good yields. However, RPW supplementation can render the cultivation medium still more efficient.

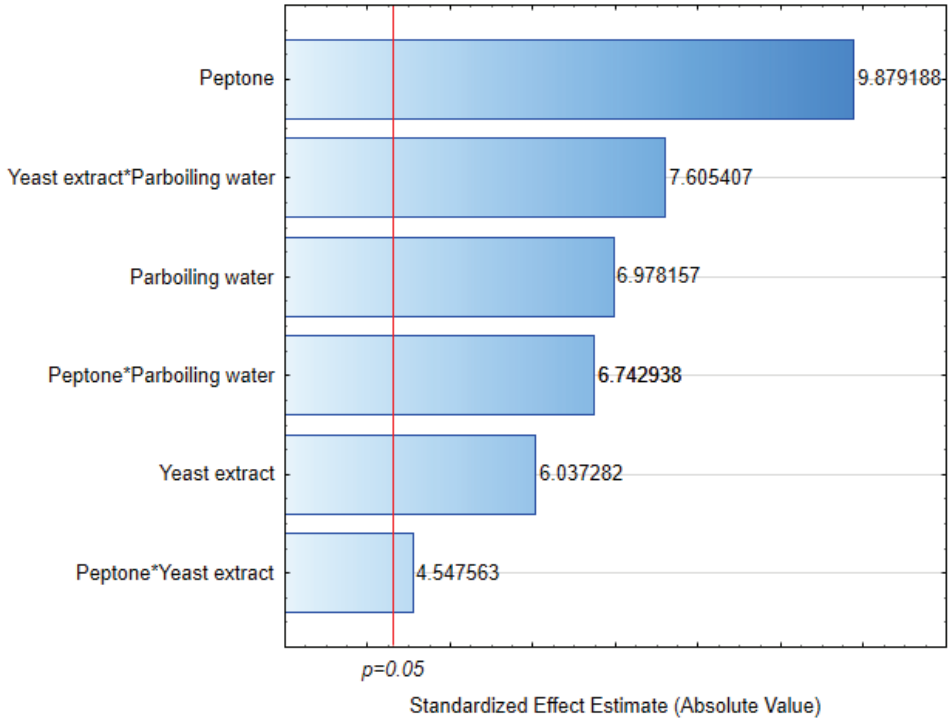

Figure 2. Effect of independent variables (peptone, yeast extract, and RPW) on yield. Asterisks (*) represents interactions between variables.

Previous studies already demonstrated the importance of organic nitrogen sources in xanthan production. Kurbanolgu and Kurbanolgu (2007) and Caegnatto et al. (2011) [28,29] highlighted that peptone and yeast extract provide soluble amino acids and minerals essential to the cultivation medium, creating favorable conditions for biopolymer synthesis. Ozdal and Kurbanolgu (2019) [9] reported a significant increase in xanthan production by using peptones extracted from hens' feathers, reaching yields in excess of 24 g/L in a shaker at 200 rpm.

In spite of the positive impact of yeast extract, yields observed (4.02 to 4.18 g/L) were lower than those obtained in this study, suggesting that yeast extract per se may be not as efficient as when combined with other components, such as peptone and RPW. Da Silva et al. (2018) [30] also utilized agro-industrial wastes such as coconut and cocoa peel, reaching values of 3.89 to 4.48 g/L. In the present study, the use of RPW as an alternative source provided yields higher than those reported in these papers, indicating that this agro-industrial waste can be a viable alternative for optimizing xanthan production.

Demirci et al. (2019) [10] obtained a superior yield (14.3 g/L) by utilizing disposed bread waste; however, the hypothesis of an inflated yield cannot be discarded in view of the presence of starch. Trivunović et al. (2024) [12] reached yields between 4 and 10 g/L by utilizing rosé wine wastewater. Yield variations can be explained by differences in substrate composition and adopted fermentation conditions. Similar yields obtained from

treatments tested in this study reinforce the viability of partial replacement of conventional medium components for RPW, peptone, and yeast extract, without compromising xanthan productivity. This finding is relevant for process scalability since it enables using agro-industrial wastes as sustainable, economically viable alternatives while maintaining a competitive performance as compared with conventional substrates.

3.3. Residual Nitrogen

Nitrogen contents measured in initial time (0 h) varied between 4.52 and 12.21 mg/dL, suggesting that culture medium composition was directly influenced by peptone, yield extract, and RPW concentrations (Table 5).

Table 5. Residual nitrogen in media containing different peptone, yield extract, and RPW concentrations at 0 and 24 h *X. arboricola* pv. pruni strain 101 cell growth.

Treat.	x1	x2	x3	Residual Nitrogen 0 h (mg/L)	Residual Nitrogen 24 h (mg/L)
1	−1 (1)	−1 (1)	−1(20)	45.2 ± 1.3 *	102.8 ± 8.6 *
2	+1 (5)	−1 (1)	−1 (20)	78.2 ± 1.9 *	280.4 ± 4.5 *
3	−1 (1)	+1 (5)	−1 (20)	81.3 ± 3.2	236.9 ± 6.1 *
4	+1 (5)	+1 (5)	−1 (20)	94.4 ± 2.8 *	449.9 ± 4.6 *
5	−1 (1)	−1 (1)	+1 (80)	48.1 ± 2.5 *	108.2 ± 8.5 *
6	+1 (5)	−1 (1)	+1 (80)	85.7 ± 1.9 *	374.0 ± 6.1
7	−1 (1)	+1 (5)	+1 (80)	82.1 ± 2.5 *	286.4 ± 7.5 *
8	+1 (5)	+1 (5)	+1 (80)	122.1 ± 9.0 *	433.9 ± 8.6 *
9	0 (3)	0 (3)	0 (50)	82.9 ± 1.6	349.4 ± 3.2 *
10	0 (3)	0 (3)	0 (50)	90.5 ± 1.9 *	336.3 ± 5.5 *
11	0 (3)	0 (3)	0 (50)	89.7 ± 0.9	359.9 ± 9.3 *
SPA	5	-	-	91.8 ± 0.6	376.4 ± 1.8

x1 = peptone (g/L), x2 = yield extract (g/L), and x3 = RPW (%). Asterisks (*) on the samples point to significant differences as compared to the standard ($p < 0.05$), according to the *t*-test.

After 24 h, a significant increase in nitrogen concentrations was observed, reaching values between 102.8 and 449.9 mg/L. This behavior was consistent for all treatments, with the highest increases being observed for those containing higher peptone and yeast extract concentrations. For example, for treatment 4 (+1 peptone and +1 yeast extract), nitrogen concentration increased from 9.44 to 44.99 mg/dL, while for treatment 8 (having the same peptone and yeast extract, but higher RPW percentage), the increase was from 12.21 to 43.99 mg/dL. Such an increase after 24 h cultivation was also observed by Macagnan et al. (2021) [31] when studying the influence of different yeast extracts on *X. arboricola* pv. pruni strain 101 cell growth.

The cause of nitrogen increase was not completely revealed, but it is suggested that the *X. arboricola* bacterium can be involved in a process of atmospheric nitrogen fixation [32]. Alternatively, gradual nitrogen release from the degradation of compounds present in peptone and in yeast extract may have contributed to the observed increase. Further studies are required to confirm possible nitrogen fixation and identify the mechanisms at the origin of this phenomenon.

As regards the effects of independent variables, peptone exhibited a positive relationship with initial nitrogen content (Figure 3). At higher concentration (+1, corresponding to 5 g/L), nitrogen contents were significantly higher, as could be observed from treatments 4 (9.44 mg/dL) and 8 (12.21 mg/dL), nitrogen values at 0 h were consistently higher, as in treatments 3 (8.13 mg/dL) and 7 (8.21 mg/dL).

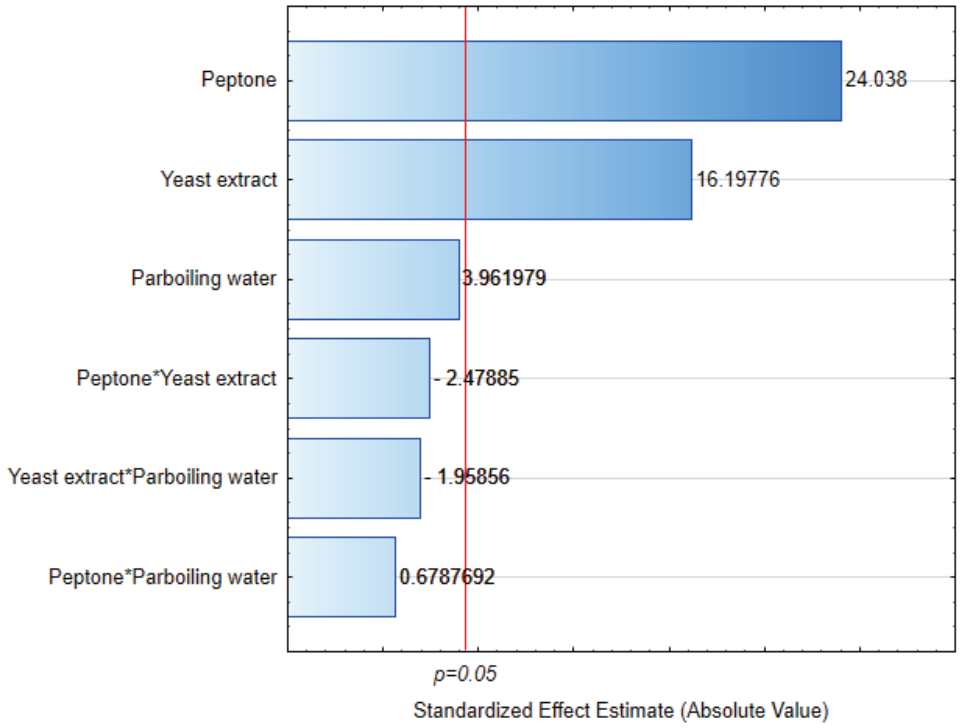

Figure 3. Effect of the independent variables (peptone, yeast extract, and RPW) on residual nitrogen. Asterisks (*) represents interactions between variables.

3.4. Viscosity

The rheological properties of xanthan were described by the Ostwald–de Waele model using *K* and η parameters, with a determination coefficient (R^2) of 0.99 (Table 6). The consistency index (*K*), which translates the resistance to fluid flow, varied from 4.874 to 0.205 for treatments 1 and 4, respectively. The flow behavior index (η) varied from 0.605 and 0.181, indicating the relationship between shear rate and viscosity. A value of (η) below 1 ($\eta < 1$) confirms the pseudoplastic behavior [1].

Table 6. *X. arboricola* pv. pruni strain 101 rheological parameters obtained from different RPW, peptone, and yeast extract concentrations.

Treat.	x1	x2	x3	Consistency (*K*)	Flow behavior (η)
1	−1 (1)	−1 (1)	−1(20)	4.874 ± 0.051 *	0.181 ± 0.004 *
2	+1 (5)	−1 (1)	−1 (20)	1.549 ± 0.018 *	0.308 ± 0.006
3	−1 (1)	+1 (5)	−1 (20)	1.702 ± 0.011 *	0.361 ± 0.000 *
4	+1 (5)	+1 (5)	−1 (20)	0.205 ± 0.002 *	0.605 ± 0.000 *
5	−1 (1)	−1 (1)	+1 (80)	2.102 ± 0.099 *	0.291 ± 0.013
6	+1 (5)	−1 (1)	+1 (80)	0.798 ± 0.024 *	0.436 ± 0.004 *
7	−1 (1)	+1 (5)	+1 (80)	0.737 ± 0.004 *	0.461 ± 0.005 *
8	+1 (5)	+1 (5)	+1 (80)	0.290 ± 0.002 *	0.590 ± 0.019 *
9	0 (3)	0 (3)	0 (50)	0.853 ± 0.018 *	0.417 ± 0.000 *
10	0 (3)	0 (3)	0 (50)	1.816 ± 0.027 *	0.337 ± 0.009 *
11	0 (3)	0 (3)	0 (50)	0.989 ± 0.071 *	0.402 ± 0.015 *
SPA	5	-	-	2.399 ± 0.066	0.298 ± 0.007

x1 = peptone (g/L), x2 = yeast extract (g/L), and x3 = RPW (%). Asterisks (*) on the samples point to significant differences as compared to the standard ($p < 0.05$), according to the *t*-test.

Treatments obtained from different RPW, peptone, and yeast extract concentrations enabled us to obtain xanthan products having different properties. For treatment 1, with the lower peptone concentrations, yeast extract, and RPW, the consistency index (*K*) was the highest, 4.874, pointing to high viscosity, while the flow behavior index (η) was the lowest,

0.181, featuring a more accentuated pseudoplastic behavior. High viscosity provides better water retention capacity, which contributes to higher stability and improvement in food texture for the food industry. On the other hand, for treatment 4, with high peptone (5 g/L) and yeast extract (5 g/L) concentrations, the consistency index (K) was the lowest, at only 0.205, and the flow behavior index (η) was the highest, 0.605.

Comparatively, Cancella et al. (2024) [1] investigated xanthan production from milk substrates, such as milk permeate and deproteinized whey in a shaker. The consistency index (K) of the obtained xanthan products was 1.829 and 0.874, respectively, which were lower than those obtained from rice parboiling water. Crugeira et al. (2023) [33] also assessed xanthan biosynthesis using wet olives bagasse, with 15% and 20% concentrations, resulting in consistency indices (K) of 4.353 and 4.216. Besides, flow behavior (η) indices were 0.2939 for 15% concentration and 0.2534 for 20%. Trivunović et al. (2024) [12] made use of vineyard wastewater and obtained viscosity values between 40 and 60 mPa.

These values are lower than those found in the present study signaling that RPW can be a highly efficient substrate for obtaining high-viscosity xanthan products. It is important to consider that cultivation medium composition, *Xanthomonas* strain employed, and production conditions, such as temperature, time, pH, agitation, and aeration, can significantly influence polymer structure and consequently the rheological properties of the produced gum [34]. Based on the results of Figure 4, it can be observed that the response value is mainly influenced by peptone and yeast extract concentration, with negative effects of 4.49 and 4.35, respectively, at a 5% significance level. This means that the higher the contents of these components, the lower the gum viscosity at the tested concentration range. This is desirable since it involves input savings.

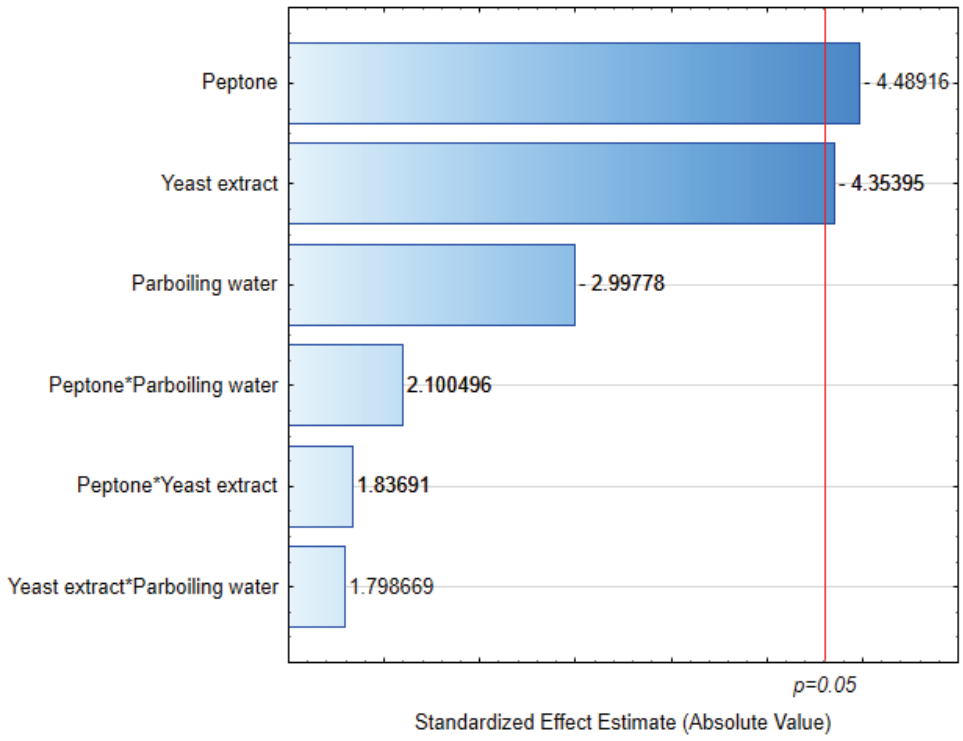

Figure 4. Effect of the independent variables (peptone, yeast extract, and RPW) on xanthan pruni solutions consistency index (K). Asterisks (*) represents interactions between variables.

In Figure 5, it is possible to observe the independent variables' effect on the flow behavior index (η). Yeast extract was the highest positive impact factor on this parameter, with a standardized effect of 6.66, followed by peptone with an effect of 5.36. This means

that both components, at higher concentrations, in the range examined, significantly increase the value of (η), which means lower pseudoplasticity.

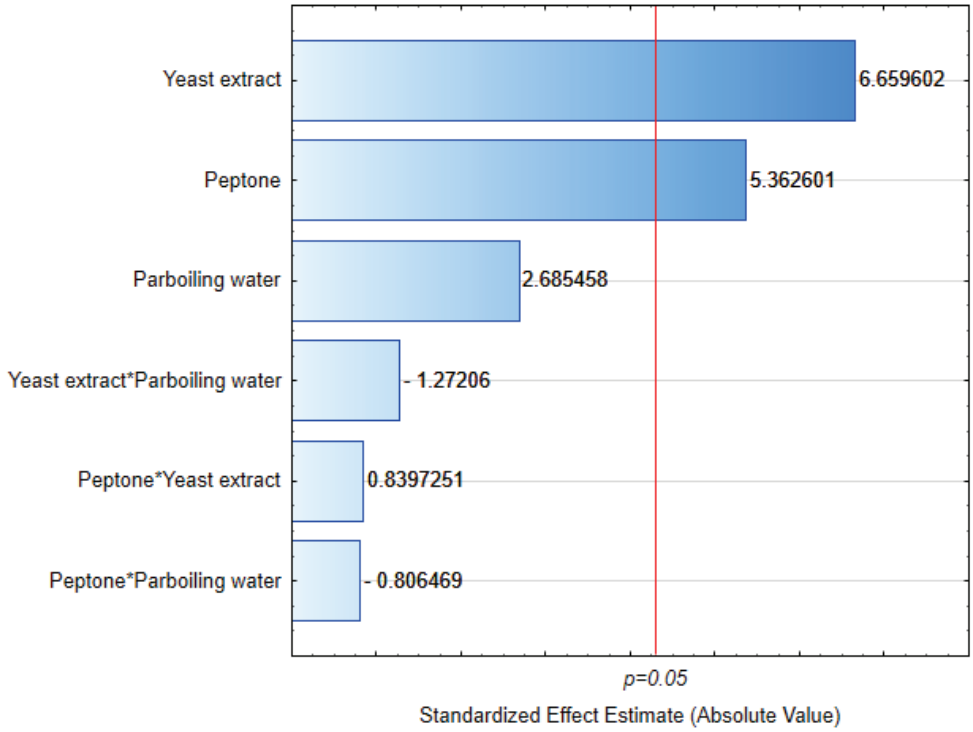

Figure 5. Effect of independent variables (peptone, yeast extract, and RPW) on flow behavior index (η) of xanthan pruni solutions. Asterisks (*) represents interactions between variables.

3.5. Minerals

The xanthan gum mineral composition varied among the treatments, influenced by the medium components. As expected, high RPW, peptone, and yeast extract concentration treatments favored the incorporation of minerals into the biopolymer. P was the element that most differed from the value ascertained for xanthan pruni synthesized in the standard medium—SPA. P, Si, Ca, and Mn exhibited higher concentration in high-RPW treatments. K was more influenced by peptone concentration and yeast extract. Na, Zn, Mg, and Mn were kept relatively stable.

Other elements, besides those listed in the Table 7, were also analyzed. Ti, B, and Al were found only as trace elements. Analyzes for Cd, Ba, Cu, Ni, Pb, Cr, and As were performed, but these elements were not detected in the obtained xanthan. According to the monography provided by the FAO/WHO Expert Committee on Food Additives [35], xanthan should not contain more than 2 mg/Kg lead in its general form, with the limit reduced to 0.5 $mg \cdot kg^{-1}$ for infant formulae. Besides, the Food Chemicals Codex [36] monography sets a limit of 3 mg/Kg for As in xanthan gum. However, the results of the present research pointed out that xanthan pruni did not exhibit any detectable lead or arsenic concentration, thus it meets the safety standards required for human consumption.

Xanthan gums exhibited variable concentrations of monovalent salts, between 2.44% and 2.93%. Torres et al. (1993) [37] observed 4.97% monovalent salts in xanthan gums produced by *X. Campestris*. Similarly, Borges (2007) [38] reported 5% monovalent salts for *X. arboricola* pv. pruni 115 strain, while commercial xanthan gums showed monovalent salts content variation from 0.67% to 3.2%. It should be mentioned that the total cation concentration is directly related to the negative hydroxyl, pyruvyl, and acetyl groups/ions [39].

The relationship among ions is crucial for understanding xanthan's functional properties. Among monovalent salts, Na's contribution to viscosity increase is higher than that of K. Moreover, the replacement of K with Na through ionic exchange [40] constitutes a strategy to increase xanthan viscosity. Treatment 1, with lower K content, had the highest viscosity (K 4.874) as compared with both the remaining treatments and the standard. In spite of the fact that monovalent salts contribute to viscosity increase, generally, these are not responsible for forming strong gels due to their weaker interactions as compared with divalent and trivalent salts [41].

Table 7. Mineral salts of xanthan gum obtained from *Xanthomonas arboricola* pv. pruni strain 101 from different concentrations of rice parboiling water, peptone, and yeast extract.

Treat.	P (mg/g)	Zn (mg/g)	Fe (mg/g)	Si (mg/g)	Ca (mg/g)	K (mg/g)	Mg (mg/g)	Mn (mg/g)	Na (mg/g)
1	13.72 ± 0.53 *	0.03 ± 0.01	0.03 ± 0.004	0.05 ± 0.003	1.84 ± 0.02	21.53 ± 0.39 *	3.51 ± 0.12	0.05 ± 0.001 *	2.85 ± 0.04
2	13.54 ± 0.29 *	0.03 ± 0.01	0.03 ± 0.004	0.05 ± 0.01	1.98 ± 0.05 *	25.33 ± 0.96	3.52 ± 0.28	0.05 ± 0.005 *	2.53 ± 0.01 *
3	15.42 ± 0.32 *	0.02 ± 0.004	0.06 ± 0.005 *	0.04 ± 0.005	1.67 ± 0.16	22.63 ± 0.35 *	3.75 ± 0.09 *	0.09 ± 0.14 *	2.67 ± 0.08 *
4	16.08 ± 0.19 *	0.05 ± 0.02	0.07 ± 0.006 *	0.10 ± 0.01 *	1.87 ± 0.01	26.36 ± 1.35	4.06 ± 0.10 *	0.05 ± 0.001 *	2.92 ± 0.08
5	31.49 ± 1.73 *	0.04 ± 0.005	0.05 ± 0.006 *	0.23 ± 0.01 *	2.41 ± 0.08 *	22.28 ± 0.15 *	4.12 ± 0.07 *	0.18 ± 0.01	2.95 ± 0.09
6	25.66 ± 2.03 *	0.06 ± 0.01	0.08 ± 0.01 *	0.16 ± 0.001 *	2.76 ± 0.30 *	26.06 ± 0.78	4.33 ± 0.25 *	0.19 ± 0.02	2.41 ± 0.13 *
7	29.21 ± 1.37 *	0.02 ± 0.008	0.05 ± 0.003 *	0.14 ± 0.01 *	2.33 ± 0.11 *	24.95 ± 0.10	4.34 ± 0.28 *	0.15 ± 0.004 *	2.40 ± 0.11 *
8	27.10 ± 0.05 *	0.02 ± 0.001	0.05 ± 0.008 *	0.15 ± 0.02 *	3.73 ± 0.07 *	26.11 ± 0.03	4.61 ± 0.40 *	0.11 ± 0.005 *	2.59 ± 0.08 *
9	16.18 ± 0.33 *	0.06 ± 0.001	0.05 ± 0.003 *	0.06 ± 0.01	2.21 ± 0.04 *	25.66 ± 0.16	3.87 ± 0.07 *	0.11 ± 0.004 *	2.59 ± 0.05 *
10	17.10 ± 0.05 *	0.06 ± 0.01	0.06 ± 0.01 *	0.08 ± 0.01 *	1.86 ± 0.003	22.28 ± 0.15 *	4.24 ± 0.10 *	0.09 ± 0.005 *	2.48 ± 0.11 *
11	18.33 ± 0.50 *	0.02 ± 0.001	0.07 ± 0.004 *	0.12 ± 0.01 *	2.24 ± 0.04	24.14 ± 0.85	3.57 ± 0.02 *	0.13 ± 0.006 *	3.12 ± 0.08 *
SPA	12.81 ± 0.03	0.03 ± 0.001	0.03 ± 0.004	0.05 ± 0.001	1.59 ± 0.13	25.80 ± 1.09	3.43 ± 0.05	0.19 ± 0.11	2.93 ± 0.04

Asterisks (*) on the samples point to significant differences as compared to the standard ($p < 0.05$), according to the *t*-test.

4. Conclusions

In the face of growing environmental challenges caused by increasing agro-industrial wastes, the use of RPW for producing biopolymers like xanthan is a sustainable, economically viable alternative. The partial (80%) replacement of peptone for rice parboiling water and yeast extract increased xanthan pruni yield and improved its rheological properties, increasing viscosity and pseudoplasticity. Besides, RPW fostered higher incorporation of minerals such as phosphorus, silicon, calcium, and magnesium. Potassium directly depended on P and YE concentration. Toxic elements such as arsenic and lead were not detected in the obtained xanthan. These findings evidence the potential of agro-industrial wastes as efficient alternatives for sustainable biopolymer production. Besides, obtained data provides important subsidies for bioprocess optimization, focusing on yield increment and end product quality. Aiming at scalability, complementary studies are being carried out in agitated flasks and bioreactors to assess the effect of RPW addition to the xanthan pruni production medium, which will contribute to future industrial production in line with sustainable development.

Author Contributions: Conceptualization, I.S.P. and A.d.S.M.; methodology, I.S.P., F.I.A., E.d.S.M.C. and J.d.R.P.; software, I.S.P. and K.L.M.; validation, I.S.P., K.L.M. and A.S.R.; formal analysis, I.S.P.; investigation, I.S.P. and A.d.S.M.; data curation, K.L.M.; writing—original draft preparation, I.S.P., K.L.M. and M.I.A.; writing—review and editing, I.S.P. and A.d.S.M.; visualization, C.T.V.; supervision, A.d.S.M.; project administration, A.d.S.M. All authors have read and agreed to the published version of the manuscript.

Funding: The authors thank the CAPES and CNPq funding agencies for their financial support.

Institutional Review Board Statement: Not applicable.

Informed Consent Statement: Not applicable.

Data Availability Statement: The original contributions presented in this study are included in the article. Further inquiries can be directed to the corresponding author.

Conflicts of Interest: Author Claire Tondo Vendruscolo is co-owner by the Biopolix Tecnological Materials. The remaining authors declare that the research was conducted in the absence of any commercial or financial relationships that could be construed as a potential conflict of interest.

Abbreviations

The following abbreviations are used in this manuscript:

RPW rice parboiling water

References

1. Cancella, M.J.; Cerqueira, A.F.L.W.; da Costa Teodoro, L.; Pereira, J.R.; da Costa Ludwig, Z.M.; de Carvalho Anjos, V.; Rodarte, M.P. Xanthan gum produced from milk permeate and deproteinized cheese whey: A comparative analysis with commercial xanthan gums. *Biocatal. Agric. Biotechnol.* **2024**, *56*, 103053.
2. Global Market Insights. Xanthan Gum Market Size, Industry Analysis Report, Regional Outlook, Growth Potential, Price Trends, Competitive Market Share & Forecast. 2024. Available online: https://www.gminsights.com/industry-analysis/xanthan-gum-market (accessed on 26 February 2025).
3. Mordor Intelligence. Xanthan Gum Market Size & Share Analysis—Growth Trends & Forecasts (2025–2030). Available online: https://www.mordorintelligence.com/industry-reports/xanthan-gum-market (accessed on 26 February 2025).
4. Li, P.; Li, T.; Zeng, Y.; Li, X.; Jiang, X.; Wang, Y.; Xie, T.; Zhang, Y. Biosynthesis of xanthan gum by *Xanthomonas campestris* LRELP-1 using kitchen waste as the sole substrate. *Carbohydr. Polym.* **2016**, *151*, 684–691. [PubMed]
5. Ramos, B.F.M.; de Almeida, P.F.; Chinalia, F.A. Bacterial xanthan and ramnolipid simultaneous production using industrial oil produced water. *Environ. Technol.* **2022**, *43*, 983–990.
6. Rashidi, A.R.; Dailin, D.J.; Ramli, S.; Hanapi, S.Z.; Ibrahim, S.F.; El Enshasy, H. Variable nitrogen sources effect on *Xanthomonas campestris* ATCC 13915 ability for xanthan production in culture supplemented with pineapple waste. *Biosci. Res.* **2023**, *20*, 7–12.
7. Vidhyalakshmi, R.; Vallinachiyar, C.; Radhika, R. Production of xanthan from agro-industrial waste. *J. Adv. Sci. Res.* **2012**, *3*, 56–59.
8. Obidah, J.S.; Owuama, C.I. Xanthan yield and conversion efficiency of pre-treated rice husk, sweet potato and cassava flours from *Xanthomonas campestris* fermentation. *Int. J. Eng. Trends Technol.* **2017**, *49*, 477–481.
9. Ozdal, M.; Kurbanoglu, E.B. Citric acid production by *Aspergillus niger* from agro-industrial by-products: Molasses and chicken feather peptone. *Waste Biomass Valorization* **2019**, *10*, 631–640.
10. Demirci, A.S.; Palabiyik, I.; Apaydın, D.; Mirik, M.; Gumus, T. Xanthan gum biosynthesis using *Xanthomonas* isolates from waste bread: Process optimization and fermentation kinetics. *LWT* **2019**, *101*, 40–47. [CrossRef]
11. Mohsin, A.; Zhang, K.; Hu, J.; Rehman, S.U.; Tariq, M.; Zaman, W.Q.; Khan, I.M.; Zhuang, Y.; Guo, M. Optimized biosynthesis of xanthan via effective valorization of orange peels using response surface methodology: A kinetic model approach. *Carbohydr. Polym.* **2018**, *181*, 793–800.
12. Trivunović, Z.; Zahović, I.; Vlajkov, V.; Grahovac, M.; Grahovac, J.; Dodić, J. Xanthan production using wastewaters from rose wine industry: Screening of *Xanthomonas euvesicatoria* isolates. *Period. Polytech. Chem. Eng.* **2024**, *68*, 428–436. [CrossRef]
13. Zohoun, E.V.; Tang, E.N.; Soumanou, M.M.; Manful, J.; Akissoe, N.H.; Bigoga, J.; Futakuchi, K.; Ndindeng, S.A. Physicochemical and nutritional properties of rice as affected by parboiling steaming time at atmospheric pressure and variety. *Food Sci. Nutr.* **2018**, *6*, 638–652. [CrossRef] [PubMed]
14. Bagchi, T.B.; Das, B.; Kumar, A.; Kumar, G.; Banerjee, J.; Gain, H.; Adhikari, A.A.; Chattopadhyay, K. Impact of cooking, parboiling and fermentation on nutritional components, predicted glycemic index and pasting properties of rice. *J. Cereal Sci.* **2023**, *114*, 103763.
15. Yang, J.; Li, X.; Zhao, S.; Yuan, W.; Zhou, Q.; Zhang, Y.; Qiu, J.; Wang, J.; Zhu, Q.; Yang, X.; et al. Light calcium carbonate improves pullulan biosynthesis by *Aureobasidium pullulans* under high concentration of sugar. *Food Chem.* **2023**, *415*, 135760. [PubMed]
16. Zhang, Y.; Wang, X.; Hu, Z.Q.; Xiao, Q.Q.; Wu, Y. Capturing and recovering phosphorus in water via composite material: Research progress, future directions, and challenges. *Sep. Purif. Technol.* **2025**, *353*, 128453.
17. Vendruscolo, C.T.; Vendruscolo, J.L.S.; da Moreira, A.S. Meio de cultura para crescimento de Xanthomonas. Brazilian patent BR1220140300158, 5 November 2004.
18. Moreira, A.D.S.; Vendruscolo, J.L.S.; Gil-Turnes, C.; Vendruscolo, C.T. Screening among 18 novel strains of Xanthomonas campestris pv pruni. *Food Hydrocoll.* **2001**, *15*, 469–474. [CrossRef]
19. Perez, I.A.; Macagnan, K.L.; Costa, E.D.S.M.; de Oliveira, G.D.; Ames, C.W.; Rossi, D.; da Silveira Moreira, A. Efeitos de novos extratos de levedura no crescimento celular, produção e viscosidade da xantana pruni por *Xanthomonas arboricola* pv pruni cepa 106. *Braz. J. Dev.* **2020**, *6*, 21543–21552.

20. Moreira, A.S.; Foresti, A.P.; Rodrigues, A.A.; Macagnam, J.L.; Alves, M.I.; Vendruscolo, C.T. Bioconversion of Agri-Food Wastes into Biopolymers: A step towards circular bioeconomy. In *Microbial Bioprocessing of Agri-Food Wastes*, 1st ed.; CRC Press: Boca Raton, FL, USA, 2023; Volume 1, pp. 81–124.
21. Instituto Adolfo Lutz. *Normas Analíticas do Instituto Adolfo Lutz*, 3rd ed.; IMESP: São Paulo, Brazil, 1985; Volume 1, p. 27.
22. Yu, S.; Olsen, C.E.; Marcussen, J. Methods for the assay of 1,5-anhydro-D-fructose and α-1,4-glucan lyase. *Carbohydr. Res.* **1997**, *305*, 73–82. [CrossRef]
23. Junior, R.A.C.; Chagas, A.V.; Felix, C.S.; Souza, R.C.; Silva, L.A.; Lemos, V.A.; Ferreira, S.L. A closed inline system for sample digestion using 70% hydrogen peroxide and UV radiation. Determination of lead in wine employing ETAAS. *Talanta* **2019**, *191*, 479–484.
24. Hayward, A.C. Bacteriophage sensitivity and biochemical group in *Xanthomonas malvacearum*. *Microbiology* **1964**, *35*, 287–298.
25. Myers, R.H.; Montgomery, D.C.; Anderson-Cook, C.M. *Response Surface Methodology: Process and Product Optimization Using Designed Experiments*, 3rd ed.; John Wiley & Sons: Hoboken, NJ, USA, 2016.
26. Da Rosa, M.B.; Oreste, E.Q.; Bonemann, D.H.; Rodrigues, A.A.; Vendruscolo, C.T.; Moreira, A.S.; Ribeiro, A.S.; Nunes, A.M. Evaluation of the use of a reflux system for sample preparation of xanthan gum and subsequent determination of Ca, Cu, K, Mg, Na and Zn by atomic spectrometry techniques. *J. Braz. Chem. Soc.* **2016**, *27*, 919–924.
27. Murad, H.A.; Mohamed, S.H.; Abu-El-Khair, A.G. Impact of amino acids, nitrogen source, and buffering system on xanthan yield produced on hydrolyzed whey lactose. *Biotechnology* **2017**, *16*, 69–76. [CrossRef]
28. Kurbanoglu, E.B.; Kurbanoglu, N.I. Ram horn hydrolysate as enhancer of xanthan production in batch culture of *Xanthomonas campestris* EBK-4 isolate. *Process Biochem.* **2007**, *42*, 1146–1149. [CrossRef]
29. Carignatto, C.R.R.; Oliveira, K.S.M.; de Lima, V.M.G.; de Oliva Neto, P. New culture medium to xanthan production by *Xanthomonas campestris* pv. campestris. *Indian J. Microbiol.* **2011**, *51*, 283–288. [CrossRef] [PubMed]
30. da Silva, J.A.; Cardoso, L.G.; de Jesus Assis, D.; Gomes, G.V.P.; Oliveira, M.B.P.P.; de Souza, C.O.; Druzian, J.I. Xanthan gum production by *Xanthomonas campestris* pv. campestris IBSBF 1866 and 1867 from lignocellulosic agroindustrial wastes. *Appl. Biochem. Biotechnol.* **2018**, *186*, 750–763. [CrossRef]
31. Macagnan, K.L.; Perez, I.A.; Costa, E.D.S.M.; Ames, C.W.; Soares, J.C.M.; Sourabié, A.; da Silveira Moreira, A. Influência de diferentes extratos de levedura (insumos) no crescimento celular de *Xanthomonas arboricola* pv. pruni cepa 101. *Braz. J. Dev.* **2021**, *7*, 15816–15824. [CrossRef]
32. Ouyabe, M.; Kikuno, H.; Tanaka, N.; Babil, P.; Shiwachi, H. Isolation and identification of nitrogen-fixing bacteria associated with *Dioscorea alata* L. and *Dioscorea esculenta* L. *Microb. Resour. Syst.* **2019**, *35*, 3–11.
33. Crugeira, P.J.L.; Almeida, H.H.S.; Marcet, I.; Rendueles, M.; Pires, M.G.; Rafael, H.M.; Rodrigues, A.I.G.; Santamaria-Echart, A.; Barreiro, M.F. Biosynthesis of antioxidant xanthan gum by *Xanthomonas campestris* using substrates added with moist olive pomace. *Food Bioprod. Process.* **2023**, *141*, 210–218. [CrossRef]
34. Garcia-Ochoa, F.; Santos, V.E.; Casas, J.A.; Gomez, E. Xanthan gum: Production, recovery, and properties. *Biotechnol. Adv.* **2000**, *18*, 549–579. [CrossRef]
35. Food and Agriculture Organization (FAO); World Health Organization (WHO). Xanthan Gum. Compendium of Food Additive Specifications. In Proceedings of the Joint FAO/WHO Expert Committee on Food Additives (JECFA), 82nd Meeting 2016, FAO JECFA Monographs 19. Geneva, Switzerland, 7–16 June 2016.
36. Burdock, G.A. *Food Chemicals Codex*, 4th ed.; National Academy Press: Washington, DC, USA, 1994.
37. Torres, L.G.; Brito, E.; Galindo, E.; Choplin, L. Viscous behaviour of xanthan aqueous solutions from a variant strain of *Xanthomonas campestris*. *J. Ferment. Bioeng.* **1993**, *75*, 58–64. [CrossRef]
38. Borges, C.D.; Bastos, C.P.; Vendruscolo, C.T. Avaliação das características físicas e químicas de gomas xantanas. *Ciênc. Exatas Technol.* **2007**, *28*, 107–114. [CrossRef]
39. Klaic, P.M.A.; Nunes, A.M.; da Silveira Moreira, A.; Vendruscolo, C.T.; Ribeiro, A.S. Determination of Na, K, Ca and Mg in xanthan gum: Sample treatment by acid digestion. *Carbohydr. Polym.* **2011**, *83*, 1895–1900.
40. Galván, Z.R.N.; Soares, L.D.S.; Medeiros, E.A.A.; Soares, N.D.F.F.; Ramos, A.M.; Coimbra, J.S.D.R.; de Oliveira, E.B. Rheological properties of aqueous dispersions of xanthan gum containing different chloride salts are impacted by both sizes and net electric charges of the cations. *Food Biophys.* **2018**, *13*, 186–197. [CrossRef]
41. Luporani, S.; Bretas, R. Rheological characterization of xanthan gum: Influence from univalent and trivalent metallic ions and from the temperature in dynamic experiments. *Polímeros* **2011**, *21*, 188–194.

fermentation

MDPI

Article

Exopolysaccharide (EPS) Production by Endophytic and Basidiomycete Fungi

Wai Prathumpai [1,*], Umpawa Pinruan [2], Sujinda Sommai [2], Somjit Komwijit [1] and Kwanruthai Malairuang [1]

[1] Biocontrol Technology Research Team, Integrative Crop Biotechnology and Management Research Group, National Center for Genetic Engineering and Biotechnology, National Science and Technology Development Agency, 113 Thailand Science Park, Phahonyothin Rd., Khlong Nueng, Khlong Luang, Pathum Thani 12120, Thailand; somjit.kom@biotec.or.th (S.K.); kwanruthai.mal@ncr.nstda.or.th (K.M.)

[2] Plant Microbe Interaction Research Team, Integrative Crop Biotechnology and Management Research Group, National Center for Genetic Engineering and Biotechnology, National Science and Technology Development Agency, 113 Thailand Science Park, Phahonyothin Rd., Khlong Nueng, Khlong Luang, Pathum Thani 12120, Thailand; umpawa.pin@biotec.or.th (U.P.); sujinda.som@biotec.or.th (S.S.)

* Correspondence: wai.pra@biotec.or.th; Tel.: +66-2564-6700 (ext. 3525-6-0)

Abstract: The screening of exopolysaccharides (EPS) produced by 52 isolates of endophytic and basidiomycete fungi was studied on two different media, PDB and PYGM. There were five isolates that could produce dried exopolysaccharide of more than 4 g/L (*S. commune* LF01962, LF01001, LF01581, *Pycnoporus* sp. MMCR00271.1, *Pestalotiopsis* sp. PP0005). The molecular weights of these exopolymers were found to be in the range of 2.5–500 kDa. These five exopolysaccharides, produced by five different fungal isolates, showed non-cytotoxic activity against NCTC clone 929 and HDFn cell lines. The selected fungal isolate of *S. commune* LF01962 was used for further optimization of different medium compositions affecting exopolysaccharide production using statistical methods. Among four conditions tested in the first step (xylose + peptone, glucose + $(NH_4)_2HPO_4$, fructose + peptone, and mannose + yeast extract), mannose + yeast extract resulted in the highest exopolysaccharide production of 5.10 ± 2.00 g/L. In the second step using Plackett–Burman design, the optimal medium for *S. commune* exopolysaccharide production was found to consist of 40 g/L glucose, 5 g/L mannose, 20 g/L $(NH_4)_2HPO_4$, 5 g/L yeast extract, 3 g/L monosodium glutamate, 0.5 g/L KH_2PO_4, 0.5 g/L K_2HPO_4, 0.2 g/L $MgSO_4$, 1 mL/L trace elements, and 3 mL/L vitamin solution, which resulted in 8.16 g/L exopolysaccharide production. Exopolysaccharide production in a 5 L bioreactor using small pellets as seed inoculum was found to produce 18.28 g/L exopolysaccharide.

Keywords: exobiopolymer; schizophyllan; *Schizophyllum commune*; endophytic; basidiomycete

1. Introduction

Fungal exopolysaccharides (EPSs) are high-molecular-weight polysaccharides composed of sugar monomer subunits that are secreted into the surrounding environments and/or dispersed in their growth media [1]. Some of these possess novel bioactive components, exhibit low toxicity, and have potential applications in various industries including cosmetics, pharmaceuticals, medicine, and food [2,3]. Although EPSs have been produced, isolated, and studied for many different fungi [1,4], novel EPSs have not yet been fully explored due to the high diversity of fungal species in nature [3]. Endophytes, a group

of fungi of interest, have the potential to produce EPSs with novel characteristics and properties [5]. The exploration and utilization of microbial polysaccharides for potential industrial applications have significantly increased in recent years [3,4]. Several studies have indicated that endophytes are potent producers of bioactive EPSs with unique properties, structures, and biological activities, making them suitable for applications in cosmetic, pharmaceutical, medical, and food industries [3,5]. Furthermore, many researchers have documented procedures for the production, isolation, and identification of EPS-producing endophytic fungi [1,6–8]. Optimization of EPS production by an endophytic fungus, *Pestalotiopsis* sp. BC55, resulted in the production of 4.320 $\pm$ 0.022 g/L of EPS with a molecular weight of approximately 2×10^5 Da. Structural elucidation of the EPS indicated the presence of only (1→3)-linked β-D-glucopyranosyl moieties [1]. Furthermore, the production of EPS by *Agrocybe cylindracea* reached a maximum of 3.0 g/L within 10 days [6]. A medicinal mushroom, *Fomes fomentarius*, produced a maximum EPS concentration of 3.64 g/L under optimal culture conditions [6,7]. Schizophyllan, produced by *S. commune* in an optimized medium in a 5 L fermenter, reached a concentration of 12.80 g/L [8]. Schizophyllan produced by a similar strain of the fungus *Schizophyllum commune* using cheaply available sago starch as a carbon source was observed to be thermally stable up to 125 °C with a high molecular weight of 14.73×10^3 kDa [9]. Additionally, exopolysaccharides were isolated from the submerged fermentation broth of *Morchella conica*, and the chemical structure of the isolated polysaccharide was elucidated [10]. In another study, eight endophytes isolated from *Piper hispidum* Sw., belonging to genera *Diaporthe*, *Marasmius*, *Phlebia*, *Phoma*, *Phyllosticta*, and *Schizophyllum*, were reported to produce EPSs in submerged cultures. These EPSs were rich in glucose (51%) and had a molecular weight of 46.6 kDa [11]. The medicinal mushroom *Ganoderma lingzhi* yielded EPSs at a concentration of 3.57 $\pm$ 0.21 g/L. These EPSs were heteropolysaccharides with high molecular weights (475,000 kDa and 21.6 kDa, 87.97%) and were composed of uronic acid, D-mannose, L-rhamnose, and D-glucose [12]. In submerged culture, *Ganoderma lucidum* achieved an EPS production of 4.7 g/L when the pH was adjusted from 3.0 to 6.0 after the fourth day [13]. The endophytic fungus *Bionectria ochroleuca* M21 produced EPS in submerged culture, reaching a production of 2.65 $\pm$ 0.16 g/L after 4 days of fermentation in a 5 L bioreactor [14]. Endophytes, therefore, represent a group of fungi of interest that can produce EPSs with the novel characteristics of EPS such as molecular weight distributions, being non-cytotoxic to human cell lines, and having high product yield, etc. This research aimed to study non-cytotoxic EPSs against human cell lines of the threshold of 20% cytotoxicity which serves as a critical point in categorizing exopolysaccharides as toxic to tested cells with different molecular weights and high yields by the fungal potential candidates. These EPSs can then be used for commercial applications in the future.

2. Materials and Methods

2.1. Microorganism and Growth Conditions

Fifty two isolates of mushroom and endophytic fungi (Table 1) were obtained from Biotec Culture Collection (BCC), Pathum Thani, Thailand, and from Plant Microbe Interaction Research Team, Integrative Crop Biotechnology and Management Research Group, National Center for Genetic Engineering and Biotechnology, Pathum Thani, Thailand. All strains were identified by morphological study, phylogeny, and 16 S rRNA gene sequence analysis. Stock cultures were maintained on potato dextrose agar (PDA, Difco™ and BBL™, Becton, Dickinson, MD, USA) that was cut into the cryotube containing 10% of glycerol and stored at −80 °C.

Table 1. List of 52 strains of endophytic and basidiomycete fungi for exopolysaccharide screening.

No	Original Code	BCC Code	Microorganisms
1	LF00466	56724	*Schizophyllum commune*
2	LF00467	56725	*Schizophyllum commune*
3	LF00469	56727	*Schizophyllum commune*
4	LF00470	56728	*Schizophyllum commune*
5	LF00473	56731	*Schizophyllum commune*
6	LF00534	61999	*Schizophyllum commune*
7	LF00543	62007	*Schizophyllum commune*
8	LF01001	66090	*Schizophyllum commune*
9	LF01581		*Schizophyllum commune*
10	LF01962	82612	*Schizophyllum commune*
11	MMCR00071		*Schizophyllum commune*
12	MMCR00176		*Schizophyllum commune*
13	MMCR00333		*Schizophyllum commune*
14	MMCR00334		*Schizophyllum commune*
15	MMCR00336		*Schizophyllum commune*
16	LF01222		*Auricularia* cf. *auricula*
17	LF01580		*Auricularia* cf. *delicata*
18	LF01616		*Auricularia* cf. *polytricha*
19	MMCR00014		*Auricularia* sp.
20	MMCR00107		*Auricularia* sp.
21	MMCR00108		*Auricularia* sp.
22	MMCR00157.1		*Auricularia* sp.
23	MMCR00171		*Auricularia* sp.
24	MMCR00177		*Auricularia* sp.
25	PHD00142		*Auricularia* sp.
26	MMCR00214.2		*Calvatia* sp.
27	MMCR00215.1		*Ganoderma* sp.
28	MMCR00216.1		*Ganoderma* sp.
29	MMCR00271.1		*Pycnoporus* sp.
30	MMCR00309.2		*Coprinus* cf. *fimetarius*
31	MMCR00347.1		*Amauroderma* sp.
32	PP0005		*Pestalotiopsis* sp.
33	PP0013		*Nigrospora* sp.
34	PP0049.1		*Mucor-like* sp.
35	ENFER0001		*Lasiodiplodia-like* sp.
36	ENFER0002		*Phomopsis* sp.
37	ENFER0003		*Mucor-like* sp.
38	ENFER0004		*Unidentified* sp.
39	ENFER0005		*Unidentified* sp.
40	ENFER0006		*Unidentified* sp.
41	ENFER0007		*Unidentified* sp.
42	ENFER0008		*Unidentified* sp.
43	ENFER0009		*Unidentified* sp.
44	MMCR00035		*Panus* sp.
45	MMCR00041		*Panus* sp.
46	MMCR00120		*Panus* sp.
47	MMCR00199		*Lentinus* cf. *polychrous*
48	MG0001		*Volvariella volvacea*
49	MG0002		*Flammulina velutipes*
50	MCR366.3		*Hericium erinaceus*
51	MCR369.1		*Pleurotus* cf. *djamor*
52	MCR370	56724	*Lentinus polychrous*

2.2. Seed Culture Preparation

Storage stock was activated on PDA medium in a Petri dish for 7 days. The activated culture was transferred and grown in a 250 mL flask containing 50 mL of potato dextrose broth (PDB) at 25 °C on a rotary shaker incubator (200 rpm/min) for 5 days.

2.3. Production of Exopolysaccharide by Selected Fungi

2.3.1. Growth Condition and Exopolysaccharide Extraction

Exopolysaccharide production in submerge cultures was performed in 250 mL flasks containing 50 mL of PDB (standard medium) and Peptone Yeast extract Glucose Medium (PYGM) (10 g/L glucose, 5 g/L bacteriological peptone, 20 g/L yeast extract, 1 g/L KH_2PO_4, 0.5 g/L $MgSO_4 \cdot 7H_2O$) after inoculation with 10% (*v/v*) of the seed culture. The experimental cultures were incubated at 25 °C on a rotary incubator (200 rpm/min) for 7 days.

After 7 days, the cultures were vacuum filtered through pre-weight Whatman® No. 1 filter paper. Cold-95% ethanol (4:1) was then added to mycelium-free filtrate for exopolysaccharide precipitation and then the solutions were kept at –20 °C overnight. The precipitants were lyophilized to obtain the exopolysaccharide dried weight. Mycelium on pre-weight filter papers was oven dried at 80 °C for 3 days to obtain the mycelium dried weight [15,16].

2.3.2. In Vitro Cytotoxicity Against Mouse Lung Fibroblasts (NTCT Clone 929) and Human Dermal Fibroblasts, Neonatal (HDFn)

NCTC clone 929 (ATCC, Manassas, VA, USA) and HDFn (Invitrogen, Carlsbad, CA, USA) were grown in Eagle's Minimum Essential Medium (EMEM) containing 10% FBS and 1 mM pyruvate and were incubated in 5% CO_2 chamber at 37 °C. For experiments, NCTC clone 929 and HDFn cells were seeded into 96-well plates at 1×10^3 and 5×10^3 cells/well, respectively. After 48 h of incubation for NCTC clone 929 and 72 h for HDFn, each cell type was challenged with exopolysaccharides at 100, 50, 20, and 10 μg/mL for 48 h. After challenging, cell viability was measured as described by Riss T.L. et al. [17]. Then, the cell viability was measured by MTT assay to obtain the average cell viability number in the tested solution compared with the control. The average of the cell viability was obtained from 8 wells using ellipeticine as a positive control.

2.3.3. Molecular Weight of Exopolysaccharide Measurement

The lyophilized exopolysaccharides were dissolved in 5 mg/mL water and were filtered through a 0.2 μm syringe filter to avoid the insolubilizing agent. The average molecular weight of the exopolysaccharides was determined with High Performance Liquid Chromatography (HPLC), RI detector, using a gel permeation column (PL aquagel-OH MIXED-H; Agilent, Santa Clara, CA, USA) eluted with deionized water at a flow rate of 0.5 mL/min at 80 °C. The standard of 6–450 kDa dextrans was used as references.

2.4. Medium Optimization for Maximized Exopolysaccharide from S. commune BCC 82612

After obtaining the high potential fungal strain for exopolysaccharide production, medium optimization for maximum exopolysaccharide production was performed by Design-Expert®13 (Stat-Ease).

2.4.1. Seed Culture Preparation for *S. commune* BCC 82612

Storage stock was activated on PDA medium in a Petri dish for 7 days. The activated culture was transferred and grown in a 1000 mL flask containing 200 mL of potato dextrose broth (PDB) at 25 °C on a rotary shaker incubator (200 rpm/min) for 5 days.

After 5 days, a big pellet of seed culture was ready for use. For the mycelial seed culture, the grown culture was homogenized with a sterile blender before use. The small pellet seed culture was prepared by the inoculation of the mycelial seed culture into PDB and incubated on the rotary shaker for 2 days before use.

2.4.2. Selection of Carbon and Nitrogen Sources

Six carbon sources (fructose, glucose, sucrose, maltose, mannose, xylose) and 8 nitrogen sources ($(NH_4)_2HPO_4$, $NH_4H_2PO_4$, $(NH_4)_2SO_4$, bacteriological peptone, casein hydrolysate, KNO_3, malt extract, yeast extract) were used in this experiment. A total of 20 g of carbon source and 10 g of nitrogen source were added to the basal medium (0.5 g/L KH_2PO_4, 0.5 g/L K_2HPO_4, 0.2 g/L $MgSO_4$). The pH of the experimental medium was adjusted to 5.5. Every combination of each source was performed in triplicate. At the end of the experiment, the mycelium dried weight and exopolysaccharide dried weight were analyzed for the selection of each source.

2.4.3. Screening of the Significant Medium Component by Plackett–Burman Design

A total of 11 variables (Table 2) were used in this experiment to generate a set of 26 experimental designs. All components were added to the basal medium as above with the final pH at 5.5. All of the experiments were carried out in triplicate.

Table 2. The selected variables of 26 treatments with different medium composition using Plackett–Burman Design.

No.	Factors										
	A g/L	**B g/L**	**C g/L**	**D g/L**	**E g/L**	**F g/L**	**G g/L**	**H g/L**	**J g/L**	**K ml/L**	**L ml/L**
1	40	5	0	20	5	5	0	0	0	3	1
2	20	5	5	10	5	5	5	0	0	1	3
3	40	0	5	20	0	5	5	0.5	0	1	1
4	20	5	0	20	5	0	5	0.5	3	1	1
5	20	0	5	10	5	5	0	0.5	3	3	1
6	20	0	0	20	0	5	5	0	3	3	3
7	40	0	0	10	5	0	5	0.5	0	3	3
8	40	5	0	10	0	5	0	0.5	3	1	3
9	40	5	5	10	0	0	5	0	3	3	1
10	20	5	5	20	0	0	0	0.5	0	3	3
11	40	0	5	20	5	0	0	0	3	1	3
12	20	0	0	10	0	0	0	0	0	1	1
13	30	2.5	2.5	15	2.5	2.5	2.5	0.25	1.5	2	2
14	20	0	5	10	0	0	5	0.5	3	1	3
15	40	0	0	20	0	0	0	0.5	3	3	1
16	20	5	0	10	5	0	0	0	3	3	3
17	40	0	5	10	0	5	0	0	0	3	3
18	40	5	0	20	0	0	5	0	0	1	3
19	40	5	5	10	5	0	0	0.5	0	1	1
20	20	5	5	20	0	5	0	0	3	1	1
21	20	0	5	20	5	0	5	0	0	3	1
22	20	0	0	20	5	5	0	0.5	0	1	3
23	40	0	0	10	5	5	5	0	3	1	1
24	20	5	0	10	0	5	5	0.5	0	3	1
25	40	5	5	20	5	5	5	0.5	3	3	3
26	30	2.5	2.5	15	2.5	2.5	2.5	0.25	1.5	2	2

Remarks: A = glucose, B = Xylose, C = Mannose, D = $(NH_4)_2HPO_4$, E = yeast extract, F = casein hydrolysate, G = Peptone, H = $MnSO_4$, J = Monosodium glutamate, K = Trace elements, L = Vitamin solution.

The significant effects of the variables on the production were identified for the isolates based on confidence levels above 95% ($p < 0.05$).

2.5. Exopolysaccharide Production by S. commune BCC 82612 in Laboratory Scale Bioreactor

Exopolysaccharide production by *S. commune BCC 82612* was carried out in a 5 L bioreactor (Satorius) with 4 L of optimized production medium. The bioreactor was equipped with two Rushton type turbines and baffles. The optimized medium (pH 5.5) was sterilized in situ at 121 °C for 15 min. Glucose was sterilized separately and was mixed aseptically with the other components of the medium in the bioreactor. The medium was inoculated with 10% (*v/v*) inoculum, and fermentation was carried out at 25 °C with uncontrolled pH. The impeller speed was initially adjusted to 100 rpm at the first 2 days of culture and adjusted to 300 after that, and compressed sterile air was sparged into the medium at the rate of 1 vvm. The samples were withdrawn every day and analyzed for dried mycelial weight, dried exopolysaccharide weight, and residual glucose. Three different types of seed cultures (mycelium, small pellet, big pellet) were studied for the production of exopolysaccharides in the laboratory bioreactor.

3. Results

3.1. Screening of the High Potential Fungi for Exopolysaccharide Production

By employing a multi-criteria screening approach involving the ability to produce exopolysaccharides (>4 g/L), assessing toxicity to human cells, and determining molecular weight, this comprehensive selection process ensures that the chosen strains not only exhibit high exopolysaccharide yields but also demonstrate favorable characteristics in terms of safety and structural properties. Ultimately, this systematic screening methodology enables the identification of fungal strains with the most promising attributes for further exploration and potential industrial applications.

3.1.1. Production of Exopolysaccharides in PDB and PYGM Media

Exopolysaccharide and mycelium dried weights were obtained from the experiments that were shown in Table 3. The fungi produced exopolysaccharides with dried weights of 0.01 ± 0.00–4.01 ± 2.32 g/L in PDB medium and 0.11 ± 0.03–6.59 ± 0.98 g/L in PYGM medium. The mycelium dried weights of the fungi of 0.55 ± 0.15–5.01 ± 0.31 and 1.77 ± 0.15–9.76 ± 0.09 g/L were obtained on PDB and PYGM media, respectively. The identification of five strains capable of producing dried exopolysaccharides exceeding 4 g/L showed their remarkable potential for industrial applications and further research. For instance, the high-yield exopolysaccharide-producing strains included *S. commune* LF01962, LF01001, LF01581, MMCR00333, and *Pycnoporus* sp. MMCR00271.1. The exopolysaccharides produced by the identified high-yield strains were utilized in subsequent experiments of in vitro human cell toxicity tests and molecular weight determinations.

Table 3. Exopolysaccharide and mycelium dried weights produced by 52 fungal strains in different media.

No	Code	Genus	Epithet	Mycelium Dried Weight (g/L)		Exopolysaccharide Dried Weight (g/L)	
				PDB	PYGM	PDB	PYGM
1	LF00466	*Schizophyllum*	*commune*	3.20 ± 0.38	8.57 ± 1.34	0.10 ± 0.02	2.41 ± 0.06
2	LF00467	*Schizophyllum*	*commune*	3.75 ± 0.24	10.23 ± 1.64	0.37 ± 0.27	1.91 ± 0.13
3	LF00469	*Schizophyllum*	*commune*	3.05 ± 0.13	7.29 ± 2.11	0.02 ± 0.01	2.26 ± 0.12
4	LF00470	*Schizophyllum*	*commune*	3.00 ± 0.27	11.42 ± 1.59	0.17 ± 0.05	1.25 ± 0.66
5	LF00473	*Schizophyllum*	*commune*	2.93 ± 0.25	10.90 ± 1.33	0.25 ± 0.31	1.81 ± 0.23

Table 3. *Cont.*

No	Code	Genus	Epithet	Mycelium Dried Weight (g/L)		Exopolysaccharide Dried Weight (g/L)	
				PDB	PYGM	PDB	PYGM
6	LF00534	*Schizophyllum*	*commune*	4.09 ± 0.11	13.92 ± 2.53	0.64 ± 0.24	0.72 ± 0.28
7	LF00543	*Schizophyllum*	*commune*	2.87 ± 2.48	12.07 ± 3.78	0.01 ± 0.01	1.94 ± 0.21
8	LF01001	*Schizophyllum*	*commune*	2.83 ± 0.22	13.30 ± 0.34	4.01 ± 2.32	5.07 ± 0.78
9	LF01581	*Schizophyllum*	*commune*	3.04 ± 0.14	8.50 ± 1.00	0.32 ± 0.14	2.04 ± 0.27
10	LF01962	*Schizophyllum*	*commune*	3.44 ± 0.46	11.03 ± 0.63	2.72 ± 0.26	6.39 ± 0.14
11	MMCR00071	*Schizophyllum*	*commune*	2.58 ± 0.23	7.46 ± 0.28	0.13 ± 0.04	2.07 ± 0.11
12	MMCR00176	*Schizophyllum*	*commune*	3.31 ± 0.39	10.64 ± 1.15	0.30 ± 0.15	1.67 ± 0.61
13	MMCR00333	*Schizophyllum*	*commune*	3.57 ± 0.28	12.35 ± 1.54	1.70 ± 0.96	4.29 ± 0.61
14	MMCR00334	*Schizophyllum*	*commune*	2.95 ± 0.24	6.05 ± 1.61	0.12 ± 0.04	1.56 ± 0.22
15	MMCR00336	*Schizophyllum*	*commune*	2.71 ± 0.09	7.66 ± 1.74	0.31 ± 0.23	1.54 ± 0.88
16	LF01222	*Auricularia*	cf. *auricula*	2.60 ± 0.24	5.06 ± 1.51	0.31 ± 0.34	1.90 ± 0.44
17	LF01580	*Auricularia*	cf. *delicata*	2.61 ± 0.12	4.19 ± 0.62	0.17 ± 0.07	0.93 ± 0.04
18	LF01616	*Auricularia*	cf. *polytricha*	2.39 ± 0.68	3.29 ± 0.28	0.75 ± 0.19	3.01 ± 0.22
19	MMCR00014	*Auricularia*	sp.	1.82 ± 0.13	5.81 ± 0.94	0.05 ± 0.01	1.54 ± 0.47
20	MMCR00107	*Auricularia*	sp.	3.12 ± 0.42	7.69 ± 0.86	0.20 ± 0.10	1.40 ± 0.46
21	MMCR00108	*Auricularia*	sp.	2.99 ± 0.02	6.07 ± 0.30	1.15 ± 0.10	2.62 ± 0.19
22	MMCR00157.1	*Auricularia*	sp.	4.39 ± 0.39	7.27 ± 2.90	0.38 ± 0.19	0.11 ± 0.03
23	MMCR00171	*Auricularia*	sp.	1.46 ± 0.12	3.48 ± 0.78	0.08 ± 0.02	2.29 ± 0.26
24	MMCR00177	*Auricularia*	sp.	1.17 ± 0.14	5.65 ± 0.95	0.33 ± 0.34	2.52 ± 0.18
25	PHD00142	*Auricularia*	sp.	0.91 ± 0.26	1.84 ± 0.48	0.46 ± 0.13	2.74 ± 0.29
26	MMCR00214.2	*Calvatia*	sp.	0.55 ± 0.15	1.32 ± 0.28	0.85 ± 0.31	3.03 ± 0.23
27	MMCR00215.1	*Ganoderma*	sp.	1.64 ± 0.17	2.64 ± 0.31	0.41 ± 0.18	2.89 ± 0.60
28	MMCR00216.1	*Ganoderma*	sp.	2.37 ± 0.07	7.01 ± 1.68	1.80 ± 1.13	4.21 ± 0.64
29	MMCR00271.1	*Pycnoporus*	sp.	2.63 ± 0.09	3.35 ± 0.19	0.41 ± 0.13	2.82 ± 0.15
30	MMCR00309.2	*Coprinus*	cf. *fimetarius*	2.47 ± 0.40	11.43 ± 1.13	1.15 ± 0.20	1.29 ± 0.16
31	MMCR00347.1	*Amauroderma*	sp.	1.29 ± 0.10	6.44 ± 2.06	0.51 ± 0.06	0.38 ± 0.11
32	PP0005	*Pestalotiopsis*	sp.	4.73 ± 0.34	7.19 ± 0.10	0.72 ± 0.27	6.59 ± 0.98
33	PP0013	*Nigrospora*	sp.	3.50 ± 0.30	8.62 ± 0.28	0.07 ± 0.04	2.05 ± 0.05
34	PP0049.1	*Mucor-like*	sp.	5.01 ± 0.31	5.79 ± 0.69	1.08 ± 0.07	2.77 ± 0.25
35	ENFER0001	*Lasiodiplodia-like*	sp.	3.70 ± 0.32	9.76 ± 0.09	0.11 ± 0.04	1.55 ± 0.21
36	ENFER0002	*Phomopsis*	sp.	3.61 ± 1.05	4.52 ± 2.49	0.70 ± 0.14	1.59 ± 0.59
37	ENFER0003	*Mucor-like*	sp.	4.07 ± 0.30	5.19 ± 0.23	0.42 ± 0.10	2.37 ± 0.25
38	ENFER0004	*Unidentified*	*Unidentified*	4.28 ± 0.25	8.11 ± 0.25	0.01 ± 0.00	2.45 ± 0.12
39	ENFER0005	*Unidentified*	*Unidentified*	2.91 ± 0.29	7.07 ± 0.11	1.74 ± 0.11	2.52 ± 0.06
40	ENFER0006	*Unidentified*	*Unidentified*	4.20 ± 0.60	6.79 ± 0.06	0.50 ± 0.23	2.23 ± 0.10
41	ENFER0007	*Unidentified*	*Unidentified*	4.27 ± 0.33	6.40 ± 0.17	0.18 ± 0.08	2.53 ± 0.19
42	ENFER0008	*Unidentified*	*Unidentified*	2.57 ± 0.32	5.84 ± 0.08	0.90 ± 0.29	2.77 ± 0.05
43	ENFER0009	*Unidentified*	*Unidentified*	3.37 ± 0.58	6.70 ± 0.46	1.21 ± 0.07	1.51 ± 0.04
44	MMCR00035	*Panus*	sp.	4.55 ± 2.64	6.54 ± 2.94	0.62 ± 0.32	1.72 ± 0.42
45	MMCR00041	*Panus*	sp.	1.33 ± 0.24	3.20 ± 0.71	1.03 ± 0.13	2.34 ± 0.20
46	MMCR00120	*Panus*	sp.	2.29 ± 0.22	6.75 ± 0.69	0.73 ± 0.06	2.14 ± 0.06
47	MMCR00199	*Lentinus*	cf. *polychrous*	2.10 ± 0.73	6.63 ± 0.36	0.27 ± 0.05	2.21 ± 0.19
48	MG0001	*Volvariella*	*volvacea*	1.60 ± 0.29	1.17 ± 0.15	0.66 ± 0.20	2.67 ± 0.68
49	MG0002	*Flammulina*	*velutipes*	2.52 ± 0.41	7.38 ± 1.34	0.13 ± 0.06	1.95 ± 0.13
50	MCR366.3	*Hericium*	*erinaceus*	1.81 ± 0.13	3.22 ± 0.16	0.78 ± 0.11	1.73 ± 0.21
51	MCR369.1	*Pleurotus*	cf. *djamor*	3.41 ± 0.35	12.69 ± 0.96	0.11 ± 0.02	1.68 ± 0.04
52	MCR370	*Lentinus*	*polychrous*	1.92 ± 0.43	7.07 ± 3.98	0.20 ± 0.13	1.71 ± 0.24

3.1.2. Cytotoxicity Test of Exopolysaccharides Produced by Fungi Against NTCT Clone 929 and HDFn Cells

Exopolysaccharides produced by the 52 selected fungal strains were challenged with NCTC clone 929 and HDFn cells for 48 h. Cytotoxicity was calculated by normalizing with the non-exopolysaccharides in percentage. At the highest concentration of the challenging reaction, the cytotoxicity of the exopolysaccharides is shown in Table 4. The threshold of 20% cytotoxicity serves as a critical point in categorizing exopolysaccharides as toxic to the tested cells. Exceeding this threshold indicates a significant detrimental effect on cell viability, warranting classification into the toxic category. The identification of non-cytotoxic exopolysaccharides in the experiments signifies their safety for cell viability. On the other

hand, the discovery of exopolysaccharides yielding negative results would potentially stimulate cell growth.

Table 4. Cytotoxicity of 100 mg/mL exopolysaccharides produced by 52 fungal strains against HDFn and NCTC clone 929 cells.

No	Code	Genus	Epithet	Cytotoxicity (%)			
				HDFn		NCTC Clone 929	
				PDB	PYGM	PDB	PYGM
1	LF00466	*Schizophyllum*	*commune*	−13.4	−3.13	2.11	8.72
2	LF00467	*Schizophyllum*	*commune*	14.32	15.33	4.05	3.98
3	LF00469	*Schizophyllum*	*commune*	0	5.47	0	1.6
4	LF00470	*Schizophyllum*	*commune*	10.95	6.66	5.29	4.71
5	LF00473	*Schizophyllum*	*commune*	14.65	15.84	4.51	6.89
6	LF00534	*Schizophyllum*	*commune*	0.07	−3.73	8.03	1.7
7	LF00543	*Schizophyllum*	*commune*	0	−0.64	0	4.69
8	LF01001	*Schizophyllum*	*commune*	7.98	8.19	5.18	9.52
9	LF01581	*Schizophyllum*	*commune*	6.85	−0.63	4.07	−1.73
10	LF01962	*Schizophyllum*	*commune*	9.6	11.32	4.38	6.72
11	MMCR00071	*Schizophyllum*	*commune*	12.67	1.61	11.63	15.45
12	MMCR00176	*Schizophyllum*	*commune*	0.38	4.65	5.78	16.06
13	MMCR00333	*Schizophyllum*	*commune*	1.55	0.97	10.51	11.65
14	MMCR00334	*Schizophyllum*	*commune*	−6.18	7.8	7.45	12.86
15	MMCR00336	*Schizophyllum*	*commune*	12.34	4.9	4.54	8.52
16	LF01222	*Auricularia*	cf. *auricula*	−0.21	7.69	2.14	8.34
17	LF01580	*Auricularia*	cf. *delicata*	9.79	6.74	9.26	4.2
18	LF01616	*Auricularia*	cf. *polytricha*	3.57	10.56	1.42	2.39
19	MMCR00014	*Auricularia*	sp.	0	8.61	0	−4.78
20	MMCR00107	*Auricularia*	sp.	9.45	6.51	−4.76	−4.73
21	MMCR00108	*Auricularia*	sp.	7.79	4.53	−0.02	−4.7
22	MMCR00157.1	*Auricularia*	sp.	13.21	4.12	−3.61	4.5
23	MMCR00171	*Auricularia*	sp.	0	3.53	0	1.59
24	MMCR00177	*Auricularia*	sp.	−10.59	−10.38	1.45	1.15
25	PHD00142	*Auricularia*	sp.	−21.4	−21.88	5.93	7.62
26	MMCR00214.2	*Calvatia*	sp.	−11.75	−14.68	−2.36	−2
27	MMCR00215.1	*Ganoderma*	sp.	−10.31	−15.9	3.8	−0.26
28	MMCR00216.1	*Ganoderma*	sp.	−5.1	−15.56	4.45	0.06
29	MMCR00271.1	*Pycnoporus*	sp.	−9.97	−1.49	12.42	0.47
30	MMCR00309.2	*Coprinus*	cf. *fimetarius*	−15.73	−9.37	4.44	6.52
31	MMCR00347.1	*Amauroderma*	sp.	5.79	−4.78	2.51	9.48
32	PP0005	*Pestalotiopsis*	sp.	−13.99	−1.82	−0.78	0.01
33	PP0013	*Nigrospora*	sp.	−12.39	−7.84	6.02	3.71
34	PP0049.1	*Mucor-like*	sp.	−9.86	−2.17	−0.12	3.98
35	ENFER0001	*Lasiodiplodia-like*	sp.	−1.35	−10.39	6.02	4.21
36	ENFER0002	*Phomopsis*	sp.	3.38	−1.14	7.27	4.05
37	ENFER0003	*Mucor-like*	sp.	10.11	8.43	5.01	10.01
38	ENFER0004	*Unidentified*	*Unidentified*	0	12.06	0	8.76
39	ENFER0005	*Unidentified*	*Unidentified*	8.14	11.7	5.63	1.95
40	ENFER0006	*Unidentified*	*Unidentified*	1.18	4.67	2.35	4.07
41	ENFER0007	*Unidentified*	*Unidentified*	−0.13	10.35	−0.12	3.41
42	ENFER0008	*Unidentified*	*Unidentified*	8	12.12	3.78	2.02
43	ENFER0009	*Unidentified*	*Unidentified*	5.81	8.97	4.35	−2.37
44	MMCR00035	*Panus*	sp.	7.58	4.22	−3.39	−7.34
45	MMCR00041	*Panus*	sp.	1.04	10.03	4.32	1.82
46	MMCR00120	*Panus*	sp.	14.99	11.76	−3.67	−8.52
47	MMCR00199	*Lentinus*	cf. *polychrous*	6.52	6.24	−8.33	5.48
48	MG0001	*Volvariella*	*volvacea*	4.97	5.69	−3.22	5.29
49	MG0002	*Flammulina*	*velutipes*	5.07	11.45	−1.01	2.89
50	MCR366.3	*Hericium*	*erinaceus*	8.2	13.94	2.77	7.92
51	MCR369.1	*Pleurotus*	cf. *djamor*	2.66	8.17	5.1	0.07
52	MCR370	*Lentinus*	*polychrous*	1.65	1.51	2.11	3.41

3.1.3. Molecular Weight Measurement of Exopolysaccharides

The molecular weight analysis of the exopolysaccharides from *S. commune* LF01581 and *Pycnoporus* sp. MMCR00271.1 revealed that their peaks were outside the expected range when compared to the standard dextran with a molecular weight of 6–450 kDa. This

observation indicates that these exopolysaccharides may have molecular weights that are significantly higher or lower than the standard range, highlighting potential variations in their structural characteristics. In Table 5, *S. commune* LF01962, LF01001, and *Pestalotiopsis* sp. PP0005 exhibit varying molecular weights of the exopolysaccharides. It is interesting to note that *Pestalotiopsis* sp. PP0005 produced exopolysaccharides with a molecular weight of 494.5 kDa in PYGM medium. However, when cultivated in PBD medium, the molecular weight of the exopolysaccharides exceeded 500 kDa. This shift in molecular weight based on the growth medium suggests the influence of different cultivation conditions on the properties of the exopolysaccharides produced by *Pestalotiopsis* sp. PP0005. The data on *S. commune* LF01001 reveal that it produced exopolysaccharides of various sizes in PYGM medium. However, when cultivated in PDB medium, higher molecular weight sizes of the exopolysaccharides were observed, resembling the exopolysaccharides produced by *S. commune* LF01962, which maintained a consistent molecular weight across both media types. The data in Table 5 indicate that the fungus produced a uniform size of exopolysaccharide on both types of media components. From the results, *S. commune* LF01962 was chosen as the high potential strain for further study based on the exopolysaccharide production, molecular weight, and cytotoxicity.

Table 5. Molecular weights of exopolysaccharides produced by 52 fungal strains in different media.

No	Code	Genus	Epithet	Molecular Weight (kDa)			
				PDB		PYGM	
1	LF00466	*Schizophyllum*	*commune*	-	-	20.87	-
2	LF00467	*Schizophyllum*	*commune*	-	-	-	-
3	LF00469	*Schizophyllum*	*commune*	-	-	1383.87 (9)	37.64 (91)
4	LF00470	*Schizophyllum*	*commune*	-	-	-	-
5	LF00473	*Schizophyllum*	*commune*	-	-	-	-
6	LF00534	*Schizophyllum*	*commune*	-	-	-	-
7	LF00543	*Schizophyllum*	*commune*	-	-	-	-
8	LF01001	*Schizophyllum*	*commune*	59.39 (35)	2.45 (65)	260.82 (25)	15.83 (75)
9	LF01581	*Schizophyllum*	*commune*	-	-	-	-
10	LF01962	*Schizophyllum*	*commune*	2.56	-	18.14	-
11	MMCR00071	*Schizophyllum*	*commune*	-	-	-	-
12	MMCR00176	*Schizophyllum*	*commune*	-	-	-	-
13	MMCR00333	*Schizophyllum*	*commune*	0.15		2.81	
14	MMCR00334	*Schizophyllum*	*commune*	-	-	-	-
15	MMCR00336	*Schizophyllum*	*commune*	-	-	-	-
16	LF01222	*Auricularia*	cf. *auricula*	-	-	-	-
17	LF01580	*Auricularia*	cf. *delicata*	-	-	-	-
18	LF01616	*Auricularia*	cf. *polytricha*	-	-	0.88	-
19	MMCR00014	*Auricularia*	sp.	-	-	-	-
20	MMCR00107	*Auricularia*	sp.	-	-	-	-
21	MMCR00108	*Auricularia*	sp.	5.08		603.50 (45)	15.43 (55)
22	MMCR00157.1	*Auricularia*	sp.	-	-	-	-
23	MMCR00171	*Auricularia*	sp.	-	-	229.5	-
24	MMCR00177	*Auricularia*	sp.	-	-	220.73 (23)	30.55 (87)
25	PHD00142	*Auricularia*	sp.	-	-	298.07	-
26	MMCR00214.2	*Calvatia*	sp.	-	-	307.76	4.73
27	MMCR00215.1	*Ganoderma*	sp.	-	-	1234.73 (41)	19.17 (59)
28	MMCR00216.1	*Ganoderma*	sp.	2.15	-	4.23 (24)	0.82 (76)
29	MMCR00271.1	*Pycnoporus*	sp.	-	-	3.39 (64)	0.72 (46)
30	MMCR00309.2	*Coprinus*	cf. *fimetarius*	2.61	-	-	-
31	MMCR00347.1	*Amauroderma*	sp.	-	-	-	-
32	PP0005	*Pestalotiopsis*	sp.	-	-	494.5	-
33	PP0013	*Nigrospora*	sp.	494.5	-	317.76	-
34	PP0049.1	*Mucor-like*	sp.	-	-	-	-
35	ENFER0001	*Lasiodiplodia-like*	sp.	-	-	-	-
36	ENFER0002	*Phomopsis*	sp.	-	-	-	-
37	ENFER0003	*Mucor-like*	sp.	-	-	75.44	-
38	ENFER0004	*Unidentified*	*Unidentified*	-	-	216.18	-
39	ENFER0005	*Unidentified*	*Unidentified*	3.98	-	458.08 (28)	273.45 (72)
40	ENFER0006	*Unidentified*	*Unidentified*	-	-	175.96	-
41	ENFER0007	*Unidentified*	*Unidentified*	-	-	144.23	-
42	ENFER0008	*Unidentified*	*Unidentified*	-	-	281.55	-
43	ENFER0009	*Unidentified*	*Unidentified*	2.87	-	-	-
44	MMCR00035	*Panus*	sp.	-	-	-	-
45	MMCR00041	*Panus*	sp.	4.21		503.52 (61)	335.94 (49)
46	MMCR00120	*Panus*	sp.	-	-	-	-

Table 5. *Cont.*

No	Code	Genus	Epithet	Molecular Weight (kDa)			
				PDB		PYGM	
47	MMCR00199	*Lentinus*	cf. *polychrous*	-	-	1214.29	-
48	MG0001	*Volvariella*	*volvacea*	-	-	234.66 (24)	2.09 (76)
49	MG0002	*Flammulina*	*velutipes*	-	-	-	-
50	MCR366.3	*Hericium*	*erinaceus*	-	-	-	-
51	MCR369.1	*Pleurotus*	cf. *djamor*	-	-	-	-
52	MCR370	*Lentinus*	*polychrous*	-	-	-	-

Remarks: Numbers in brackets are the percentage of molecular weight distribution.

3.2. Media Components Optimization for Exopolysaccharides Production by S. commune LF01962

3.2.1. Production of Exopolysaccharides by *S. commune* LF01962 on Different Carbon and Nitrogen Sources

In the initial step of optimizing the production medium components, *S. commune* LF01962 underwent screening for suitable carbon and nitrogen sources. The production of exopolysaccharide and mycelium dried weights by *S. commune* LF01962 is detailed in Table 6. The fungus produced exopolysaccharides ranging from 0.7 g/L to 5.1 g/L using various carbon and nitrogen sources. Notably, there were four conditions that resulted in higher exopolysaccharide production: xylose + peptone, glucose + $(NH_4)_2HPO_4$, fructose + peptone, and mannose + yeast extract. These successful carbon and nitrogen sources were then utilized as variables along with other factors in the Plackett–Burman design to optimize the significant components of the exopolysaccharide production medium.

Table 6. Exopolysaccharide and mycelium dried weight production by *S. commune* LF01962 on different carbon and nitrogen sources.

Treatments Carbon Source	Nitrogen Source	Exopolysaccharide Weight (g/L)	Mycelium Weight (g/L)
xylose	malt extract	0.70 ± 0.00	5.10 ± 0.10
	yeast extract	3.50 ± 0.70	14.20 ± 0.40
	KNO_3	1.00 ± 0.20	4.00 ± 0.50
	casein hydrolysate	3.00 ± 1.00	13.40 ± 1.10
	peptone	4.80 ± 0.80	12.00 ± 0.80
	$(NH_4)_2HPO_4$	1.40 ± 0.60	4.8 ± 0.50
	$(NH_4)_2SO_4$	1.20 ± 0.10	4.00 ± 0.40
	$NH_4H_2PO_4$	0.60 ± 0.40	3.5 ± 0.40
glucose	malt extract	0.90 ± 0.00	4.40 ± 0.20
	yeast extract	3.50 ± 0.00	12.10 ± 1.20
	KNO_3	1.3 ± 0.10	4.90 ± 0.90
	casein hydrolysate	3.00 ± 0.50	11.80 ± 1.30
	peptone	2.30 ± 0.20	9.60 ± 0.50
	$(NH_4)_2HPO_4$	4.00 ± 0.70	9.00 ± 1.00
	$(NH_4)_2SO_4$	1.00 ± 0.20	6.30 ± 1.00
	$NH_4H_2PO_4$	0.50 ± 0.00	4.30 ± 0.30
fructose	malt extract	0.80 ± 0.00	4.60 ± 0.50
	yeast extract	3.90 ± 0.8	14.50 ± 0.40
	KNO_3	1.30 ± 1.00	4.50 ± 0.50
	casein hydrolysate	3.20 ± 0.50	15.20 ± 2.00
	peptone	4.10 ± 0.60	14.20 ± 0.80
	$(NH_4)_2HPO_4$	1.80 ± 0.20	8.60 ± 0.20
	$(NH_4)_2SO_4$	1.20 ± 0.10	4.20 ± 0.10
	$NH_4H_2PO_4$	0.40 ± 0.10	4.00 ± 0.30
sucrose	malt extract	1.40 ± 0.20	4.10 ± 0.30
	yeast extract	3.10 ± 0.30	14.50 ± 1.00
	KNO_3	2.40 ± 1.2	4.70 ± 0.30
	casein hydrolysate	2.70 ± 0.20	15.20 ± 0.50
	peptone	3.90 ± 0.70	14.30 ± 0.40
	$(NH_4)_2HPO_4$	2.60 ± 0.20	10.30 ± 0.30
	$(NH_4)_2SO_4$	1.00 ± 0.00	5.80 ± 0.10
	$NH_4H_2PO_4$	0.50 ± 0.10	3.70 ± 0.30

Table 6. *Cont.*

Treatments Carbon Source	Nitrogen Source	Exopolysaccharide Weight (g/L)	Mycelium Weight (g/L)
maltose	malt extract	1.00 ± 0.10	4.00 ± 0.40
	yeast extract	3.80 ± 0.20	14.20 ± 0.60
	KNO_3	1.20 ± 0.10	3.60 ± 0.40
	casein hydrolysate	3.60 ± 0.30	13.40 ± 0.90
	peptone	3.30 ± 0.50	13.30 ± 0.50
	$(NH_4)_2HPO_4$	3.00 ± 0.30	9.80 ± 0.50
	$(NH_4)_2SO_4$	1.10 ± 0.00	5.10 ± 0.30
	$NH_4H_2PO_4$	0.50 ± 0.50	3.90 ± 0.20
mannose	malt extract	0.70 ± 0.10	4.60 ± 0.50
	yeast extract	5.10 ± 2.00	14.30 ± 0.60
	KNO_3	2.50 ± 0.50	4.70 ± 0.40
	casein hydrolysate	3.10 ± 0.60	13.80 ± 0.30
	peptone	2.70 ± 0.70	13.00 ± 0.50
	$(NH_4)_2HPO_4$	2.50 ± 0.20	9.70 ± 1.10
	$(NH_4)_2SO_4$	1.30 ± 0.30	4.40 ± 0.60
	$NH_4H_2PO_4$	0.60 ± 0.10	4.40 ± 0.20
PDB		1.40 ± 1.20	11.40 ± 1.10
PYGM		3.80 ± 0.30	8.80 ± 0.00

3.2.2. Production of Exopolysaccharides by *S. commune* LF01962 Using Plackettt–Burman Design

In the Plackett–Burman design for the exopolysaccharide and mycelium dried weights of *S. commune* LF01962 with 26 treatments (Table 7), the fungus produced exopolysaccharides ranging from 0.68 g/L to 8.16 g/L, which was 2.5 times higher than in the enriched medium (PYGM). The ANOVA results (Table 8) from this experiment identified significant factors affecting exopolysaccharide production: glucose, $(NH_4)_2HPO_4$, yeast extract, monosodium glutamate, and trace elements ($p \leq 0.01$). High levels of glucose, diammonium hydrogen phosphate, yeast extract, and monosodium glutamate had a positive impact on exopolysaccharide production, while low levels of trace elements restricted maximum exopolysaccharide production. The optimal medium for *S. commune* exopolysaccharide production consisted of 40 g/L glucose, 5 g/L mannose, 20 g/L $(NH_4)_2HPO_4$, 5 g/L yeast extract, 3 g/L monosodium glutamate, 0.5 g/L KH_2PO_4, 0.5 g/L K_2HPO_4, 0.2 g/L $MgSO_4$, 1 mL/L trace elements, and 3 mL/L vitamin solution.

Table 7. Exopolysaccharide and mycelium production by *S. commune* LF01962 using Plackett–Burman design.

Treatment	Exopolysaccharide Weight (g/L)	Mycelium Dried Weight (g/L)
1	7.22 ± 0.18	22.00 ± 2.24
2	3.43 ± 0.99	22.51 ± 4.33
3	0.96 ± 0.55	4.80 ± 2.01
4	1.92 ± 0.8	5.97 ± 1.73
5	4.87 ± 0.73	18.22 ± 1.69
6	1.93 ± 0.98	11.81 ± 2.34
7	5.17 ± 0.4	24.58 ± 1.12
8	5.07 ± 0.92	21.58 ± 1.54
9	5.26 ± 1.62	25.13 ± 0.33
10	0.68 ± 0.29	5.11 ± 1.01
11	8.16 ± 1.02	22.86 ± 1.01
12	1.52 ± 0.71	10.72 ± 2.01
13	5.73 ± 0.43	20.48 ± 1.55
14	0.8 ± 0.34	10.96 ± 0.80
15	1.26 ± 0.25	7.02 ± 3.35
16	5.65 ± 0.27	16.24 ± 0.99
17	4.02 ± 0.18	19.09 ± 0.71
18	2.51 ± 0.72	14.07 ± 0.66
19	4.72 ± 0.59	26.39 ± 0.69
20	3.78 ± 1.94	12.63 ± 2.5
21	2.81 ± 1.86	10.34 ± 3.50
22	0.95 ± 0.37	5.87 ± 0.81
23	3.23 ± 1.48	22.98 ± 1.50
24	2.84 ± 1.06	16.80 ± 1.92
25	1.16 ± 0.55	3.77 ± 0.31
26	4.53 ± 2.51	18.40 ± 2.51

Table 8. ANOVA of factorial model for exopolysaccharide production by *S. commune* LF01962.

Source	Sum of Squares	df	Mean Square	*F*-Value	*p*-Value	
Model	303.15	23	13.18	12.27	<0.0001	significant
A—Glucose	38.54	1	38.54	35.87	<0.0001	
B—Xylose	9.14	1	9.14	8.51	0.0052	
C—Mannose	0.2367	1	0.2367	0.2203	0.6407	
D—Diammonium hydrogen phosphate	41.34	1	41.34	38.49	<0.0001	
E—Yeast extract	60.59	1	60.59	56.40	<0.0001	
F—Casein hydrolysate	11.31	1	11.31	10.53	0.0020	
G—Peptone	0.7248	1	0.7248	0.6747	0.4151	
H—Manganese sulfate	2.76	1	2.76	2.57	0.1152	
J—Monosodium glutamate	21.94	1	21.94	20.42	<0.0001	
K—Trace elements	20.93	1	20.93	19.49	<0.0001	
L—Vitamin solution	11.15	1	11.15	10.38	0.0022	
Curvature	17.95	1	17.95	16.71	0.0001	
Pure Error	56.94	53	1.07			
Cor Total	378.03	77				

3.3. Exopolysaccharide Production by S. commune LF01962 in Laboratory Bioreactor

The validation of the optimal medium for *S. commune* LF01962 exopolysaccharide production was conducted in a 5 L bioreactor. Three types of inocula were tested: freely dispersed mycelium, small pellets, and big pellets. The freely dispersed mycelium inoculum yielded only 3.7 g/L of exopolysaccharides (Figure 1A), which was lower than the production at the flask scale. Interestingly, the mycelium dried weight decreased during the culture due to the high shear rate of the propeller, which cut the mycelium and reduced the production efficiency.

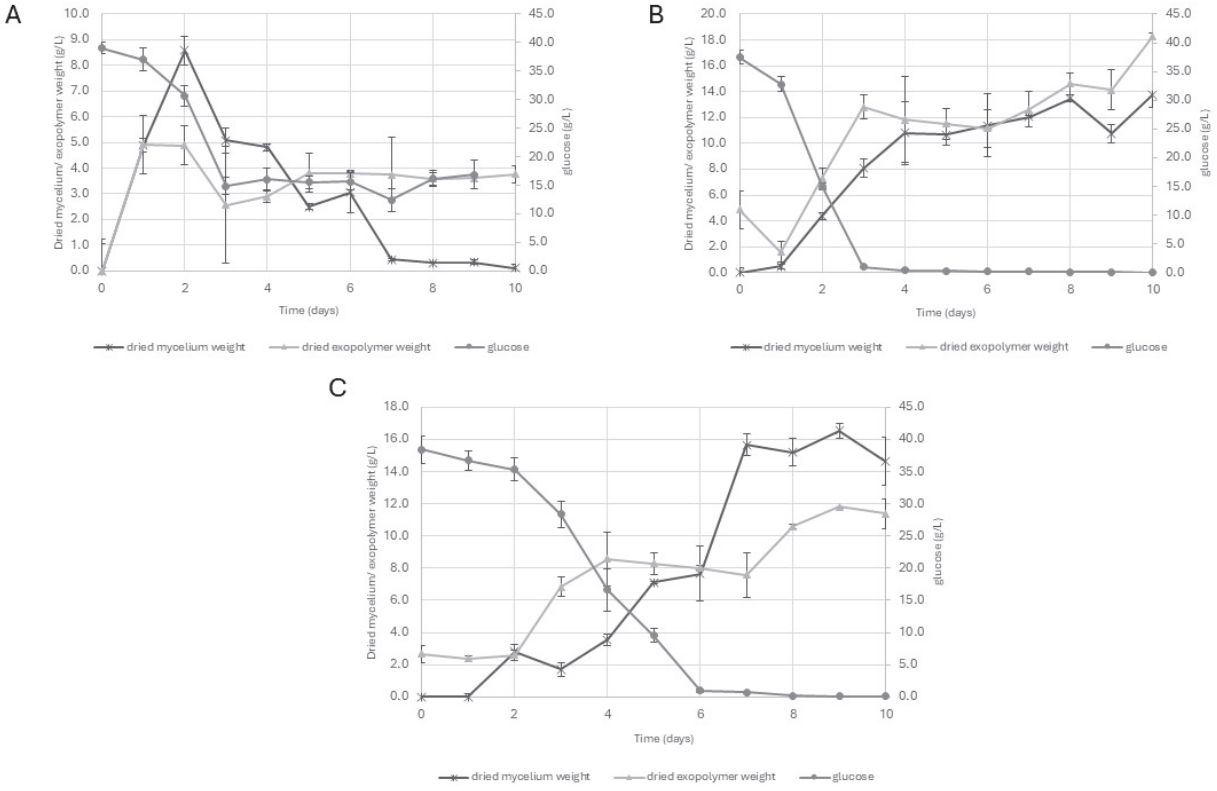

Figure 1. Mycelium and exopolysaccharide dried weights and residue glucose during *S. commune* LF01962 exopolysaccharide production with mycelium (**A**), small pellets (**B**), and big pellets (**C**) inoculum.

The study observed that the different pellet forms of the inoculum resulted in higher exopolysaccharide production, with the bigger pellets (pellet size > 5 mm diameter) producing 11.38 g/L (Figure 1C) and the smaller pellets (pellet size > 1 mm diameter) producing 18.28 g/L (Figure 1B). Interestingly, the mycelium dried weight of the pellet form continued to increase during exopolysaccharide production. These findings suggest that the use of small pellet inoculum led to higher exopolysaccharide production compared to other seed inoculum types.

4. Discussions

Endophytic and basidiomycete fungi represent promising groups capable of producing substantial amounts of exobiopolymers with varying chemical structures, cytotoxicities, and molecular weight profiles. In this study involving fifty-two fungal isolates from these groups, screened on PDB and PYGM media (Table 3), five isolates were identified as producing over 4 g/L of non-cytotoxic exopolysaccharides (Table 4) with molecular weights ranging from 2.5 to 5000 kDa (Table 5). The test of non-cytotoxic EPSs against human cell lines of the threshold of 20% cytotoxicity serves as a critical point in categorizing exopolysaccharides as toxic to tested cells with different molecular weights; and most of the selected strains possess non-cytotoxicity after being tested with these human cell lines, proving their potential in human use. The exobiopolymers produced by strains yielding less than 4 g/L were noteworthy for their diverse molecular weight sizes. Different molecular wieghts and structures can lead these exopolysaccharides to be used for different applications [15], and the molucular weight can be reduced by different techniques such as gamma radiation to signify their industrial appication [16]. However, their exclusion from further studies was based on considerations of the growth rates and mycelial yield. The identification of non-cytotoxic exopolysaccharides in the experiments signifies their safety for cell viability; their origins are from natural habitats which are edible mushrooms and which enable them to be used for human food applications, as most of them were non-cytotoxic. The strain *S. commune* LF01962 was selected for further optimization, focusing on various nutritional factors. It was discovered that the initial step involving mannose/yeast extract had the most significant impact on schizophyllan production, resulting in the highest exobiopolymer yield of 5.10 $\pm$ 2.00 g/L (Table 6). Subsequent optimization revealed that an optimal medium comprising 40 g/L glucose, 5 g/L mannose, 20 g/L $(NH_4)_2HPO_4$, 5 g/L yeast extract, 3 g/L monosodium glutamate, 0.5 g/L KH_2PO_4, 0.5 g/L K_2HPO_4, 0.2 g/L $MgSO_4$, 1 mL/L trace element, and 3 mL/L vitamin solution led to a further increase to 8.16 g/L of the exobiopolymer (Table 7). ANOVA analyses of the factorial model for exopolysaccharide production by *S. commune* LF01962, shown in Table 8, represent a significant model (>99%) with the expression of exopolysaccharides = 38.54A + 9.14B + 0.24C $-$ 41.34D + 60.59E + 11.31F + 0.73G + 2.76H + 21.94J + 20.93K + 11.15L (where A = glucose, B = xylose, C = mannose, D = diammonium hydrogen phosphate, E = yeast extract, F = casein hydrolysate, G = peptone, H = manganese sulfate, J = glutamic acid, K = trace elements, and L = vitamin solutions). Glucose and yeast extract had the highest positive effects but diammonium hydrogen phosphate had the highest negative effects on the exopolysaccharide production of *S. commune* LF01962. In the evaluation of schizophyllan production in a 5 L bioreactor by *S. commune* LF01962, three types of seed inoculum, free mycelium (Figure 1A), small pellets (Figure 1B), and big pellets (Figure 1C), were used. Interestingly, the small pellets resulted in the highest schizophyllan production of 18.28 g/L. This highlights that morphological characteristics, such as the size of pellets, can have a significant impact on schizophyllan production in a bioreactor. The study demonstrated that schizophyllan production reached 12.80 g/L in an optimized medium by

S. commune in a 5 L fermenter according to Li et al. [18], and schizophyllan was produced by *S. commune* in a similar study [8,9]. Additionally, another observation by Li et al. [18] reported a slightly higher schizophyllan production of 13.68 g/L. These results show the variations in schizophyllan production levels achieved through different experimental setups and optimization strategies. Schizophyllan's intriguing biological properties, such as antitumor and immune-stimulating activities, make this exopolysaccharide fascinating due to its unique structure of β-(1-6)-Branched β-(1-3)-glucans, gelation behavior, and natural origin [3]. The study highlighted the highest production levels compared to other reports, indicating its potential for scale-up and future applications in various fields.

5. Conclusions

The study highlighted the potential of endophytic and basidiomycete fungi to produce a variety of exopolysaccharides with non-cytotoxic properties, as they have been part of human food sources for many years. These exopolysaccharides exhibit diverse molecular weight sizes, structures, gelation properties, and compositions, making them versatile for numerous applications. The research, with 52 candidate strains, suggests that these fungi hold promise for further exploration in exopolysaccharide production, ranging from food and feed to cosmetics, pharmaceuticals, medical, and cosmeceutical industries. Notably, the high schizophyllan production of *S. commune* LF01962 indicates the potential for scalability and future commercial applications.

Author Contributions: Experimental investigation, methodology, data curation, formal analysis, and writing—original draft preparation were performed by S.K., K.M. and S.S.; investigation and methodology were performed by S.K., K.M. and S.S.; supervision was performed by U.P. and W.P.; and conceptualization, funding acquisition, project administration, resources, supervision, and writing—review and editing were performed by W.P. and U.P. All authors have read and agreed to the published version of the manuscript.

Funding: This work was financially supported by TDG-cosmeceuticals platform, National Nanotechnology Center, National Science and Technology Development Agency, Thailand. Funding code P20-50656.

Institutional Review Board Statement: Not applicable.

Informed Consent Statement: Not applicable.

Data Availability Statement: The original contributions presented in this study are included in the article. Further inquiries can be directed to the corresponding author.

Conflicts of Interest: The authors declare no conflicts of interest.

References

1. Mahapatra, S.; Banerjee, D. Production and structural elucidation of exopolysaccharide from endophytic *Pestalotiopsis* sp. BC55. *Int. J. Biol. Macromolec.* **2016**, *82*, 182–191.
2. Abdel-Monem, N.M.; El-Saadani, M.A.; Daba, A.S.; Saleh, S.R.; Aleem, E. Exopolysaccharide-peptide complex from oyster mushroom (*Pleurotus ostreatus*) protects against hepatotoxicity in rats. *Biochem. Biophys. Rep.* **2020**, *24*, 100852.
3. Zhang, Y.; Kong, H.; Fang, Y.; Nishinari, K.; Phillips, G.O. Schizophyllan: A review on its structure, properties, bioactivities and recent developments. *Bioact. Carbohydrats Diet. Fiber.* **2013**, *1*, 53–71. [CrossRef]
4. Osemwegie, O.O.; Adetunji, C.O.; Ayeni, E.A.; Adejobi, O.I.; Arise, R.O.; Nwonuma, C.O.; Oghenekaro, A.O. Exopolysaccharides from bacteria and fungi: Current status and perspectives in Africa. *Heliyon* **2020**, *6*, e04205. [CrossRef] [PubMed]
5. Liu, J.; Wang, X.; Pu, H.; Liu, S.; Kan, J.; Jin, C. Recent advances in endophytic exopolysaccharides: Production, structural characterization, physiological role and biological activity. *Carbohydr. Polym.* **2017**, *157*, 1113–1124. [PubMed]
6. Kim, H.O.; Lim, J.M.; Joo, J.H.; Kim, S.W.; Hwang, H.J.; Choi, J.W.; Yun, J.W. Optimization of submerged culture condition for the production of mycelial biomass and exopolysaccharides by *Agrocybe cylindracea*. *Biores. Tech.* **2005**, *96*, 1175–1182.

7. Chen, W.; Zhao, Z.; Chen, S.F.; Li, Y.Q. Optimization for the production of exopolysaccharide from Fomes fomentarius in submerged culture and its antitumor effect in vitro. *Biores. Tech.* **2008**, *99*, 3187–3194. [CrossRef] [PubMed]
8. Li, W.; Zhou, P.; Yu, L. Statistical Optimization of the Medium Composition by Response Surface Methodology to Enhance Schizophyllan Production by *Schizophyllum commune*. *Z Naturforsch C J. Biosci.* **2011**, *66*, 173–181. [CrossRef] [PubMed]
9. Gunaji, R.G.; Junin, R.; Bandyopadhyay, S. Production and characterization of biopolymer schizophyllan using sago starch as a carbon source. *J. Physics Conf. Ser.* **2020**, *1529*, 052063.
10. Su, C.; Xu, X.; Liu, D.; Wu, M.; Zeng, F.; Zeng, M.; Wei, W.; Jiang, N.; Luo, X. Isolation and characterization of exopolysaccharide with immunomodulatory activity from fermentation broth of *Morchella conica*. *DARU J. Pharmaceu. Sci.* **2013**, *21*, 5.
11. Si, J.; Meng, G.; Wu, Y.; Ma, H.F.; Cui, B.K.; Dai, Y.C. Medium composition optimization, structural characterization, and antioxidant activity of exopolysaccharides from the medicinal mushroom *Ganoderma lingzhi*. *Int. J. Biolo. Macromolec.* **2019**, *124*, 1186–1196.
12. Orlandelli, R.C.; Vasconcelos, A.F.D.; Azevedo, J.L.M.; Silva, L.C.; Pamphile, J.A. Screening of endophytic sources of exopolysaccharides: Preliminary characterization of crude exopolysaccharide produced by submerged culture of *Diaporthe* sp. JF766998 under different cultivation time. *Biochim. Open* **2016**, *2*, 33e40.
13. Kim, H.M.; Park, M.K.; Yun, J.W. Culture pH Affects Exopolysaccharide Production in Submerged Mycelial Culture of *Ganoderma lucidum*. *Appl. Biochem. Biotech.* **2006**, *134*, 249–262.
14. Li, Y.; Guo, S.; Zhu, H. Statistical optimization of culture medium for production of exopolysaccharide from endophytic fungus *Bionectria ochroleuca* and its antitumor effect in vitro. *EXCLI J.* **2016**, *15*, 211–220. [PubMed]
15. Madla, S.; Methacanon, P.; Prasitsil, M.; Kirtikara, K. Characterization of biocompatible fungi-derived polymers that induce IL-8 production. *Carbohydr. Polym.* **2005**, *59*, 275–280.
16. Methacanon, P.; Madla, S.; Kirtikara, K.; Prasitsil, M. Structural elucidation of bioactive fungi-derived polymers. *Carbohydr. Polym.* **2005**, *60*, 199–203. [CrossRef]
17. Riss, T.L.; Moravec, R.A.; Niles, A.L.; Duellman, S.; Benink, H.A.; Worzella, T.J.; Minor, L. Cell Viability Assays. In *Assay Guidance Manual*; Eli Lilly & Company and the National Center for Advancing Translational Sciences: Bethesda, MA, USA, 2013.
18. Li, W.; Wang, G.; Zhou, P.; Yu, L.; Zhang, Z. Optimization of conditions for schizophyllan production in submerged culture of *Schizophyllum commune*. In Proceedings of the 2011 International Conference on Human Health and Biomedical Engineering, Jilin, China, 19–22 August 2011.

fermentation

MDPI

Article

Effects of Compound Lactic Acid Bacteria Additives on the Quality of Oat and Common Vetch Silage in the Northwest Sichuan Plateau

Tianli Ma [1], Yafen Xin [1], Xuesong Chen [1], Xingjin Wen [2,*], Fei Wang [1], Hongyu Liu [1], Lanxi Zhu [1], Xiaomei Li [1], Minghong You [2,*] and Yanhong Yan [1,*]

[1] College of Grassland Science and Technology, Sichuan Agricultural University, Chengdu 611130, China; 17834451503@163.com (T.M.); xinyf13@163.com (Y.X.); cxs1278882456@126.com (X.C.); w255727wangfei@163.com (F.W.); liu57372024@126.com (H.L.); zoora042903@163.com (L.Z.); 14961@sicau.edu.cn (X.L.)

[2] Sichuan Academy of Grassland Sciences, Hongyuan 624400, China

* Correspondence: w778592700@163.com (X.W.); ymhturf@163.com (M.Y.); yanyanhong3588284@126.com (Y.Y.); Tel.: +86-184-2831-5408 (X.W.); +86-138-8028-8056 (M.Y.); +86-028-8629-0908 (Y.Y.)

Abstract: The objective of this experiment was to determine whether compound microbial inoculants could enhance the fermentation of oat and common vetch silage that were stored in the Northwest Sichuan Plateau for 60 days under extremely low temperatures. Oat and common vetch harvested from single and mixed artificially planted grassland of oat and common vetch were chopped into 2–3 cm (oat, S1; common vetch, S2; oat–common vetch = 2:1, S3), then sterile water (T1), Zhuang Lemei IV silage additive (T2), and Fu Zhengxing silage additive (T3) were added to the feed and ensiled at the local outdoor environment for 60 days. Data were analyzed as a 3 × 3 factorial arrangement of treatments with the main effects of the materials, additives, and their interaction. Interactions between the materials and additives significantly affected the fermentation quality and the content of DM, WSC, and NDF and the number of yeasts in forages. Treatments with S3 have significantly higher contents of lactic acid, acetic acid, and lactic acid bacteria in the feed than those in the S1 and S2 treatments, while the contents of AN/TN and propionic acid were significantly lower compared with the S1 and S2 treatments ($p < 0.05$). Concentrations of lactic acid, acetic acid, and propionic acid were significantly increased and the content of neutral detergent fiber in the T2-treated silage decreased compared with the T1 treatment ($p < 0.05$). The T3 treatment significantly reduced the number of yeasts in the silage but the compound lactic acid bacteria additive treatment (T1, T2) significantly decreased the butyric acid content and pH of the feed and increased the acid detergent fiber content and the number of lactic acid bacteria in the feed compared with the T1 treatment. Among them, the butyric acid content of the T3 treatment decreased by 63.64–86.05%, while that of the T2 treatment decreased by 36.36–83.33% ($p < 0.05$). The comprehensive analysis of the membership function revealed that the silage quality was the best after the S3T2 treatment, so the implementation of the S3T2 combination in the Northwest Sichuan Plateau can provide guarantees for the production of local high-quality forage grass and alleviate the shortage of forage grass.

Keywords: Zhuang Lemei IV silage additive; Fu Zhengxing silage additive; legume and grass silage; silage quality

1. Introduction

The Northwest Sichuan Plateau is one of the five major pastoral areas in China, which is rich in grassland and livestock resources, and animal husbandry is the local leading industry [1]. However, long-term overgrazing has led to the serious deterioration of the grassland ecological environment in this area, the productivity of natural forage has decreased and the quality has deteriorated, and the contradiction between forage supply and demand has intensified, which has greatly restricted the development of the local animal husbandry economy [2]. Oat (*Avena sativa* L.) and common vetch (*Vicia sativa* L.) are the main forage grasses in the Northwest Sichuan Plateau, which have the characteristics of strong acceptability, high nutritional value, and good palatability [3,4]. Studies have shown that planting oat and common vetch mixed grassland at a ratio of 2:1 in plateau areas above 3000 m above sea level not only makes full use of natural resources such as land and climate, but also improves soil fertility, increases forage production, and enhances forage quality [5,6]. In recent years, the area of oat and common vetch artificial grassland planting in the Northwest Sichuan Plateau area has been expanding year by year, but the harvest time of oat and common vetch is in the rainy season, the local temperature is low, and it is very easy for the traditional hay preparation to cause forage mildew rot and nutrient loss [1]. Therefore, the selection of a forage processing method suitable for the Northwest Sichuan Plateau is the key link to producing high-quality forage and alleviating the contradiction between forage supply and demand. Silage, as a forage preparation technology with lactic acid bacteria fermentation as the core, can effectively prevent the decay and mildew of forage grass, improve its nutritional value, and prolong the silage period [7]. However, forage silage is a complex biochemical process, and microbial community succession and external factors can affect the fermentation effect of silage [8,9]. The high altitude, strong radiation, and extremely arid and cold climate of the Northwest Sichuan Plateau significantly affected the microbial community attached to the surface of forage, resulting in a decrease in microbial metabolic activity, slow growth of lactic acid bacteria, and growth dominance of undesirable microorganisms, which increased the risk of silage failure [10,11]. Therefore, it is imperative to seek a good solution to solve the difficult problem of the unstable quality of the forage of oat and common vetch.

Exogenous addition of lactic acid bacteria preparation is one of the important means to promote the rapid dominance of forage bacteria [12]. The increase in the number of lactic acid bacteria can significantly improve the quality of silage, but different lactic acid bacteria have different functions, and the effect of lactic acid bacteria additives may vary depending on the fermentation substrate; in addition, when different types of lactic acid bacteria are compounded together in a certain ratio, their synergistic effects also vary [13,14]. Previous studies have found that the addition of *Lactobacillus buchneri* alone or in combination with *Lactobacillus plantarum* to maize and sorghum silage can improve the aerobic stability of silage under low dry matter content conditions, but the addition of *Lactobacillus buchneri* in combination with *Lactobacillus plantarum* also reduces the content of ammoniacal nitrogen and fermentation losses compared with the addition of a single *Lactobacillus buchneri*. When *Lactobacillus plantarum*, *Pediococcus pentosaceu*, and *Weissella cibaria* were used to ferment *Hemarthria compressa*, the single or compound addition of *Lactobacillus plantarum*, *Pediococcus pentosaceu*, and *Weissella cibaria* could improve the quality of *Hemarthria compressa* silage, but when lactic acid bacteria were added in pairwise, the effect on silage quality was different. Among all the additives, the compound addition of three kinds of bacteria had the best effect [15]. When Fu et al. [16] fermented *Sorghum bicolor* × *Sorghum sudanense* with *Lactobacillus plantarum*, *Pediococcus pentosaceu*, and *Lactobacillus brevis*, it was found that the combination effect of *Lactobacillus plantarum* and *Lactobacillus brevis* was the best, and the

effect of the combination of the three bacteria was worse than that of *Lactobacillus plantarum* alone or its compound with *Lactobacillus brevis* and *Pediococcus pentosaceu*. It can be seen that the effects of lactic acid bacteria additives can vary depending on the interactions between the bacteria and the fermentation substrate.

At present, there are few reports on compound lactic acid bacteria additives in the Plateau of Northwest Sichuan, and we do not know whether compound lactic acid bacteria additives can also improve forage quality in the special climate of the Northwest Sichuan Plateau. Based on this, by adding different compound lactic acid bacteria additives, the purpose of this study was to explore the effects of additives on the quality of oat and common vetch silage in the Northwest Sichuan Plateau, in order to select the most suitable compound lactic acid bacteria additives for oat and common vetch, and to provide a theoretical basis and practical guidance for the production of high-quality silage in the Northwest Sichuan Plateau.

2. Materials and Methods

2.1. Materials and Silage Additives

The seeds of oat and common vetch were supplied by Sichuan Nongken Muyuan Paradise Agriculture and Animal Husbandry Science and Technology Co (Ruoerge County, Aba Tibetan and Qiang Autonomous Prefecture, Sichuan Province, China). The oat (*Avena sativa* 'Qinyin No. 3') and the common vetch (*Vicia sativa* 'Ximu 324') were harvested from the Tangke town, Ruoergai country, Sichuan province (102°48′ E, 33°49′ N, altitude 3450 m) on 28 August 2021. When the oat was in the filling stage and the common vetch was at the podding period. Tangke Town has a plateau frigid–temperate climate, with sufficient sunshine, concentrated rainfall, large daily temperature difference, and no absolute frost-free period. The characteristics of silage raw materials are shown in Table S1.

The compound lactic acid bacteria additive Zhuang Lemei IV (*Lactobacillus plantarum* 550, *Lactobacillus plantarum* 360, *Lactobacillus buchneri*) was from Sichuan Gaofuji Biotechnology Co., Ltd. (Chengdu City, Sichuan Province, China), and Fu Zhengxing (two types of *Lactobacillus corn*, *Lactobacillus casei*) was from Sichuan Fu Zhengxing Biotechnology Co., Ltd. (Meishan City, Sichuan Province, China).

2.2. Silage Preparation and Treatments

The experiment was a two-factor completely randomized design. Three raw materials: S1, whole-plant oat silage; S2, whole-plant common vetch single; S3, oat–common vetch mixed silage (weight ratio of mixed sowing of oat and common vetch was 2:1). Two silage additives: the compound lactic acid bacteria additive Zhuang Lemei IV (T2), the compound lactic acid bacteria additive Fu Zhengxing (T3), and an equal volume of sterile water control (T1). The harvested oat and common vetch were cut into 2–3 cm, and the compound lactic acid bacteria preparations were inoculated at a rate of 5 × 105 cfu/g FW, and then evenly sprayed into each silage material. The mixed samples of 300 g were immediately vacuum-sealed in 30 cm × 40 cm single threaded polythene bags and a total of 27 silage samples (3 materials × 3 additives × 3 replicates) were stored in the local outdoor environment. After 60 days of fermentation, the silage quality, nutritional quality, and the number of microorganisms were determined.

2.3. Measurement Items and Analysis Methods

2.3.1. Chemical Compositions Analysis

Fresh samples and silage materials were de-enzymed at 105 °C for 30 min, then placed in a blast dryer at 65 °C and dried for 3 days to determine the dry matter (DM) content. The

dried materials were stored after grinding and filtering with a 1.0 mm sieve for subsequent analysis. The water-soluble carbohydrate (WSC) content was analyzed by the anthrone–sulfuric acid colorimetric method [17]. The crude protein (CP) and total nitrogen (TN) contents were detected using the Dumas combustion method [18]. The neutral detergent fiber (NDF) and acid detergent fiber (ADF) were determined according to the method of Van Soest et al. [19].

2.3.2. Fermentation Compositions Analysis

An amount of 20 g of fresh samples was evenly mixed in 180 mL of 0.85% NaCl sterile saline, extracted in a refrigerator at 4 °C for 24 h, and then the remaining liquid was filtered through 4 layers of gauze, and the extracts were stored in a −20 °C freezer for subsequent fermentation quality determination. The filtrate pH was determined with a glass electrode pH meter. The ammonia nitrogen (AN) content was analyzed by the phenol–hypochlorite method [20]. The contents of lactic acid (LA), acetic acid (AA), propionic acid (PA), and butyric acid (BA) were analyzed by high-phase liquid chromatography (HPLC, KC-811, Shimadzu Co., Ltd., Kyoto, Japan). The column used was a Shodex Rspak KC-811 S-DVB gel column (Lisennoke Scientific Instruments Co., Ltd., Shanghai, China) with an SPD-M10AVP detector (Shimadzu Co., Ltd., Kyoto, Japan). The setting parameters were as follows: the wavelength was set to 210 nm. The mobile phase was 3 mmol/L perchloric acid, the column temperature was 50 °C, and the flow rate was 1 mL/min [21].

2.3.3. Microbial Community Counting

The microbial community count was based on the method of Zeng Tairu et al. [21]. The specific method was as follows: the 20 g sample was mixed into 180 mL sterile saline (0.85% NaCl), placed on a 4 °C shaker for 1 h, then filtered, and then serial dilution was performed from 10^{-1} to 10^{-7}. Enterobacter were cultivated on Violet Red Bile Agar (Difco, Hopebil, Qingdao, China) and counted after 24 h of aerobic growth at 37 °C. Lactic acid bacteria were cultured on De Man, Rogosa, and Sharpe agar (Difco, Hopebil, Qingdao, China) and counted after 48 h of anaerobic growth at 37 °C. Molds and yeasts were determined by Potato Glucose agar (Difco, Hopebil, Qingdao, China) and counted after 72 h of aerobic growth at 28 °C. Yeasts and molds were distinguished by colony appearance and cell morphology observation.

2.4. Statistical Analyses

The data were collated and calculated using Excel 2019; the results of the microbial plate smear counts needed to be converted into log10 cfu/g of FM before statistical analysis. The one-way ANOVA and multi-way ANOVA were performed using SPSS 27.0 for the additives and materials. Duncan's multiple tests were used to compare the mean values of the different chemical compositions and the fermentation qualities of the silage. Results were expressed as mean ± standard deviations. Significant differences existed if the probability level was below 0.05.

In order to comprehensively evaluate the effects of different lactic acid bacteria additives on the silage quality of oats and common vetch silage, the membership function value method was used to analyze the measured indexes [20], in which dry matter, crude protein, water-soluble carbohydrate, lactic acid, acetic acid, and lactic acid bacteria were considered as positive indicators, and neutral detergent fibers, acid detergent fibers, pH, ammonia nitrogen/total nitrogen, butyric acid, and yeasts were considered as negative indicators. The values of the membership function of the individual indicators of the different treatments were calculated separately, and then the average membership function

value of each treatment was calculated; the larger the value, the better the quality of the silage. The membership function value formula is as follows:

$X(\mu_1) = \frac{X - X_{min}}{X_{max} - X_{min}}$ (positive correlation);

$X(\mu_2) = 1 - X(\mu_1)$ (negative correlation);

X_μ: the membership function value of a silage treatment under an additive;

X: the measured value of an index for a silage treatment;

X_{min} and X_{max}: the minimum and maximum values of an indicator in all processes, respectively.

3. Results

3.1. Fermentation Quality of Oat and Common Vetch Silage

The fermentation quality of silage treated with different compound lactic acid bacteria additives is shown in Table S2. The material, additives, and their interactions significantly affected the pH, LA, AA, and BA content of the silage ($p < 0.05$). In comparison with the T1 treatment, the pH of S1, S2, and S3 was significantly decreased in the T2 and T3 treatments ($p < 0.05$), and the pH was less than 4.2. The AN/TN of all treatments was lower than 28 g·kg^{-1} DM, and the AN/TN of the S3 treatment was lower than that of the S1 and S2 treatments. Among the S1, S2, and S3 treatments, the contents of LA and AA in the S3 treatment were the highest. Compared with the T1 treatment, the T2 treatment significantly increased the LA content of the silage ($p < 0.05$), and the S3T2 treatment had the highest LA content of 40.86 g·kg^{-1} DM ($p < 0.05$). In addition to the S1T3 treatment, the T2 and T3 treatments significantly increased the AA content of the silage compared to the T1 treatment ($p < 0.05$), and the S3T3 treatment had the highest AA content of 14.94 g·kg^{-1} DM. The LA/AA ratio was higher than 2:1 for all treatments throughout the fermentation process. The T2 treatment significantly increased the PA content of the silage ($p < 0.05$), and the highest PA content was 2.87 g·kg^{-1} DM in the S2T2 treatment. In this study, the BA content of all treatments was less than 0.9 g·kg^{-1} DM.

3.2. Chemical Characteristics of Oat and Common Vetch Silage

The chemical characteristics of silages treated with different compound lactic acid bacteria additives are shown in Table S3. The materials, additives, and their interactions significantly affected the DM, WSC, and NDF content of the silage ($p < 0.05$). The DM content of all treatments ranged from 160.62 to 262.03 g·kg^{-1} FM, and the S3 treatment had a higher DM content ($p < 0.05$). In comparison with the T1 treatment, the T2 treatment significantly decreased the CP content of the S1 and S3 treatments ($p < 0.05$). The T2 treatment significantly increased the WSC content of the silage compared to the T1 treatment, while the T3 treatment significantly decreased the WSC content of the S1 and S3 treatments, and the S1T2 treatment had the highest WSC content among all treatments at 61.27 g·kg^{-1} DM ($p < 0.05$). Except that the ADF content of the S3T2 treatment decreased compared with the S1 treatment, the NDF and ADF content of the S3 treatment increased in other treatments. In contrast to the T1 treatment, the T2 treatment decreased the NDF content of the silage, while the T3 treatment only led to a reduction in the NDF content of the S3 treatment. Both the T2 and T3 treatments demonstrated a significant increase in the ADF content of the silage ($p < 0.05$), with the T3 treatment exhibiting a more pronounced increase (7.25~18.09% vs. 23.77~34.72%).

3.3. Microorganisms of Oat and Common Vetch Silage

The number of microbial populations in the silage treated with different compound lactic acid bacteria additives is shown in Table S4. The materials, additives, and their

interactions significantly affected the number of yeasts in the silage ($p < 0.01$). Compared with the T1 treatment, the T2 and T3 treatment increased the number of lactic acid bacteria in the silage, in which the number of lactic acid bacteria treated with S3 increased significantly, and the number of lactic acid bacteria treated with S3T3 was the highest (7.52 $\log_{10}$ cfu·g^{-1} FM). The T2 treatment demonstrated a reduction in yeast populations in S2 and S3, while the T3 treatment significantly decreased the number of yeasts in the silage compared to the T1 treatment ($p < 0.05$). Notably, no yeast was detected in the S1T3 and S2T3 treatments.

3.4. Comprehensive Evaluation of Silage Quality of Oat and Common Vetch with Different LAB Additives

Using the membership function analysis method, Table S5 shows the comprehensive evaluation of oat and common vetch silages' quality with different compound lactic acid bacteria additives. The membership function analysis of each index of the tested treatment showed that the dry matter, crude protein, water-soluble carbohydrate, lactic acid, acetic acid, and lactic acid bacteria were positive indexes. The neutral detergent fiber, acid detergent fiber, pH, AN/TN, BA, and yeasts were negative indexes. According to the ranking of the membership function values of the above indexes, it can be seen that the average value of the membership function of the experimental group is higher than that of the control group, indicating that lactic acid bacteria additives can improve the quality of silage, and the ranking result of the membership function is S3T2 > S3T3 > S1T2 > S2T2 > S2T3 > S1T3 > S3T1 > S1T1 > S2T1. In general, the improvement effect of the T1 and T2 treatments on the S3 treatment tended to be the same, but the T2 treatment had a better-quality improvement effect on the S1 and S2 treatments.

4. Discussion

4.1. Effects of Different LAB Additives on Fermentation Quality of Oat and Common Vetch Silage

The pH is an important index to evaluate the fermentation quality of silage, and it is generally believed that the pH of high-quality silage should be less than 4.2 [22]. The soluble carbohydrate content of grass forage is rich, which provides sufficient substrate for the growth and reproduction of lactic acid bacteria, so after exogenous addition of lactic acid bacteria, the number of lactic acid bacteria in silage increases, accelerating the lactic acid production, and the pH value decreases. However, legume forage has a low content of water-soluble carbohydrate, a high buffering energy, and a high content of soluble proteins, which can be rapidly degraded to form NH^{4+}, and inhibit the decrease in the pH value [23]. After mixed silage, it balanced the nutrient composition of both, such as the increase in water-soluble carbohydrate in silage compared with legume forage silage alone, which provided the conditions for lactic acid bacteria to convert soluble carbohydrate into organic acids, and the increase in the lactic acid content in the silage, which in turn led to the decrease in its pH value [24]. The ability of lactic acid bacteria to utilize fermentation substrates such as water-soluble carbohydrate varies according to the species of lactic acid bacteria, which may be the reason why in the present study, the Zhuang Lemei IV additive significantly reduced the pH value of the single-silage group of oat and common vetch, while the Fu Zhengxing additive significantly reduced the pH value of the mixed-silage group [13], but the specific reasons need to be explored in the near future. AN/TN reflects the proteolysis, and generally high-quality silage requires the AN/TN to be less than 100 g·kg^{-1} DM [25]. In this study, the AN/TN of the treatments was all less than 28 g·kg^{-1} DM, and the AN/TN content of the silage was decreased after the mixed silage of oat and common vetch, which may be due to the mixed silage balancing the characteristics and microbial communities of the two kinds of forage grass, inhibiting the reproduction of

undesirable bacteria, and then decreasing the degradation of crude protein in the silage [26]. The content of organic acids can reflect the fermentation process of silage and is considered to be a homofermentation-dominated process when the ratio of lactic acid to acetic acid is at least higher than 2:1, which is a desired result in silage. Legume forages have acetic acid bacteria attached to themselves and this can produce acetic acid before anaerobic conditions are reached, thus allowing the accumulation of lactic and acetic acid in the silage [26]. The effect of two compound lactic acid bacteria additives on the accumulation of the acetic acid content of the silage was similar to its effect on the silage pH; when the Zhuang Lemei IV silage additive was added, it promoted the accumulation of lactic acid and acetic acid in the silage, but the addition of the Fu Zhengxing silage additive will cause most of the lactic acid in the oat and common vetch single-silage group and mixed-silage group to be isomerized to acetic acid, which will result in a relative decrease in the lactic acid content and an increase in the acetic acid content of the two groups [27], so it is presumed that there is also a competitive relationship between exogenous bacteria and microorganisms naturally attached to the surface of the forage, and that the addition of the Zhuang Lemei IV silage additive might introduce bacteria that have benign interactions with the forage microorganisms themselves, and that the addition of the Fu Zhengxing silage additive may have resulted in the dominance of heterogeneous fermenting lactic acid bacteria [13]. Propionic acid is a secondary metabolite produced by the fermentation of lactic acid by Propionibacterium. A small amount of propionic acid acts similarly to acetic acid and is effective in preserving silage nutrients. Butyric acid is produced by the decomposition of proteins and lactic acid by spoilage bacteria, the lower the content of which the better [28,29]. In this study, the contents of propionic acid and butyric acid in all treatments were less than 2.9 $g \cdot kg^{-1}$ DM and 0.9 $g \cdot kg^{-1}$ DM, respectively, which met the requirements of high-quality silage. However, the propionic acid content in the silage increased significantly after the addition of the Zhuang Lemei IV additive, which may be caused by the increased activity of Propionibacterium after the addition of the Zhuang Lemei IV silage additive [13], but the specific reason is still unclear and needs to be further explored. In general, the results of this study showed that the mixed silage of oat and common vetch and the addition of lactic acid bacteria could effectively improve the fermentation quality of the silage.

4.2. Effects of Different LAB Additives on Chemical Characteristics of Oat and Common Vetch Silage

The content of each nutrient composition is an important index to evaluate the nutritional quality of silage. In the silage fermentation process, lactic acid bacteria need to use forage water to promote their own life activities, so the dry matter content of silage has an important impact on fermentation [30]. This study found that the dry matter content of the oat and common vetch mixed silage was higher than when the two forages were silaged separately, but the dry matter content was consistently 259.73–262.03 $g \cdot kg^{-1}$ FM, which may be related to the high dry matter content of the oats themselves. It meets the requirements of high-quality silage [31], indicating that the mixed silage of oat and common vetch can improve the feeding value of the silage. Crude protein is an important index to reflect the quality of silage, and its content is negatively correlated with AN/TN. In this study, it was found that the crude protein content of oat and common vetch increased after mixed silage without lactic acid bacteria preparation, but if exogenous lactic acid bacteria preparation was added, the change in the silage crude protein content varied with different additives. For example, the addition of the Fu Zhengxing silage additive had no significant effect on the crude protein content of the silage, but the addition of the Zhuang Lemei IV

lactic acid bacteria additive decreased the crude protein content of the oat single-silage and mixed-silage group, which was similar to the change in AN/TN. This shows that the mixed silage of oat and common vetch can give full play to the characteristics of the two kinds of forage grass and balance their nutrients, and the difference in the effect after adding lactic acid bacteria may be related to the interaction between exogenous lactic acid bacteria and the lactic acid bacteria attached to the forage grasses themselves, as well as the different adaptability of different lactic acid bacteria to fermentation substrates [14]. Water-soluble carbohydrates are the material basis for lactic acid bacteria fermentation, and their content is an important factor in determining the fermentation process of silage. After utilizing the water-soluble carbohydrates in silage, lactic acid bacteria convert them into organic acids, which in turn inhibit the activity of undesirable microorganisms and reduce the consumption of water-soluble carbohydrate by undesirable microorganisms [32]. However, since the consumption of water-soluble carbohydrate in silage by lactic acid bacteria themselves is also larger, exogenously added lactic acid bacteria with relatively strong metabolic activity will accelerate the consumption of water-soluble carbohydrates in silage when they multiply in large quantities in silage, and the number of lactic acid bacteria under the treatment of the Fu Zhengxing silage additive is significantly higher than that under the other treatments, which explains the significant reduction in the number of lactic acid bacteria after the addition of the Fu Zhengxing silage additive in the water-soluble carbohydrate content in the oat and mixed-silage groups [16]. Fiber and its compositions are the key indexes for the routine evaluation of silage quality. The appropriate content of neutral detergent fiber can increase the saliva secretion of livestock, but too high a content will affect the digestibility of livestock and the lower the content of acid detergent fiber, the higher the feeding value [33]. The cellular respiration and rapid growth and reproduction of lactic acid bacteria in the early stage of silage will consume part of the nutrients in silage, which in turn leads to an increase in the proportion of acidic and neutral detergent fiber in silage [34], and the number of lactic acid bacteria in the mixed-silage group was higher than that in the single-silage group, which explains well the increase in the content of neutral detergent fiber and acid detergent fiber in the silage after the mixing of leguminous and grassy forage for silage. However, the effects of different additives on the forage fiber fractions were inconsistent and may also be related to the interaction between the bacteria and fermentation substrate as well as the characteristics of the two types of fibers [35], but the exact reason for this is not clear. Further exploration is needed.

4.3. Effect of Different LAB Additives on Microorganisms of Oat and Common Vetch Silage

Silage is a technology based on the vital metabolic activities of microorganisms that enable the long-term preservation of forage, and the type and number of microorganisms directly affect the fermentation quality of silage, and lactic acid bacteria are the core microorganisms of silage fermentation [36]. In this study, the mixed storage of oat and common vetch increased the number of lactic acid bacteria in the silage, indicating that the mixed silage played the complementary effect of the two kinds of forage grass, making the silage nutrition more comprehensive and providing more abundant and diversified sources of nutrition for the reproduction of lactic acid bacteria [26]. In addition, the number of lactic acid bacteria in the silage was increased by the addition of exogenous lactic acid bacteria preparations, among which the number of lactic acid bacteria treated with Fu Zhengxing additive was the highest, which indicated that the added lactic acid bacteria would multiply in large quantities in silage, but the degree of reproduction varied with different types of lactic acid bacteria [15]. Yeasts are the main microbial responsible for the aerobic deterioration of silage, which affects silage quality mainly by decomposing sugar

and lactic acid [37,38]. Yeast can utilize lactic acid for raw reproduction, and the mixed silage of oats and arrow end peas increased the yeast population of the forage, which was attributed to the higher lactic acid content of the mixed-silage group, which increased the supply of substrate needed for yeast growth and promoted yeast reproduction [39]. The addition of the Fu Zhengxing treatment significantly decreased the number of yeasts in the silage, and the treatment with the Zhuang Lemei IV additive decreased the number of yeasts in the single silage of the common vetch and mixed-silage group. This is because the addition of lactic acid bacteria decreased the pH of the silage and inhibited the growth and reproduction of yeasts [40], but it is doubtful that the addition of the Zhuang Lemei IV silage additive significantly increased the number of yeasts in the oat single-silage treatment, which may be the result of bacterial interactions [13], but the specific reasons need to be further explored. Molds and Enterobacter are undesirable bacteria that affect silage fermentation, and their excessive growth and reproduction will lead to silage failure.

5. Conclusions

In this study, we compared the effects of different compound lactic acid bacteria additives on the quality of oat and common vetch silage quality. It was found that oat and common vetch mixed silage balanced the nutritional characteristics of the two kinds of forage grass and made the nutrients of silage more comprehensive compared with the silage of the two forages alone. Both the Zhuang Lemei IV silage additive and Fu Zhengxing silage additive were beneficial in improving the quality of the silage. Combined with the comprehensive analysis of the affiliation function, the use of Zhuang Lemei IV compound lactic acid bacterial additive is recommended for oat and common vetch silage under the special climatic conditions of the Northwest Sichuan Plateau, which has a better effect on quality enhancement and efficiency.

Supplementary Materials: The following supporting information can be downloaded at: https://www.mdpi.com/article/10.3390/fermentation11020093/s1. Table S1. chemical composition and microbial population of fresh material. Table S2. effect of lactic acid bacteria additives on fermentation quality of oat and common vetch silage. Table S3. effect of lactic acid bacteria additives on nutritional quality of oat and common vetch silage. Table S4. effect of lactic acid bacteria additives on microbes of oat and common vetch silage. Table S5. comprehensive evaluation of silage quality of oat and common vetch with compound lactic acid bacteria additives.

Author Contributions: Conceptualization, T.M.; methodology, T.M. and Y.X.; formal analysis, T.M.; investigation, T.M., Y.X., X.C., X.W., F.W., H.L., L.Z. and X.L.; writing—original draft preparation, T.M.; writing—review and editing, Y.Y, M.Y., X.L. and Y.X.; supervision, Y.Y. and M.Y.; project administration, Y.Y. and M.Y.; funding acquisition, Y.Y. and M.Y. All authors have read and agreed to the published version of the manuscript.

Funding: This research was funded by the National forage industry technology system (grant number CARS-34-45), Special Funds for Sichuan Innovation Team Building of National Modern Agricultural Industrial Technology System (grant number SCCXTD-2024-21), National Key Research and Development Programs—Integration and demonstration of High efficiency breeding techniques of Yak in Hongyuan County (grant number 2022YFD1601602), and Sichuan Provincial Public Welfare Research Institutes Basic Research Operating Expenses Project (grant number 2023JDKY0033).

Institutional Review Board Statement: Not applicable.

Informed Consent Statement: Not applicable.

Data Availability Statement: The data in this study are included in the Supplementary Material.

Acknowledgments: The authors are grateful for the participants in this experiment, especially Yanhong Yan, Minghong You and Xingjin Wen for their generous support of this study.

Conflicts of Interest: The authors declare no conflicts of interest.

References

1. Wang, S.; Yuan, X.; Dong, Z.; Li, J.; Shao, T. Characteristics of lactic acid bacteria isolated from different sources and their effects on the silage quality of oat (*Avena sativa* L.) straw on the Tibetan Plateau. *Grassl. Sci.* **2018**, *64*, 128–136. [CrossRef]
2. Li, L.; Zhao, H.; Gou, W.; Lu, G.; Xiao, B.; Chen, C.; Li, P. Effects of Lactic Acid Bacteria Inoculants and Stage-Increased Storage Temperature on Silage Fermentation of Oat on the Qinghai–Tibet Plateau. *Fermentation* **2022**, *8*, 631. [CrossRef]
3. Dong, S.; Kang, M.; Yun, X.; Long, R.; Hu, Z. Economic comparison of forage production from annual crops, perennial pasture and native grassland in the alpine region of the Qinghai-Tibetan Plateau, China. *Grass Forage Sci.* **2007**, *62*, 405–415. [CrossRef]
4. Pflueger, N.; Redfearn, D.; Volesky, J.; Bolze, R.; Stephenson, M. Influence of oat and spring pea mixtures on forage characteristics in different environments. *Agron. J.* **2020**, *112*, 1911–1920. [CrossRef]
5. Qin, Y.; Liu, Y.; Zhang, Y.; Liang, G.; Liu, W. Effects of Mixed Ratios on Plant Growth Characteristics in Mixed Grassland of the Oat and Vetch Pea. *Acta Agrestia Sin.* **2020**, *28*, 1768–1774.
6. Xin, Y.; Zhang, L.; Chen, C.; Li, J.; She, L.; He, W.; Liu, Z.; Yan, Y. Study on Pasture Yield and Interspecific Relationship of Mixed Pasture of *Avena sativa* and Vicia sativa. *J. Sichuan Agric. Univ.* **2022**, *40*, 935–941.
7. Dong, D.; Lin, Z.; Dai, T.; Dong, Z.; Li, J.; Shao, T. Dynamics associated with fermentation and aerobic deterioration of high-moisture Italian ryegrass silage made using Lactobacillus plantarum and caproic acid. *J. Appl. Microbiol.* **2023**, *134*, 188. [CrossRef]
8. McEniry, J.; O'Kiely, P.; Clipson, N.; Forristal, P.; Doyle, E. Bacterial community dynamics during the ensilage of wilted grass. *J. Appl. Microbiol.* **2008**, *105*, 359–371. [CrossRef] [PubMed]
9. Zhang, Q.; Wu, B.; Nishino, N.; Wang, X.; Yu, Z. Fermentation and microbial population dynamics during the ensiling of native grass and subsequent exposure to air. *Anim. Sci. J.* **2016**, *87*, 389–397. [CrossRef]
10. Li, P.; Bai, S.; You, M.; Shen, Y. Effects of maturity stage and lactic acid bacteria on the fermentation quality and aerobic stability of Siberian wildrye silage. *Food Sci. Nutr.* **2016**, *4*, 664–670. [CrossRef] [PubMed]
11. Chen, C. Regulatory Mechanism of Hybrid *Pennisetum purpureum* Silage Quality by Self-Selected Lactic Acid Bacteria LP149 and Cellulase. Ph.D. Thesis, Sichuan Agricultural University, Chengdu, China, 2023.
12. Ma, J.; Dai, H.; Liu, H.; Du, W. Effects of harvest stages and lactic acid bacteria additives on the nutritional quality of silage derived from triticale, rye, and oat on the Qinghai-Tibet Plateau. *PeerJ.* **2023**, *11*, e15772. [CrossRef] [PubMed]
13. Liu, Q.; Li, X.; Desta, S.; Zhang, J.; Shao, T. Effects of Lactobacillus plantarum and fibrolytic enzyme on the fermentation quality and in vitro digestibility of total mixed rations silage including rape straw. *J. Integr. Agric.* **2016**, *15*, 2087–2096. [CrossRef]
14. Zhang, Q.; Li, X.; Zhao, M.; Yu, Z. Isolating and evaluating lactic acid bacteria strains for effectiveness of *Leymus chinensis* silage fermentation. *Lett. Appl. Microbiol.* **2014**, *59*, 391–397. [CrossRef] [PubMed]
15. Li, X.; Guan, H.; Shuai, Y.; Li, X.; Peng, A.; Li, C.; Pu, Q.; Yan, Y.; Zhang, X. Effects of single and multiple inoculants on *Hemarthria compressa* silage quality. *Acta Pratacult. Sin.* **2019**, *28*, 119–127.
16. Fu, W.; Chen, W.; Wang, X.; Zhou, L.; Qin, T.; Han, T.; Han, Y.; Meng, J. Effects of adding single and multiple lactic acid bacteria on silage of *Sorghum bicolor* × *Sorghum sudanense*. *J. South. Agric.* **2022**, *53*, 2060–2067.
17. Koehler, L. Differentiation of Carbohydrates by Anthrone Reaction Rate and Color Intensity. *Anal. Chem.* **2002**, *24*, 1576–1579. [CrossRef]
18. Chen, C.; Xin, Y.; Li, X.; Ni, H.; Zeng, T.; Du, Z.; Guan, H.; Wu, Y.; Yang, W.; Cai, Y.; et al. Effects of Acremonium cellulase and heat-resistant lactic acid bacteria on lignocellulose degradation, fermentation quality, and microbial community structure of hybrid elephant grass silage in humid and hot areas. *Front. Microbiol.* **2022**, *13*, 1066753. [CrossRef] [PubMed]
19. Van Soest, P.J.; Robertson, J.B.; Lewis, B.A. Methods for dietary fiber, neutral detergent fiber, and nonstarch polysaccharides in relation to animal nutrition. *J. Dairy Sci.* **1991**, *74*, 3583–3597. [CrossRef] [PubMed]
20. Li, J.; Wen, X.; Yang, J.; Yang, W.; Zhang, L.; Liu, H.; He, Y.; Yan, Y. Effects of maize varieties on biomass yield and silage quality of maize-soybean intercropping in the Qinghai-Tibet Plateau. *Fermentation* **2022**, *8*, 542. [CrossRef]
21. Zeng, T.; Li, X.; Guan, H.; Yang, W.; Liu, W.; Liu, J.; Du, Z.; Li, X.; Xiao, Q.; Wang, X.; et al. Dynamic microbial diversity and fermentation quality of the mixed silage of corn and soybean grown in strip intercropping system. *Bioresour. Technol.* **2020**, *313*, 123655. [CrossRef] [PubMed]
22. Soundharrajan, I.; Jung, J.; Muthusamy, K.; Lee, B.; Park, H.; Sivanesan, R.; Choi, K. Effects of Different Lactic Acid Bacteria in Single or Mixed Form on the Fermentative Parameters and Nutrient Contents of Early Heading Triticale Silage for Livestock. *Foods* **2023**, *12*, 4296. [CrossRef]

23. Yang, M.; Wang, F.; Xu, W.; Li, X.; Yin, H.; Tuluhong, M.; Qiu, R.; Li, B.; Cui, G. Effects of the fermentation quality and microbial community of waxy maize mixed with fodder soybean silage. *Front. Microbiol.* **2024**, *15*, 1405018. [CrossRef]
24. Zhang, Z.; Zhao, K.; Yang, S.; Min, L.; Tong, X.; Chen, W.; Li, D. Analysis on Fermentation Quality, Chemical Composition and Bacterial Communities of Corn Straw and Soybean Straw Mixed Silage. *Fermentation* **2023**, *9*, 500. [CrossRef]
25. Zhang, J.; Yuan, X.; Guo, G.; Wen, A.; Wang, J.; Xiao, S.; Ba, S.; Yu, C.; Shan, T. Effect of additive on fermentation quality of mixed silages of oat (*Avena sativa*) and common vetch (*Vicia sativa*) in Tibet. *Acta Pratacult. Sin.* **2014**, *23*, 359–364.
26. Lai, X.; Wang, H.; Yan, J.; Zhang, Y.; Yan, L. Exploring the differences between sole silages of gramineous forages and mixed silages with forage legumes using 16S/ITS full-length sequencing. *Front. Microbiol.* **2023**, *14*, 1120027. [CrossRef]
27. Xu, J.; Ma, J.; Sa, R.; Sui, H.; Wang, X.; Li, Q.; Zhu, X.; Wu, B.; Hu, Z.; Niu, H. Effects of lactic acid bacteria inoculants on the nutrient composition, fermentation quality, and microbial diversity of whole-plant soybean-corn mixed silage. *Front. Microbiol.* **2024**, *15*, 1347293. [CrossRef] [PubMed]
28. da Silva, J.; Ribeiro, K.; Pereira, O.; Mantovani, H.; Cecon, P.; Pereira, R.; Silva, J. Nutritive value and fermentation quality of palisadegrass and stylo mixed silages. *Anim. Sci. J.* **2018**, *89*, 72–78. [CrossRef]
29. Jiang, Y.; Tian, F.; Zi, X.; Li, M.; Tang, J.; Zhou, H.; Hou, G. Effect of Lactic Acid Bacteria and Molasses on Fermentation Quality of King Grass Silage. *J. Domest. Anim. Ecol.* **2022**, *43*, 67–70.
30. Guan, H.; Yan, Y.; Li, X.; Shuai, Y.; Feng, G.; Ran, Q.; Cai, Y.; Li, Y.; Zhang, X. Microbial communities and natural fermentation of corn silages prepared with farm bunker-silo in Southwest China. *Bioresour. Technol.* **2018**, *265*, 282–290. [CrossRef] [PubMed]
31. Luo, Y.; Chen, T.; Li, J.; Guo, X.; Yu, Z.; Zhang, X.; Yan, Y. Study on the Nutritional Quality of Italian Ryegrass and Soybean Straw Mixed Silages. *Acta Agrestia Sin.* **2015**, *23*, 200–204.
32. Wang, S.; Li, J.; Zhao, J.; Dong, Z.; Dong, D.; Shao, T. Dynamics of the bacterial communities and predicted functional profiles in wilted alfalfa silage. *J. Appl. Microbiol.* **2022**, *132*, 2613–2624. [CrossRef] [PubMed]
33. Li, M.; Zi, X.; Zhou, H.; Lv, R.; Tang, J.; Cai, Y. Silage fermentation and ruminal degradation of cassava foliage prepared with microbial additive. *Amb Express* **2019**, *9*, 180. [CrossRef] [PubMed]
34. Wang, X.; Qi, J.; Che, M. Quality and rumen fermentation characteristics of mixed silage intercropping with corn and sorghum hybrid sudan grass. *Grassl. Turf* **2023**, *43*, 101–108.
35. Xia, T.; Tahir, M.; Wang, T.; Wang, Y.; Zhang, X.; Liu, S.; Teng, K.; Fu, Z.; Yun, F.; Wang, S.; et al. Lactobacillus cocktail and cellulase synergistically improve the fiber transformation rate in Sesbania cannabina and sweet sorghum mixed silage. *Chem. Biol. Technol. Agric.* **2024**, *11*, 81. [CrossRef]
36. Holzer, M.; Danner, H.; Mayrhuber, E.; Braun, R. The aerobic stability of silages influenced by metabolites of lactic acid bacteria. *Meded. Rijksuniv. Gent. Fak. Landbouwkd. Toegepaste Biol. Wet.* **2001**, *66*, 459–461.
37. Borreani, G.; Piano, S.; Tabacco, E. Aerobic stability of maize silage stored under plastic films with different oxygen permeability. *J. Sci. Food Agric.* **2014**, *94*, 2684–2690. [CrossRef] [PubMed]
38. Tabacco, E.; Piano, S.; Revello-Chion, A.; Borreani, G. Effect of *Lactobacillus buchneri* LN4637 and *Lactobacillus buchneri* LN40177 on the aerobic stability, fermentation products, and microbial populations of corn silage under farm conditions. *J. Dairy Sci.* **2011**, *94*, 5589–5598. [CrossRef] [PubMed]
39. Oliveira, A.; Weinberg, Z.; Ogunade, I.; Cervantes, A.; Arriola, K.; Jiang, Y.; Kim, D.; Li, X.; Goncalves, M.; Vyas, D.; et al. Meta-analysis of effects of inoculation with homofermentative and facultative heterofermentative lactic acid bacteria on silage fermentation, aerobic stability, and the performance of dairy cows. *J. Dairy Sci.* **2017**, *100*, 4587–4603. [CrossRef] [PubMed]
40. Wang, Y.; He, L.; Xing, Y.; Zhou, W.; Pian, R.; Yang, F.; Chen, X.; Zhang, Q. Bacterial diversity and fermentation quality of Moringa oleifera leaves silage prepared with lactic acid bacteria inoculants and stored at different temperatures. *Bioresour. Technol.* **2019**, *284*, 349–358. [CrossRef]

fermentation

MDPI

Article

The Optimization of the Nutrient Medium Composition for the Submerged Cultivation of the *Mycolicibacterium neoaurum* Strain VKM Ac-3067D in a 100 L Bioreactor Under Controlled Conditions by Mathematical Planning

Vera V. Yaderets, Nataliya V. Karpova, Elena V. Glagoleva, Alexandra S. Shibaeva and Vakhtang V. Dzhavakhiya *

Laboratory of Biotechnology of Industrial Microorganisms, Department of Biotechnology and Technology of Bioorganic Synthesis Products, Russian Biotechnological University (ROSBIOTECH), Moscow 125080, Russia; verayaderetz@yandex.ru (V.V.Y.)

* Correspondence: vahoru@mail.ru

Abstract: The biotechnological production of carotenoids offers a promising alternative to their chemical synthesis or extraction from plants. *Mycolicibacterium* species have shown potential as pigment-producing microorganisms. However, bacterial strains typically exhibit lower productivity compared to fungal and yeast strains. Earlier, we enhanced the β-carotene biosynthesis in *M. neoaurum* strain VKM Ac-3067D by modifying the cultivation medium. Key changes included replacing glucose with glycerol and soybean meal with skimmed milk powder (SMP) and increasing the urea content from 0.5 to 1.0 g/L. To further optimize β-carotene yield, a steepest ascent method was applied combining factorial design with a gradient-based optimization (Wilson–Box method). The resulting regression model showed that the most influential factors were the glycerol concentration and SPM use. The in-flask fermentation of the Ac-3067D strain in a medium containing 25.5 g/L of glycerol (carbon source) and 12.80 g/L of SMP (nitrogen source) increased β-carotene yield to 318.4 ± 8.3 mg/kg. In a 15 L bioreactor, β-carotene yield increased to 432.3 ± 10.4 mg/kg, while the biomass concentration reached 23.2 ± 1.2 g/L. The further scaling up to a 100 L bioreactor increased both β-carotene yield (450.4 ± 8.2 mg/kg) and biomass concentration (25.2 ± 1.1 g/L). Thus, β-carotene production technology using the *M. neoaurum* strain AC-3067D was successfully scaled up from 750 mL flasks to a 100 L bioreactor, confirming its potential for industrial-scale application.

Keywords: mathematical planning; β-carotene; *Mycolicibacterium neoaurum*; nutrient medium; fermentation; bioreactor; scaling up

1. Introduction

A high biological activity of carotenoids and their wide range of applications determine the ongoing interest of researchers in finding effective methods for their production [1–5]. According to the available data, there are three main methods of the production of these compounds, chemical synthesis [6,7], extraction [3,6,8–10], and biosynthesis, which is based on the use of various microorganisms including fungi, yeast, bacteria, and microalgae [2–5].

To date, the majority of commercial carotenoids on the global market are of a chemical origin [11,12] that is explained by low production costs, relatively high yield of target products, and the lack of the productivity dependence on a season [12]. However, chemical

synthesis has several drawbacks. First, not all carotenoids can be produced via chemical synthesis. Second, toxic by-products are generated during their production, thus contributing to environmental pollution. Third, chemically synthesized compounds can differ from their natural analogues in their isomeric composition and effectiveness, and may also cause allergic and other undesirable reactions. For example, natural astaxanthin consists mainly of esterified forms (95%), while synthetic astaxanthin is non-esterified; as a result, natural astaxanthin is 50-fold more effective in relation to the singlet oxygen neutralization and 20-fold more effective in scavenging of free radicals [13]. In addition, a global trend to prefer natural carotenoids has been observed in recent years among consumers. All these facts suggest that in the nearest future, the focus of carotenoid production may shift towards the use of natural sources.

Technologies related to the carotenoid extraction from natural plant sources are certainly positively assessed by consumers. However, the stability of the manufacturing processes is complicated by a seasonality of carotenoid sources, relatively low yield, and the need for the purification of the target product from other metabolites that does not completely meet the requirements of industrial production, and it is often labor-consuming, and requires significant land areas for the cultivation of target plants [14].

Bacteria represent another potential type of producers suitable for the microbiological production of carotenoids, because they are widely used in the large-scale production of various biological compounds and have a short life cycle [3,15–17]. The suitable producers may include either naturally pigmented bacteria, or genetically modified bacteria, which initially were not able to synthesize pigments.

The ability of a producer strain to synthesize compounds with specific properties depends not only on individual characteristics of the strain, but also on the conditions, under which the target product is obtained. Determining the composition of a cultivation medium is an effective method for increasing biosynthetic activity of microorganisms producing biologically active compounds [18,19]. The medium composition can be determined by two ways: empirical selection, or the use of mathematical design of experiments. The traditional empirical selection method is widely used for determining the optimal cultivation conditions for microorganisms [19]. However, experimental design makes it possible to simultaneously vary all factors and to provide a quantitative evaluation of the influence of key factors and interactions on the yield of the target parameter with smaller errors compared to the traditional one-factor methods [20–24]. The ultimate goal of the mathematical modeling is the controlled cultivation of producer strains to achieve the maximum yield of the biomass or target metabolites.

For example, modeling of the nutrient medium composition for *Candida melibiosica* strain 2491 enabled its optimization, so its use for the yeast cultivation increased the phytase biosynthesis by 22.5% [23]. This approach was also used in the planning of β-carotene production by *Rhodotorula glutinis* ATCC 4054. Rice bran, molasses, and sugarcane bagasse were tested as substrates. As a result, rice bran was found to be the best inexpensive substrate for the biomass growth and β-carotene production. Using mathematical planning, the optimal contents of medium components were determined, including sucrose (18.6 g/L), NaCl (0.66 g/L), and KH_2PO_4 (1.01 g/L). In addition, the optimal amount of the inoculum, pH (5.4), and stirring rate were established, which provided a several-fold increase in the biosynthesis of the target product [24].

Fast-growing, non-pathogenic bacteria from the genus *Mycolicibacterium*, which have been shown to synthesize β-carotene and lycopene as well as several other pigments [17,24–26], can be considered as promising producers of carotenoids. In our earlier studies, we developed the *M. neoaurum* strain AC-501/22 via chemical mutagenesis and optimized its

cultivation conditions in a 3 L bioreactor to achieve a β-carotene yield of 262.4 mg/kg of dry biomass [27]. The strain was deposited in the All-Russian Collection of Microorganisms (accession number *M. neoaurum* VKM AC-3067D). The purpose of this study was the optimization of the nutrient medium composition using mathematical planning and its approbation under conditions of a submerged cultivation of the AC-3067D strain during the scaling up of the process from flasks to a 100 L bioreactor.

2. Materials and Methods

2.1. Reagents and Media Components

Skimmed milk powder was manufactured by HiMedia Laboratories (Mumbai, India). Urea was manufactured by NeoFroxx GmbH (Einhausen, Germany). Skimmed deodorated soybean flour was purchased from Soyanta 200 (Irkutsk, Russia). Citric acid was manufactured by Component-reactiv Ltd. (Moscow, Russia). Agar was manufactured by Difco (Detroit, MI, USA). Inorganic salts, glycerol, glucose, and organic solvents (acetone, hexane, benzene) were purchased from Acros Organics (Geel, Belgium).

2.2. Producer Strain

M. neoaurum strain AC-3067D was stored in the working collection of the Laboratory of Biotechnology of Industrial Microorganisms of the Russian Biotechnological University (Moscow, Russia).

2.3. Nutrient Media for M. neoaurum Cultivation and Maintenance

M. neoaurum VKM Ac-3067D was cultivated on the A1 medium of the following composition (g/L): agar, 17.0; glucose, 10.0; soybean meal, 10.0; citric acid, 2.2; urea, 0.5; NH_4Cl, 1.0; KH_2PO_4, 0.5; $MgSO_4 \cdot 7H_2O$, 0.5; $FeSO_4 \cdot 7H_2O$, 0.05; and $CaCO_3$, 1.5 (pH 6.8–7.2). After being stored on an agarized medium at 4 °C for one month, the cultures were transferred to a fresh medium. For long-term preservation, the cultures were freeze-dried with a powdered milk as a carrier and stored at 4 °C.

2.4. Cultivation of M. neoaurum VKM Ac-3067D on a Liquid Nutrient Medium

The control liquid medium (AM medium) used for the further modification had the following composition (g/L): glycerol, 20.0; skimmed milk powder (SMP), 10.0; citric acid, 2.2; urea, 1.0; NH_4Cl, 1.0; KH_2PO_4, 0.5; $MgSO_4 \cdot 7H_2O$, 0.5; $FeSO_4 \cdot 7H_2O$, 0.05; and $CaCO_3$, 1.5 (pH 6.8–7.2).

The inoculum was prepared as follows. A tube containing the bacterial culture was supplemented with 10 mL of a sterile physiological solution. The agar surface was gently scraped using an inoculation loop, and the obtained cell suspension was transferred into 750 mL flasks containing 100 mL of the AM medium followed by the 48-h incubation of flasks at 220 rpm and 35 °C in an Innova 44 shaker (New Brunswick, Germany). The obtained inoculate (10 vol. %) was then transferred to fresh flasks containing 100 mL of the same medium and cultivated for 72 h under identical conditions. The resulting culture broth was either used to inoculate the bioreactor, or dried and then analyzed for the carotenoid content.

2.5. Carotenoid Content Determination

The carotenoid content in the cell biomass of *M. neoaurum* VKM Ac-3067D was measured spectrophotometrically [27]. The procedure was conducted under low illumination with the room temperature maintained below 20 °C. A 30-mL aliquot of culture broth was centrifuged for 5 min at 7500 rpm. The supernatant was discarded, and the remaining

biomass underwent a 3-fold extraction using 10 mL of acetone. The resulting acetone extracts were pooled, transferred into a separating funnel, and mixed with petroleum ether (10 mL). After vigorous shaking, the resulted emulsion was broken by a adding a saturated NaCl solution dropwise. Once the acetone layer separated, the solution was re-extracted with petroleum ether. The petroleum ether extracts were pooled and filtered through a glass filter. The absorption spectrum of the carotenoid extract was recorded at 450 nm using a Thermo Spectronic spectrophotometer (Thermo Fisher Scientific, Waltham, MA, USA) with petroleum ether used as a reference. The total carotenoid content was determined using the following formula:

$$Carotenoid\ content\ \ (\mu g/g\ d.w.) = \frac{V(mL) \times A_{450} \times 10^6}{2592 \times 100 \times m(g)}, \quad (1)$$

where A_{450} is the experimentally determined adsorption of the measured solution; 2592 is the value of a 1% extinction; and m is the weight of dried cells (g).

2.6. Nutrient Medium Optimization Using the Mathematical Planning Method (Complete Factorial Experiment, CFE 2^3)

2.6.1. Nutrient Medium Optimization by a Complete Factorial Experiment (CFE)

To perform the nutrient medium optimization by CFE [28], three factors were chosen: glycerol concentration (X1), SPM concentration (X2), and urea concentration (X3). Variations of these factors were arranged on two levels, bottom (–1) and upper (+1). The plan center (Z) was chosen based on the research executed on the influence of these components on the β-carotene biosynthesis and the biomass yield [28]. The sizes of variation steps (δ) for these factors are shown in Table 1.

Table 1. The plan center and the variation step of the studied factors.

Factors	**X1**	**X2**	**X3**
Variables	Glycerol	SMP	Urea
Concentration, g/L	20.0	10.0	1.0
δ, g/L	2.5	1.5	0.15
Low level (–1), g/L	17.5	7.5	0.85
High level (+1), g/L	22.5	11.5	1.15

The number of experiments N was determined by the following formula:

$$N = n \times k, \quad (2)$$

where n is the number of the levels of variation and k is the number of factors.

The regression coefficients were determined using Formulas (3) and (4):

$$b_0 = \frac{\sum \overline{y}}{N}, \quad (3)$$

$$b_i = \frac{\sum [(x)]_{iu} \overline{y}_u}{N}, \quad (4)$$

where N is the number of experiments calculated by Formula (2), $\bar{y}$ is the experimentally obtained value of the parameter, x_{iu} is the value of the variable in the corresponding column of the experiment plan, u is the number of the experimental variant, and i is the number of a factor.

The coefficients of interaction (b_{12}, b_{13}, b_{23}, b_{123}) were determined using Formulas (5) and (6):

$$b_{ij} = \frac{\sum_{u=l}^{N} x_{iu} x_{ji} \overline{y}_u}{N} \tag{5}$$

$$b_{ijk} = \frac{\sum_{u=l}^{N} x_{iu} x_{ji} x_{ku} \overline{y}_u}{N} \tag{6}$$

where x_{iu}, x_{ju}, and x_{ku} are variable values in the corresponding column of the planning matrix and $\bar{y}_u$ is the average value of the optimization parameter.

The line-by-line dispersion was determined by Formula (7):

$$S^2_{y_{ul}} = \frac{\sum (y_{ul})^2 - \frac{(\sum y_{ul})^2}{m}}{m-1}, \tag{7}$$

where u is the row number in the planning matrix, l is the number in each row, and m is the number of parallel experiments.

A single-value dispersion is calculated using Formulas (8) and (9):

$$S^2_{b_i} = \frac{\sum S^2_{y_{ul}}}{mN^2}, \tag{8}$$

$$S_{b_i} = \sqrt{S^2_{b_i}}. \tag{9}$$

The error determination is calculated by Formula (10):

$$| b_i | = t \times S_{bi}, \tag{10}$$

where t is Student's coefficient at $t_{0.9S}$ determined as a tabulated value for the given number of the degrees of freedom (f).

Degrees of freedom were calculated using Formulas (11) and (12):

$$f = (m - 1) \cdot N, \tag{11}$$

where m is the number of parallel experiments and N is the total number of experiments.

$$f_{ad} = N - N', \tag{12}$$

where N is the number of experiments and N' is the number of significant regression coefficients.

The dispersion of adequacy was calculated using Formula (13):

$$S^2_{ad} = \frac{\sum (\overline{y}_u - y_u)^2}{N - N'}, \tag{13}$$

where N is the total number of experiments, N' is the number of significant regression coefficients including b_0, $\bar{y}$ is the experimentally obtained factor value, and y is the factor value calculated by the obtained regression formula.

Then, using Formula (14), the dispersion of reproduction was calculated:

$$S^2_{\overline{y}} = \frac{\sum S^2_{y_{ul}}}{mM}. \tag{14}$$

The Fisher criterion was calculated using Formula (15):

$$F_p = \frac{S_{ad}^2}{S_{\overline{y}}^2}. \quad (15)$$

The uniformity and reproducibility of the experiment were evaluated by the Cochran test (Gp) using table data.

2.6.2. Nutrient Medium Optimization Using the Steepest Ascent Method

The nutrient medium optimization by the steepest ascent method was performed according to [29]. After the assessment of the adequacy of the regression equation and the fulfillment of the $F_m > F_p$ condition, the next optimization stage is carried out using the above-mentioned method. First, the L_i coefficient is found according to Formula (16) to calculate the steepest ascent program:

$$L_i = \delta \times b_i, \quad (16)$$

where δ is the variation step and b_i is the regression coefficient.

The L_i value can be either positive or negative. Therefore, the factor can either increase or decrease. The factor with the maximum $|L_i|$ value is considered as the basic one. Then, the new γ_i coefficients are calculated using Formula (17):

$$\gamma_i = \frac{L_i}{|L_{\max}|}. \quad (17)$$

In the case of the base factor (hbase, Formula (18)), the step for the movement along the gradient is calculated according to Formula (19). First, the "reserve" for the movement along each factor from the basic level up to a practical worthwhile value in the decreasing or increasing direction is calculated by Formula (19).

$$h_{base} = \frac{\Delta i}{n}, \quad (18)$$

$$\Delta i = Xi_{\max} - Xi_0 \ (\Delta i = Xi_0 - Xi_{\min}), \quad (19)$$

were n is the number of steps towards the maximum or minimum value of the Xi_{max} factor. The n number is chosen arbitrarily; as a rule, it varies within 5–8 steps.

The movement step for other factors is calculated using Formula (20):

$$h = h_{base} \times \gamma_i \quad (20)$$

If the regression coefficient of a planning factor is insignificant, then during a calculation of the steepest ascent program, it can be used at the basic level. A new matrix is constructed on the basis of the performed calculations, and then new experiments are performed.

All experiments on the mathematical planning were performed three times, each in three replications. The data shown in the Section 3 represent the means of these experiments.

2.7. M. neoaurum Fermentation in a 3 L Bioreactor

2.7.1. Inoculum Preparation

The procedure of inoculum obtaining was similar to that described in Section 2.4; the following medium composition was used (g/L): glycerol, 25.5; powdered milk, 12.8; citric

acid, 2.2; urea, 1.0; NH_4Cl, 1.0; KH_2PO_4, 0.5; $MgSO_4 \cdot 7H_2O$, 0.5; $FeSO_4 \cdot 7H_2O$, 0.05; and $CaCO_3$, 1.5 (pre-sterilization pH 6.8–7.2). Prior to the inoculation of the bioreactor, the inoculum was microscoped using a Carl Zeiss Primo Star microscope (Carl Zeiss, Jena, Germany) for the quality control. The inoculum volume further used for the bioreactor seeding was 10% of the fermentation medium volume (150 mL). The inoculum was added in the bioreactor via a sterile inoculum feeding line.

2.7.2. Bioreactor Preparation and Fermentation

M. neoaurum fermentation in a 3 L bioreactor was performed as described earlier [27]. After the completion of the process, the biomass was inactivated by a 30-min heating at 80–85 °C with continuous stirring, then transferred out into a collection vessel, centrifuged, and dried in a Martin Christ ALPHA 2-4LD plus freeze dryer (Martin Christ Gefriertrocknungsanlagen GmbH, Osterode am Harz, Germany).

2.8. M. neoaurum Fermentation in a 15 L Bioreactor

2.8.1. Inoculum Preparation

An inoculum was produced in accordance with the procedure described in Section 2.4; the medium composition was the same as described in Section 2.7.1. The inoculum obtained in flasks was combined under sterile conditions into one 2 L flask with the bottom outlet. The total volume of the inoculum was 1.0 L. Prior to the inoculation of the bioreactor, the quality of inoculum was examined using a Carl Zeiss Primo Star microscope (Carl Zeiss, Jena, Germany). The inoculum was transferred into the bioreactor via a sterile inoculum feeding line.

2.8.2. Bioreactor Preparation

The fermentation system used in the study consisted of a computer-based automatic control unit and three 15 L bioreactors (Prointech-Bio, Pushchino, Russia) connected via the coupling elements with the feed lines for the direct steam, compressed air, and water. The effective volume of bioreactors was 10 L. The units for monitoring culture broth parameters included a Buk-3 thermal sensor connected to a controller (Keklab Group, Moscow, Russia); an InPro 6800/12/220 oxygen sensor (Mettler Toledo, Greifensee, Switzerland) connected to a controller regulating the work of the mechanical stirring device; and an InPro3300/225/PT1000 pH sensor (Mettler Toledo, Greifensee, Switzerland) connected via a controller to a peristaltic pump delivering a titrating solution.

Bioreactors were equipped with 0.2 μm fine filters for compressed air. The preparation and sterilization of the fermentation medium (see Section 2.8.1 for the medium composition) were carried out directly within the bioreactor. Preliminarily, bioreactors with the air filters were sterilized for 1 h at 121 ± 2 °C. Then, all components of the fermentation medium were sequentially loaded into each bioreactor through a receiver, and the volume of the medium was adjusted to 10.0 L with purified water. If necessary, the pH level was adjusted to 6.8–7.2. The medium was sterilized for 1 h at 125 ± 1 °C by introducing direct steam into the bioreactor through a bubbler, sample collector, and bottom outlet.

2.8.3. *M. neoaurum* Fermentation

The pre-inoculation fermentation regime is shown in Table 2. The level of pO_2 was controlled by changing the air supply volume to culture broth volume ratio (manual mode) via changes in the stirrer's rpm number (automatic mode). For both regimes, the fermentation process duration was 82 h. The basic fermentation parameters are shown in Table 3.

Table 2. Pre-inoculation fermentation regime (15 L bioreactor).

Parameter	Value
Medium volume	10.0 L
Temperature	35 ± 1 °C
Aeration	0.1 L/min

Table 2. *Cont.*

Parameter	Value
Stirring rate	250 rpm
pO_2 level	100% of saturation
Pressure within the bioreactor	0.03–0.05 MPa
Medium pH	6.8–7.2

Table 3. Basic parameters for the *M. neoaurum* strain AC-3067D fermentation in a 15 L bioreactor.

Parameter	Value
Temperature	35 ± 1 °C
Aeration	5–10 L/min
pH	6.8–7.2
Stirring rate	400–450 rpm to maintain the required level of dissolved oxygen
Feeding addition	Glycerol (2.5 g/L) after 30 h of fermentation
Fermentation time	72–76 h
Process control	The first sampling to control the culture purity and crude biomass weight is performed after 18–24 h of fermentation. The further sampling is performed as required, but at least one time a day.

Upon the completion of fermentation, the biomass of *M. neoaurum* was either inactivated (see Section 2.7.2) or transferred via a seed train to seed a 100 L bioreactor.

2.9. M. neoaurum Fermentation in a 100 L Bioreactor

2.9.1. Inoculum Preparation

The inoculum for the bioreactor was obtained as described in Section 2.8.

2.9.2. Bioreactor Preparation

A 100 L bioreactor was connected via the control unit with the feed lines for the steam, compressed air, and water as well as with an automatic control unit. The effective volume of the bioreactor ranged from 60 to 70 L. The measurement devices required to control fermentation medium parameters included a Buk-3 thermal sensor connected to a controller (Keklab Group, Moscow, Russia), an InPro 6800/12/220 sensor for dissolved oxygen (Mettler Toledo, Greifensee, Switzerland), connected via a controller to the mechanical stirring device, and an InPro3300/225/PT1000 pH sensor (Mettler Toledo, Greifensee, Switzerland) intended to manage the supply of a titrant solution by a peristaltic pump via the controller.

The fermentation medium was mixed by a mechanical stirring device characterized by the motor located on the top and the end seal; the stirring rate ranged from 50 to 600 rpm. The pO_2 level was regulated by manual adjusting the air flow volume compared to the fermentation medium volume and by automatic change in the stirring rate. The medium

was sterilized directly in the bioreactor. After sterilization, the air flow rate and the pressure within the bioreactor were set to be 35 L/min and 0.03 MPa, respectively; the dissolved oxygen concentration in the medium was set to 100%. After the cooling of the bioreactor to 29–30 °C, a sterile medium sample was taken for a microbiological analysis.

2.9.3. *M. neoaurum* Fermentation

The pre-inoculation fermentation regime is shown in Table 4. The pO_2 level was regulated by manual adjusting the air flow rate relative to the volume of the culture medium with the automatic changes in the rpm number of the stirrer. For both regimes, the process was conducted for 72–74 h. The basic fermentation parameters are shown in Table 5.

Table 4. Pre-inoculation fermentation regime (100 L bioreactor).

Parameter	Value
Medium volume	70.0 L
Temperature	35 ± 1 °C
Aeration	3.5 L/min
Stirring rate	250 rpm
pO_2 level	100% of saturation
Pressure within the bioreactor	0.03–0.05 MPa
Medium pH	6.8–7.2

Table 5. Basic parameters for a *M. neoaurum* strain AC-3067D fermentation in a 100 L bioreactor.

Parameter	Value
Temperature	35 °C
Aeration	35–70 L/min
pH	Maintained at 6.8–7.2 using a sterile 10% HCl solution
Stirring rate	400–450 rpm to maintain the required level of dissolved oxygen
Feeding addition	50% glycerol solution (2.5 g/L of medium) after 30 h of fermentation
Fermentation time	72–80 h

Upon the completion of fermentation, the biomass of *M. neoaurum* was inactivated (see Section 2.7.2) and collected into a collector. After centrifugation, it was dried in a Martin Christ ALPHA 2-4LD plus freeze dryer (Martin Christ Gefriertrocknungsanlagen GmbH, Osterode am Harz, Germany).

3. Results

3.1. Optimization of Nutrient Medium Composition by CFE 2^3

In this study, the composition of the nutrient medium was optimized by the steepest ascent method, which combines CFE with the Wilson–Box method. The planning factors included the concentrations of glycerol, a surfactant (SMP), and urea (see Table 1). The output parameter of optimization (y) was determined as the content of β-carotene (mg/g) in the culture broth (CB). The number of experiments was determined using Formula (2) (N = 8 for this study); based on this, the experimental planning matrix for CFE 2^3 was constructed (Table 6). Using this matrix, a series of experiments was conducted, each in three replications. The results are shown in Table 3.

The mathematical model equation should be the following:

$$\bar{y} = b_0 + b_1x_1 + b_2x_2 + b_3x_3,$$

where $\bar{y}$ is the process optimization parameter, b_i is a regression coefficient indicating the influence of factors on the optimization parameters, and x is the value of a factor level in encoded units. The homogeneity and reproducibility of the experiment were evaluated using Cochran's criterion (Gp). For the obtained data, Gp = 0.2594, which is less than the tabulated value for the used degrees of freedom (0.2594 < 0.5157). Thus, we concluded that the obtained data are homogenous and reproducible.

Table 6. The experimental matrix in natural and encoded units of factor values and the results of the experiment (output parameter values).

Experiment No.	Encoded Factors			Natural-Scale Factors, g/L			β-Carotene Yield, mg/kg			
	x_1	x_2	x_3	x_1	x_2	x_3	y_1 *	y_2 *	y_3 *	$\bar{y}_u$ **
1	−1	−1	−1	17.5	8.5	0.85	182.5	170.4	186.2	179.70
2	+1	−1	−1	22.5	8.5	0.85	206.2	196.5	188.4	197.03
3	−1	+1	−1	17.5	11.5	0.85	190.6	198.5	188.6	192.57
4	+1	+1	−1	22.5	11.5	0.85	248.3	220.4	229.5	232.73
5	−1	−1	+1	17.5	8.5	1.15	180.8	188.5	183.8	184.37
6	+1	−1	+1	22.5	8.5	1.15	204.3	227.4	214.5	215.40
7	−1	+1	+1	17.5	11.5	1.15	196.6	202.6	220.7	206.63
8	+1	+1	+1	22.5	11.5	1.15	216.7	200.8	218.7	212.07

* y_1, y_2, and y_3 represent the numerical values of the response function for each of the replications obtained after the completion of the experiment, mg/kg; ** $\bar{y}_u$ is the mean arithmetical value of the response function, mg/kg.

To determine the direction of action for each factor, regression coefficients were calculated using Formulas (3) and (4): b_0 = 202.56, b_1 = 11.75, b_2 = 8.44, and b_3 = 2.05. Then, using the data presented in Table 6, the significance of the calculated regression coefficients was determined for m = 3, where m is the number of parallel experiments. The line-by-line dispersion was calculated using Formula (7), where m = 3 represents the number of parallel experiments and N = 8 represents the total number of experiments. The results are shown in Table 7.

Table 7. Determination of line-by-line dispersions.

u	y_{ul}			$\sum(y_{ul})^2$	$(\sum y_{ul})^2$	$\frac{(\sum y_{ul})^2}{m}$	$S^2_{y_{ul}}$
1	182.5	170.4	186.2	97,012.85	290,628.81	96,876.27	68.29
2	206.2	196.5	188.4	116,625.25	349,399.21	116,466.40	79.42
3	190.6	198.5	188.6	111,300.57	333,737.29	111,245.76	27.40
4	248.3	220.4	229.5	162,899.3	487,483.24	162,494.41	202.44
5	180.8	188.5	183.8	102,003.33	305,919.61	101,973.20	15.06
6	204.3	227.4	214.5	139,459.5	417,574.44	139,191.48	134.01
7	196.6	202.6	220.7	128,406.81	384,276.01	128,092.00	157.40
8	216.7	200.8	218.7	135,109.22	404,750.44	134,916.81	96.20
							$\sum$ = 780.24

Using Formulas (8) and (9), a single-value dispersion (S_{bi}) was calculated to be equal to 2.02. Then, using Formula (10) with t = 2.09, the error determination was calculated

(tS_{b_i} = 4.21). Therefore, regression coefficients are significant in the case when $|bi| > 4.21$, and the regression equation takes the following form:

$$y = 202.56 + 11.75x_1 + 8.44x_2 \quad (21)$$

To evaluate the adequacy of the obtained linear approximation equation, Equation (21), the β-carotene yield (y) was calculated for each variant. The x_1 and x_2 values were taken from Table 6. The results of the performed calculations are shown in Table 8.

Using Formula (12), the dispersion of adequacy S^2_{ad} was determined at $N - N' = 5$. According to the performed calculations, S^2_{ad} = 164.33. Using Formula (13), the dispersion of reproducibility $S^2_{\bar{y}}$ = 32.51 was calculated. The Fisher criterion Fp = 5.05 was calculated by Formula (14).

Table 8. The determination of the deviation square for the average values obtained experimentally and those calculated by the linear approximation equation.

u	y_{ul}	$\bar{y}_u$	$\bar{y}_u - y_u$	$(\bar{y}_u - y_u)^2$
1	182.38	179.70	−2.68	7.18
2	205.87	197.03	−8.84	78.10
3	199.25	192.57	−6.69	44.72
4	222.75	232.73	9.99	99.75
5	182.38	184.37	1.99	3.95
6	205.87	215.40	9.53	90.81
7	199.25	206.63	7.38	54.45
8	222.75	212.07	−10.68	114.04
				$\sum$ = 493.00

The tabulated value of the Fisher criterion (F_t) is located at the intersection of the values of the degree of freedom of the dispersion of adequacy (f_{ad} = 5) and the number of degrees of freedom of the dispersion of reproducibility (f = 16).

Since $F_p > F_t$ (5.05 > 2.85), then, first, the equation is inadequate (i.e., the process cannot be described by the linear approximation equation). Second, the obtained results evidence that the process is close to the near-optimum area, when the influence of the interaction between factors is enhanced.

If the process cannot be described by the linear approximation equation, it is possible to use a complete factorial experiment with allowance for all interactions between factors. A new planning matrix and the results obtained during the experiment implementation are shown in Table 9.

Table 9. Experimental plan and obtained results.

Experiment No.	Factors at a Natural Scale, g/L			Encoded Factors			Auxiliary Graphs in a CFE 23 Matrix				B-Carotene Yield, mg/kg			
	x_1	x_2	x_3	x_1	x_2	x_3	x_1x_2	x_2x_3	x_1x_3	$x_1x_2x_3$	y_1 *	y_2 *	y_3 *	$\bar{y}_u$ **
1	17.5	8.5	0.85	−1	−1	−1	+1	+1	+1	−1	182.5	170.4	186.2	179.70
2	22.5	8.5	0.85	+1	−1	−1	−1	+1	−1	+	206.2	196.5	188.4	197.03
3	17.5	11.5	0.85	−1	+1	−1	−1	−1	+1	+1	190.6	198.5	188.6	192.57
4	22.5	11.5	0.85	+1	+1	−1	+1	−1	−1	−1	248.3	220.4	229.5	232.73
5	17.5	8.5	1.15	−1	−1	+1	+1	−1	−1	+	180.8	188.5	183.8	184.37
6	22.5	8.5	1.15	+1	−1	+1	−1	−1	+1	−1	204.3	227.4	214.5	215.40
7	17.5	11.5	1.15	−1	+1	+1	−1	+1	−1	−1	196.6	202.6	220.7	206.63
8	22.5	11.5	1.15	+1	+1	+1	+1	+1	+1	+1	216.7	200.8	218.7	212.07

* y_1, y_2, and y_3 represent the numerical values of the response function for each of the replications obtained after the completion of the experiment, mg/kg; ** $\bar{y}_u$ is the mean arithmetical value of the response function, mg/kg.

The regression equation obtained by the use of CFE 2^3 is the following:

$$y = b_0 + b_1x_1 + b_2x_2 + b_3x_3 + b_{12}x_1x_2 + + b_{13}x_1x_3 + + b_{23}x_2x_3 + b_{123}x_1x_2x_3.$$

Using Formulas (3)–(6), coefficients of regression were calculated. The regression equation has the following form:

$$y = 202.56 + 11.75x_1 + 8.44x_2 - 6.05x_2x_3 - 6.5x_1x_2x_3 \quad (22)$$

Then, the adequacy of the obtained linear approximation equation, Equation (22), was determined. To achieve this, a dry biomass yield (y) was calculated for each variant using the regression equation. The results of this calculation are shown in Table 10.

Table 10. The deviation square for the means determined experimentally and by the linear approximation equation.

u	y_{ul}	$\bar{y}_u$	$\bar{y}_u - y_u$	$(\bar{y}_u - y_u)^2$
1	194.49	179.70	−14.79	218.67
2	193.76	197.03	3.27	10.70
3	187.15	192.57	5.42	29.39
4	234.85	232.73	−2.12	4.50
5	170.27	184.37	14.10	198.69
6	217.98	215.40	−2.58	6.65
7	211.36	206.63	−4.73	22.37
8	210.64	212.07	1.43	2.04
				$\sum = 493.00$

The dispersion of adequacy was calculated using Formula (13). According to the performed calculations, the dispersion of adequacy was equal to 98.60. The dispersion of reproduction calculated earlier by Formula (14) was 32.51. The Fisher criterion F_p calculated by Formula (15) was equal to 3.03. The tabulated value of the Fisher criterion (F_t) was determined at $f_{ad} = 3$ and $f = 16$. Since $F_p < F_t$ (3.03 < 3.24), then, the obtained regression equation (Formula (21)) is adequate to the studied process. Therefore, the biomass yield within the studied concentration range is positively influenced by an increase in the glycerol and SMP concentrations. At the same time, the effect of these factors is enhanced in the case of a combined action of x_1 and x_2 or x_1, x_2, and x_3 factors (if these factors are at the highest coordination level).

3.2. The Optimization of the Nutrient Medium Composition by the Steepest Ascent Method

Based on the results of the performed CFE, one can suppose the efficiency of the steepest ascent method for the further medium optimization. Since the coefficient of regression b_3 was determined as insignificant, then the urea concentration was further considered as a constant variable equal to 1.0 g/L.

The initial data required for the construction of a new planning matrix are shown in Table 11.

Table 11. The calculation of the steepest ascent for the determination of the quantitative ratio of medium components.

Factor and Experiment Characteristics	X_1 Glycerol Concentration	X_2 SPM Concentration
Base level, g/L	22.5	11.5
Maximum level, g/L	30.0	15.0
Stock, Δ_i	7.5	4.5
Variation interval (δ_i)	2.5	1.5
Coefficient of regression (b_i)	11.75	8.44
Production $L_i = b_i\delta_i$	29.34	12.66
Coefficient (γ_i)	0.26	0.59
Steepest ascent step (h_i), g/L	1.5	0.65

Since the value of the γ_i coefficient for glycerol is less than that for SMP, this factor was considered as the base one. The steepest ascent steps for glycerol and SMP are presented in Table 11. In all variants, the urea concentration was 1.0 g/L. A new experimental design matrix was created, and the β-carotene yield was determined. The results are shown in Table 12.

Table 12. The planning matrix for the experiment based on the steepest ascent method.

Experiment No.	X_1 (Glycerol Concentration, g/L)	X_2 (SMP Concentration, g/L)	β-Carotene Yield, mg/kg
1 (initial medium)	22.5	11.5	248.3 ± 5.7
2	24.0	12.15	284.5 ± 8.2
3	25.5	12.80	318.4 ± 8.3
4	27.0	13.45	292.4 ± 6.4
5	28.5	14.10	252.1 ± 5.5
6	30.0	14.75	224.6 ± 8.2

The maximum β-carotene yield (318.4 ± 8.3 mg/kg) was obtained for variant 3, where the nutrient medium contained 25.5 g/L of glycerol and 12.8 g/L SMP. The further increase in the glycerol and SMP concentrations up to 30.0 and 14.75 g/L, respectively, was accompanied with the inhibition of a pigment accumulation process.

Thus, a new composition of the fermentation medium was proposed. The next stage of work included the examination of this medium composition for the cultivation of *M. neoaurum* in a 3 L bioreactor.

3.3. M. neoaurum Fermentation in a 3 L Bioreactor

Earlier, we studied the effect of the temperature, dissolved oxygen level, and acidity of a culture medium on the biomass accumulation and β-carotene production by *M. neoaurum* [27]. The optimal pH values were found to fall within the range of 6.8–7.0, and the optimal O_2 concentration was 50%. Therefore, these parameters were maintained at a constant level during *M. neoaurum* fermentation in the bioreactor as described in the Section 2.

After 30 h of fermentation, a sterile 50% glycerol solution (2.5 g/L of fermentation medium) was added under controlled optimal pH and O_2 concentration (6.8–7.2 and 50%, respectively). Glycerol addition started automatically, when pH exceeded 7.0, and the dissolved oxygen concentration decreased. The results are shown in Figure 1. The productivity of *M. neoaurum* in terms of the β-carotene production and the maximum biomass increase was recorded after 72 h of fermentation and reached 370.5 mg/kg and 25.4 g/L, respectively.

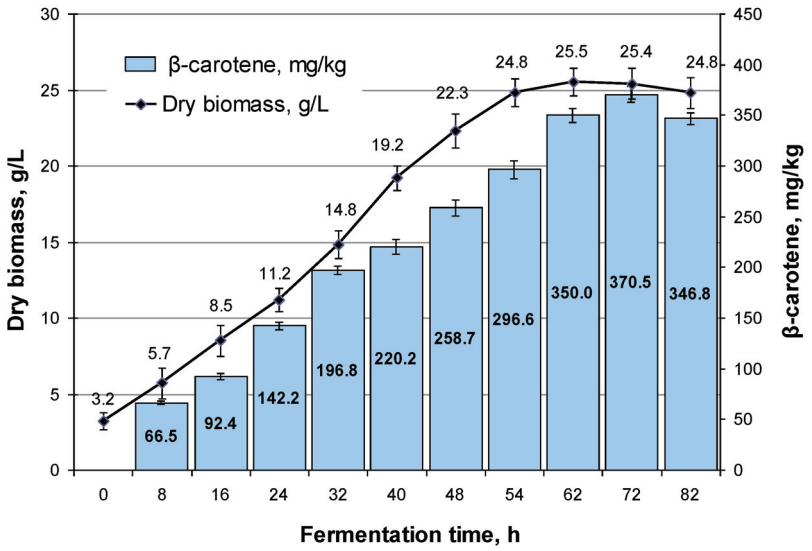

Figure 1. Biomass yield and β-carotene accumulation during fermentation of *M. neoaurum* in 3 L fermenter with culture feeding by 2.5 g/L glycerol after 30 h of cultivation.

3.4. M. neoaurum Fermentation in a 15 L Bioreactor

The fermentation of *M. neoaurum* in a 15 L bioreactor was performed under the same conditions as described in Section 3.3. The results are shown in Figure 2. The β-carotene productivity of *M. neoaurum* and the maximum biomass yield observed after 72 h of fermentation reached 432.3 ± 10.4 mg/kg and 23.2 ± 1.2 g/L, respectively.

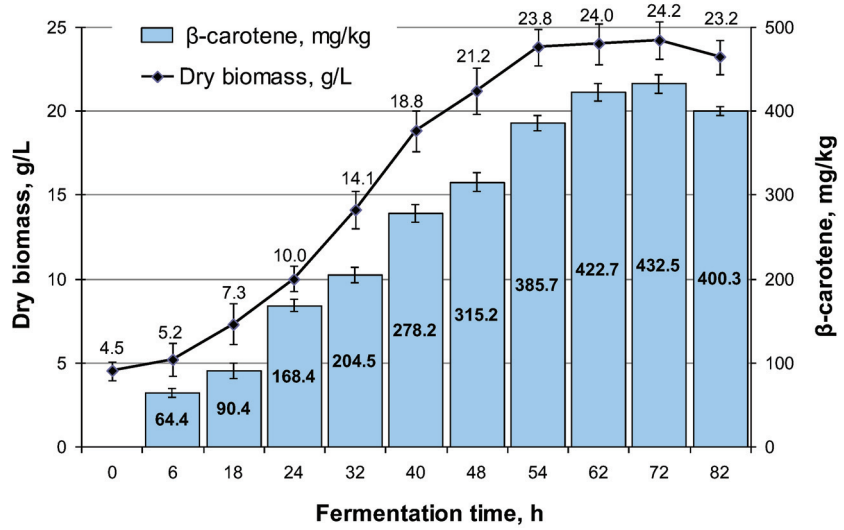

Figure 2. Biomass yield and β-carotene accumulation during fermentation of *M. neoaurum* in 15 L fermenter with culture feeding (50% glycerol, 2.5 g/L) after 30 h of cultivation.

3.5. M. neoaurum Fermentation in a 100 L Bioreactor

The fermentation of *M. neoaurum* in a 100 L bioreactor was performed under the constant pH (6.8–7.2), and the pO_2 value of 50% or more. After 30 h of fermentation, a sterile 50% glycerol solution (2.5 g/L of fermentation medium) was added in an automatic mode. The results are shown in Figure 3. The β-carotene productivity and the maximum biomass yield of the Ac-3067D strain observed after 72 h of fermentation reached 450.4 ± 8.2 mg/kg and 25.2 ± 1.1 g/L, respectively.

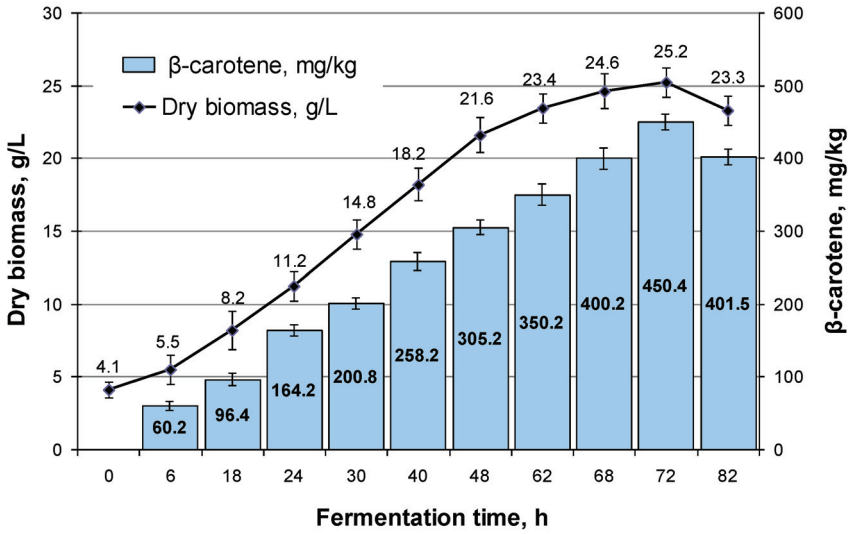

Figure 3. Biomass yield and β-carotene accumulation during fermentation of *M. neoaurum* in 100 L fermenter with culture feeding (50% glycerol, 2.5 g/L) after 30 h of cultivation.

4. Discussion

One of the most challenging tasks for biotechnological processes based on the use of overproducing strains is the selection and optimization of fermentation conditions. The analysis of numerous data shows that the growth of a culture and the biosynthesis of secondary metabolites are influenced by such factors as the viability of the planting material, the composition of the cultivation medium, and physicochemical conditions of fermentation. However, one should note that optimal conditions for the cell growth and the target product biosynthesis may not coincide [29–31].

Traditional approaches for the optimization of the β-carotene production are based on the change in one parameter at a time. However, this approach often does not allow a researcher to determine variables responsible for the optimal result, since such approaches do not take into account possible interaction between different factors [24]. One of the effective methods for optimizing cultivation conditions is a combination of the experimental and mathematical modeling with the conduction of a computational experiment, which includes an important step, namely, the determination of a mathematical model, i.e., a regression equation, which characterizes the relationship between the optimization parameter and the main factors. An approach based on the design of experiments (DOE) makes it possible to not only efficiently evaluate the main effects and interactions using a minimal number of experiments, but also relatively rapidly conclude on the significance of various components of the nutrient medium as well as to determine its qualitative and quantitative composition [20–24]. Mathematical modeling is widely used to determine optimal cultivation conditions for highly active strains. Numerous publications describe different examples of the DOE use for the development of processes occurring in biotechnological plants. However, one should note that this study represents the first attempt to use mathematical modeling for the optimization of the *M. neoaurum* cultivation conditions.

This study investigated the influence of three key factors (glycerol, SMP, and urea) on the β-carotene productivity of *M. neoaurum*. We found that glycerol and SMP provided the greatest impact on the pigment yield. The stimulation of the carotenoid biosynthesis can be explained by the fact that glycerol is involved in the biosynthesis of isoprenoids representing precursors of carotenoids (Figure 4). Use of glycerol as a carbon source for the β-carotene biosynthesis was also demonstrated in some other studies. For example, Bindea et al. [32] studied the effect of pH and glycerol concentration on a pigment accu-

mulation. In addition, a positive effect of a glycerol addition into the nutrient medium on the carotenoid biosynthesis was reported by Suwaleerat et al. [33] for *Rhodococcus opacus* PD630. According to the obtained regression equation, the factors that have the greatest influence on the biosynthesis of β-carotene by *M. neoaurum* cells include glycerol and SMP concentrations. Using the mathematical planning method, the optimal values of these concentrations were determined as 25.5 and 12.80 g/L, respectively.

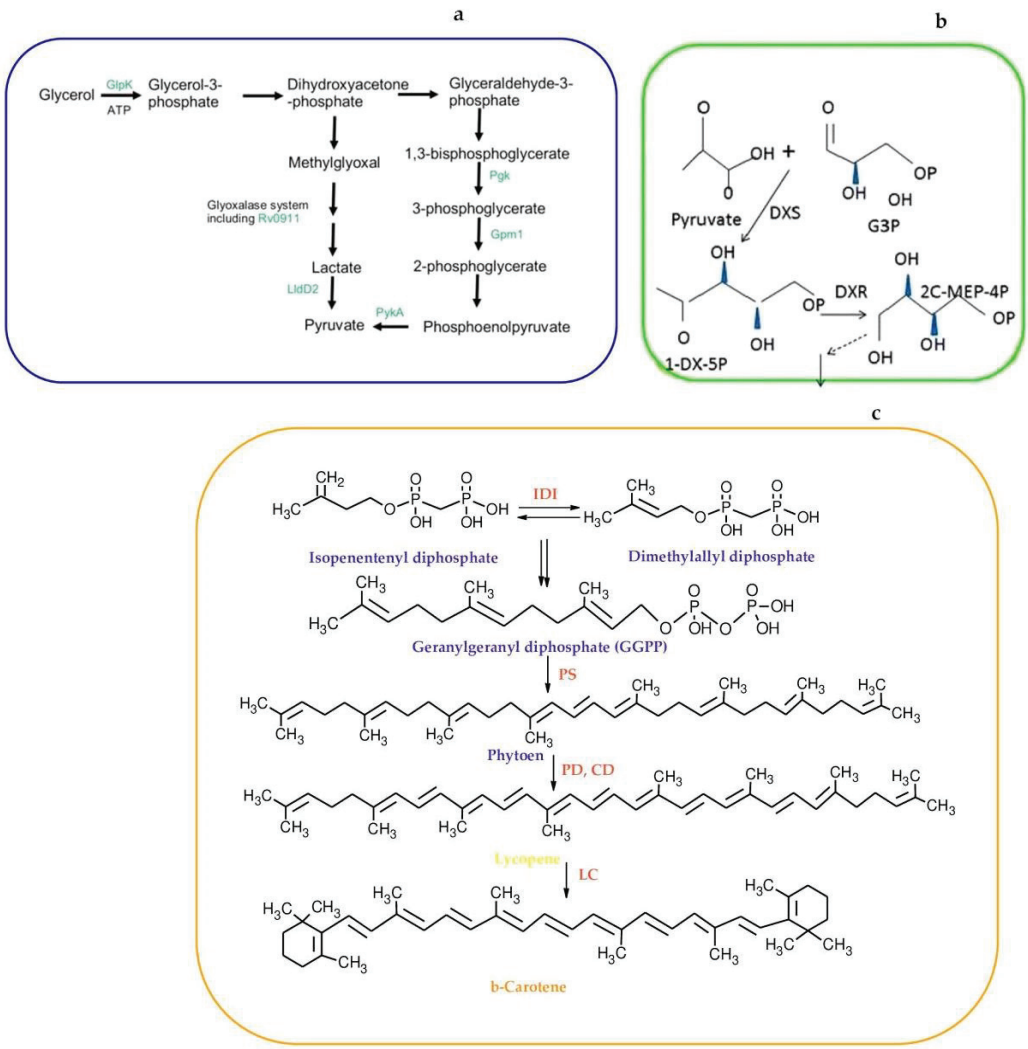

Figure 4. Proposed pathway for carotenoid biosynthesis in *M. neoaurum* based on published data: (**a**) pyruvate production from glycerol [34]; (**b**) biosynthetic pathways of isoprenoids [35]; (**c**) general scheme of carotenoid biosynthesis [36]. 1-DX-5P, deoxyxylulose 5-phosphate; 2C-MEP-4P, 2-C-methyl-D-erythritol 4-phosphate; CD, carotene desaturase; DXR, 1-deoxy-D-xylose 5-phosphate reducto-isomerase; DXS, 1-deoxy-D-xylose 5-phosphate synthase; G3P, glycerolaldehyde-3-phosphate; Glpk, glycerol kinase; Gpm1, phosphoglycerate mutase 1; IDI, diphosphate isomerase; LC, lycopene β-cyclase; LldD2, lactate dehydrogenase; PD, phytoene desaturase; Pgk, phosphoglycerate kinase; PS, phytoene synthase; PykA, pyruvate kinase; Rv0911, putative glyoxalase.

The influence of the nitrogen sources on the development and morphology of microorganisms and also on the synthesis of secondary metabolites is determined by the importance of this element as a constituent of nucleotides and amino acids representing building blocks of enzymes providing the biosynthetic processes. However, according to some data, the greatest effect on the carotenoid biosynthesis is provided by carbon rather than nitrogen [37], which was confirmed in the current study.

As a rule, microbial biosynthesis technologies are initially developed under laboratory conditions and then scaled up to the pilot and then industrial scales. The main task of the scale-up process is to increase the volume of production while maintaining or even increasing the productivity of the used strain [38,39]. High cell density in fermenters significantly differs from their natural growth conditions and results in some stresses related to various environmental factors such as changes in temperature, pH, osmotic concentrations, etc. [40].

Published data related to the industrial technologies of β-carotene production by *M. neoaurum* are rather poor. The majority of publications are focused on optimizing fermentation conditions for such producers as *Blakeslea trispora* and *Rhodotorula* spp. There is also a study describing the optimization of fermentation conditions of *Yarrowia lipolytica*. A successful modification of the original strain and optimization of batch fermentation conditions for a 5 L bioreactor provided a β-carotene yield of 2.7 g/L [41]. Another study reports about the fermentation of a genetically modified *Yarrowia lipolytica* strain, YL-C0, in a 5 L bioreactor with the constant glucose concentration of 10.0 g/L, pO_2 level maintained at 20–30% by adjusting the stirring rate, and pH level maintained at 5.5 using a 15% ammonia solution; under such conditions, the maximum β-carotene yield reached 1.7 g/L [42].

It is known that the reduction in the concentration of carbon and/or nitrogen sources causes some disorders in the biosynthesis of secondary metabolites including β-carotene. In the case of periodic processes, this problem can be solved by additional feeding of the limiting substrate, thus avoiding a suppressive effect of initially high substrate concentrations and increasing the yield of a target metabolite. Therefore, after 30 h of fermentation, a sterile 50% glycerol solution (2.5 g/L of a fermentation medium) was added under controlled optimal pH and pO_2 conditions (6.8–7.2 and 50%, respectively). A continuous supply of a 50% glycerol solution during fermentation also helps to stabilize the pH level due to the formation of organic acids during its metabolization [43]. Such pH stabilization promotes more active biosynthesis of β-carotene.

In this study, *M. neoaurum* cultivation in flasks under selected conditions resulted in a β-carotene yield of 318.4 ± 8.3 mg/kg. When the optimized medium was tested in a 3 L bioreactor, β-carotene and dry biomass yields were 370.5 ± 8.0 mg/kg and 25.4 ± 1.0 g/L, respectively. These results allowed us to perform a step-by-step scaling up of the process in 15 L and 100 L bioreactors. For the 15 L bioreactor, β-carotene and dry biomass yields reached 432.3 ± 10.4 mg/kg and 22.2 ± 1.2 g/L, respectively. In the case of the 100 L bioreactor, the strain productivity for β-carotene was 450.4 ± 11.0 mg/kg, while the dry biomass yield was 25.2 ± 1.1 g/L. Note that the scaling up from the 3 L to 100 L bioreactor provided an increase in the β-carotene yield by 21.7% that can be associated with the improved aeration conditions.

Aeration is a key parameter, which should be considered for the production of this class of pigments, since the biosynthesis of carotenoids is an aerobic process. The air flow rate during microbial fermentation is an important factor providing the nutrient absorption, growth rate, cell mass accumulation, and carotenoid biosynthesis. In addition, according to some published data, a decrease in the oxygen content in the culture medium affects the production of carotenoids and xanthophylls [31]. The effect of aeration can depend on the microorganism species.

Moreover, the development of a biotechnological process should take into account such factors as the design of the bioreactor, used raw materials, and fermentation type (batch, fed-batch, or continuous). These factors play a very important role in achieving the desired yield of target metabolites, including β-carotene [31].

5. Conclusions

The performed study showed that the biosynthesis of β-carotene by *M. neoaurum* cells is influenced mainly by the glycerol and SMP concentration. Using mathematical planning, we optimized a nutrient medium composition for *M. neoaurum* fermentation and β-carotene biosynthesis and determined the optimal glycerol and SMP concentrations (25.5 and 12.8 g/L, respectively). Under such cultivation conditions, the β-carotene production by the *M. neoaurum* strain AC-3067D in 750 mL flasks was 318.4 ± 8.3 mg/kg. In the case of a 15 L bioreactor, the β-carotene and biomass yields were 432.3 ± 10.4 mg/kg and 23.2 ± 1.2 g/L, respectively. The further scaling up to a 100 L bioreactor increased the yield of β-carotene and the biomass up to 450.4 ± 8.2 mg/kg and 25.2 ± 1.1 g/L, respectively.

The obtained results demonstrate the potential of the application of the *M. neoaurum* strain AC-3067D for industrial β-carotene production. The further work planned with this strain includes determining cultivation conditions and optimal fermentation parameters for pilot-scale and industrial conditions with the process scaling up to a 1000 L bioreactor.

Author Contributions: Conceptualization, V.V.Y. and E.V.G.; methodology, N.V.K., E.V.G. and A.S.S.; software, V.V.Y.; validation, E.V.G., N.V.K. and V.V.Y.; formal analysis, V.V.D.; investigation, N.V.K., V.V.Y. and V.V.D.; data curation, V.V.Y.; writing—original draft preparation, N.V.K. and A.S.S.; writing—review and editing, V.V.Y. and V.V.D.; visualization, V.V.Y. and A.S.S.; supervision, V.V.D. and E.V.G.; project administration, V.V.D.; funding acquisition, V.V.D. All authors have read and agreed to the published version of the manuscript.

Funding: The study was carried out within the State Assignment of the Ministry of Science and Higher Education of the Russian Federation (theme no. 123012000071-1).

Institutional Review Board Statement: Not applicable.

Informed Consent Statement: Not applicable.

Data Availability Statement: The original contributions presented in this study are included in the article. Further inquiries can be directed to the corresponding author(s).

Conflicts of Interest: The authors declare no conflicts of interest.

References

1. Maoka, T. Carotenoids: Distribution, function in nature, and analysis using LC-photodiode array detector (DAD)-MS and MS/MS system. *Mass Spectrom* **2023**, *12*, A0133. [CrossRef]
2. Maoka, T. Carotenoids as natural functional pigments. *J. Nat. Med.* **2020**, *74*, 1–16. [CrossRef]
3. Yaderets, V.V.; Karpova, N.V.; Glagoleva, E.V.; Petrova, K.S.; Shibaeva, A.S.; Dzhavakhiya, V.V. Carotenoids: Overview of the main methods and conditions of their preparation. *Proc. Univ. Appl. Chem. Biotechnol.* **2024**, *14*, 41–54. (In Russian) [CrossRef]
4. Ashokkumar, V.; Flora, G.; Sevanan, M.; Sripriya, R.; Chen, W.H.; Park, J.H.; Rajesh Banu, J.; Kumar, G. Technological advances in the production of carotenoids and their applications—A critical review. *Bioresour. Technol.* **2023**, *367*, 128215. [CrossRef] [PubMed]
5. Foong, L.C.; Loh, C.W.L.; Ng, H.S.; Lan, J.C. Recent development in the production strategies of microbial carotenoids. *World J. Microbiol. Biotechnol.* **2021**, *37*, 12. [CrossRef] [PubMed]
6. Ernst, H. Recent advances in industrial carotenoid synthesis. *Pure Appl. Chem.* **2002**, *74*, 2213–2226. [CrossRef]
7. Lim, K.C.; Yusoff, F.M.; Shariff, M.; Kamarudin, M.S. Astaxanthin as feed supplement in aquatic animals. *Rev. Aquac.* **2017**, *10*, 738–773. [CrossRef]
8. Botella-Pavía, P.; Rodríguez-Concepción, M. Carotenoid biotechnology in plants for nutritionally improved foods. *Physiol. Plant.* **2006**, *126*, 369–381. [CrossRef]
9. Gong, M.; Bassi, A. Carotenoids from microalgae: A review of recent developments. *Biotechnol. Adv.* **2016**, *34*, 1396–1412. [CrossRef] [PubMed]
10. Rodriguez-Amaya, D.B. Update on natural food pigments – A mini-review on carotenoids, anthocyanins, and betalains. *Food Res. Int.* **2019**, *124*, 200–205. [CrossRef] [PubMed]

11. Choi, S.S.; Kim, G.D. Production of carotenoids by bacteria: Carotenoid productivity and availability. *J. Life Sci.* **2022**, *32*, 411–419. [CrossRef]
12. El Baky, H.H.A.; El Baroty, G.S.; Mostafa, E.M. Optimization growth of *Spirulina (Arthrospira) platensis* in photobioreactor under varied nitrogen concentration for maximized biomass, carotenoids and lipid contents. *Recent Pat. Food. Nutr. Agric.* **2018**, *11*, 40–48. [CrossRef] [PubMed]
13. Aneesh, P.A.; Ajeeshkumar, K.K.R.G.; Kumar Lekshmi, R.; Anandan, C.N.; Ravishankar, S.M. Bioactivities of astaxanthin from natural sources, augmenting its biomedical potential: A review. *Trends Food Sci. Technol.* **2022**, *125*, 81–90. [CrossRef]
14. Frusciante, S.; Diretto, G.; Bruno, M.; Ferrante, P.; Pietrella, M.; Prado-Cabrero, A.; Rubio-Moraga, A.; Beyer, P.; Gomez-Gomez, L.; Al-Babili, S.; et al. Novel carotenoid cleavage dioxygenase catalyzes the first dedicated step in saffron crocin biosynthesis. *Proc. Natl. Acad. Sci. USA* **2014**, *111*, 12246–12251. [CrossRef]
15. Asker, D. Isolation and characterization of a novel, highly selective astaxanthin-producing marine bacterium. *Agric. Food Chem.* **2017**, *65*, 101–9109. [CrossRef] [PubMed]
16. Silva, T.P.; Paixão, S.M.; Alves, L. Ability of *Gordonia alkanivorans* strain 1B for high added value carotenoids production. *RSC Adv.* **2018**, *5*, 58055. [CrossRef]
17. Tran, T.; Dawrs, S.N.; Norton, G.J.; Virdi, R.; Honda, J.R. Brought to you courtesy of the red, white, and blue pigments of nontuberculous mycobacteria. *AIMS Microbiol.* **2020**, *6*, 434–450. [CrossRef] [PubMed]
18. Igreja, W.S.; Maia, F.A.; Lopes, A.S.; Chisté, R.C. Biotechnological production of carotenoids using low-cost substrates is influenced by cultivation parameters: A review. *Int. J. Mol. Sci.* **2021**, *22*, 8819. [CrossRef] [PubMed]
19. Pagels, F.; Vasconcelos, V.; Guedes, A.C. Carotenoids from Cyanobacteria: Biotechnological potential and optimization strategies. *Biomolecules* **2021**, *11*, 735. [CrossRef]
20. Dyaa, A.; Soliman, H.; Abdelrazak, A.; Samra, B.N.; Khojah, E.; Ahmed, A.F.; El-Esawi, M.A.; Elsayed, A. Optimization of carotenoids production from *Rhodotorula* sp. strain ATL72 for enhancing its biotechnological applications. *J. Fungi* **2022**, *8*, 160. [CrossRef]
21. Xu, X.; Liu, W.; Niu, H.; Hua, M.; Su, Y.; Miao, X.; Chi, Y.; Xu, H.; Wang, J.; Sun, M.; et al. Study on the fermentation effect of *Rhodotorula glutinis* utilizing tofu whey wastewater and the influence of *Rhodotorula glutinis* on lying hens. *Front. Nutr.* **2023**, *10*, 1125720. [CrossRef]
22. Siziya, I.N.; Yoon, D.J.; Kim, M.; Seo, M.J. Enhanced production of C30 carotenoid 4,4′-diaponeurosporene by optimizing culture conditions of *Lactiplantibacillus plantarum* subsp. *plantarum* KCCP11226T. *J. Microbiol. Biotechnol.* **2022**, *32*, 892–901. [CrossRef] [PubMed]
23. Stanchev, V.; Georfiev, D.; Gargova, S. Mathematical modeling of the nutrient medium composition for the production of yeast phytase. *Bulg. J. Agric. Sci.* **2010**, *16*, 628–634.
24. Husseiny, S.M.; Abdelhafez, A.A.; Ali, A.A.; Sand, H.M. Optimization of b-carotene production from *Rhodotorula glutinis* ATCC 4054 growing on agro-industrial substrate using Plackett–Burman design. *Proc. Natl. Acad. Sci. India Sect. B Biol. Sci.* **2017**, *88*, 1637–1646. [CrossRef]
25. da Costa Cardoso, L.A.; Kanno, K.Y.F.; Karp, S.G. Microbial production of carotenoids—A review. *Afr. J. Biotechnol.* **2017**, *16*, 139–146. [CrossRef]
26. Kerr, S.; Calé, C.; Cabral, J.M.; van Keulen, F. Factors enhancing lycopene production by a new *Mycobacterium aurum* mutant. *Biotechnol. Lett.* **2004**, *26*, 103–108. [CrossRef]
27. Yaderets, V.; Karpova, N.; Glagoleva, E.; Shibaeva, A.; Dzhavakhiya, V. Enhanced β-carotene production in *Mycolicibacterium neoaurum* Ac-501/22 by combining mutagenesis, strain selection, and subsequent fermentation optimization. *Fermentation* **2023**, *9*, 1007. [CrossRef]
28. Rozhnov, E.D. *Modeling of Biotechnological Processes: Methodological Recommendations for Performing Laboratory Work, Conducting Practical Classes and Organizing Independent Work of Students for the Speciality 04/19/2011—Biotechnology*; Altai State Technical University: Biysk, Russia, 2019; pp. 40–96.
29. Zhernosekova, I.V.; Chernogor, N.P.; Tymchuk, A.A.; Vinnikov, A.I. Methods of experiments planning by optimization of the nutrient medium for Streptomycete. *Visnyk Dnipropetrovsk Univ. Biol. Ecol.* **2001**, *18*, 20–28. [CrossRef]
30. Zeni, J.; Colet, R.; Cence, K.; Tiggeman, L.; Toniazzo, G.; Cansian, R.L.; Di Luccio, M.; Oliveira, D.; Valduga, E. Screening of microorganisms for production of carotenoids. *CyTA J. Food* **2011**, *9*, 160–166. [CrossRef]
31. Mata-Gómez, L.C.; Montañez, J.C.; Méndez-Zavala, A.; Aguilar, C. Biotechnological production of carotenoids by yeasts: An overview. *Microb. Cell Fact.* **2014**, *13*, 12. [CrossRef] [PubMed]
32. Bindea, M.; Rusu, B.; Rusu, A.; Trif, M.; Leopold, L.F.; Dulf, F.; Vodnar, D.C. Valorification of crude glycerol for pure fractions of docosahexaenoic acid and β-carotene production by using *Schizochytrium limacinum* and *Blakeslea trispora*. *Microb. Cell Fact.* **2018**, *17*, 97. [CrossRef] [PubMed]

33. Suwaleerat, T.; Thanapimmetha, A.; Srisaiyoot, M.; Chisti, Y.; Srinophakun, P. Enhanced production of carotenoids and lipids by *Rhodococcus opacus* PD630. *J. Chem. Technol. Biotechnol.* **2018**, *93*, 2160–2169. [CrossRef]
34. Baughn, A.D.; Rhee, K.Y. Metabolomics of central carbon metabolism in *Mycobacterium tuberculosis*. *Microbiol. Spectr.* **2014**, *2*. [CrossRef] [PubMed]
35. Paniagua-Michel, J.; Olmos-Soto, J.; Ruiz, M.A. Pathways of carotenoid biosynthesis in bacteria and microalgae. *Methods Mol. Biol.* **2012**, *892*, 1–12. [CrossRef]
36. Janisch, N.; Levendosky, K.; Budell, W.C.; Quadri, L.E.N. Genetic underpinnings of carotenogenesis and light-induced transcriptome remodeling in the opportunistic pathogen *Mycobacterium kansasii*. *Pathogens* **2023**, *12*, 86. [CrossRef]
37. Zheng, X.; Hu, R.; Chen, D.; Chen, J.; He, W.; Huang, L.; Lin, C.; Chen, H.; Chen, Y.; Zhu, J.; et al. Lipid and carotenoid production by the *Rhodosporidium toruloides* mutant in cane molasses. *Biores. Technol.* **2021**, *326*, 124816. [CrossRef] [PubMed]
38. Dzhavakhiya, V.; Savushkin, V.; Ovchinnikov, A.; Glagolev, V.; Savelyeva, V.; Popova, E.; Novak, N.; Glagoleva, E. Scaling up a virginiamycin production by a high-yield *Streptomyces virginiae* VKM Ac-2738D strain using adsorbing resin addition and fed-batch fermentation under controlled conditions. *3 Biotech* **2016**, *6*, 240. [CrossRef]
39. Schmidt, F.R. Optimization and scale up of industrial fermentation processes. *Appl. Microbiol. Biotechnol.* **2005**, *68*, 425–435. [CrossRef]
40. Liu, W.C.; Gong, T.; Wang, Q.H.; Liang, X.; Chen, J.J.; Zhu, P. Scaling-up fermentation of *Pichia pastoris* to demonstration-scale using new methanol-feeding strategy and increased air pressure instead of pure oxygen supplement. *Sci. Rep.* **2016**, *6*, 18439. [CrossRef]
41. Jing, Y.; Wang, J.; Gao, H.; Jiang, Y.; Jiang, W.; Jiang, M.; Xin, F.; Zhang, W. Enhanced β-carotene production in *Yarrowia lipolytica* through the metabolic and fermentation engineering. *J. Ind. Microbiol. Biotechnol.* **2023**, *50*, kuad009. [CrossRef]
42. Liu, L.; Qu, Y.L.; Dong, G.R.; Wang, J.; Hu, C.Y.; Meng, Y.H. Elevated β-carotene production using codon-adapted CarRA&B and metabolic balance in engineered *Yarrowia lipolytica*. *Front. Microbiol.* **2021**, *12*, 627150. [CrossRef]
43. Hunter, G.J. The oxidation of glycerol by Mycobacteria. *Biochem. J.* **1953**, *55*, 320–328. [CrossRef] [PubMed]

fermentation

MDPI

Article

A New Concept for the Rapid Development of Digital Twin Core Models for Bioprocesses in Various Reactor Designs

André Moser [1,2], Christian Appl [3], Ralf Pörtner [2], Frank Baganz [4] and Volker C. Hass [1,4,*]

[1] Institute of Applied Biology, Faculty of Medical and Life Sciences, Furtwangen University, 78054 VS-Schwenningen, Germany; andre.moser@hs-furtwangen.de
[2] Institute of Bioprocess and Biosystems Engineering, Hamburg University of Technology, 21073 Hamburg, Germany; poertner@tuhh.de
[3] s&h Ingenieurgesellschaft mbH, 21109 Hamburg, Germany; cbappl@sh-ingenieure.de
[4] Department of Biochemical Engineering, University College London, London WC1H 0AH, UK; f.baganz@ucl.ac.uk
* Correspondence: volkerclaus.hass@hs-furtwangen.de

Abstract: In this research work, a new software tool concept and its application for the rapid and flexible development of mechanistic digital twin core models for bioprocesses in various reactor designs are presented. The newly developed software tool concept automatically combines user-selected submodels into an overall digital twin core model. The main part is a biokinetic submodel, of which three were designed for enzymatic, microbial and biocatalytic processes, which can be adapted to specific processes. Furthermore, the digital twin core model contains a physico-chemical submodel (e.g., calculating pH or oxygen transfer) and a reactor submodel. The basis of the reactor submodel is an ideally mixed stirred tank reactor. The biokinetic submodel is decoupled from the reactor submodels and enables an independent parameterisation of submodels. Connecting ideally mixed stirred tank reactor models allows for the simulation of different reactor designs. The implementation of an executable digital twin core model was accelerated, creating a new software tool concept. When the concept was applied, the development time and the computing time of digital twin core models for the cultivation of *Saccharomyces cerevisiae* in two coupled stirred tank reactors as well as for enzymatic hydrolysis processes in a packed-bed reactor were reduced by 90%.

Keywords: digital twin; mathematical model; model development; submodel framework; reactor model; bioprocesses

1. Introduction

Digital twins (DTs) are becoming increasingly important in the biotechnology sector. They can be utilised for fast and resource-saving development and improvement of bioprocesses [1]. Due to the increasing demand for bioprocess DTs, there is a growing need for new strategies for the rapid and flexible development of dynamic process models and DTs.

In the early 2000s, the DT concept was first applied in mechanical engineering [2–4]. DTs are often seen as virtual representations of physical systems. They may be able to map the entire life cycle of the physical system [3]. Various authors have already published definitions of the term "digital twin" [2–6]. This work is mainly based on the definition given by El Saddik [4]:

> *"Digital twins are (. . .) digital replications of living as well as non-living entities that enable data to be seamlessly transmitted between the physical and virtual worlds".*

Therefore, DTs for biotechnological processes must be able to mimic and predict the dynamic behaviour of the biokinetic processes, the biological system (e.g., microorganisms, enzymes), the environment in which the process takes place (e.g., nutrient media, carrier material (immobilisation)), the physical-chemical system, the bioreactor and the periphery

connected to the bioreactor (e.g., pumps, valves, pipes). Besides this, the DT should also include control and automation functions, a graphical user interface and a connection to the real system for information exchange.

To realise the elements of a bioprocess DT, a shell structure was established by our group in previous works (Figure 1) to assist DT development [7,8].

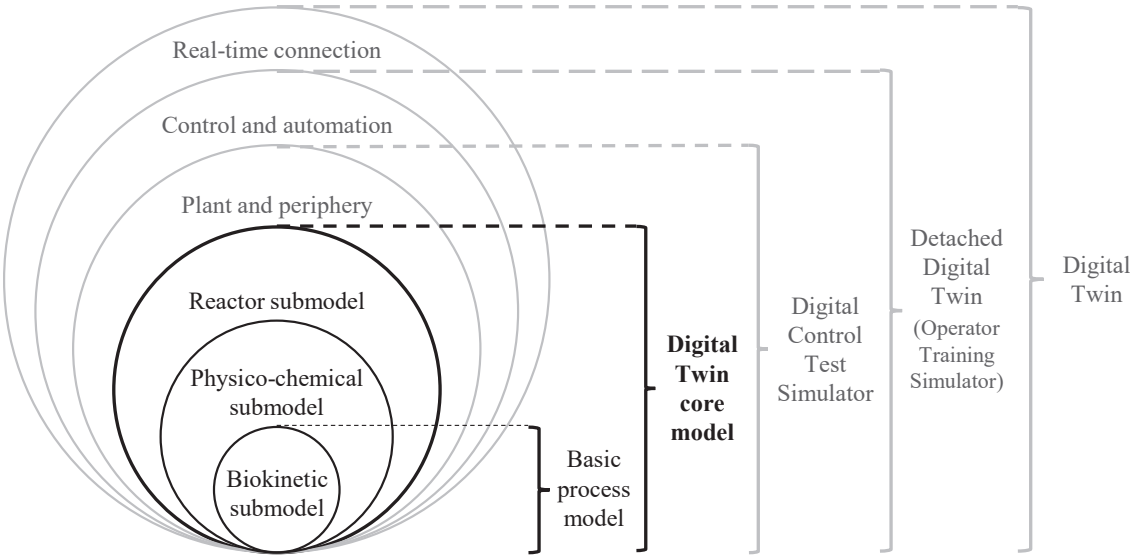

Figure 1. Shell structure for bioprocess DTs based on [7,8]. Extended by definitions for DT core model, digital control test simulator and detached DT.

A DT core model consists of biokinetic, physico-chemical and reactor submodels, which are continuously exchanging information. The biokinetic submodel calculates all rates concerning the growth and product formation of microorganisms, mammalian cells or enzymatic and biocatalytic reactions. The physico-chemical submodel may include models for calculating broth temperature, pH, foam level and dissolved gas concentrations. The physico-chemical submodel may be influenced by the results of reactions calculated by biokinetic equations in the biokinetic submodel, e.g., through heat generation caused by reactions. In turn, the resulting physico-chemical properties may influence the biokinetics reflected by the biokinetic submodel. The reactor submodel describes the properties of the reactor in which the process is performed and may include information about flow patterns.

For the creation of a full DT, the DT core model may be implemented in a simulation, process control and automation software like WinErs 7.7.A [9] to realise the real-time connection between the physical and virtual instances [1,8]. Submodels representing the plant and periphery, as well as the control and automation, may also be implemented in the process control and automation system.

The development of the DT core model requires a considerable amount of time and is a major bottleneck in DT development.

There are various modelling approaches for the creation of the submodels used for DT core models. Usually, a distinction is made between mechanistic and non-mechanistic modelling approaches. Most types of non-mechanistic modelling approaches like big data, artificial intelligence (AI) or machine learning utilise provided data resources to predict trends and behaviour of a system [10–13]. Non-mechanistic models calculate probabilities and correlations. Large amounts of high-quality data are needed for model training. Strictly speaking, non-mechanistic models are only capable of prediction within the scope of the data used for learning and allow for a very limited change of process conditions. Non-mechanistic models are based on correlation, not causation, and therefore provide limited insight into biotechnological processes [3]. For this reason, non-mechanistic models can only support biotechnological DT core models as hybrid models [11,14–16] but can't be

applied as the sole process model. Fuzzy sets may be seen as an intermediate between non-mechanistic and mechanistic models, as they utilise expert knowledge to a considerable extent [13,17–20].

In this work, mechanistic modelling approaches are used for the development of bioprocess DT core models [8], which are based on biological, physical and chemical relationships and equations. In biotechnology, equations are usually based on kinetic reactions, e.g., Monod kinetics [21] for fermentations or Michaelis–Menten kinetics [22,23] for enzymatic processes. The development of mechanistic models is often far more time-consuming than the development of non-mechanistic models, but less experimental data are needed for parameter identification and model calibration. An essential benefit of mechanistic models is that the model parameters have an actual physical meaning, which facilitates the scientific interpretation of the results [8].

Mechanistic models can be divided into structured (compartmentalised) and unstructured models [24–27]. In unstructured models, all cells are viewed as one black box, whereas in structured models, the biomass is split into multiple compartments with different tasks, which allows for a more realistic representation of the biocatalysts [28,29].

To avoid the DT core model becoming too complex, it is practical to divide it into several submodels that exchange relevant information. This combination could be performed with simple functional state models where different models describe specific states of the process [7,8,30], hybrid models, which combine mechanistic and non-mechanistic approaches [11,14,15] or submodel frameworks [7,8].

Using structured, mechanistic submodels integrated into a submodel framework for the development of DT core models has proven to be very advantageous [1,7,8,30]. By using a submodel framework, different DT core model configurations can be created in a flexible way [31]. However, developing DT core models using this modelling approach is labour-intensive and complex, and modelling experts are needed.

To facilitate the development process, a new software tool concept was established and tested for the realisation of DT core models for the cultivation of *S. cerevisiae* in two coupled parallel stirred tank reactors (STRs) and the enzymatic hydrolysis with immobilised enzymes in a packed-bed flow tube reactor (PBR).

2. Materials and Methods

The C++-based programming and simulation package C-eStIM 2021-11 [32] was used to create the dynamic mathematical biokinetic, physico-chemical and reactor submodels.

The software tool concept was realised using *R* programming language [33], which offers the possibility to combine the desired submodels in an overall DT core model.

WinErs [9] was used to create the plant and periphery and control and automation submodels of the DT, as well as the PCS of the reactors. Specific interfaces were created in WinErs for data exchange between DT and PCS.

The recommended *S. cerevisiae* cultivation experiments were performed in two connected 1 L stirred tank reactors (STRs) (MDX, Nörten-Hardenberg, Germany). Genetically unmodified *S. cerevisiae* (Agrano, Riegel am Kaiserstuhl, Germany) was cultivated in media consisting of water, glucose (Glc), yeast extract (YE) and soy peptone (Pep, all Carl Roth, Karlsruhe, Germany). No preculture was carried out, and dried active yeast was directly inoculated. The initial concentration of yeast was set at 10 g L^{-1}, Glc at 20 g L^{-1} and YE as well as Pep at 25 g L^{-1}. The temperature was set to 28 °C. The pH and DO were not controlled during the process. The airflow rate was adjusted at ~1 vvm and the stirring rate at 800 rpm to maintain aerobic conditions (DO > 10%) in the aerobic compartment. The anaerobic compartment was stirred at 600 rpm, and the reactor was not aerated. Antifoam was fed when required. Glucose and ethanol concentrations were measured with enzymatic test kits (Art. No.: 10716251035 and 10176290035, R-Biopharm AG, Pfungstadt, Germany). Dry biomass density was determined by filtrating the medium through cellulose acetate filters (0.45 m, VWR, Radnor, PA, USA) and measuring the weight of the retentate after drying in a moisture analyser (MA45, Sartorius, Göttingen, Germany). The percentages of O_2 and CO_2 in

the exhaust gas were measured via an extractive gas analyser (Sick, Waldkirch, Germany). The pH value of the medium was measured in situ with an amperometric pH probe (EasyFerm Plus PHI S8 225, Hamilton, Bonaduz, Switzerland). The DO was measured with an optical dissolved oxygen (DO) probe (VisiFerm DO ECS 225 H0, Hamilton).

3. Results

Three main challenging tasks within the process of DT core model development were identified and shall be addressed in this chapter:

1. Adding, exchanging or removing submodels requires changes throughout the entire source code of the DTs core model. A manual adaptation of the model structure takes at least a few hours, or even multiple days, of work for more elaborate changes;
2. Non-ideal flow patterns in bioreactors may have an impact on the kinetics, performance and dynamics of the process under consideration. Thus, for a realistic representation of these effects in DTs, possibilities should be created to represent non-ideal reactor behaviour and/or different reactor types with the reactor submodel;
3. The numerical solution of large mechanistic models, consisting of systems of a high number of nonlinear coupled differential equations, requires high computational effort. It is particularly important to keep the computation times of DTs, especially for their parameterisation and application in process optimisation, as short as possible.

3.1. Characteristics of the New Software Tool Concept for Automated Bioprocess DT Core Model Development

The software tool concept realised in the programming language R 4.2.2 [33] automatically creates DT core models in the simulation and programming environment C-eStIM [32] by implementing user-selected submodels from a model library, thus eliminating laborious manual changes throughout the model code (Figure 2).

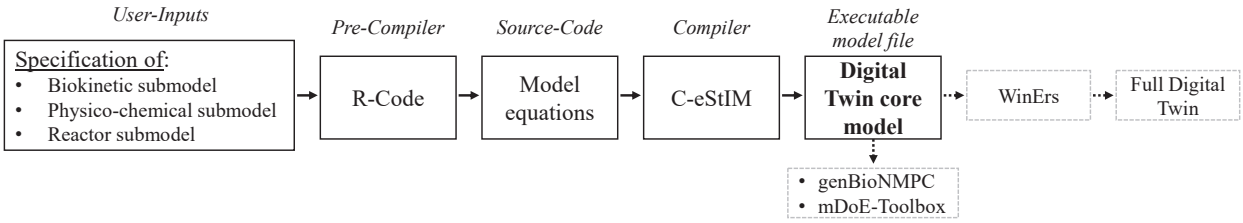

Figure 2. Software tool concept for the rapid development of mechanistic DT core models for bioprocesses in various reactor designs.

It also introduces the option to model different reactor configurations using a system of networked STR models, including a cascade of STR models to replicate the behaviour of a flow tube reactor. To minimise the computing time, only the equations necessary for the selected submodels are implemented in the DT core model.

All submodels available for the formulation of the biokinetic and physico-chemical submodels are listed in Table 1.

Table 1. Available submodels for the implementation in the biokinetic and physico-chemical submodels.

Submodel	Model	Options/Specification
Biokinetic	Microbiological	*Saccharomyces cerevisiae* *Cyathus striatus* *Lactobacillus delbrueckii* *Escherichia coli*
	Mammalian cells	Hybridoma cells Chinese hamster ovary (CHO) cells
	Biocatalysis	Whole-cell biocatalysis
	Enzymatic reactions	Starch hydrolysis Proteolysis

Table 1. *Cont.*

Submodel	Model	Options/Specification
Physico-chemical	Gas-phase	*Calculation*
	pH value	*Calculation* *Fixed profile* *Fixed value*
	Dissolved oxygen	*Algebraic equations* *Differential equations* *Fixed profile* *Fixed value*
	Temperature	*Calculation* *Fixed profile* *Fixed value*
	Foam level	*Calculation*

3.1.1. Biokinetic Submodel

The selectable options for the biokinetic submodel include a cultivation model for different microorganisms [8] and mammalian cell lines [8,31], as well as biokinetic models for whole-cell biocatalysis [34], enzymatic starch hydrolysis and proteolysis [30].

By summarising individual metabolic reactions to generalised stoichiometric functions according to stoichiometric Equation (1), it is possible to create one biokinetic submodel for different organisms and their respective reactions [31].

$$C_xH_yO_z + \alpha O_2 + \beta H_gO_hN_i \rightarrow \gamma C_aH_bO_cN_d + \delta CO_2 + \varepsilon H_2O_t + \zeta C_jH_kO_lN_m \quad (1)$$

Several metabolic pathways are integrated into the model, e.g., biomass production, total oxidation or partial oxidation of substrates (e.g., overflow metabolism). Furthermore, product formation mechanisms for growth-associated products or non-growth-associated products are included. The resulting rates (r_S) are modelled using Monod kinetics (Equation (2)). The maximum possible substrate uptake rate $r_{S,max}$ is multiplied by a quotient that encompasses the substrate concentration c_S divided by the sum of c_S and the half-saturation constant K_S. The result is multiplied by the product of multiple (double) sigmoidal functions (Equation (3)) [31].

$$r_S = r_{S,\,max}\left(\frac{c_S}{Ks + c_S}\right)\prod_{i=1}^{n} f_{Dsig}(x_i) \quad (2)$$

$$f_{Dsig}(x) = \left(Y_l + \frac{Y_{mid} - Y_l}{1 + e^{-K_{sl,l}(x - X_{50,l})}}\right)\cdot\left(1 + \frac{Y_h/Y_{mid} - 1}{1 + e^{-K_{sl,h}(x - X_{50,h})}}\right) \quad (3)$$

Y_l is the value at low x, Y_h is the value at high x and Y_{mid} is the value between $X_{50,l}$ and $X_{50,h}$. $X_{50,l}$ and $X_{50,h}$ are location parameters of the low/high side of the function, $K_{sl,l}$ determines the slope on the low side of the function and $K_{sl,h}$ determines the slope on the high side of the function [31,35]. Gerlach et al. discussed the properties of double-sigmoidal functions [35]. (Double) sigmoidal functions are also utilised to describe the influence of state and physico-chemical variables on yield coefficients as well as activation, inactivation and mortality rates [31,36].

3.1.2. Physico-Chemical Submodel

Multiple options are available for the formulation of the physico-chemical submodel, including the calculation of pH, the dissolved oxygen concentration, the foam level and the temperatures of the broth in the reactor as well as in the heating jacket (Table 1, physico-chemical submodel).

For the physico-chemical submodel, the user can specify if the variables pH and temperature should be calculated with the respective model or if they should be predefined. The variables can be predefined with a fixed value or profile. Two models exist for the

dissolved oxygen concentration. One model utilises differential equations, and the other model uses algebraic equations. The approach using differential equations is more accurate but slower because of relatively small time constants requiring smaller step sizes. The DO can also be set at a fixed value or profile.

The computation time can be reduced by increasing the step size or reducing the number of ODEs to be solved. Therefore, for parameterisation of the biokinetic submodel, it might be an advantage to set the values of measured physico-chemical variables as input profiles and not include physico-chemical submodels in the mathematical model. This decoupling of submodels, which is easily achieved with the presented software tool concept, makes it possible to carry out simulations with the biokinetic model with longer step sizes. This reduces the computing time of a single simulation by more than 90% (compared to a model with all physico-chemical submodels) and, thus, the time required for the entire parameterisation process. After parameterisation of the biokinetic submodel, the physico-chemical submodels can be included again in the DT core model.

3.1.3. Reactor Submodel

The biokinetic submodel and the physico-chemical submodel are connected with (values of state variables) the reactor submodel, which consists of a user-defined network of interlinked ideal STR models and exchange values of state variables (Figure 3).

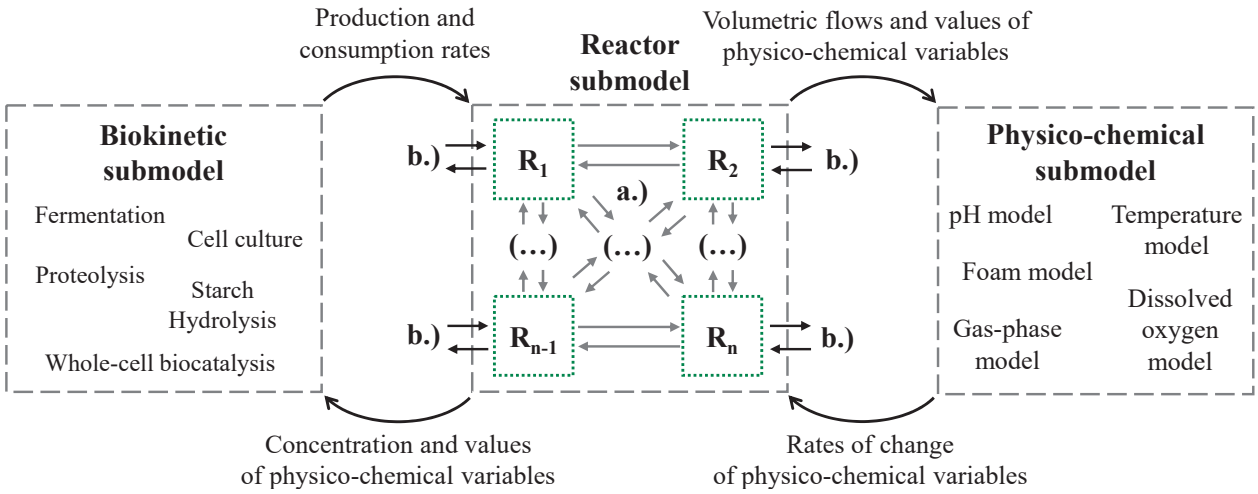

Figure 3. Combination of the DT submodels to enable the simulation of various reactor designs, (a) mass transfer flows between STR models, and (b) individually adjustable inputs and outputs.

All STR models in the reactor submodel can be linked to each other in any way, and each STR model is linked to the biokinetic and physico-chemical submodels. The reactor submodel processes all the inputs and outputs, e.g., feed streams, aeration rate or sample volumes. The biokinetic submodel transfers the production and consumption rates of biomass and metabolites to the reactor submodel. The reactor submodel calculates the concentration of the biomass and metabolites as well as the values of physico-chemical variables and transfers them back to the biokinetic submodel. Furthermore, the reactor submodel calculates the values of physico-chemical variables, which are transferred to the physico-chemical submodel. The physico-chemical submodel calculates the rate of change of each physico-chemical value. Only one set of parameters is required for the biokinetic and physico-chemical submodels in a specific DT.

The differential equation calculating the change of volume is derived from the mass balance using the assumption that changes in density might be neglected and processes all

inputs and outputs of the reactor submodel. Equation (4) describes the differential equation for calculating the volume of each STR model (V_i) implemented in the reactor submodel.

$$\frac{dV_i}{dt} = F_{in,i} - F_{out,i} + F_{in,\ Comp,i} - F_{out,Comp,i} \quad (4)$$

$F_{in,i}$ is the sum of all input flows to the STR model, and $F_{out,i}$ is the sum of all output flows from the STR model. $F_{in,Comp,i}$ is the sum of all input flows from other STR models, and $F_{out,Comp,i}$ is the sum of all output flows to other STR models.

The differential equations of all concentrations have the following standardised structure.

$$\frac{dc_i}{dt} = r_i^+ \cdot Xv_i - r_i^- \cdot Xv_i + c_{i,F} \cdot \frac{F_i}{V_i} - c_i \cdot \frac{F_{in,i}}{V_i} + \sum_{j=1}^{n_{Comp}} c_{i,j} \cdot \frac{F_{i,j}}{V_i} \quad (5)$$

$$\frac{dc_i}{dt} = production - uptake + input - dilution + inputs\ from\ other\ STR\ models \quad (6)$$

The production rate r_i^+ and the uptake rate r_i^- are multiplied by the viable biomass Xv_i. The input is calculated with the concentration of the feed $c_{i,F}$ multiplied by the flow rate of the feed F_i divided by the volume of the STR model V_i. The dilution is calculated with the concentration c_i, the sum of all input flows $F_{in,i}$ into the STR model and the volume V_i of the STR model. The inputs from other STR models are accounted for via the sum of the concentration of all (n_{Comp}) STR models $c_{i,j}$, multiplied by their flow $F_{i,j}$ to the considered STR model divided by the volume V_i.

By networking STR models, DTs with a wide variety of reactor configurations can be created (Figure 4).

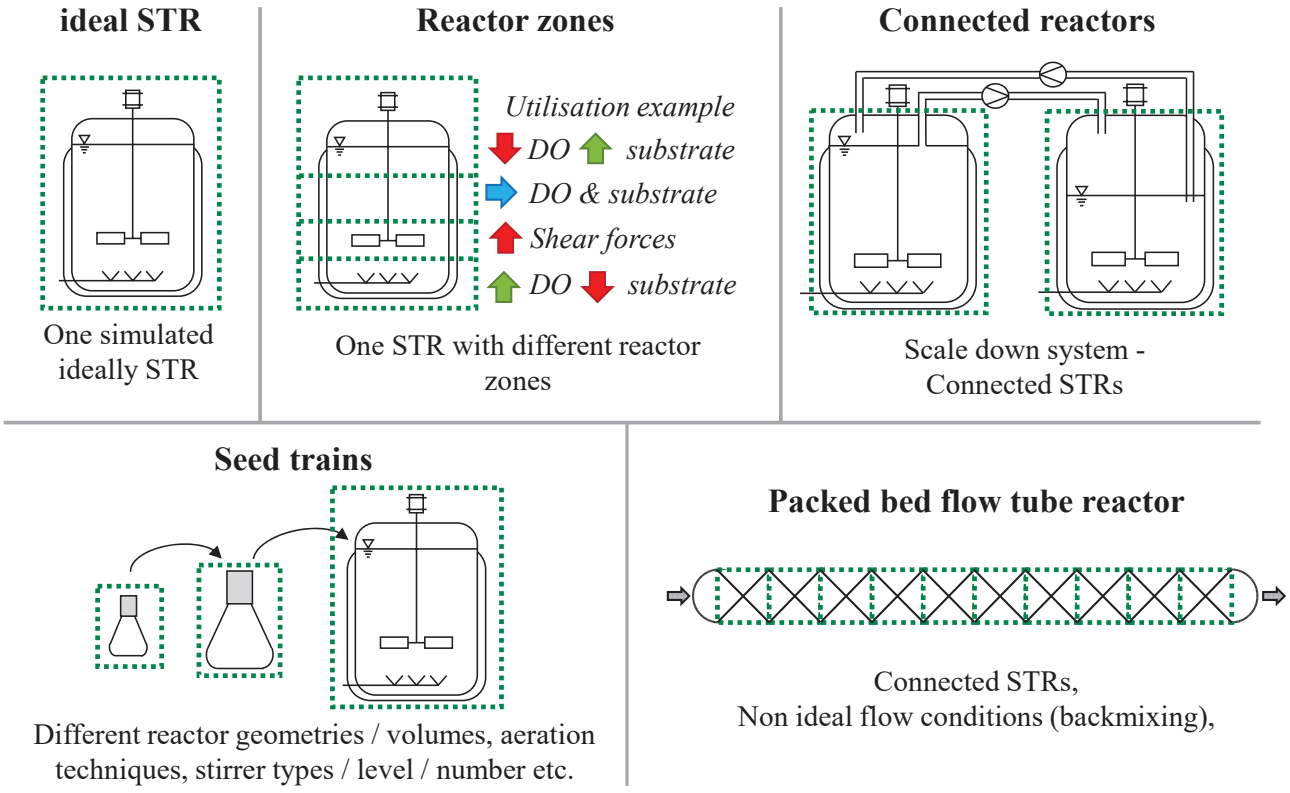

Figure 4. DT reactor configurations that can be created with the new software tool concept. Each green-dotted box indicates one individual STR model.

This strategy offers the possibility of an innovative flexible modelling approach. It is possible to calculate non-ideally mixed reactor systems by interconnecting multiple ideally

mixed STR models with specific properties (volume, geometry, etc.) that are continuously exchanging material flows. The reactor systems that may be modelled include tubular flow reactors (e.g., packed-bed flow tube reactors) with a flowing phase and a stationary phase, large-scale reactors or systems of connected reactors (e.g., scale-down systems) or building sequences of reactors with different geometries (e.g., seed trains). Since the biokinetic submodel is decoupled from the reactor and physico-chemical submodel, it can be used in different reactor configurations. This enables and accelerates a process transfer between different bioreactors.

The user inputs are transferred to the pre-compiler written in the programming language R [33]. The R-Code writes the selected and necessary mathematical model equations into the source code of the DT core model based on the user selection. These mathematical equations of the DT are written in the programming language C++. The source code is then compiled using the C-eStIM compiler [32] into an executable model file (.exe), a DLL (dynamic link library) for Windows or a shared object file (.so) for UNIX systems, respectively. This accelerates, simplifies and reduces the risk of errors during model implementation to an executable model; the manual modelling work is reduced to a few seconds.

Since computation time should be as short as possible, multiple methods for model reduction and acceleration of calculation are implemented into the software tool concept:

- Only the required models are implemented into the final DT core model. The user can decide which models to include. Temperature, DO and pH can be defined as fixed values or fixed profiles if a calculation is not necessary;
- Only necessary double-sigmoidal functions are implemented into the DT. These functions demand a high computational effort since two exponential functions must be solved (Equation (3)). For this purpose, a user-predefined configuration file comprising the parameters of the double-sigmoidal functions is scanned using the software tool concept. If the parameters are defined in such a way that the function yields the neutral element for multiplications ($y_h = y_{mid} = y_l = 1$), the function is not transferred into the DT core model because the result of the function equals one in any case;
- A fast calculation mode is selectable by the user. The temperature submodel (based on dynamic energy and mass balances) and the DO submodel (based on dynamic mass balances and mass transfer theory, see reference [31]) have faster time constants (in their differential equations) compared to the biokinetic submodel and are thus decisive for the number of necessary calculation steps. The fast calculation mode enables a more than 80% shorter calculation time at the expense of simulation accuracy by reducing necessary calculation steps. In the temperature model, the fast calculation mode lowers heat transfer coefficients and thus slows down the heat transfer rates. In the DO model, for the fast calculation mode, the differential equations for the calculation of the DO and the gas phase composition are replaced by algebraic equations.

In addition, the DT core model can be combined with process development tools, such as the "genBioNMPC" [8], which is a parameterisation algorithm and a nonlinear model predictive controller (NMPC) [37,38] of the open-loop-feedback-optimal (OLFO) type [1,8], or the model-assisted design of experiment (mDoE-toolbox) [39], which combines mathematical models, statistical design of experiments [40] and uncertainty analysis [41] to accelerate and optimise process development [42].

3.2. Application of the New Software Tool Concept for the Development of Bioprocess DTs

Using the new software tool concept, a DT core model for the cultivation of *S. cerevisiae* in two coupled parallel STRs and a DT core model for enzymatic hydrolysis processes in a PBR were created.

3.2.1. DT Core Model for the Cultivation of *S. cerevisiae* in Two Coupled Parallel 1 L STRs

The reactor system is utilised to simulate inhomogeneities (such as concentration differences) occurring in large-scale reactors on a laboratory scale [43,44]. These inhomo-

geneities could potentially have a severe impact on process performance at the production scale [45–48]. For this reason, it is important to understand the influence of inhomogeneities on the bioprocess [49]. The approach chosen is the utilisation of a physical scale-down model that can emulate specific inhomogeneities of large-scale reactors [44,50–52] in combination with a corresponding DT of the system [8,31]. The detailed model equations and parameters used can also be found in [8,31].

The experimental scale-down system consists of two 1 L STRs connected via pipes. The broth is pumped between the two STRs with a peristaltic pump (Figure 5).

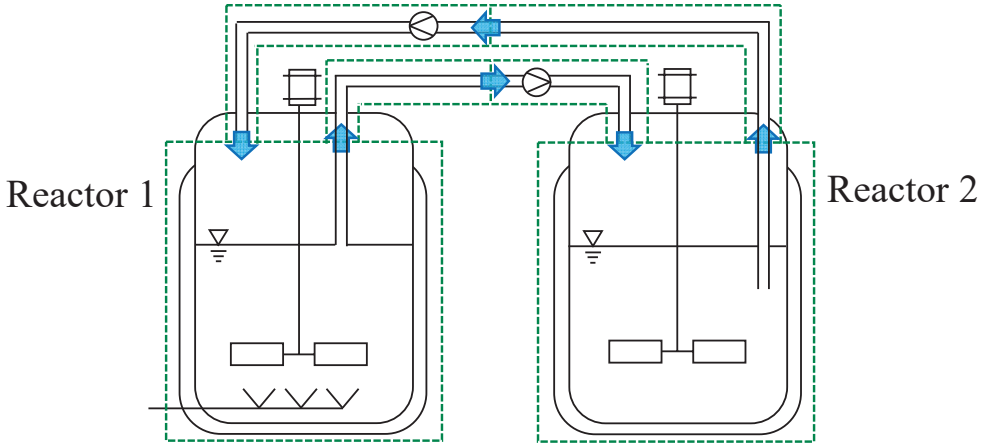

Figure 5. DT for the cultivation of *S. cerevisiae* in two connected parallel ideal STRs. Blue arrows symbolise the flow between the ideal STR models (green dotted boxes).

The chosen microbial system was the cultivation of baker's yeast (*S. cerevisiae*). Yeast has the advantage of having a well-known aerobic and anaerobic metabolism. *S. cerevisiae* produces ethanol, even under aerobic conditions, if glucose concentration is above a certain limit. This phenomenon is known as the Crabtree effect [53,54]. Ethanol formation is crucial due to its inhibitory effect on cell growth and activity [55]. Furthermore, yeast can metabolise ethanol for cell growth and energy under aerobic conditions if no glucose is available [56].

The design of the DT core model was achieved using the developed software tool concept. First, a biokinetic submodel with a predefined parameter set for yeast cultivations was chosen (see Brüning [31]). The biokinetic submodel was parameterised with data from 16 previously performed experiments under different conditions and reactor configurations (aerobic, anaerobic, aerobic and anaerobic scale-down systems). The validation experiment was not part of the data set used for parameterisation. Parameterisation was performed conventionally by minimising the total absolute deviation between experimental and simulated values of the offline data (biomass density, glucose concentration, ethanol concentration) with an optimisation algorithm based on the Nelder–Mead algorithm [57]. After parameterisation, the models for the physico-chemical submodel, consisting of a gas-phase model to simulate the gas-phase concentrations in the exhaust gas and a pH model to calculate the pH of the medium, were included in the model. Temperature and DO models are not needed because both temperature and oxygen levels are kept constant in the calculations to simulate the conditions of the physical system. Assuming ideally mixed conditions in the physical STRs, one STR model was chosen for each physical reactor (Figure 5). Since a flow through the pipes should be simulated by two or more STR models, two connected STR models were combined to simulate each pipe of the experimental system. In total, six connected ideal STR models were used. Without the possibility of selecting models and methods for model reduction, 378 differential equations would be necessary for the model to perform the desired calculations. Through model reduction (excluding submodels from the DT core model used for parameter identification), this number was reduced to 174. At the same time, larger calculation step sizes were applied.

Both measures lead to over 90% faster simulation times (reduction from, initially, 30 s to 1.5 s for the simulation of a process with a duration of 48 h). The step size was selected to be as large as possible, where only a minor deviation (less than 1%) from a baseline simulation (one computation step per second) was determined.

In the next step, the planned process conditions are implemented into the model. Both reactors are initially filled with 0.5 L of a nutrient medium. The total volume of the pipe between the reactors is 0.05 L per pipe. The flow between the compartments is adjusted to 0.125 L min^{-1}, which results in a long mixing time of the system of about 5 min to mimic inhomogeneities [58]. Mixing time is defined as the time elapsed until 90% of the equilibrium state is reached, determined via pH measurements [59]. Reactor 1 (R1) is aerated (0.5 L min^{-1}) and operated under aerobic conditions; the second reactor 2 (R2) is operated under anaerobic conditions. R1 is stirred at 800 rpm and R2 at 600 rpm.

Figure 6 shows a comparison between predicted simulation results from the DT core model and data from a subsequently performed experiment under the simulated conditions. Initially, the pH value could not be quantitatively predicted with sufficient accuracy. Adjusting the initial buffer capacity led to an improved adaption. This altered buffer capacity can be explained by a change in the experimental medium composition. Further reparameterisation of the model after the experiment was not necessary.

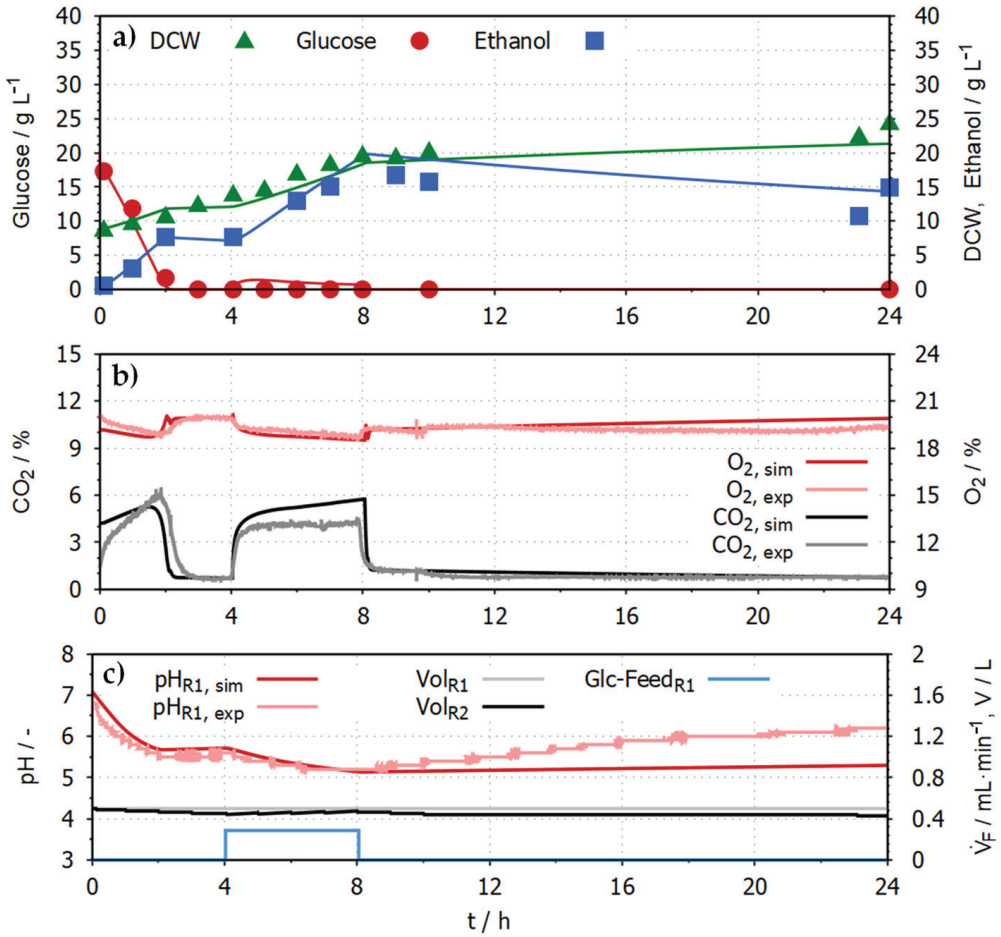

Figure 6. Experimental data in comparison to simulation results using the DT for the system of two interconnected 1 L STRs. (**a**) shows the concentrations of glucose (red, circle), ethanol (blue, square) and the dry cell weight (DCW, green, triangle) in R1. (**b**) shows the online data of the exhaust gas concentration of O_2 (simulated = dark red, experimental = light red) and CO_2 (simulated = black, experimental = grey) of R1 and R2. (**c**) shows the pH (simulated = dark red, experimental = light red), the feed rate of the glucose medium (500 g L^{-1} glucose) and the simulated volume of the reactor medium of both reactors (R1 = black, R2 = grey).

The process was planned to start with a batch phase for 4 h in which 20 g L^{-1} glucose is metabolised by 10 g L^{-1} *S. cerevisiae*. This is followed by a fed-batch phase in which a glucose feed (500 g L^{-1} glucose) was fed with 0.289 mL min^{-1} into R1 for 4 h. In the remaining 16 h of the process, no glucose is measurable, and the yeast consumes ethanol. The ethanol concentration reaches its highest concentration of around 20 g L^{-1} at about 8 h and is reduced to 10-15 g L^{-1} at the end of the process. Dry biomass density reaches about 25 g L^{-1} after 24 h. The simulated offline data from the biokinetic submodel show close agreement with the experimental data. The combined R^2 for all offline data is 0.92 ($R^2_{Glucose}$ = 0.97, $R^2_{Ethanol}$ = 0.87, R^2_{DCW} = 0.90).

The physico-chemical variables also show qualitatively and quantitatively good agreement between simulated and experimental data. The CO_2 concentration in the exhaust gas reaches 6% during the batch phase of the process. After the complete consumption of glucose, it sharply drops to 0.8%. When the feed is turned on, the CO_2 concentration reaches 4% and drops again after turning off the feed. Since the pH value is nearly identical in both compartments, only the pH value in R1 is shown. The experimental and simulated pH drops from about 7 to 5 throughout the first 8 h; afterwards, the experimental pH value rises back to over 6. This might be caused by a combination of several factors, such as changes in the buffer capacity of the system, production and consumption of organic acids and bases or changes in the dissolved CO_2 concentration. The simulated pH only rose slightly to 5.2 since not all factors potentially influencing the pH were included in the pH submodel.

The software tool concept enabled the rapid creation of the DT core model for the cultivation of *S. cerevisiae* in two coupled parallel 1 L STRs. The definition of the reactor submodel structure using six networked STR models and the specification of the biokinetic and physico-chemical submodels was accomplished by the authors within one hour. These DT specifications were entered into the user interface of the new software tool concept. When the authors were utilising the new software tool concept, the source code creation of the DT core model took less than one minute, instead of several days, if this had to be performed manually. The faster code implementation could also be performed by less experienced users (students). The accelerated model code generation enables the testing of model compositions and sequential parameterisation of submodels.

3.2.2. DT Core Model for Enzymatic Hydrolysis Processes in a PBR

Using the new software tool concept, a DT core model for enzymatic hydrolysis processes in a PBR was created to demonstrate that the conditions in a PBR can be modelled by combining a series of STRs. In the STR models, a model representing immobilised biocatalysts was included. The biokinetic and physico-chemical submodels implemented in the STRs correspond to those of the DT for enzymatic hydrolysis processes in a STR [30]. Models for enzymatic starch hydrolysis and proteolysis are forming the biokinetic submodel of the DT. In starch hydrolysis, the substrate starch is converted into glucose by α- and glucoamylases [30]. In proteolysis, proteins are the substrates that are cleaved into free amino acids (products) by endo- and exopeptidases [30]. The physico-chemical submodel is formed by models calculating the temperature and pH of the broth in the reactor.

The DT core model can map the enzymatic hydrolysis processes in a PBR with a length (l_{PBR}) of 0.3 m, a diameter (d_{PBR}) of 0.03 m and a volume (V_{PBR}) of 0.212 L. To reflect the conditions in the PBR, a cascade of ten modified STRs (l_{STR} = 0.03 m, d_{STR} = 0.03 m, V_{STR} = 0.0212 L) was created in the reactor submodel (Figure 7).

The enzymes are immobilised on a carrier substance that is retained in the individual STRs. The ideally mixed substrate solution passes through the STRs from one end of the reactor to the other. In addition, back mixing between the individual STRs can be simulated to represent different flow types.

Figure 8a shows how the product concentration in a simulated proteolysis process in the PBR changes over the length of the reactor from STR_1 to STR_{10}.

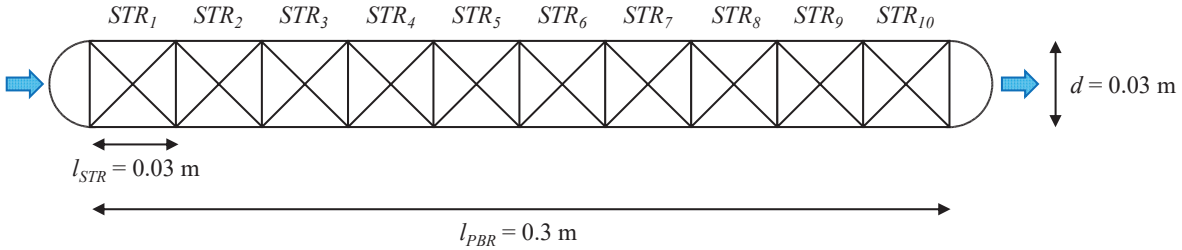

Figure 7. DT for enzymatic hydrolysis processes in a PBR (ten connected STRs) with immobilised enzymes. Blue arrows symbolise the flow direction of nutrient media through the PBR.

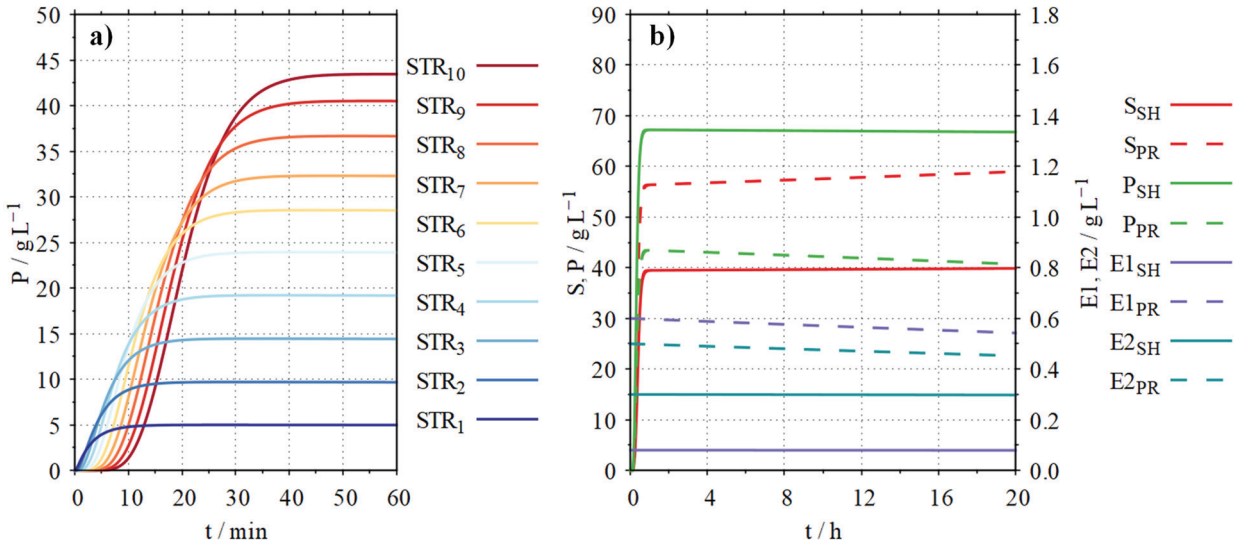

Figure 8. DT simulation of the combined enzymatic starch hydrolysis (SH) and proteolysis (PR) in ten STRs representing a PBR (l = 0.3 m, d = 0.03 m) with T = 60 °C, pH = 6, inflow of substrate solution = 10 mL min^{-1} (100 g L^{-1} substrate SH (80% hydrolysable), 100 g L^{-1} substrate PR (50% hydrolysable)), back mixing = 1 mL min^{-1}; (**a**) proteolysis start-up phase in the STRs 1–10 with P: product (free amino acids) concentration; (**b**) continuous process over 20 h with S: substrate concentration, P: product concentration, E1: active α-amylase (SH) or endopeptidase (PR) concentration, E2: active glucoamylase concentration (SH) exopeptidase (PR).

It can be seen how the product concentration increases over the length of the PBR from STR_1 (5 g L^{-1}) to STR_{10} (44 g L^{-1}). After about 45 min, almost stationary conditions are reached in the PBR.

Using the developed DT, a scenario for the combined starch hydrolysis and proteolysis was simulated. The substrate solution containing 100 g L^{-1} soluble maise starch (80% hydrolysable components) and 100 g L^{-1} sunflower protein powder (50% hydrolysable components) continuously passed through the PBR (Figure 8b).

For the simulation of the starch hydrolysis process, it can be seen that after the start-up phase of approx. 45 min, the concentration of the substrate rises to approx. 39 g L^{-1}, and the product concentration rises to approx. 68 g L^{-1}. During the processing time of 20 h, the concentration of active enzyme 1 decreases from 0.08 to 0.079 g L^{-1}, and the concentration of active enzyme 2 decreases from 0.3 to 0.29 g L^{-1} due to enzyme denaturation. This effect can also be recognised in the concentrations of substrate and product. The substrate concentration increases to approx. 40 g L^{-1}, and the product concentration decreases to 67 g L^{-1} towards the end of the process.

For the simulation of the proteolysis process, it can be seen that after the start-up phase of approx. 45 min, the concentration of the substrate rises to approx. 56 g L^{-1}, and the product concentration rises to approx. 44 g L^{-1}. During a processing time of 20 h, the concentration of active enzyme 1 decreases from 0.6 to 0.55 g L^{-1}, and the concentration

of active enzyme 2 decreases from 0.5 to 0.46 g L^{-1} due to enzyme denaturation. This effect can also be recognised in the concentrations of substrate and product. The substrate concentration increases up to approx. 59 g L^{-1}, and the product concentration decreases to 41 g L^{-1} towards the end of the process.

A decrease in enzyme activity affects the conversion of the substrate to the product in starch hydrolysis, as well as in proteolysis. By determining the content of the substrate and product, the enzyme denaturation constant can be identified. With the help of the DT core model, future experiments can be planned in which the enzyme stability can be determined under different process conditions (temperature, pH value).

The new software tool concept enabled the rapid creation of the DT core model for enzymatic hydrolysis processes in a PBR. The desired specifications of the DT core model were entered into the user interface of the new software tool concept. After that, the source code creation of the DT core model took less than one minute, instead of several days if this had to be performed manually. One STR model of this DT core model contains 25 differential equations. The network of ten connected STR models increases the number of differential equations to 250. As the volume in the individual STRs of the PBR does not change, the dilution term in the differential equations for the calculation of the concentrations (see Equations (5) and (6)) could be removed. Since each STR model of the DT core model contains the same biokinetic and physico-chemical submodels, the number of model parameters increases only slightly using ten connected STR models. There are 10 additional parameters describing the exchange area between the STRs. In addition, 20 new control files are added, which specify the flow between the STRs.

Since the newly developed DT core model can map the dynamic behaviour of a PBR approximately, it can serve as a basis for the development of control and automation strategies and thus accelerate the design of a future real process.

4. Conclusions

The new software tool concept enables the rapid and flexible development of bioprocess DT core models. It is possible to create DT core models for various reactor configurations by linking multiple STR models into a network in the reactor submodel. The software tool concept is based on a model library comprising nine different biokinetics with initial parameterisations for a variety of microorganisms and cell lines as well enzymatic systems that can be used as a basis for new biokinetic models. Furthermore, the model library contains five different physico-chemical models that can calculate the most important physico-chemical variables occurring in bioprocesses. In addition, the physico-chemical variables can be predefined with a fixed value or profile. The user can choose the organism, additional enzymatic and biocatalytic reactions and physico-chemical models and create a custom bioprocess DT core model within an hour, compared to several days. This rapid development based on a modular submodel framework also enables faster parameterisations of the developed custom bioprocess DT core models. Submodels can be parameterised independently and sequentially from each other. In the first step, the biokinetic submodel is parameterised with the values of physico-chemical variables as fixed profiles. In the next step, physico-chemical models are added to the DT core model and parameterised. This accelerates parameterisation by at least 90% since time constants in the biokinetic model for microorganisms are generally greater than in the physico-chemical submodel (e.g., temperature model). Despite a user-defined number of STR models, only one biokinetic and one physico-chemical submodel with only one set of parameters are required since the same microorganisms are used in the whole system. The number of connected STR models is only limited by the performance of the PC used for computing.

In the future, the software tool concept for the development of bioprocess DT core models will be continuously upgraded. This includes a systematic expansion of the model library, further options for accelerating the computing time and a further increase in user-friendliness. Using the new software tool concept, the creation and parameterisation of various bioprocess DT core models can be accelerated, and the application possibili-

ties of the DT core models, e.g., for process, control and automation development, can be increased.

Author Contributions: A.M., C.A. and V.C.H. carried out the programming and simulation work. A.M., C.A., R.P., F.B. and V.C.H. conceived the experiments. A.M. conducted the experiments. A.M. and C.A. performed the statistical analysis and figure generation and A.M., C.A., R.P., F.B. and V.C.H. reviewed the manuscript. All authors have read and agreed to the published version of the manuscript.

Funding: Parts of this research were funded by the Federal Ministry of Education and Research (Germany) and conducted in cooperation with the Ingenieurbüro Dr.-Ing. Schoop GmbH (Hamburg, Germany), within the research projects "protP.S.I.", grant numbers: BMBF 031B0405C and BMBF 031B1080D and "genBioNMPC: New generic Bio-NMPC for the development of dynamic bioeconomic processes", grant number: BMBF 031B1032.

Institutional Review Board Statement: Not applicable.

Informed Consent Statement: Not applicable.

Data Availability Statement: All data necessary for the comprehensibility of this work can be found in this publication or the references given.

Conflicts of Interest: Author Christian Appl is employed by the company "s&h Ingenieurgesellschaft mbH". But for purposes of this investigation, there was no financing relationship with the company; therefore, there are no conflicts of interest. The remaining authors declare that the research was conducted in the absence of any commercial or financial relationships that could be construed as a potential conflict of interest.

References

1. Appl, C.; Moser, A.; Baganz, F.; Hass, V.C. Digital Twins for Bioprocess Control Strategy Development and Realisation. *Adv. Biochem. Eng. Biotechnol.* **2020**, *177*, 63–94. [CrossRef]
2. Grieves, M. *Origins of the Digital Twin Concept*; Working Paper; Florida Institute of Technology: Melbourne, FL, USA, 2016.
3. Glaessgen, E.; Stargel, D. The Digital Twin Paradigm for Future NASA and U.S. Air Force Vehicles. In Proceedings of the 53rd AIAA/ASME/ASCE/AHS/ASC Structures, Structural Dynamics and Materials Conference, Honolulu, HI, USA, 23–26 April 2012. [CrossRef]
4. El Saddik, A. Digital Twins: The Convergence of Multimedia Technologies. *IEEE MultiMedia* **2018**, *25*, 87–92. [CrossRef]
5. He, R.; Chen, G.; Dong, C.; Sun, S.; Shen, X. Data-driven digital twin technology for optimized control in process systems. *ISA Trans.* **2019**, *95*, 221–234. [CrossRef]
6. Zobel-Roos, S.; Schmidt, A.; Mestmäcker, F.; Mouellef, M.; Huter, M.; Uhlenbrock, L.; Kornecki, M.; Lohmann, L.; Ditz, R.; Strube, J. Accelerating Biologics Manufacturing by Modeling or: Is Approval under the QbD and PAT Approaches Demanded by Authorities Acceptable Without a Digital-Twin? *Processes* **2019**, *7*, 94. [CrossRef]
7. Blesgen, A.; Hass, V.C. Operator Training Simulator for Anaerobic Digestion Processes. *IFAC Proc. Vol.* **2010**, *43*, 353–358. [CrossRef]
8. Moser, A.; Appl, C.; Brüning, S.; Hass, V.C. Mechanistic Mathematical Models as a Basis for Digital Twins. *Adv. Biochem. Eng. Biotechnol.* **2020**, *176*, 133–180. [CrossRef]
9. Ingenieurbüro Dr.-Ing.Schoop GmbH. *WinErs*; Ingenieurbüro Dr.-Ing.Schoop GmbH: Hamburg, Germany, 2018.
10. Nagy, Z.K. Model based control of a yeast fermentation bioreactor using optimally designed artificial neural networks. *Chem. Eng. J.* **2007**, *127*, 95–109. [CrossRef]
11. Chen, L.; Nguang, S.K.; Chen, X.D.; Li, X.M. Modelling and optimization of fed-batch fermentation processes using dynamic neural networks and genetic algorithms. *Biochem. Eng. J.* **2004**, *22*, 51–61. [CrossRef]
12. Grahovac, J.; Jokić, A.; Dodić, J.; Vučurović, D.; Dodić, S. Modelling and prediction of bioethanol production from intermediates and byproduct of sugar beet processing using neural networks. *Renew. Energy* **2016**, *85*, 953–958. [CrossRef]
13. Konstantinov, K.B.; Yoshida, T. An expert approach for control of fermentation processes as variable structure plants. *J. Ferment. Bioeng.* **1990**, *70*, 48–57. [CrossRef]
14. Sahakyan, M.; Aung, Z.; Rahwan, T. Explainable Artificial Intelligence for Tabular Data: A Survey. *IEEE Access* **2021**, *9*, 135392–135422. [CrossRef]
15. Treloar, N.J.; Fedorec, A.J.H.; Ingalls, B.; Barnes, C.P. Deep reinforcement learning for the control of microbial co-cultures in bioreactors. *PLoS Comput. Biol.* **2020**, *16*, e1007783. [CrossRef] [PubMed]
16. Von Stosch, M.; Davy, S.; Francois, K.; Galvanauskas, V.; Hamelink, J.-M.; Luebbert, A.; Mayer, M.; Oliveira, R.; O'Kennedy, R.; Rice, P.; et al. Hybrid modeling for quality by design and PAT-benefits and challenges of applications in biopharmaceutical industry. *Biotechnol. J.* **2014**, *9*, 719–726. [CrossRef] [PubMed]

17. Zadeh, L.A. Fuzzy sets. *Inf. Control* **1965**, *8*, 338–353. [CrossRef]
18. Ying, H. Essentials of fuzzy modeling and control. *J. Am. Soc. Inf. Sci.* **1995**, *46*, 791–792. [CrossRef]
19. Karakuzu, C.; Türker, M.; Öztürk, S. Modelling, on-line state estimation and fuzzy control of production scale fed-batch baker's yeast fermentation. *Control. Eng. Pract.* **2006**, *14*, 959–974. [CrossRef]
20. Horiuchi, J.-I. Fuzzy modeling and control of biological processes. *J. Biosci. Bioeng.* **2002**, *94*, 574–578. [CrossRef]
21. Monod, J. The Growth of Bacterial Cultures. *Annu. Rev. Microbiol.* **1949**, *3*, 371–394. [CrossRef]
22. Michaelis, L.; Menten, M.L. Kinetik der Invertinwirkung. *Biochem. Ztg.* **1913**, *49*, 333–369.
23. Cornish-Bowden, A. One hundred years of Michaelis–Menten kinetics. *Perspect. Sci.* **2015**, *4*, 3–9. [CrossRef]
24. González-Figueredo, C.; Flores-Estrella, R.A.; Rojas-Rejón, O.A. Fermentation: Metabolism, Kinetic Models, and Bioprocessing. In *Current Topics in Biochemical Engineering*; Shiomi, N., Ed.; IntechOpen: London, UK, 2019; ISBN 978-1-83881-209-6.
25. Craven, S.; Shirsat, N.; Whelan, J.; Glennon, B. Process model comparison and transferability across bioreactor scales and modes of operation for a mammalian cell bioprocess. *Biotechnol. Prog.* **2013**, *29*, 186–196. [CrossRef] [PubMed]
26. Hodgson, B.J.; Taylor, C.N.; Ushio, M.; Leigh, J.R.; Kalganova, T.; Baganz, F. Intelligent modelling of bioprocesses: A comparison of structured and unstructured approaches. *Bioprocess Biosyst. Eng.* **2004**, *26*, 353–359. [CrossRef]
27. Esener, A.A.; Roels, J.A.; Kossen, N.W. Theory and applications of unstructured growth models: Kinetic and energetic aspects. *Biotechnol. Bioeng.* **1983**, *25*, 2803–2841. [CrossRef] [PubMed]
28. Shuler, M.L.; Leung, S.; Dick, C.C. A Mathematical Model for the Growth of a Single Bacterial Cell. *Ann. N. Y. Acad. Sci.* **1979**, *326*, 35–52. [CrossRef]
29. Nielsen, J.; Nikolajsen, K.; Villadsen, J. Structured modeling of a microbial system: I. A theoretical study of lactic acid fermentation. *Biotechnol. Bioeng.* **1991**, *38*, 1–10. [CrossRef]
30. Appl, C.; Baganz, F.; Hass, V.C. Development of a Digital Twin for Enzymatic Hydrolysis Processes. *Processes* **2021**, *9*, 1734. [CrossRef]
31. Brüning, S. Development of a Generalized Process Model for Optimization of Biotechnological Processes. Ph.D. Thesis, Jacobs University, Bremen, Germany, 2016.
32. Hass, V.C.; Kuhnen, F.; Schoop, K.-M. An environment for the development of operator training systems (OTS) from chemical engineering models. *Comput. Aided Chem. Eng.* **2005**, *20*, 289–293. [CrossRef]
33. R Core Team. *R Foundation for Statistical Computing*; R Core Team: Vienna, Austria, 2014.
34. Hirschmann, R. Evaluating the Potential of Anaerobic Production of Ethyl(3)Hydroxybutyrate for Integration in Biorefineries. Ph.D. Thesis, University College London, London, UK, 2022.
35. Gerlach, I.; Brüning, S.; Gustavsson, R.; Mandenius, C.-F.; Hass, V.C. Operator training in recombinant protein production using a structured simulator model. *J. Biotechnol.* **2014**, *177*, 53–59. [CrossRef]
36. Kuntzsch, S. Energy Efficiency Investigations with a New Operator Training Simulator for Biorefineries. Ph.D. Thesis, Jacobs University, Bremen, Germany, 2014.
37. Laurí, D.; Lennox, B.; Camacho, J. Model predictive control for batch processes: Ensuring validity of predictions. *J. Process. Control.* **2014**, *24*, 239–249. [CrossRef]
38. Mears, L.; Stocks, S.M.; Sin, G.; Gernaey, K.V. A review of control strategies for manipulating the feed rate in fed-batch fermentation processes. *J. Biotechnol.* **2017**, *245*, 34–46. [CrossRef]
39. Moser, A.; Kuchemüller, K.B.; Deppe, S.; Hernández Rodríguez, T.; Frahm, B.; Pörtner, R.; Hass, V.C.; Möller, J. Model-assisted DoE software: Optimization of growth and biocatalysis in Saccharomyces cerevisiae bioprocesses. *Bioprocess Biosyst. Eng.* **2021**, *44*, 683–700. [CrossRef] [PubMed]
40. Mandenius, C.-F.; Brundin, A. Bioprocess optimization using design-of-experiments methodology. *Biotechnol. Prog.* **2008**, *24*, 1191–1203. [CrossRef]
41. Candioti, L.V.; de Zan, M.M.; Cámara, M.S.; Goicoechea, H.C. Experimental design and multiple response optimization. Using the desirability function in analytical methods development. *Talanta* **2014**, *124*, 123–138. [CrossRef] [PubMed]
42. Möller, J.; Kuchemüller, K.B.; Steinmetz, T.; Koopmann, K.S.; Pörtner, R. Model-assisted Design of Experiments as a concept for knowledge-based bioprocess development. *Bioprocess Biosyst. Eng.* **2019**, *42*, 867–882. [CrossRef] [PubMed]
43. Neubauer, P.; Junne, S. Scale-down simulators for metabolic analysis of large-scale bioprocesses. *Curr. Opin. Biotechnol.* **2010**, *21*, 114–121. [CrossRef] [PubMed]
44. Oosterhuis, N.M.; Kossen, N.W. Dissolved oxygen concentration profiles in a production-scale bioreactor. *Biotechnol. Bioeng.* **1984**, *26*, 546–550. [CrossRef]
45. Hewitt, C.J.; Nienow, A.W. The scale-up of microbial batch and fed-batch fermentation processes. *Adv. Appl. Microbiol.* **2007**, *62*, 105–135. [CrossRef]
46. Enfors, S.O.; Jahic, M.; Rozkov, A.; Xu, B.; Hecker, M.; Jürgen, B.; Krüger, E.; Schweder, T.; Hamer, G.; O'Beirne, D.; et al. Physiological responses to mixing in large scale bioreactors. *J. Biotechnol.* **2001**, *85*, 175–185. [CrossRef]
47. George, S.; Larsson, G.; Olsson, K.; Enfors, S.-O. Comparison of the Baker's yeast process performance in laboratory and production scale. *Bioprocess Eng.* **1998**, *18*, 135–142. [CrossRef]
48. Larsson, G.; Trnkvist, M.; Wernersson, E.S.; Trgrdh, C.; Noorman, H.; Enfors, S.-O. Substrate gradients in bioreactors: Origin and consequences. *Bioprocess Eng.* **1996**, *14*, 281–289. [CrossRef]

49. Formenti, L.R.; Nørregaard, A.; Bolic, A.; Hernandez, D.Q.; Hagemann, T.; Heins, A.-L.; Larsson, H.; Mears, L.; Mauricio-Iglesias, M.; Krühne, U.; et al. Challenges in industrial fermentation technology research. *Biotechnol. J.* **2014**, *9*, 727–738. [CrossRef] [PubMed]
50. Sweere, A.P.J.; Matla, Y.A.; Zandvliet, J.; Luyben, K.C.A.M.; Kossen, N.W.F. Experimental simulation of glucose fluctuations. *Appl. Microbiol. Biotechnol.* **1988**, *28*, 109–115. [CrossRef]
51. Sandoval-Basurto, E.A.; Gosset, G.; Bolívar, F.; Ramírez, O.T. Culture of Escherichia coli under dissolved oxygen gradients simulated in a two-compartment scale-down system: Metabolic response and production of recombinant protein. *Biotechnol. Bioeng.* **2005**, *89*, 453–463. [CrossRef] [PubMed]
52. Lara, A.R.; Galindo, E.; Ramírez, O.T.; Palomares, L.A. Living with heterogeneities in bioreactors: Understanding the effects of environmental gradients on cells. *Mol. Biotechnol.* **2006**, *34*, 355–381. [CrossRef]
53. Fiechter, A.; Fuhrmann, G.F.; Käppeli, O. Regulation of Glucose Metabolism in Growing Yeast Cells. *Adv. Microb. Physiol.* **1981**, *22*, 123–183. [CrossRef]
54. Sonnleitner, B.; Käppeli, O. Growth of Saccharomyces cerevisiae is controlled by its limited respiratory capacity: Formulation and verification of a hypothesis. *Biotechnol. Bioeng.* **1986**, *28*, 927–937. [CrossRef]
55. Bai, F.W.; Anderson, W.A.; Moo-Young, M. Ethanol fermentation technologies from sugar and starch feedstocks. *Biotechnol. Adv.* **2008**, *26*, 89–105. [CrossRef]
56. Larsson, C.; von Stockar, U.; Marison, I.; Gustafsson, L. Growth and Metabolism of Saccharomyces cerevisiae in Chemostat Cultures under Carbon-, Nitrogen-, or Carbon- and Nitrogen-Limiting Conditions. *J. Bacteriol.* **1993**, *175*, 4809–4816. [CrossRef]
57. Nelder, J.A.; Mead, R. A Simplex Method for Function Minimization. *Comput. J.* **1965**, *7*, 308–313. [CrossRef]
58. Nienow, A.W. Scale-Up, Stirred Tank Reactors. In *Encyclopedia of Industrial Biotechnology: Bioprocess, Bioseparation, and Cell Technology*; John Wiley & Sons, Inc.: Hoboken, NJ, USA, 2010; pp. 1–38. [CrossRef]
59. Van't Riet, K.; Tramper, J. *Basic Bioreactor Design*, 1st ed.; CRC Press: Boca Raton, FL, USA, 1991; ISBN 9781482293333.

fermentation

MDPI

Article

Enhanced Fermentation Process for Production of High Docosahexaenoic Acid Content by *Schizochytrium* sp. GCD2032

Liucheng Long [1,2,†], Xiaoqing Ren [3,†], Feiyu Zhang [3], Aijia Shi [2], Yida Zhai [2], Wuxi Chen [2], Yu Duan [2], Pengbao Shi [1,*], Limei Chen [2,*] and Demao Li [2,*]

[1] College of Food Science & Technology, Hebei Normal University of Science & Technology, Qinhuangdao 066004, China; longlc0324@163.com
[2] Tianjin Key Laboratory for Industrial Biological System and Bioprocessing Engineering, Tianjin Institute of Industrial Biotechnology, Chinese Academy of Sciences, Tianjin 300308, China; ssshiaijia@163.com (A.S.); zhaiyd@tib.cas.cn (Y.Z.); chen_wx@tib.cas.cn (W.C.); duanyu@tib.cas.cn (Y.D.)
[3] College of Food Science and Bioengineering, Tianjin Agricultural University, Tianjin 300392, China; xiaoqingren@tjau.edu.cn (X.R.); zfy970501@163.com (F.Z.)
* Correspondence: spb2651@hevttc.edu.cn (P.S.); chen_lm@tib.cas.cn (L.C.); li_dm@tib.cas.cn (D.L.); Tel.: +86-(022)-84861993 (D.L.)
† Authors that contribute equally.

Abstract: There is significant demand for high-purity DHA in the pharmaceutical industry. Traditionally, this high-purity DHA is extracted from raw materials with relatively low DHA content (10–20%), such as fish oil. Recently, through electroporation-induced mutation, a high-DHA-content strain of *Schizochytrium* sp. GCD2032 was isolated. To further enhance its DHA production, optimizations were conducted on the culture medium and fermentation conditions (in shaking flasks), as well as different nitrogen source concentrations (in a 5 L fermenter) for biomass, fatty acid content, and DHA content (as a percentage of total fatty acids). In a 5 L fermenter, *Schizochytrium* sp. GCD2032 achieved a biomass of 50 g/L, with fatty acid content of 55.71% and DHA content of 61.29%. Notably, the DHA content reached an impressive 341.45 mg/g of dry weight. This strain consistently produces high levels of fatty acids and DHA, demonstrating significant potential for pharmaceutical applications.

Keywords: *Schizochytrium* sp. GCD2032; fermentation optimization; nitrogen source; fatty acids; DHA

1. Introduction

Docosahexaenoic acid (DHA) is a member of the omega-3 series of polyunsaturated fatty acids (PUFAs) and is abundantly found in the human nervous system, retina, and breast milk [1]. It plays critical roles in human physiology, including promoting brain development, protecting vision, and exerting anti-cancer and anti-inflammatory effects [2–4]. Furthermore, DHA is beneficial in the prevention and treatment of cardiovascular diseases, Alzheimer's disease, and immune disorders [5]. Recent research indicates that PUFAs like Arachidonic acid (ARA) and DHA can inactivate the severe acute respiratory syndrome coronavirus, enhancing human resilience and recovery from viral infections. They may also improve the structure of gut microbiota [6,7]. Consequently, DHA is increasingly recognized and applied in pharmaceuticals. High-purity polyunsaturated fatty acids (>95%) are essential for synthesizing specialized pro-resolving mediators (SPMs) such as protectins, resolvins, and maresins used in clinical settings [8]. However, the current primary source of high-purity DHA is primarily extracted from raw materials with low content, such as fish oil. The preparation of raw materials with high DHA content remains a significant factor limiting production costs.

In recent years, *Schizochytrium* has gained significant value as an ideal industrial strain for DHA production due to its high DHA content, rapid growth rate, safety certification, and ease of cultivation [9–13]. Currently, industrial strains can achieve DHA content as high as 50–55%. Some studies have attempted to further increase DHA content. For instance,

Wang et al. successfully engineered a strain of *Schizochytrium* with DHA content comprising 61% of total fatty acids, reaching 331 mg/g [14]. Chen et al. developed a high-voltage electroporation-induced mutagenesis method and identified a strain named *Schizochytrium* sp. GCD2032 with 3.51%, 95.51%, and 71.67% higher fatty acid content, DHA content, and DHA yield than those of the wild strain, although its fermentation process has not yet been optimized [10].

The yield and quality of DHA are influenced not only by the strain itself but also by the fermentation process. For example, variations in carbon/nitrogen (C/N) source supply and cultivation temperature can lead to coordinated changes in DHA content, lipid content, and microbial biomass [15]. A high C/N ratio favours lipid accumulation, but excessively high ratios can decrease DHA content within the lipids. During nitrogen starvation, decreased AMP levels in the mitochondrial matrix inhibit the conversion of isocitrate to α-ketoglutarate, leading to citrate accumulation. Once citrate reaches a critical concentration, it is converted by ATP-citrate lyase into acetyl-CoA and oxaloacetate, facilitating lipid accumulation through reverse β-oxidation [16]. Researchers have conducted extensive studies on fermentation optimization [17–19], but only a few reports have achieved DHA content exceeding 60%. However, these instances often come at the cost of lower lipid content, resulting in reduced conversion efficiency [20].

In this study, the strain *Schizochytrium* sp. GCD2032 with a high DHA production capacity, which was screened out in the previous study, was used [10]. Initially, the stability of *Schizochytrium* sp. GCD2032 was assessed, and following the establishment of a stable culture, optimization of the fermentation medium and conditions was performed in shaking flasks. Subsequently, scale-up fermentation was conducted in a 5 L fermenter, with particular attention given to the impact of different nitrogen source compositions and concentrations on DHA production (Figure 1). The study aimed to investigate the synergistic changes among various components of *Schizochytrium* sp. GCD2032 during fermentation, providing technical support for future industrial-scale production of high DHA content.

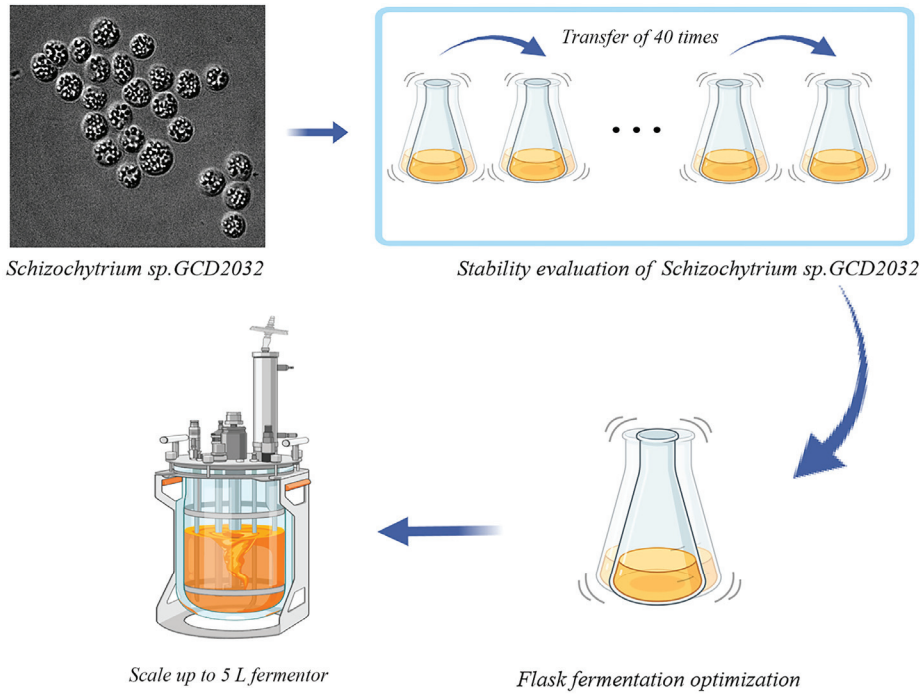

Figure 1. The main research process.

2. Materials and Methods

2.1. Strain and Medium

Schizochytrium sp. GCD2032, a mutant strain screened by our laboratory, is stored in a −80 °C ultra-low temperature freezer [10]. The seed liquid medium and basic fermentation medium were prepared according to references in the literature [10,21]. The seed medium contained glucose (30 g/L; AR, Fufeng Biotechnology Co., Qingdao, China), yeast extract (2 g/L; AR, OXOID, Cheshire, UK), soya peptone (2 g/L; AR, OXOID), and artificial seawater salt (15 g/L; AR, Tianjin Damao Chemical Reagent Factory, Tianjin, China). The original fermentation medium was comprised of glucose (80 g/L), yeast extract (4 g/L), soya peptone (4 g/L), artificial seawater salt (15 g/L), $MgCl_2 \cdot 6H_2O$ (6.4 g/L; AR, Shanghai McLean Biochemical Technology Co., Shanghai, China), $CaCl_2 \cdot 2H_2O$ (1 g/L; AR, Tianjin Damao Chemical Reagent Factory), $MgSO_4 \cdot 7H_2O$ (5 g/L; AR, Shanghai McLean Biochemical Technology Co.), and KCl (2 g/L; AR, Shanghai McLean Biochemical Technology Co.). Both media were sterilized for 20 min at 115 °C before inoculation [21].

2.2. Experimental Methods

2.2.1. Preparation of Seeds

Schizochytrium sp. GCD2032, retrieved from the −80 °C ultra-low temperature freezer (Thermo 900), was streaked onto glycerol tubes after thawing. A 100 µL aliquot was spread onto seed medium plates (including 18 g/L agar) and incubated at 28 °C for 48 h. Single colonies were picked and transferred to 50 mL seed liquid medium in 250 mL Erlenmeyer flasks. The cultures were shaken at 180 rpm for 19–25 h until an OD 600 of 0.6 was reached. This was the seed ready for inoculation.

2.2.2. Strain Stability Evaluation

The seed culture (10% v/v) was transferred to 50 mL of fermentation medium in 250 mL Erlenmeyer flasks and incubated at 180 rpm and 28 °C. After fermentation in the 250 mL flask for 96 h, 5 mL of the fermentation broth was transferred to a new flask with the same medium for the same amount of time. This process was repeated 40 times and the biomass, fatty acid content, and DHA content were determined every 10 cycles during fermentation.

2.2.3. Single-Factor Fermentation Optimization of *Schizochytrium* sp. GCD2032

Various parameters were investigated in shake flasks to optimize DHA production by *Schizochytrium* sp. GCD2032. Factors examined included glucose concentration, nitrogen source and concentration, and inoculum volume in flasks (250 mL) with 50 mL liquid medium (natural pH, 2% inoculum, 28 °C, 180 rpm) after 96 h of incubation.

Carbon Source

Glucose, xylose, fructose, sucrose, glycerol, and lactose were tested for the effects of different carbon sources. The fermentation medium was modified from the original fermentation medium with a different carbon source at 80 g/L. After fermentation, residual glucose, biomass, fatty acid content, and DHA content were determined.

Glucose Concentration

Different glucose concentrations (60 g/L, 70 g/L, 80 g/L, 90 g/L, 100 g/L) were tested for the effects of glucose concentration. The fermentation medium was modified from the original fermentation medium with different concentrations of glucose. After fermentation, residual glucose, biomass, fatty acid content, and DHA content were determined.

Nitrogen Source

Yeast extract, corn steep powder, peptone, tryptone, ammonium sulfate, ammonium chloride, and ammonium nitrate at 5 g/L were tested for the effects of different nitrogen sources. The fermentation medium was modified from the original fermentation medium

with different nitrogen sources. After fermentation, residual glucose, biomass, fatty acid content, and DHA content were determined.

Yeast Extract Concentration

Different concentrations of yeast extract (3 g/L, 5 g/L, 7 g/L, 9 g/L, 11 g/L) were tested for the effects of yeast extract concentration. The fermentation medium was modified from the original fermentation medium with different concentrations of yeast extract. After fermentation, residual glucose, biomass, fatty acid content, and DHA content were determined.

Inoculation Volume

Single-factor experiments were conducted using inoculation volumes of 2%, 4%, 6%, 8%, and 10% for fermentation. The fermentation medium was the original fermentation medium with 80 g/L of glucose and 5 g/L of yeast extract. When preparing the fermentation medium, a certain volume of seed liquid was reserved according to its volume to maintain the total volume at 50 mL. After fermentation, residual glucose, biomass, fatty acid content, and DHA content were determined.

Effects of Different Concentrations of Yeast Extract in a 5 L Stirred Tank Fermenter

Fermentation was scaled up to 5 L in a glass fermenter (Shanghai Baoxing Biological Equipment Engineering Co., Shanghai, China) with single-blade agitation technology and jacketed for temperature control. The optimized medium in 2.2.3 named 5-N, the medium modified from 5-N by fed-batch of glucose named 5-F, the media modified from 5-F using 10 g/L, 15 g/L, 20 g/L, and 25 g/L of yeast extract named 10-F, 15-F, 20-F, and 25-F were used to study the effects on biomass, fatty acid content, and DHA content.

The seed was prepared in a 250 mL flask with 50 mL working volume in the seed medium and was inoculated into the 5 L fermenter when the OD reached 0.6. Fed-batch fermentation was carried out in the 5 L fermenter at 300 rpm rotation speed, 1 vvm aeration rate, 28 °C, and pH 6.0. The initial volume in the 5 L fermenter was set at 3.15 L. Before inoculation, 0.35 L of 400 g/L glucose solution was added to the fermenter to a final concentration of 33 g/L. Subsequently, when the residual glucose was less than 20 g/L after 36 h, 400 g/L of glucose solution was continuously added to the fermenter to maintain its glucose concentration at between 20 and 30 g/L. During the fermentation process, 2 M sodium hydroxide solution and 1 M sulfuric acid solution were used to adjust the pH value, and samples were collected every 12 h to determine the biomass, fatty acid content, and DHA content. The fermentation was carried out for 142 h and the down-tanking was carried out when the biomass did not increase any more or when the growth of the biomass slowed down.

2.3. Analytical Methods

2.3.1. Glucose Concentration and Glucose Consumption Rate Determination

The glucose concentration was determined by a biosensor (SBA-40D, Shandong Academy of Sciences, Jinan, China) according to Guo et al. as follows: Absorb 2 mL fermentation liquid into a 2 mL centrifuge tube, centrifuge at 8000 r/min for 5 min [22], and run the supernatant through the water filter membrane to filter impurities. The filtered liquid was diluted 100 times with deionized water (the glucose concentration was stable in the range of 0.05–1 g/L) and loaded into 2 mL centrifuge tubes for determination (M0, g/L). The glucose curve was calibrated by its program.

$$\text{Glucose Concentration (g/L)} = \text{M0} \times 100 \quad (1)$$

The glucose consumption rate was defined as the glucose consumed (g/L) per hour, calculated as shown in Equation (2).

$$\text{Glucose consumption rate (g/L/h)} = \text{glucose consumed (g/L)/time used (h)} \quad (2)$$

2.3.2. Determination of the Biomass

Biomass represents the total dry weight of *Schizochytrium* sp. GCD2032 in a given volume (g/L). The method from Keskin et al. was used to determine the biomass [23]. At the end of cultivation, centrifuged cell pellets from a given volume (V, L) were washed three times with deionized water. Subsequently, the centrifuged samples were frozen and dried in a freeze dryer (F-D1A-50+, Beijing Boyikang Co., Ltd., Tianjin, China) until a constant weight was achieved (M1, g). The calculation was performed using Equation (3).

$$\text{Biomass (g/L)} = \text{M1}/\text{V} \quad (3)$$

2.3.3. Fatty Acid Extraction and Quantification

According to Zhao et al., the following improved methods were used for fatty acid extraction [24]. 0.2 g mass of biomass powder was weighed to perform lipid extraction. An aqua distillate/hydrochloric acid mixture of 10 mL (1:1 v/v) was added to the powder and placed into 75 °C water baths for 2 h after mixing. After the sample was cooled, 10 mL n-hexane was added and mixed; this was repeated three times. Supernatants were collected and evaporated in a nitrogen purging instrument (Hangzhou Aosheng Instrument Co., Hangzhou, China) to get a constant weight (M2, g). The fatty acid content was defined as the ratio of the total amount of fatty acids to the dry weight of the cells required to extract the fatty acid, which was quantified using Equation (4).

$$\text{Fatty acid content (\%)} = (\text{M2}/0.2) \times 100 \quad (4)$$

2.3.4. Fatty Acid Composition and DHA Content Analysis

The total fatty acid composition was determined using an improved method from our previous study [12]. Fatty acid methyl esters (FAMEs) were prepared by a modified standard method as follows: 1 mL potassium hydroxide/methanol (0.5 M) was added to extracted fatty acids samples. Samples were heated at 60 °C in water baths for 15 min to saponify. After the samples were cooled, 2 mL of 14% boron trifluoride–methanol complex was added as a catalyst for a 2 min reaction at 60 °C for transesterification. After transesterification, 2 mL of saturated sodium chloride solution was added to prevent emulsification. Then, 2 mL of chromatographically pure n-hexane was added and the transesterified FAMEs were extracted into the n-hexane layer. Finally, 0.5 g anhydrous sodium sulfate was added and gas chromatography (GC) analysis was performed [25].

A gas chromatograph (Agilent 7200 Q-TOF GC/MS) was used for qualitative analysis of all fatty acid fractions in the lipids in *Schizochytrium* sp. GCD2032. The fatty acid fractions of *Schizochytrium* sp. GCD2032 were identified by referring to the peak times of Supelco's 37 fatty acid methyl ester fractions (crm47885) or fatty acid methyl ester standards such as DHA methyl ester [26].

A Shimadzu GC2010 (GC-2010, Shimadzu, Japan) equipped with a hydrogen flame ionization detector (FID) and a Supelco SP-2560 gas-phase capillary column (100 m × 0.25 mm × 0.20 μm, Supelco, Bellefonte, PA, USA) was selected for the gas chromatographic analysis. The parameters were as follows: injection volume: 1 μL; shunt ratio: 30:1; carrier gas: nitrogen; heating procedure: inlet temperature of 250 °C, detector temperature of 260 °C; column chamber procedure: firstly, keep the column at 150 °C for 5 min, then increase it to 180 °C at 8 °C/min, keep it at 180 °C for 5 min, and then increase it to 240 °C at the same temperature increase rate, and finally keep it at 240 °C for 16 min. Samples were injected in split mode during sample collection. DHA content (%) is calculated as the percentage of the DHA peak area to the total peak area of all eluted fatty acids in the determined samples.

2.3.5. DHA Conversion Rate Analysis

The DHA conversion rate is the ratio of DHA production to the glucose used, which is indicated in Equation (5).

$$\text{DHA conversion rate (g/g)} = [\text{Biomass (g/L)} \times \text{Fatty acid content (\%)} \times \text{DHA content (\%)}]/\text{Glucose consumed (g/L)} \quad (5)$$

2.4. Data Statistics and Analysis

The above experiments were repeated three times and are presented as mean ± standard deviation. All data were analyzed using SPSS 20.0 for *t*-tests to determine significant differences in experimental data, with * $p < 0.05$, ** $p < 0.01$, and *** $p < 0.001$.

3. Results

3.1. Stability Assessment of Schizochytrium sp. GCD2032 Fermentation

Schizochytrium sp. GCD2032 is a mutant isolated from an accidental electroporation treatment [10], which needs further evaluation for stable fatty acid production capacity. To evaluate the stability of *Schizochytrium* sp. GCD2032, continuous fermentation over 40 generations was conducted, and biomass, fatty acid content, and DHA content were determined at the 10th, 20th, 30th, and 40th cycles of fermentation (Figure 2A). The results showed that the biomass, fatty acid content, and DHA content of the 10th fermentation cycle strain were 22.9 g/L, 70.24%, and 61.22%, respectively, which were comparable to the original strain [10]. (This also means that there were no differences from the 1st to the 10th generations). However, from the 20th generation of fermentation to the 40th generation of fermentation, the biomass, fatty acid content, and DHA content decreased compared to the 10th generation of fermentation. The biomasses of the 20th, 30th, and 40th generation fermentation strains were 16.35%, 15.66%, and 16.88% lower than that of the 10th generation, while at the same time, the fatty acid content and DHA content were 14.41% and 15.67%, 15.30% and 13.07%, and 13.31% and 13.66% lower, respectively. Notably, there was no significant difference in biomass, fatty acid content, and DHA content of the strain in the 20th, 30th, and 40th fermentation cycles, indicating that it was stable after the 20th consecutive fermentation.

Fermentation stability refers to the ability of a given microbial population to maintain desired morphological and biosynthetic characteristics in qualitative and quantitative terms. The reduced stability of fungi during continuous cultivation is a well-known phenomenon; however, reports in the literature are rather rare [27]. The loss of production capacity of a microorganism may be caused by genetic or epigenetic factors, and factors such as genetic mutations, culture conditions, stress, or ageing may play important roles [28]. For example, scholars have developed a protocol for inducing denaturation in *Trichoderma reesei*, a technique that can be used to calculate the extent of strain denaturation and to compare the denaturing behaviours of different evolved strains. Research has found that *T. reesei* QM6a shows no degeneration and *T. reesei* Rut-C30 exhibits minimal degeneration. This is followed by *T. reesei* Iogen-M4 with approximately 10% degeneration and *T. reesei* Iogen-M10 with nearly 100% degeneration [27]. This variability may enable fungi to better adapt to changing environments; however, it leads to a loss of production capacity in an industrial strain. Thus, it may take some time for *Schizochytrium* sp. GCD2032 to recover after mutations in the genome that lead to loss of biomass and reduced fatty acid content and DHA content.

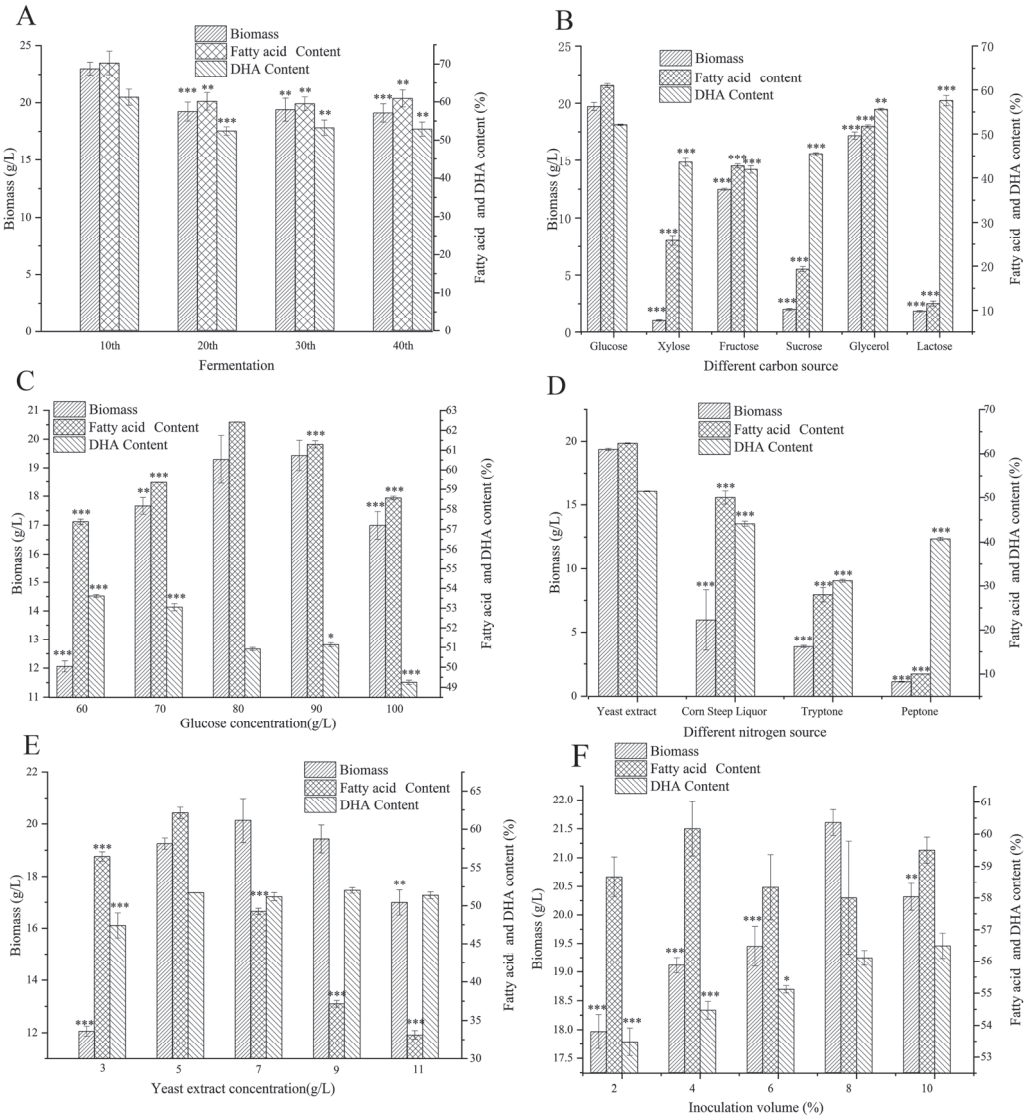

Figure 2. Fermentation characteristics of *Schizochytrium* sp. GCD2032. (**A**) Comparison of the biomass, fatty acid content, and DHA content at the 10th, 20th, 30th, and 40th cycles of fermentation of *Schizochytrium* sp. GCD2032. (**B**) Effects of different carbon sources on fermentation biomass and fatty acid and DHA contents. (**C**) Effects of glucose concentrations on fermentation biomass and fatty acid and DHA contents. (**D**) Effects of different nitrogen sources on fermentation biomass and fatty acid and DHA contents. (**E**) Effects of yeast extract concentrations on fermentation biomass and fatty acid and DHA contents. (**F**) Effects of inoculum volume on fermentation biomass and fatty acid and DHA contents. The statistical significances of the final results were analyzed by *t*-test, * $p < 0.05$, ** $p < 0.01$, *** $p < 0.001$.

3.2. Shake Flask Fermentation Optimization of Schizochytrium sp. GCD2032

To optimize the fermentation conditions of *Schizochytrium* sp. GCD2032, the effects of different carbon sources, carbon concentrations, nitrogen sources, nitrogen concentrations, and inoculum volumes on biomass, fatty acid content, and DHA content were investigated in flasks. The results are shown in Figure 2B–F. *Schizochytrium* sp. GCD2032 demonstrated efficient utilization of glucose, fructose, and glycerol; the highest biomass of 19.71 g/L was observed when glucose was used as a carbon source and the highest DHA content of 55.57% was observed when glycerol was used as a carbon source. In contrast, cultivation with xylose, sucrose, and lactose limited its growth, resulting in generally lower biomass, fatty acids, and DHA production, with minimal utilization (Figure 2B). Biomass and fatty acid content

increased with glucose concentrations ranging from 60 to 80 g/L; however, when the glucose concentration was over 80 g/L, both biomass and fatty acid content decreased. Meanwhile, as glucose concentration increased, DHA content gradually decreased (Figure 2C).

Organic nitrogen sources are more suitable for the growth of *Schizochytrium* sp. GCD2032 compared to inorganic nitrogen sources. *Schizochytrium* sp. GCD2032 grew poorly (biomass less than 1 g/L) when an inorganic nitrogen source (such as NH_4SO_4, $NaNO_3$, etc.,) was used. In a medium where yeast extract was used as the nitrogen source, 69.21%, 80.11%, and 94.21% higher dry weight, 19.86%, 55.11%, and 83.97% higher fatty acids, and 14.09%, 39.34%, and 20.67% higher DHA content were obtained compared to fermentation performed in media with corn steep, tryptone, or peptone as nitrogen sources (Figure 2D). The concentration of yeast extract is one of the important factors affecting DHA content; as yeast extract concentration increases, biomass increases. However, excessive yeast extract hinders the rapid accumulation of fatty acids; therefore, when the yeast extract concentration is 5 g/L, the biomass, fatty acid content, and DHA content are optimal (Figure 2E).

Inoculum volume is also an important parameter. A too-low inoculum volume can lead to a low initial density of microorganisms in the culture medium, thereby affecting their growth rate and metabolic efficiency. Conversely, an excessively high inoculum volume results in a high initial cell density, leading to rapid *Schizochytrium* sp. GCD2032 growth that can cause insufficient oxygen levels in the fermentation broth, which is unfavourable for cellular division metabolism. Optimal inoculum volume ensures proportional substrate consumption and fermentation time, thereby improving nutrient substrate utilization efficiency. In the range from 2% to 8%, the biomass of *Schizochytrium* sp. GCD2032 increased as the inoculum volume increased. When the inoculum reached the maximum value of 8%, the biomass was 21.61 g/L and did not increase further. Subsequently, as the inoculum continued to increase, the biomass of the strain decreased. However, there was no significant effect on the fatty acid content, whereas the DHA content gradually increased to 56.49% with increasing inoculum volume. Taking everything into consideration, an inoculum volume of 8% was chosen as appropriate (Figure 2F).

Research has shown that the addition of citric acid and malic acid can enhance DHA content [13,19]. However, during single-factor fermentation optimization, the influence of citric acid and malic acid on DHA content was examined, and the results indicated that their addition did not affect the biomass, fatty acid content, and DHA content (data not published).

3.3. Scale up in 5 L Fermenters

The effects of different yeast extract concentrations under batch and fed-batch fermentation conditions on fermentation biomass, fatty acid content, and DHA content were investigated (Figure 3). Results of fermentation in 5 L fermenters using optimized shake flask media showed biomass, fatty acid content, and DHA content comparable to shake flask results, maybe indicating glucose limitations for *Schizochytrium* sp. GCD2032 in the 5 L fermenter despite its better oxygen availability (Figure 3A). During fed-batch fermentation with increasing yeast extract concentrations, the highest biomass and DHA content were achieved after 132 h, reaching peak values with 20 g/L of yeast extract before declining. Total fatty acid content varied minimally between 5 and 15 g/L of yeast extract as the nitrogen source, decreasing gradually as yeast extract concentration increased from 20 to 25 g/L, where 25 g/L of yeast extract resulted in only 25% fatty acid content. Glucose uptake and the rate of DHA conversion by *Schizochytrium* sp. GCD2032 also increased gradually with increasing yeast extract concentration, reaching maximum levels at 20 g/L of yeast extract, indicating that 20 g/L of yeast extract was optimal for biomass and fatty acid production in the 5 L fermenters, with a DHA conversion rate of 0.17 g/g (Figure 3B).

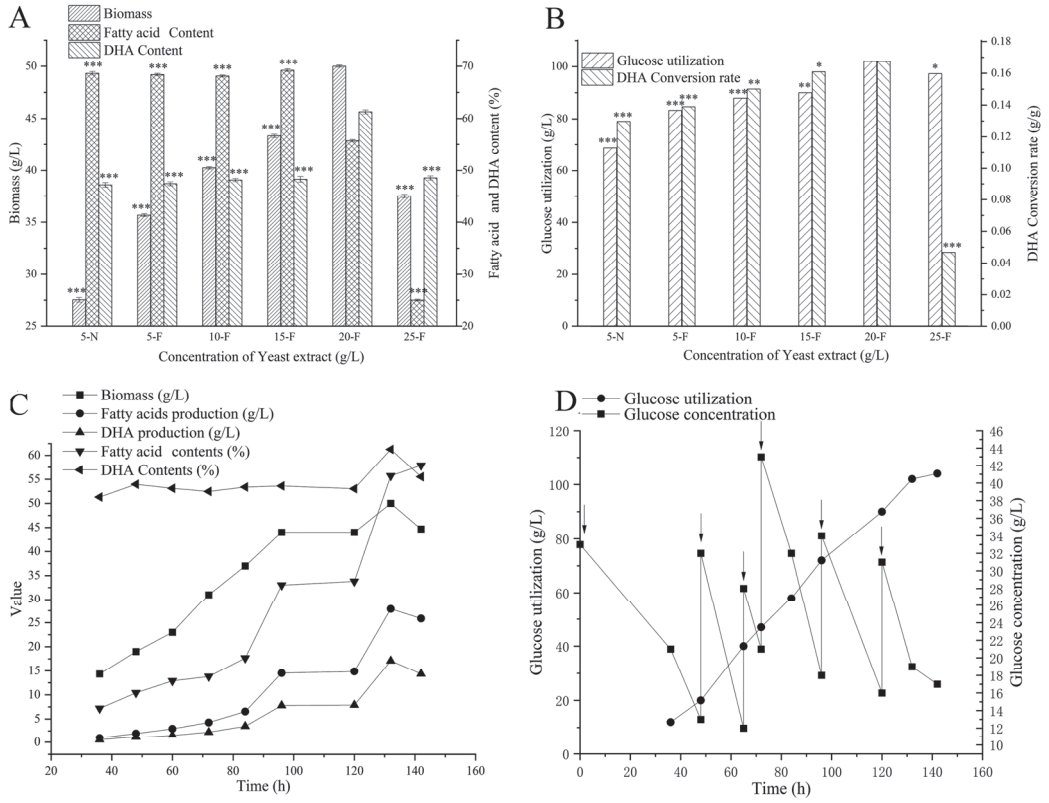

Figure 3. Fermentation of *Schizochytrium* sp. GCD2032 in a stirred tank fermenter. (**A**) Effects of yeast extract concentrations on biomass and fatty acid and DHA contents; (**B**) effects of yeast extract concentrations on glucose utilization and DHA conversion rate; (**C**) fermentation curve of *Schizochytrium* GCD2032 with 20 g/L of yeast extract as nitrogen source (the data and the units are all shown in the legend); and (**D**) glucose utilization and glucose-fed curve of GCD2032 with 20 g/L of yeast extract as nitrogen source. The statistical significances of the final results were analyzed by *t*-test, * $p < 0.05$, ** $p < 0.01$, *** $p < 0.001$.

Figure 3C displays the variations in biomass, fatty acid production and content, and DHA production and content, with feeding glucose as the carbon source (Figure 3D) and 20 g/L of yeast extract as the nitrogen source. The results show that as fermentation progresses, biomass, fatty acid production, fatty acid content, and DHA content reach their peaks at 132 h, with the maximum DHA content reaching 61.29%, followed by a decline; meanwhile, fatty acid content continues to increase. Glucose consumption increases linearly throughout the fermentation process, reaching its highest point at 132 h, after which its rate gradually slows down (Figure 3D).

Nitrogen deficiency is a major trigger for initiating fatty acid synthesis [29]. Compared with flask fermentation, a 5 L fermenter requires better oxygenation and space, thereby improving the efficiency of microorganism growth and fatty acid accumulation. Therefore, in fed-batch fermentation, if the optimal nitrogen source concentration from shake flasks is used in the 5 L fermenter, the nitrogen source concentration will limit the fermentation yield, and increasing the nitrogen source concentration is necessary to improve the fatty acid yield. Therefore, in theory, excessively high nitrogen source concentrations may delay the initiation of fatty acid accumulation, resulting in high biomass but insufficient fatty acid accumulation. Conversely, too low nitrogen source concentrations may halt cell division and initiate fatty acid accumulation without accumulating enough cells, resulting in high fatty acid content per cell but overall low fatty acid production.

Table 1 indicates different DHA contents from various studies. Not all studies provide exact DHA content data; some derive it from the ratio of DHA production to fatty acid production. According to Table 1, the DHA content reported in this study for *Schizochytrium*

sp. GCD2032 is relatively high compared to others in the literature. Only one study reported a DHA content of 62.4% [19], achieved at a scale of 50 L with a fatty acid content of 38.00%. In contrast, this study achieved a fatty acid content of 55.71% while maintaining a high DHA content of 61.29%. This difference may be attributed to variations in strains and fermenter conditions.

Table 1. Comparison of DHA contents in different studies.

Strains	Working Volume/Reactor Volume	Biomass	Fatty Acid Content	DHA Content
A recombinant strain of OPKSABC-PPT originated from *Schizochytrium* sp. ATCC20888 [30]	-	-	-	40.60%
Schizochytrium sp. HX-308 (CCTCC M209059) overexpressing the diacylglycerol acyltransferase (ScDGAT2C) gene [19]	100 mL/250 mL	-	-	50.10%
Schizochytrium sp. ATCC 20888 with 5 mg/L proanthocyanidins [31]	50 mL/250 mL	36.7 g/L	55.31%	48.30%
Aurantiochytrium sp. 6–2 [32]	1 L/2 L	-	-	28.80%
Thraustochytrium sp. [33]	100 mL/250 mL	9.88 g/L	66.50%	24.80%
Schizochytrium sp. co-overexpressed PPTase and ω-3 FAD. [34]	-/5 L	-	-	55.70%
Schizochytrium sp. with seawater and fermentation wastewater as fermentation broth [20]	30 L/50 L	195.8 g/L	38%	62.40%
The synergistic effect of chemical regulators is applied to *Schizochytrium* sp. [35]	1.5 L/2 L	2.04 ± 1.12 g/L/d	49.02%	38.60%
Schizochytrium sp. GCD2032	3.5 L/5 L	50 g/L	55.71%	61.29% (this study)

Note: "-" indicates no data in the reference.

Currently, the extraction and purification of DHA from microalgae still face challenges, including high energy consumption during cell drying and fatty acid extraction, making large-scale production difficult. This issue mainly arises from the low DHA content. Therefore, if a *Schizochytrium* species with high DHA content can be constructed, for example, *Schizochytrium* sp. GCD2032, it would significantly reduce the cost of fatty acid extraction and achieve energy and resource savings. In the future, further exploration of gene mutation sites in *Schizochytrium* sp. GCD2032 through technologies like genome sequencing should be conducted to elucidate the mechanisms and regulatory pathways behind its high DHA content. Additionally, genome editing techniques can be used to create new cell factories that are both high in DHA content and production. Concurrently, efficient extraction and purification technologies for DHA should be developed, laying a solid foundation for the development of DHA-based pharmaceuticals.

4. Conclusions

The pharmaceutical and food industries have a huge demand for high-purity DHA products, while traditional methods only extract it from fish oil, whose low concentration leads to higher product costs. This study observed that the mutant strain *Schizochytrium* sp. GCD2032 initially showed a decrease in DHA content after 10 cycles of fermentation but stabilized in its ability to produce fatty acids and DHA after 40 transfer cycles. Using this stable strain, optimal fermentation conditions were established through the optimization of shake flask media and fed-batch fermentation with glucose addition and varied nitrogen source concentrations in a 5 L fermenter. After optimization, the DHA content increased by 16.06%, DHA production increased by 179.24%, and the final DHA content reached 341.45 mg/g cell dry weight. These optimizations resulted in the highest fatty

acid fermentation outcomes, providing a robust foundation for future high-purity DHA production.

Author Contributions: Conceptualization, P.S., L.C., X.R. and D.L.; methodology, L.C. and F.Z.; software, L.L. and L.C.; validation, A.S., W.C. and Y.D.; formal analysis, L.C.; investigation, L.L., F.Z., A.S., Y.Z., W.C. and Y.D.; resources, D.L.; data curation, L.L. and L.C.; writing—original draft preparation, L.L. and L.C.; writing—review and editing, D.L., L.C. and Y.D.; visualization, L.C.; supervision, P.S., L.C., X.R. and D.L.; project administration, D.L.; funding acquisition, L.C. All authors have read and agreed to the published version of the manuscript.

Funding: This research was funded by the National Key Research and Development Program of MOST of China (2023YFA0914400).

Institutional Review Board Statement: Not applicable.

Informed Consent Statement: Not applicable.

Data Availability Statement: The raw data supporting the conclusions of this article will be made available by the authors upon request.

Conflicts of Interest: The authors declare no conflicts of interest.

References

1. He, Y.; Zhang, Y.; Su, G. Recent advances in treatment of retinitis pigmentosa. *Curr. Stem. Cell Res. Ther.* **2015**, *10*, 258–265. [CrossRef] [PubMed]
2. Allaire, J.; Couture, P.; Leclerc, M.; Charest, A.; Marin, J.; Lépine, M.C.; Talbot, D.; Tchernof, A.; Lamarche, B. A randomized, crossover, head-to-head comparison of eicosapentaenoic acid and docosahexaenoic acid supplementation to reduce inflammation markers in men and women: The Comparing EPA to DHA (ComparED) Study. *Am. J. Clin. Nutr.* **2016**, *104*, 280–287. [CrossRef]
3. Asztalos, I.B.; Gleason, J.A.; Sever, S.; Gedik, R.; Asztalos, B.F.; Horvath, K.V.; Dansinger, M.L.; Lamon-Fava, S.; Schaefer, E.J. Effects of eicosapentaenoic acid and docosahexaenoic acid on cardiovascular disease risk factors: A randomized clinical trial. *Metabolism* **2016**, *65*, 1636–1645. [CrossRef] [PubMed]
4. Bernstein, A.M.; Ding, E.L.; Willett, W.C.; Rimm, E.B. A meta-analysis shows that docosahexaenoic acid from algal oil reduces serum triglycerides and increases HDL-cholesterol and LDL-cholesterol in Persons without coronary heart disease1–23. *J. Nutr.* **2012**, *142*, 99–104. [CrossRef] [PubMed]
5. Das, U.N. Can Bioactive Lipids Inactivate Coronavirus (COVID-19)? *Arch. Med. Res.* **2020**, *51*, 282–286. [CrossRef]
6. Fu, Y.; Wang, Y.; Gao, H.; Li, D.; Jiang, R.; Ge, L.; Tong, C.; Xu, K. Associations among Dietary omega-3 polyunsaturated fatty acids, the Gut Microbiota, and Intestinal Immunity. *Mediat. Inflamm.* **2021**, *2021*, 8879227. [CrossRef]
7. Younge, N.; Yang, Q.; Seed, P.C. Enteral high fat-polyunsaturated fatty acid blend alters the pathogen composition of the intestinal microbiome in premature infants with an enterostomy. *J. Pediatr.* **2017**, *181*, 93–101. [CrossRef] [PubMed]
8. Oh, C.E.; Kim, G.J.; Park, S.J.; Choi, S.; Park, M.J.; Lee, O.M.; Seo, J.W.; Son, H.J. Purification of high purity docosahexaenoic acid from *Schizochytrium* sp. SH103 using preparative-scale HPLC. *Appl. Biol. Chem.* **2020**, *63*, 56. [CrossRef]
9. Chen, L.; Liu, X.; Li, C.; Li, H.; Chen, W.; Li, D. Transcriptome analyses reveal the DHA enhancement mechanism in *Schizochytrium limacinum* LD11 mutant. *Algal Res.* **2022**, *67*, 102868. [CrossRef]
10. Chen, L.; Tong, S.; Liu, W.; Zhang, Y.; Khalid, H.; Long, L.; Li, Y.; Li, D.; Yan, B.; Chen, G. Electroporation-induced mutation and transcriptome analysis for high DHA production in *Schizochytrium limacinum* GCD2032. *Algal Res.* **2023**, *76*, 103297. [CrossRef]
11. Jiang, Y.; Fan, K.W.; Wong, R.T.; Chen, F. Fatty acid composition and squalene content of the marine microalga *Schizochytrium mangrovei*. *J. Agric. Food. Chem.* **2004**, *52*, 1196–1200. [CrossRef] [PubMed]
12. Zhang, K.; Chen, L.; Liu, J.; Gao, F.; He, R.; Chen, W.; Guo, W.; Chen, S.; Li, D. Effects of butanol on high value product production in *Schizochytrium limacinum* B4D1. *Enzyme Microb. Technol.* **2017**, *102*, 9–15. [CrossRef] [PubMed]
13. Zhang, Y.; Min, Q.; Xu, J.; Zhang, K.; Chen, S.; Wang, H.; Li, D. Effect of malate on docosahexaenoic acid production from *Schizochytrium* sp. B4D1 Electron. *J. Biotechnol.* **2016**, *19*, 56–60.
14. Wang, Z.; Wang, S.; Feng, Y.; Wan, W.; Zhang, H.; Bai, X.; Cui, Q.; Song, X. Obtaining high-purity docosahexaenoic acid oil in *Thraustochytrid aurantiochytrium* through a combined metabolic engineering strategy. *J. Agric. Food Chem.* **2021**, *69*, 10215–10222. [CrossRef] [PubMed]
15. Castro-Cosio, P.; Monreal-Escalante, E.; Romero-Geraldo, R.; Angulo, C. Natural and recombinant bioactive compounds from *Schizochytrium* sp.: Recent advances and future prospects. *Algal Res.* **2023**, *75*, 103273. [CrossRef]
16. Półbrat, T.; Konkol, D.; Korczyński, M. Optimization of docosahexaenoic acid production by *Schizochytrium* sp.—A review. Biocatal. *Agric. Biotechnol.* **2021**, *35*, 102076.
17. Ding, J.; Fu, Z.; Zhu, Y.; He, J.; Ma, L.; Bu, D. Enhancing docosahexaenoic acid production of *Schizochytrium* sp. by optimizing fermentation using central composite design. *BMC Biotechnol.* **2022**, *22*, 39. [CrossRef]

18. Yokochi, T.; Honda, D.; Higashihara, T.; Nakahara, T. Optimization of docosahexaenoic acid production by *Schizochytrium limacinum* SR21. *Appl. Microbiol. Biotechnol.* **1998**, *49*, 72–76. [CrossRef]
19. Jia, Y.L.; Zhang, Y.; Xu, L.W.; Zhang, Z.X.; Xu, Y.S.; Ma, W.; Gu, Y.; Sun, X.M. Enhanced fatty acid storage combined with the multi-factor optimization of fermentation for high-level production of docosahexaenoic acid in *Schizochytrium* sp. *Bioresour. Technol.* **2024**, *398*, 130532. [CrossRef] [PubMed]
20. Chen, Z.L.; Yang, L.H.; He, S.J.; Du, Y.H.; Guo, D.S. Development of a green fermentation strategy with resource cycle for the docosahexaenoic acid production by *Schizochytrium* sp. *Bioresour. Technol.* **2023**, *385*, 129434. [CrossRef]
21. Zhu, X.; Meng, C.; Du, H.; Chen, L.; Sun, F.; Chen, W.; Wei, Z.; Ren, J.; Gao, Z.; Li, D. Enhancement of astaxanthin production in *Schizochytrium limacinum* B4D1 under ethanol induction. *Algal Res.* **2022**, *61*, 102537. [CrossRef]
22. Guo, D.S.; Ji, X.J.; Ren, L.J.; Yin, F.W.; Sun, X.M.; Huang, H.; Zhen, G. Development of a multi-stage continuous fermentation strategy for docosahexaenoic acid production by *Schizochytrium* sp. *Bioresour. Technol.* **2018**, *269*, 32–39. [CrossRef]
23. Keskin, A.; Ünlü, A.E.; Takaç, S. Utilization of olive mill wastewater for selective production of lipids and carotenoids by *Rhodotorula glutinis*. *Appl. Microbiol. Biotechnol.* **2023**, *107*, 4973–4985. [CrossRef] [PubMed]
24. Zhao, B.; Li, Y.; Mbifile, M.D.; Li, C.; Yang, H.; Wang, W. Improvement of docosahexaenoic acid fermentation from *Schizochytrium* sp. AB-610 by staged pH control based on cell morphological changes. *Eng. Life Sci.* **2017**, *17*, 981–988. [CrossRef] [PubMed]
25. Ren, L.J.; Huang, H.; Xiao, A.H.; Lian, M.; Jin, L.J.; Ji, X.J. Enhanced docosahexaenoic acid production by reinforcing acetyl-CoA and NADPH supply in *Schizochytrium* sp. HX-308. *Bioprocess. Biosyst. Eng.* **2009**, *32*, 837–843. [CrossRef]
26. Tene, S.T.; Zokou, R.; Albendea, P.; Bemmo, L.G.D.; Purcaro, G.; Womeni, H.M. Effect of derivatization method (KOH and BF3) on fatty acid profile data of boiled *Tetracarpidium conophorum*, and egusi pudding oils. *Data Brief.* **2024**, *54*, 110362. [CrossRef] [PubMed]
27. Martzy, R.; Mello-de-Sousa, T.M.; Mach, R.L.; Yaver, D.; Mach-Aigner, A.R. The phenomenon of degeneration of industrial *Trichoderma reesei* strains. *Biotechnol. Biofuels* **2021**, *14*, 193. [CrossRef] [PubMed]
28. Danner, C.; Mach, R.L.; Mach-Aigner, A.R. The phenomenon of strain degeneration in biotechnologically relevant fungi. *Appl. Microbiol. Biotechnol.* **2023**, *107*, 4745–4758. [CrossRef]
29. Heggeset, T.M.B.; Ertesvåg, H.; Liu, B.; Ellingsen, T.E.; Vadstein, O.; Aasen, I.M. Lipid and DHA-production in *Aurantiochytrium* sp.—Responses to nitrogen starvation and oxygen limitation revealed by analyses of production kinetics and global transcriptomes. *Sci. Rep.* **2019**, *9*, 19470. [CrossRef] [PubMed]
30. Liu, Y.; Han, X.; Chen, Z.; Yan, Y.; Chen, Z. Selectively superior production of docosahexaenoic acid in *Schizochytrium* sp. through engineering the fatty acid biosynthetic pathways. *Biotechnol. Biofuels* **2024**, *17*, 75. [CrossRef]
31. Zhao, G.; Chen, M.; Liu, J.; Wang, S.; Fu, D.; Zhang, C. Concentration-dependent dual roles of proanthocyanidins on oxidative stress and docosahexaenoic acid production in *Schizochytrium* sp. ATCC 20888. *Bioresour. Technol.* **2024**, *398*, 130537. [CrossRef] [PubMed]
32. Ip, C.H.; Higuchi, H.; Wu, C.Y.; Okuda, T.; Katsuya, S.; Ogawa, J.; Ando, A. Production of docosahexaenoic acid by a novel isolated *Aurantiochytrium* sp. 6-2 using fermented defatted soybean as a nitrogen source for sustainable fish feed development. *Biosci. Biotechnol. Biochem.* **2024**, *88*, 696–704. [CrossRef] [PubMed]
33. Chauhan, A.S.; Patel, A.K.; Singhania, R.R.; Vadrale, A.P.; Chen, C.W.; Giri, B.S.; Chang, J.S.; Dong, C.D. Fine-tuning of key parameters to enhance biomass and nutritional polyunsaturated fatty acids production from *Thraustochytrium* sp. *Bioresour. Technol.* **2024**, *394*, 130252. [CrossRef]
34. Li, J.; Zheng, Y.; Yang, W.Q.; Wei, Z.Y.; Xu, Y.S.; Zhang, Z.X.; Ma, W.; Sun, X.M. Enhancing the accumulation of lipid and docosahexaenoic acid in *Schizochytrium* sp. by co-overexpression of phosphopantetheinyl transferase and ω-3 fatty acid desaturase. *Biotechnol. J.* **2023**, *18*, 2300314. [CrossRef] [PubMed]
35. Mehta, P.; Rani, R.; Gupta, R.; Mathur, A.; Ramakumar, S.S.V. Simultaneous production of high-value lipids in *Schizochytrium* sp. by synergism of chemical modulators. *Appl. Microbiol. Biot.* **2023**, *107*, 6135–6149. [CrossRef] [PubMed]

fermentation

MDPI

Article

Assessing Waste Sunflower Oil as a Substrate for Citric Acid Production: The Inhibitory Effect of Triton X-100

Bilge Sayın [1,*], Akif Göktuğ Bozkurt [2] and Güzin Kaban [3]

[1] Department of Gastronomy and Culinary Arts, School of Tourism and Hotel Management, Ardahan University, Ardahan 75002, Türkiye
[2] Department of Food Processing, Vocational School of Technical Sciences, Ardahan University, Ardahan 75002, Türkiye; akifgoktugbozkurt@ardahan.edu.tr
[3] Department of Food Engineering, Faculty of Agriculture, Atatürk University, Erzurum 25240, Türkiye; gkaban@atauni.edu.tr
* Correspondence: bilgesayin@ardahan.edu.tr

Abstract: In this study, waste sunflower oils were evaluated as substrates for citric acid (CA) production by *Yarrowia lipolytica* IFP29 (ATCC 20460). This strain was selected based on its capacity to produce organic acids in a selective medium. Attempts were made to optimize the process using the Taguchi statistical method in terms of the oil polarity, oil concentration, fermentation time, and Triton X-100 concentration. The results indicated that *Y. lipolytica* IFP29 utilized waste sunflower oil as a substrate and produced a maximum CA of 32.17 ± 1.44 g/L. Additionally, Triton X-100 inhibited the production of CA. For this reason, this process could not be optimized. These results were obtained by periodically adjusting the pH with NaOH during the fermentation period. On the other hand, a new experimental design was created without Triton X-100. As a buffering agent, 2-morpholinoethanesulfonic acid monohydrate (MES) was used to prevent a drop in pH; the maximum concentration of CA was found to be 20.31 ± 2.76. The optimum conditions were as follows: 90 g/L of waste sunflower oil with a polarity of 16 and 12 days of fermentation. According to the analysis of variance results, the effects of factors other than polarity on CA production were found to be significant ($p < 0.05$).

Keywords: citric acid; *Yarrowia lipolytica*; isocitric acid; Taguchi; waste oil; FTIR; fatty acids

1. Introduction

Approximately 80% of vegetable oils produced are partitioned for human consumption [1]. Therefore, large quantities of waste cooking oil (WCOs) are generated daily from various sources, including the food processing industry, fast-food establishments, restaurants, and households. Bio-refineries offer the potential for achieving "zero waste" and promoting "green chemistry" by encouraging the recycling and utilization of waste and by-products through eco-friendly processes. The removal of WCOs poses an environmental challenge that can be addressed by using them for biodiesel production or as bio-lubricants [2]. Utilizing WCOs directly as feedstock for microbial processes presents an opportunity to reduce the production costs of valuable compounds and enhance the economic value of these wastes, which are hazardous to the environment. Certain species of yeast, fungi, and bacteria can utilize WCOs as carbon and energy sources and convert them into metabolites of added value [3].

Citric acid (CA) is the second-largest fermentation product produced by tonnage after ethanol production [4]. Citric acid is used in the food, pharmaceutical, chemical, and metallurgical industries because of its nontoxic nature and ability to chelate and sequester metal ions [5]. According to the Global Citric Acid Market Outlook (2023), the global CA market reached approximately 2.59 million tons in 2022; approximately 70% of the production is used in the food industry, 12% in pharmacological preparations, and 18% in

technical applications. Furthermore, production is expected to reach 3.29 million tons by 2028 [6]. CA is an intermediate product of the tricarboxylic acid cycle [7]. *Y. lipolytica* is one of the most commonly used yeast species in CA production via fermentation [8]. However, the biggest disadvantage of *Yarrowia lipolytica* production is the production of isocitric acid (ICA) as a by-product. As a strategy, reducing ICA and fatty acid biosynthesis of *Y. lipolytica* increases CA production. One of the most important parameters in production is the excess carbon source and nitrogen limitation in the fermentation medium [9].

Y. lipolytica can use hydrophobic substrates to produce organic acids, single-cell oils, and lipases [10]. The initial step involves the hydrolysis of triacylglycerols by extracellular lipases and the release of glycerol and fatty acids into the culture medium depending on the source of WCO. This hydrolysate can then be used to synthesize CA in the mitochondria of *Y. lipolytica* [11]. Although waste oils are generally preferred for biodiesel production [12–15], various bioproducts, such as biosurfactant [16–23], lipase [24–30], microbial lipids [25,31–38], single-cell protein [39], limonene [40], itaconic acid [41], and succinic acid [42], can also be produced using WCOs in yeast-based processes. Moreover, non-waste sunflower and canola oils have been used as substrates for CA production by *Y. lipolytica* strains, and high concentrations were obtained [7,43–47]. However, only a few studies have been conducted on CA production by *Y. lipolytica* using WCO in the production medium [11,48].

Optimizing and scaling up fermentation processes can significantly improve the performance of high-yield strains, resulting in increased productivity and reduced cost [49]. Among these optimization methods, the Taguchi method utilizes fractional factorial designs known as orthogonal arrays (OAs). This approach helps optimize multiple process variables while minimizing the total number of experiments required. The selection of an appropriate OA depends on the number of control factors and their respective levels [50].

CA is an important organic acid that is frequently used in various industries and is typically produced via fermentation. The fact that demand for CA has increased every year has caused studies on its production to continue. In this study, CA production by *Y. lipolytica* using the waste sunflower oil obtained from potato frying was investigated. The Taguchi experimental design was used to optimize production in terms of oil polarity, oil concentration, fermentation time, and Triton X-100 concentration. This study also characterized waste oil in more detail compared to similar studies in the literature and made a difference through process optimization. In addition, the effects of different buffering agents and Triton X-100 on CA production were revealed for the first time.

2. Materials and Methods

2.1. Microorganisms

Strains of *Y. lipolytica* NRRL Y-1094 (ATCC 8662), *Y. lipolytica* NRRL YB-423 (ATCC 18942), *Y. lipolytica* IFP29 (ATCC 20460), and *Y. lipolytica* NRRL YB 423-12 (ATCC 18944) were sourced from the American Type Culture Collection (ATCC, Manassas, VA, USA). The cells were preserved at −80 °C in MEB with 50% (*v*/*v*) glycerol and activated in Malt Extract Broth (MEB).

2.2. Collection of Sunflower Oils

Waste oil samples were obtained by frying potatoes with sunflower oil (a well-known brand in Türkiye) in a kitchen-type deep fryer. The polarities of the samples were adjusted using a Testo 270 frying oil tester (Testo, Lenzkirch, Germany). The samples could not be obtained from small- and medium-sized enterprises because they generally do not use pure sunflower oil and sometimes fry products other than potatoes. In this context, controlled conditions were created to elucidate the mechanism of CA production using waste sunflower oils.

2.3. Characterization of Sunflower Oils

2.3.1. Determination of Fatty Acid Compositions of Oils

The fatty acid compositions of the samples were determined using an Agilent 7890 B gas chromatograph equipped with a Flame Ionization Detector (Agilent Technologies, Palo Alto, CA, USA) and Agilent J&W DB-FastFAME column (30 m × 0.25 mm, 0.25 μm, p/n G3903-63011). The inlet temperature was set to 250 °C and a 1 μL sample injection was performed. Hydrogen gas was used at a flow rate of 40 mL/min. The oven program was set as follows: 0.5 min at 50 °C, 194 °C at a rate of 30 °C/min for 3.5 min, and 240 °C at a rate of 5 °C/min for 1 min. A mixture of fatty acid methyl esters (37 components, C4-C24, ANPEL, Shanghai, China) was used as the external standard.

2.3.2. FTIR Analysis

The Fourier Transform Infrared (FTIR) spectra of oils were obtained utilizing an FTIR spectrometer (Thermo Scientific, Nicolet iS50 Spectrometer, Waltham, MA, USA) equipped with an ATR (Attenuated Total Reflectance) sampling accessory featuring a single bounce diamond crystal. The spectra were measured in absorbance mode over the range of 4000 cm^{-1} to 600 cm^{-1}, with 7 scans accumulated at a spectral resolution of 4 cm^{-1}.

2.4. Screening of Y. lipolytica Strains for Acid Production Capacities

The medium proposed by Hesham et al. [51] was modified and used to select producer microorganisms. The medium components and concentrations (g/L) were as follows: waste oil, 60; NH_4Cl, 0.6; KH_2PO_4, 1; $MgSO_47H_2O$, 1; yeast extract, 1; bromocresol green, 0.2; Triton X-100, 1.5; and agar, 20. Waste sunflower oil (60 g/L) with a polarity of 16 was added to the culture medium instead of glucose but the pH was not adjusted. Wells were created on each agar plate and 150 μL of the active yeast culture was separately added to each well. The yellow-colored zones formed by acid formation of the strains incubated at 28 °C for 48 h were measured.

2.5. Fermentation Conditions

The fermentation medium components and concentrations (g/L) are as follows: yeast extract, 0.8; KH_2PO_4, 1; $MgSO_47H_2O$, 1.5; $FeCl_36H_2O$, 0.2; $ZnSO_47H_2O$, 0.02; and $CuSO_4$, 0.02. Active cultures were transferred to a fermentation medium (at a 2% inoculation rate) and prepared according to the experimental design conditions. Fermentations were performed on a rotary shaker (50 mL medium/250 mL flask/28 °C, 180 rpm).

During fermentation, the pH was adjusted to 5.5–6.5 with 5 N NaOH on days 4 and 8, to prevent a decrease in pH. For the second experimental design, pH was adjusted using 100 mM 2-Morpholinoethanesulfonic acid monohydrate (MES) buffer at pH 6.5.

2.6. Determination of CA, ICA, and Biomass Concentrations

After fermentation, the medium was centrifuged at 9000 rpm for 15 min to separate the cells and the obtained supernatant was passed through a syringe filter (0.45 μm) and mixed with 8% $HClO_4$ in equal volume. Measurements were performed on an HPLC system (Agilent Technologies 1100 Series, Palo Alto, CA, USA) and a reverse-phase column (Inertsil ODS-3, 4.6 × 250 mm) was used. The wavelength was set to 210 nm. The column temperature was 40 °C and the flow rate of the mobile phase was 1 mL/min. The mobile phase was selected as 0.01 M H_2SO_4 [52]. The concentrations of CA and ICA were determined using a calibration curve obtained with standards (Sigma-Aldrich, St. Louis, MO, USA).

Biomass concentration was determined by centrifuging the fermentation liquids to separate the cells, followed by drying at 80 °C for 18–24 h.

The CA production process is presented in Figure S1 (Supplementary Materials).

2.7. Process Optimization

An experimental design was created using Minitab statistical software (version 17) by the Taguchi method to optimize CA and ICA production. The experiments were conducted with four replicates (considering possible adverse effects of pH adjustment) and the results were based on two samples. Table 1 lists the factors and levels used in the experiments and Table 2 lists the experimental design.

Table 1. Factors and levels used in the experiments.

Factors	Level 1	Level 2	Level 3
Sunflower oil polarity	8	16	24
Oil concentration (g/L)	60	90	120
Fermentation time (days)	4	8	12
* Triton X-100 concentration (g/L)	0	1	2

* This factor was used only in the first experimental design.

Table 2. Experimental design used for the optimization of CA production.

Run	Polarity	Oil (g/L)	Time (Days)	Triton X-100 (g/L) *
1	8	60	4	0
2	8	90	8	1
3	8	120	12	2
4	16	60	8	2
5	16	90	12	0
6	16	120	4	1
7	24	60	12	1
8	24	90	4	2
9	24	120	8	0

* This factor was used only in the first experimental design. Other factors and levels remained the same in the second experimental design.

Optimal parametric conditions can be determined using a signal-to-noise (S/N) ratio. This ratio reflects the deviation of the experimental results from the desired performance values, indicating closeness to the ideal performance. The S/N ratio values can be analyzed based on three performance characteristics: "larger is better", "nominal is best", and "smaller is better". As we aimed to maximize CA production in our study, the "larger is better" criterion was preferred [53]. The Mean Square Deviation (MSD) represents all variations around the designated target and can be calculated from S/N [54]. The study employing a larger is a better criterion for calculating the S/N ratio, which is defined as

$$\mathrm{S/N} = -10 \log \mathrm{MSD}$$

$$\mathrm{MSD} = [(1/y_1)^2 + (1/y_2)^2 + \cdots + (1/y_n)^2]/n,$$

where n is the representative number of measurements (9 in our case) and y is the experimental value. Combinations of experimental factors were selected from the L9 orthogonal test table to determine the optimum process conditions.

After determining the inhibitory effect of Triton X-100 on CA production, this factor was excluded, and a new experimental design was created (Table 2). Analysis of variance (ANOVA) was used to determine the statistical significance of the factors. Both the S/N ratio and ANOVA were instrumental in predicting the optimal combinations of process parameters.

3. Results and Discussion

3.1. Characterization of Sunflower Oil Samples

The spectra of sunflower oils were obtained using Fourier Transform Infrared (FTIR) spectrometry before and after use as sunflower oils. The wavenumbers corresponding to the oleic (C18:1), linoleic (C18:2), palmitic (C16:0), and stearic acid (C18:0) fatty acids present in sunflower oil were characterized. This method enables the detection of polymerization, oxidation, and esterification reaction products in oils based on the wave numbers and regions where bands occur because of the vibrational energies of the molecules constituting these acids in the oil. Each band observed in the spectrum facilitated the identification of functional groups in the measured sample. The FTIR spectra of the oils are shown in Figure 1. The polarity of the non-waste oil was determined to be eight and the sample was coded as SF-8. This sample was used as the control. Waste oils with polarities of 16 and 24 were coded as SF-16 and SF-24, respectively.

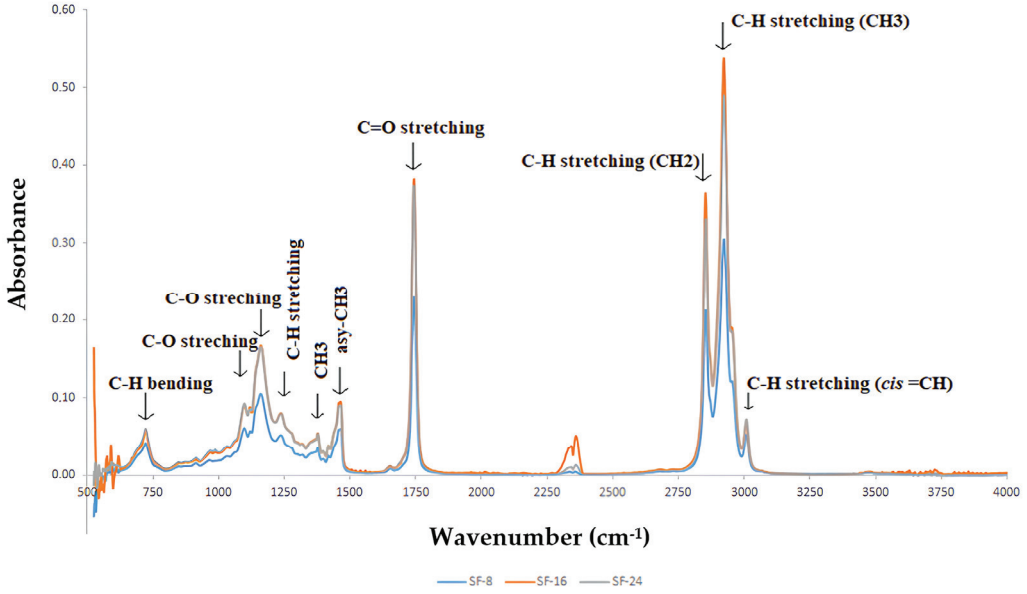

Figure 1. FTIR spectra of sunflower oils and vibration modes of corresponding observed bands.

As the polarization degree increased (from SF-8 to SF-24), there was a noticeable change in the absorbance of the bands. Especially, the C=O stretching band around 1740 cm^{-1} showed a significant increase, indicating higher levels of saturated aldehyde functional groups or other secondary oxidation and polymerization products. The C-H stretching bands around 2850–2925 cm^{-1} also showed changes in absorbance, reflecting the alteration in the alkyl chain structure due to frying. An increase in the absorbance of the C=O stretching band and changes in the C-H stretching band were direct indicators of polymerization and oxidation. These changes were consistent with the chemical transformations that occurred during prolonged frying, which led to the formation of larger and more complex molecules. Figure 1 shows the spectra of sunflower oils and the band vibration assignments are listed in Table 3.

Table 3. FTIR band vibration assignments with fatty acid correlation.

Wavenumber (cm^{-1})	Assignment	Functional Group	Fatty Acid Containing
720	C-H bending [55]	methylene (CH_2) groups and alkanes	long-chain fatty acids (e.g., palmitic acid and stearic acid)
1100–1200	C-O stretching [56]	esters	triglycerides formed from fatty acids (e.g., oleic acid, linoleic acid, palmitic acid, and stearic acid)
1375–1385	CH_3 bending (symmetric) [57]	methyl (CH_3) groups in alkanes	fatty acids with methyl groups (e.g., palmitic acid and stearic acid)
1465	CH_2 bending [58]	alkanes	long-chain fatty acids (e.g., palmitic acid and stearic acid)
1740	C=O stretching [59]	esters	triglycerides and fatty acids (e.g., oleic acid, linoleic acid, palmitic acid, and stearic acid)
2850	C-H stretching (CH_2) [60]	methylene (CH_2) groups and alkanes	long-chain fatty acids (e.g., palmitic acid and stearic acid)
2925	C-H stretching (CH_3) [58,61]	methyl (CH_3) groups in alkanes	fatty acids with methyl groups (e.g., palmitic acid and stearic acid)
3008	C-H stretching (*cis*=CH) [62]	aromatic rings and alkanes (unsaturated)	unsaturated fatty acids (e.g., oleic acid and linoleic acid)

Ester groups were observed in the carbonyl stretching band (C=O ~ 1740 cm^{-1}). The increase in the absorbance of this band might be related to polymerization-induced creation of new ester molecules and oxidation products. We observed an increase in the absorbance of this band because the oil was fried for longer periods (greater degrees of polarization). The stretching vibrations of the methylene (CH_2) and methyl (CH_3) groups were correlated with the C-H stretching (2850–2925 cm^{-1}) bands. Larger polymeric structures and cross-linking of fatty acids were indicated by changes in these bands, particularly their broadening or increase in absorbance.

The fatty acid compositions of the samples are recorded in Table S1 (Supplementary Materials). Linoleic, oleic, palmitic, and stearic acids were the most abundant fatty acids in sunflower oils. It is thought that the lack of a regular increase or decrease in the amount of fatty acids as the polarity increased was due to the samples being obtained at different times.

3.2. Screening of Y. lipolytica Strains for CA Production

At the end of the incubation period, *Y. lipolytica* IFP29, which had the largest zone diameter (2.00 ± 0.00 cm), was selected as the potential producer strain (Table 4). Figure 2 shows the zone formation of *Y. lipolytica* IFP29 in a selective growth medium.

Table 4. The zone diameters in the selective medium for *Y. lipolytica* strains.

Microorganisms	Diameter (cm)	
	24 h	**48 h**
Y. lipolytica NRRLY-1094	0.60 ± 0.07	1.00 ± 0.14
Y. lipolytica NRRL YB-423	0.05 ± 0.07	0.50 ± 0.00
Y. lipolytica IFP29	0.75 ± 0.07	2.00 ± 0.00
Y. lipolytica NRRL YB 423-12	0.40 ± 0.14	1.25 ± 0.07

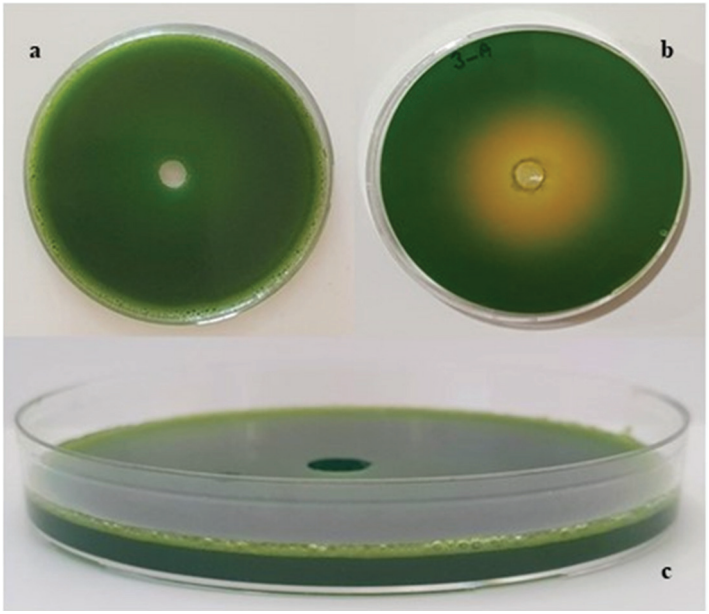

Figure 2. (**a**) Selective medium, (**b**) Zone image of *Y. lipolytica* IFP29 after 48 h, (**c**) The oil layer on the selective medium.

3.3. Results of Experimental Design 1

The data obtained from the applied experimental design are presented in Table 5. Overall, it can be concluded that Triton X-100 reduced the biomass concentration and inhibited CA production. As is evident from the table, the highest biomass concentration (3.30 ± 0.42) was achieved when the condition of the 1st run was applied. This outcome was expected because of the non-waste oil used and the absence of Triton X-100. The lowest biomass concentration was observed as 1.51 ± 0.10, using the highest polarity and Triton X-100 concentration. The highest CA and ICA production were 32.17 ± 2.04 and 29.44 ± 1.80, respectively. One noteworthy parameter was the considerable concentration of ICA formed as a byproduct (CA/ICA ratio of 1.09). Although the CA concentration remained relatively consistent, the ICA concentration decreased when non-waste oil and 1 g/L Triton X-100 were used. Additionally, it was evident that Triton X-100 adversely affected production compared with condition 2, even though the highest polarity level and oil concentration were used under condition 9 (with the same fermentation time).

Table 5. Results of biomass, CA, and ICA concentrations and the final pH.

Run	Polarity	Oil (g/L)	Time (Days)	Triton X-100 (g/L)	Biomass (g/L)	CA (g/L)	ICA (g/L)	Final pH
1	8	60	4	0	3.30 ± 0.42	4.36 ± 0.24	3.76 ± 0.38	2.74 ± 0.14
2	8	90	8	1	2.83 ± 0.18	4.53 ± 1.44	1.64 ± 0.26	3.60 ± 0.23
3	8	120	12	2	2.34 ± 0.25	-	-	5.15 ± 0.28
4	16	60	8	2	2.11 ± 0.31	-	-	4.78 ± 0.27
5	16	90	12	0	3.10 ± 0.17	32.17 ± 2.04	29.44 ± 1.80	4.65 ± 0.41
6	16	120	4	1	2.52 ± 0.20	-	-	3.42 ± 0.50
7	24	60	12	1	2.22 ± 0.61	-	-	5.50 ± 0.21
8	24	90	4	2	1.51 ± 0.10	-	-	4.48 ± 0.06
9	24	120	8	0	3.00 ± 0.41	11.40 ± 1.27	7.27 ± 1.10	3.68 ± 0.64

Liu et al. [11] showed that 30.3 g/L of CA by *Y. lipolytica* SWJ-1b was obtained after 336 h in a medium containing 80 g/L waste oil. Under these conditions, the concentrations of ICA and biomass were calculated as 6.9 and 6.1 g/L, respectively. Upon increasing the waste oil concentration to 120 and 140 g/L, a decrease in the CA concentration and an increase in the ICA concentration were observed. In our study, achieving a higher CA yield after 288 h was significant; however, a high ICA concentration was disadvantageous. Another important point is that the CA concentration reached was obtained in shake flasks but not in the bioreactor. Therefore, using less than 90 g/L waste oil in the fermentation medium without a surfactant may reduce the concentration of ICA. In another study, 12.2 g/L of CA was achieved in a fermentation medium containing 30 g/L of waste oil when 20 g/L of NaCl (for an initial osmotic pressure of 0.75 osmol/L) was used. Moreover, the synergistic effect of osmotic pressure with pH was investigated and 12.6 g/L of CA was obtained, with a combination of 0.75 osmol/L and pH 6.0 [48].

3.4. Results of Experimental Design 2

The data obtained from the new experimental design are given in Table 6. Except for the conditions in the seventh trial, the pH value did not drop below four. Biomass values ranged between 1.64 ± 0.35 and 3.89 ± 0.47. The highest CA concentration, calculated as 20.31 ± 2.76, was obtained under the fifth condition, similar to the first experimental design. The concentration of ICA produced under these conditions was calculated to be 13.63 ± 1.46. Compared with the experimental designs, the difference in CA concentrations obtained under the fifth condition was attributed solely to pH adjustment. This difference could be due to the substances used for buffering and/or the stabilization of the pH around four with MES buffer, which may decrease or block the rate of CA production. While the use of MES buffer aimed to provide more standard production, it is anticipated that continuous pH control with NaOH would yield better results if a bioreactor were used.

Table 6. The results were obtained by applying the new experimental design.

Run	Oil (g/L)	Polarity	Time (Days)	Biomass (g/L)	Final pH	CA (g/L)	S/N Ratio	ICA (g/L)	S/N Ratio
1	60	8	4	3.14 ± 0.27	4.48 ± 0.07	8.18 ± 1.22	18.26	6.32 ± 1.15	16.01
2	60	16	8	2.19 ± 0.21	4.03 ± 0.08	10.97 ± 0.49	20.80	7.66 ± 1.10	17.68
3	60	24	12	1.64 ± 0.35	4.01 ± 0.01	13.98 ± 0.18	22.91	10.03 ± 1.54	20.03
4	90	8	8	3.76 ± 0.61	4.01 ± 0.16	13.92 ± 0.47	22.87	10.59 ± 0.93	20.50
5	90	16	12	2.97 ± 0.27	4.36 ± 0.06	20.31 ± 2.76	26.15	13.63 ± 1.46	22.69
6	90	24	4	1.79 ± 0.10	4.95 ± 0.03	6.77 ± 0.66	16.61	5.76 ± 0.71	15.21
7	120	8	12	3.89 ± 0.47	3.88 ± 0.11	14.25 ± 1.09	23.08	10.65 ± 0.89	20.55
8	120	16	4	3.86 ± 0.28	5.00 ± 0.02	5.02 ± 0.20	14.01	4.99 ± 0.34	13.96
9	120	24	8	3.64 ± 0.51	4.51 ± 0.01	7.68 ± 0.69	17.70	6.44 ± 1.20	16.18

The objective of optimizing the process parameters was to enhance the S/N ratio, thereby achieving superior outcomes. The optimal levels for each factor were identified to minimize the variability and maximize the concentrations of CA and ICA. The highest S/N ratios for each factor were observed using 90 g/L of non-waste sunflower oil after 12 days of fermentation. The main effects plots for the S/N ratios are shown in Figures 3 and 4.

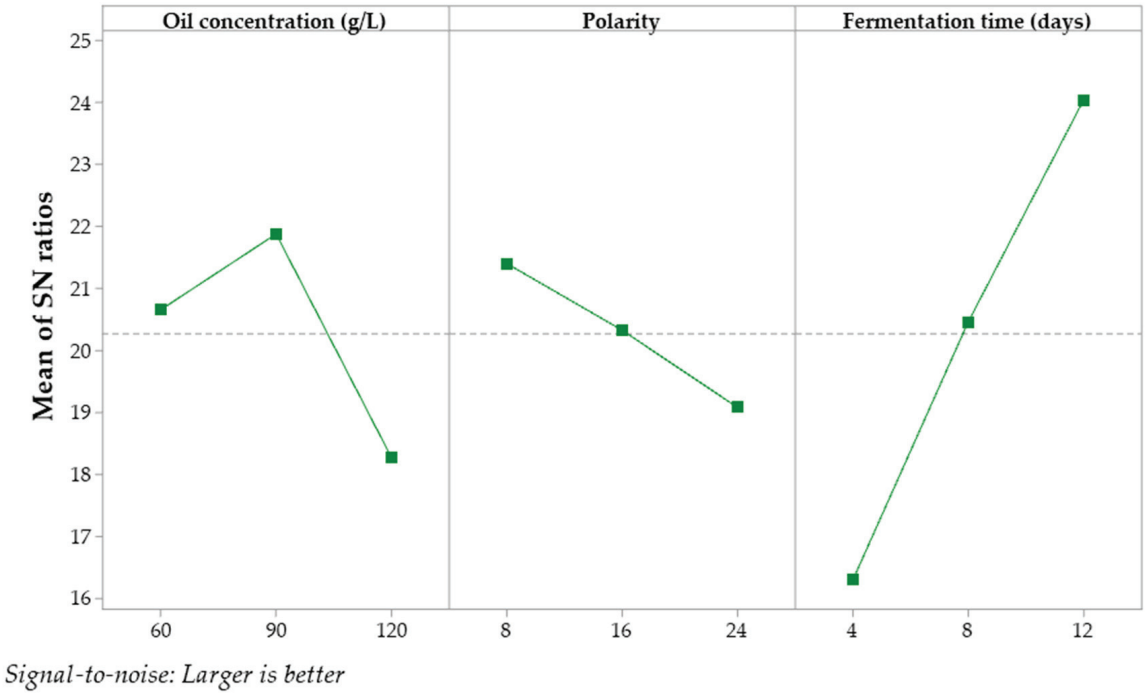

Figure 3. Main effects plot for the S/N ratio (CA concentration).

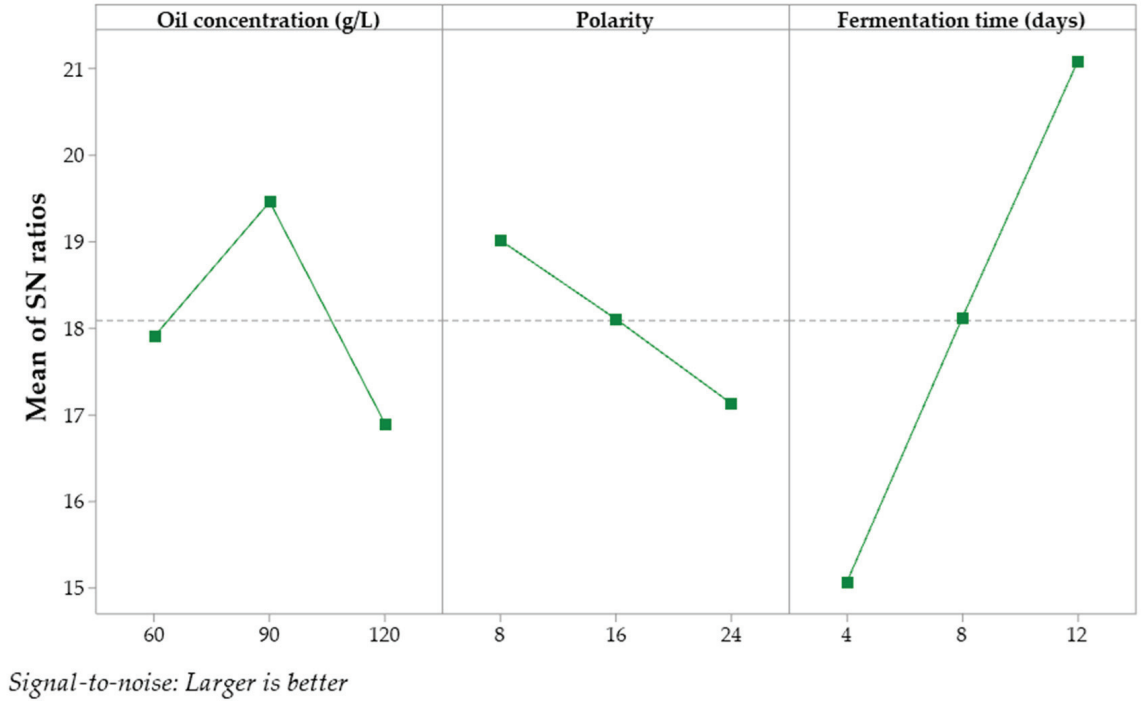

Figure 4. Main effects plot for the S/N ratio (ICA concentration).

The ANOVA results (Tables 7 and 8) revealed that among the selected factors, fermentation time had a stronger influence on CA and ICA concentrations (75.49% and 77.58%, respectively), while polarity had the least influence. The effects of oil concentration and fermentation time were statistically significant for both CA and ICA ($p < 0.05$).

Table 7. Analysis of variance for CA production.

Source	DF	Seq SS	Contribution	Adj SS	Adj MS	F	P
Oil concentration (g/L)	2	20.27	16.94%	20.27	10.14	21.46	0.05
Polarity	2	8.12	6.79%	8.12	4.06	8.60	0.10
Fermentation time (days)	2	90.34	75.49%	90.34	45.17	95.63	0.01
Error	2	0.95	0.79%	0.94	0.47		
Total	8	119.68	100%				

DF: Degrees of freedom, Seq SS: Sequential sums of squares, Adj SS: Adjusted sum of square, Adj MS: Adjusted mean square (R^2: 99.21%, R^2 (adj): 96.84%).

Table 8. Analysis of variance for ICA production.

Source	DF	Seq SS	Contribution	Adj SS	Adj MS	F	P
Oil concentration (g/L)	2	10.05	14.32%	10.05	5.03	27.17	0.04
Polarity	2	5.32	7.57%	5.32	2.66	14.37	0.07
Fermentation time (days)	2	54.47	77.58%	54.47	27.24	147.22	0.01
Error	2	0.37	0.53%	0.37	0.19		
Total	8	70.22	100%				

DF: Degrees of freedom, Seq SS: Sequential sums of squares, Adj SS: Adjusted sum of square, Adj MS: Adjusted mean square. (R^2: 99.47%, R^2 (adj): 97.89%).

Kamzolova et al. [44] indicated that plant oils are promising substrates for CA production by *Y. lipolytica* strains. They also emphasized the effectiveness of strain selection for ICA formation. The application of genetic manipulation tools is easier in yeasts because of their less complex genetic background than filamentous fungi. Studies have reported that genetically modified yeast strains can produce more CA, generate less ICA, and reduce residual sugar content [63]. Holz et al. [64] constructed a recombinant *Y. lipolytica* strain containing multiple copies of the aconitase-encoding gene *ACO1*. This high-level expression of aconitase in the *ACO1* multicopy integrative transformant led to a significant decrease in the CA/ICA ratio toward the ICA. ICA formation increased markedly compared to that in the wild-type strain using sunflower oil in the fermentation medium. In another study, two transformants of *Y. lipolytica* A101.1.31, overexpressing either *CIT1* or *CIT2* (encoding proteins with citrate synthase activity), were generated and overexpression of either of these genes was found to increase citrate synthase activity. Moreover, a significant increase in ICA biosynthesis was observed in the overexpressed mutants. Finally, *CIT1* and *CIT2* overexpressing strains produced CA and ICA from vegetable oil at a ratio close to 1. This study is similar to the findings of the present study in terms of the utilization of vegetable oil in production and the CA/ICA ratio [65]. It is noteworthy that the strain used in our study was not a mutant strain but yielded similar results. A major challenge in CA production using yeast is the simultaneous secretion of ICA, which is undesirable and disrupts crystallization. Förster et al. [66] detected that high-level expression of ICL (isocitrate lyase) in *ICL1* (isocitrate lyase-encoding gene) multicopy integrative transformants resulted in an important shift of the CA/ICA ratio in the direction of CA. ICA concentration decreased from 37 to 6% when sunflower oil was used in the fermentation medium. Lastly, in the respective mutant strains, a decrease in aconitase activity and an increase in isocitrate lyase activity resulted in the predominant accumulation of CA. Yuzbasheva et al. [67] stated that the mitochondrial succinate–fumarate carrier YlSfc1 of *Y. lipolytica* controls the ICA efflux from the mitochondria. Overexpression of *YlSFC1* shifted the ICA/CA ratio in favor of ICA. *YlSFC1* expression was repressed in the wild-type strain grown in a glucose-based medium compared to that in an olive oil medium, explaining the preference for CA production when *Y. lipolytica* was grown on carbohydrates.

Finogenova et al. [68] reported that the predominant production of CA or ICA was affected by intracellular iron concentration. Kamzolova et al. [69] stated that the limitation of nitrogen, phosphorus, sulfur, or magnesium is required in the fermentation medium for ICA formation by *Y. lipolytica*. Because CA and ICA are chiral compounds [70], separating them is challenging. Therefore, it is essential to reduce the concentration of ICA to improve process efficiency and ease the purification stage.

Venter et al. [46] discovered that adding 10 g/L of acetate in a medium containing 30 g/L of sunflower oil significantly increased CA production by *Y. lipolytica* UOFS Y-1701 while also significantly increasing the CA/ICA ratio. Mitrea et al. [42] used the pure glycerol as a hydrophilic source, stimulating de novo metabolic pathways and waste cooking oil as a hydrophobic source, promoting ex novo metabolic pathways in the yeast cells. Crude glycerol was a mixture of hydrophilic and hydrophobic carbon sources. Importantly, *Y. lipolytica* ATCC 20177 exhibited superior performance when cultivated on waste oil compared with glycerol. After 192 h of fermentation, 3.50 $\pm$ 0.04 g/L CA and 21 $\pm$ 0.16 g/L of succinic acid were obtained.

A significant challenge in using oily substrates is their water insolubility, which leads to insufficient substrate utilization and low mass transfer of air and nutrients into the medium [71]. To address these issues, the nonionic detergent Triton X-100 was added in the present study. Surfactants and their concentrations must be carefully selected; they can be toxic to microorganisms and either promote or inhibit metabolite production [72]. Contrary to our results, Mirbagheri et al. [73] found that the addition of Triton X-100 in the production medium increased the CA concentration of *Y. lipolytica* DSM 3286 and M7. In another study, adding Triton X-100 at 0–1% increased the CA concentration but inhibited mannitol and xylitol production [74]. Ping et al. [75] reported that Tween 80, Tween 20, and Triton X-100 inhibited the lipase activity.

Considering the results of the present study, it was concluded that changes in medium composition and pH values, as well as advanced optimizations and genetic modifications, could effectively reduce ICA concentration and increase CA concentration.

The cost of the culture medium generally accounts for 50–80% of the total cost of the end products. Biological processes can be more economical and sustainable, using low-cost substrates, such as various wastes and by-products from agriculture and other industries [76]. The composition of the culture medium is crucial for CA production by *Y. lipolytica*. Therefore, selecting waste cooking oils produced in large quantities as substrates for fermentation can reduce production costs. Additionally, these oils can be used directly without sterilization or filtering [77]. This approach can also lower the processing costs associated with pretreatment and raw material sterilization. Similarly, in the present study, oil was added to the medium by filtration. It was concluded that the industrial production potential is high because the raw material is cheap, easily accessible, requires no pretreatment, and competes with non-waste oils. However, the concentration of by-products must be reduced.

4. Conclusions

Frying oils used in the food industry have become waste oils because of their prolonged use and loss of physical and chemical properties. The resulting waste oils are harmful to the environment and to human health. One of the greatest advantages of biotechnological production is the ability to use waste as a raw material to produce value-added products. This enables the reduction in waste volume and environmental pollution and saves energy that would otherwise be spent on waste disposal, thus contributing to the country's economy.

In microbial production, different concentrations of detergents can have different effects on yeast cells, such as increasing cell permeability and causing cell membrane lysis and cell death. In the present study, the selection of Triton X-100 in the fermentation medium was aimed at reducing the increased surface tension associated with sunflower oil use and increasing the availability of oil as a substrate for CA production by *Y. lipolytica*

IFP29 (ATCC 20460). However, these results were unexpected. This study is important in terms of characterizing oils in more detail than other studies, revealing the inhibitory effect of Triton X-100 on CA production and determining the effects of different buffers on CA production. In addition, it was found that using waste and non-waste oils for CA production had a statistically insignificant effect ($p > 0.05$), which would increase the interest in preferring waste oils instead of non-waste oils.

Finally, we determined that waste sunflower oil could be a promising substrate for CA production using *Y. lipolytica*. However, to reduce the formation of by-products and further increase the production yield, further optimization studies, changes in some components of the fermentation medium, and genetic engineering approaches can be employed in future studies.

Supplementary Materials: The following supporting information can be downloaded at https://www.mdpi.com/article/10.3390/fermentation10070374/s1, Figure S1: Citric acid production process; Table S1: Fatty acid composition of sunflower oils.

Author Contributions: B.S.: Conceptualization, Investigation, Formal analysis, Writing—original draft, Funding acquisition. A.G.B.: Formal analysis and Writing—review and editing. G.K.: Formal analysis, Validation, and Writing—review and editing. All authors have read and agreed to the published version of the manuscript.

Funding: This study was supported by the Ardahan University Scientific Research Project Coordination under project number 2020-009.

Institutional Review Board Statement: Not applicable.

Informed Consent Statement: Not applicable.

Data Availability Statement: The data are presented in the article and Supplementary Materials.

Conflicts of Interest: The authors declare no conflicts of interest.

References

1. Suzuki, A.H.; Botelho, B.G.; Oliveira, L.S.; Franca, A.S. Sustainable synthesis of epoxidized waste cooking oil and its application as a plasticizer for polyvinyl chloride films. *Eur. Polym. J.* **2018**, *99*, 142–149. [CrossRef]
2. Sarno, M.; Iuliano, M.; Cirillo, C. Optimized procedure for the preparation of an enzymatic nanocatalyst to produce a bio-lubricant from waste cooking oil. *J. Chem. Eng.* **2019**, *377*, 120273. [CrossRef]
3. Lopes, M.; Miranda, S.M.; Belo, I. Microbial valorization of waste cooking oils for valuable compounds production–a review. *Crit. Rev. Environ. Sci. Technol.* **2020**, *50*, 2583–2616. [CrossRef]
4. Tong, Z.; Tong, Y.; Wang, D.; Shi, Y.C. Whole maize flour and isolated maize starch for production of citric acid by *Aspergillus niger:* A review. *Starch-Stärke* **2023**, *75*, 2000014. [CrossRef]
5. Książek, E. Citric acid: Properties, microbial production, and applications in industries. *Molecules* **2023**, *29*, 22. [CrossRef] [PubMed]
6. Kamzolova, S.V. A Review on citric acid production by *Yarrowia lipolytica* yeast: Past and present challenges and developments. *Processes* **2023**, *1*, 3435. [CrossRef]
7. Kamzolova, S.V.; Lunina, J.N.; Morgunov, I.G. Biochemistry of citric acid production from rapeseed oil by *Yarrowia lipolytica* yeast. *J. Am. Oil Chem. Soc.* **2011**, *88*, 1965–1976. [CrossRef]
8. Börekçi, B.S.; Kaban, G.; Kaya, M. Citric acid production of yeasts: An overview. *EuroBiotech J.* **2021**, *5*, 79–91. [CrossRef]
9. Tan, M.J.; Chen, X.; Wang, Y.K.; Liu, G.L.; Chi, Z.M. Enhanced citric acid production by a yeast *Yarrowia lipolytica* over-expressing a pyruvate carboxylase gene. *Bioprocess Biosyst. Eng.* **2016**, *39*, 1289–1296. [CrossRef]
10. Darvishi, F.; Nahvi, I.; Zarkesh-Esfahani, H.; Momenbeik, F. Effect of plant oils upon lipase and citric acid production in *Yarrowia lipolytica* yeast. *J Biomed Biotechnol.* **2009**, *2009*, 562943. [CrossRef]
11. Liu, X.; Lv, J.; Xu, J.; Zhang, T.; Deng, Y.; He, J. Citric acid production in *Yarrowia lipolytica* SWJ-1b yeast when grown on waste cooking oil. *Appl. Biochem. Biotechnol.* **2015**, *175*, 2347–2356. [CrossRef] [PubMed]
12. Katre, G.; Ajmera, N.; Zinjarde, S.; RaviKumar, A. Mutants of *Yarrowia lipolytica* NCIM 3589 grown on waste cooking oil as a biofactory for biodiesel production. *Microb. Cell Fact.* **2017**, *16*, 176. [CrossRef] [PubMed]
13. Katre, G.; Raskar, S.; Zinjarde, S.; Kumar, V.R.; Kulkarni, B.D.; RaviKumar, A. Optimization of the in situ transesterification step for biodiesel production using biomass of *Yarrowia lipolytica* NCIM 3589 grown on waste cooking oil. *Energy* **2018**, *142*, 944–952. [CrossRef]

14. Gohain, M.; Bardhan, P.; Laskar, K.; Sarmah, S.; Mandal, M.; Bora, U.; Kalita, M.C.; Goud, V.V.; Deka, D. *Rhodotorula mucilaginosa*: A source of heterogeneous catalyst for biodiesel production from yeast single cell oil and waste cooking oil. *Renew. Energy* **2020**, *160*, 220–230. [CrossRef]
15. Raut, G.; Jagtap, S.; Kumar, V.R.; RaviKumar, A. Enhancing lipid content of oleaginous *Yarrowia lipolytica* biomass grown on waste cooking oil and its conversion to biodiesel by statistical optimization. *Biomass Convers. Biorefin.* **2022**, 1–18. [CrossRef]
16. Batista, R.M.; Rufino, R.D.; Luna, J.M.; Souza, J.E.G.; Sarubbo, L.A. Effect of medium components on the production of a biosurfactant from *Candida tropicalis* applied to the removal of hydrophobic contaminants in soil. *Water Environ. Res.* **2010**, *82*, 418–425. [CrossRef] [PubMed]
17. Dzięgielewska, E.; Adamczak, M. Evaluation of waste products in the synthesis of surfactants by yeasts. *Chem. Pap.* **2013**, *67*, 1113–1122. [CrossRef]
18. Campos, J.M.; Stamford, T.L.M.; Sarubbo, L.A. Production of a bioemulsifier with potential application in the food industry. *Appl. Biochem. Biotechnol.* **2014**, *172*, 3234–3252. [CrossRef]
19. Almeida, D.G.; Silva, R.C.F.S.; Luna, J.M.; Rufino, R.D.; Santos, V.A.; Sarubbo, L.A. Response surface methodology for optimizing the production of biosurfactant by *Candida tropicalis* on industrial waste substrates. *Front. Microbiol.* **2017**, *8*, 157. [CrossRef]
20. Csutak, O.; Corbu, V.; Stoica, I.; Vassu, T. Fatty acids effect on lipase and biosurfactant induction in *Rhodotorula glutinis* CMGB-RG5. In *"Agriculture for Life, Life for Agriculture", Conference Proceedings*; Sciendo: Warsaw, Poland, 2018; Volume 1, pp. 515–522. [CrossRef]
21. Junior, R.B.R.; Meira, H.M.; Almeida, D.G.; Rufino, R.D.; Luna, J.M.; Santos, V.A.; Sarubbo, L.A. Application of a low-cost biosurfactant in heavy metal remediation processes. *Biodegradation* **2018**, *30*, 215–233. [CrossRef]
22. Souza, P.M.; Silva, N.R.A.; Souza, D.G.; Silva, T.A.L.; Freitas-Silva, M.C.; Andrade, R.F.S.; Silva, G.K.B.; Albuquerque, C.D.C.; Messias, A.S.; Campos-Takaki, G.M. Production of a biosurfactant by *Cunninghamella echinulata* using renewable substrates and its applications in enhanced oil spill recovery. *Colloids Interfaces* **2018**, *2*, 63–74. [CrossRef]
23. Liepins, J.; Balina, K.; Soloha, R.; Berzina, I.; Lukasa, L.K.; Dace, E. Glycolipid biosurfactant production from waste cooking oils by yeast: Review of substrates, producers and products. *Fermentation* **2021**, *7*, 136. [CrossRef]
24. Nunes, P.M.B.; Martins, A.B.; Brigida, A.I.S.; Rocha-Leao, M.H.M.; Amaral, P. Intracellular lipase production by *Yarrowia lipolytica* using different carbon sources. *Chem. Eng. Trans.* **2014**, *38*, 421–426.
25. Lopes, M.; Miranda, S.M.; Alves, J.M.; Pereira, A.S.; Belo, I. Waste cooking oils as feedstock for lipase and lipid-rich biomass production. *Eur. J. Lipid Sci. Technol.* **2019**, *121*, 1800188. [CrossRef]
26. Domínguez, A.; Deive, F.J.; Angeles Sanromán, M.; Longo, M.A. Biodegradation and utilization of waste cooking oil by *Yarrowia lipolytica* CECT 1240. *Eur. J. Lipid Sci. Technol.* **2010**, *112*, 1200–1208. [CrossRef]
27. Moftah, O.A.S.; Grbavčić, S.; Žuža, M.; Luković, N.; Bezbradica, D.; Knežević-Jugović, Z. Adding value to the oil cake as a waste from oil processing industry: Production of lipase and protease by *Candida utilis* in solid state fermentation. *Appl. Biochem. Biotechnol.* **2012**, *166*, 348–364. [CrossRef]
28. Snopek, P.; Nowak, D.; Zieniuk, B.; Fabiszewska, A. Aeration and stirring in *Yarrowia lipolytica* lipase biosynthesis during batch cultures with waste fish oil as a carbon source. *Fermentation* **2021**, *7*, 88. [CrossRef]
29. Fraga, J.L.; Souza, C.P.; Pereira, A.D.S.; Aguieiras, E.C.; de Silva, L.O.; Torres, A.G.; Freire, D.G.; Amaral, P.F. Palm oil wastes as feedstock for lipase production by *Yarrowia lipolytica* and biocatalyst application/reuse. *3 Biotech* **2021**, *11*, 191. [CrossRef]
30. Colacicco, M.; Ciliberti, C.; Agrimi, G.; Biundo, A.; Pisano, I. Towards the physiological understanding of *Yarrowia lipolytica* growth and lipase production using waste cooking oils. *Energies* **2022**, *15*, 5217. [CrossRef]
31. El Bialy, H.; Gomaa, O.M.; Azab, K.S. Conversion of oil waste to valuable fatty acids using oleaginous yeast. *World J. Microbiol. Biotechnol.* **2011**, *27*, 2791–2798. [CrossRef]
32. Katre, G.; Joshi, C.; Khot, M.; Zinjarde, S.; Ravikumar, A. Evaluation of single cell oil (SCO) from a tropical marine yeast *Yarrowia lipolytica* NCIM 3589 as a potential feedstock for biodiesel. *AMB Express* **2012**, *2*, 36–49. [CrossRef] [PubMed]
33. Poli, J.S.; da Silva, M.A.N.; Siqueira, E.P.; Pasa, V.M.; Rosa, C.A.; Valente, P. Microbial lipid produced by *Yarrowia lipolytica* QU21 using industrial waste: A potential feedstock for biodiesel production. *Bioresour. Technol.* **2014**, *161*, 320–326. [CrossRef] [PubMed]
34. Miranda, S.M.; Pereira, A.S.; Belo, I.; Lopes, M. Waste cooking oils: Low-cost substrate for co-production of lipase and microbial lipids. In *WASTES—Solutions, Treatments and Opportunities II*; CRC Press: Boca Raton, FL, USA, 2017; pp. 99–104.
35. Niehus, X.; Casas-Godoy, L.; Rodríguez-Valadez, F.J.; Sandoval, G. Evaluation of *Yarrowia lipolytica* oil for biodiesel production: Land use oil yield, carbon, and energy balance. *J. Lipids* **2018**, *2018*, 6393749. [CrossRef] [PubMed]
36. Tzirita, M.; Papanikolaou, S.; Chatzifragkou, A.; Quilty, B. Waste fat biodegradation and biomodification by *Yarrowia lipolytica* and a bacterial consortium composed of *Bacillus* spp. and *Pseudomonas putida*. *Eng. Life Sci.* **2018**, *18*, 932–942. [CrossRef] [PubMed]
37. Radha, P.; Narayanan, S.; Chaudhuri, A.; Anjum, S.; Thomas, D.L.; Pandey, R.; Ramani, K. Synthesis of single-cell oil by *Yarrowia lipolytica* MTCC 9520 utilizing slaughterhouse lipid waste for biodiesel production. *Biomass Convers. Biorefin.* **2020**, *13*, 1–12. [CrossRef]
38. Pereira, A.S.; Lopes, M.; Miranda, S.M.; Belo, I. Bio-oil production for biodiesel industry by *Yarrowia lipolytica* from volatile fatty acids in two-stage batch culture. *Appl. Biochem. Biotechnol.* **2022**, *106*, 2869–2881. [CrossRef]
39. Spalvins, K.; Geiba, Z.; Kusnere, Z.; Blumberga, D. Waste cooking oil as substrate for single cell protein production by yeast *Yarrowia lipolytica*. *Rigas Teh. Univ. Zinat. Raksti.* **2020**, *24*, 457–469. [CrossRef]

40. Pang, Y.; Zhao, Y.; Li, S.; Zhao, Y.; Li, J.; Hu, Z.; Zhang, C.; Xiao, D.; Yu, A. Engineering the oleaginous yeast *Yarrowia lipolytica* to produce limonene from waste cooking oil. *Biotechnol. Biofuels.* **2019**, *12*, 1–18. [CrossRef] [PubMed]
41. Rong, L.; Miao, L.; Wang, S.; Wang, Y.; Liu, S.; Lu, Z.; Zhao, B.; Zhang, C.; Xiao, D.; Pushpanathan, K.; et al. Engineering *Yarrowia lipolytica* to produce itaconic acid from waste cooking oil. *Front. Bioeng. Biotechnol.* **2022**, *10*, 888869. [CrossRef]
42. Mitrea, L.; Călinoiu, L.F.; Teleky, B.E.; Szabo, K.; Martău, A.G.; Ştefănescu, B.E.; Dulf, F.-V.; Vodnar, D.C. Waste cooking oil and crude glycerol as efficient renewable biomass for the production of platform organic chemicals through oleophilic yeast strain of *Yarrowia lipolytica*. *Environ. Technol. Innov.* **2022**, *28*, 102943. [CrossRef]
43. Good, D.W.; Droniuk, R.; Lawford, G.R.; Fein, J.E. Isolation and characterization of a *Saccharomycopsis lipolytica* mutant showing increased production of citric acid from canola oil. *Can. J. Microbiol.* **1985**, *31*, 436–440. [CrossRef]
44. Kamzolova, S.V.; Morgunov, I.G.; Aurich, A.; Perevoznikova, O.A.; Shishkanova, N.V.; Stottmeister, U.; Finogenova, T.V. Lipase secretion and citric acid production in *Yarrowia lipolytica* yeast grown on animal and vegetable fat. *Food Technol. Biotech.* **2005**, *43*, 113–122.
45. Kamzolova, S.V.; Finogenova, T.V.; Morgunov, I.G. Microbiological production of citric and isocitric acids from sunflower oil. *Food Technol. Biotech.* **2008**, *46*, 51–59.
46. Venter, T.; Kock, J.L.F.; Botes, P.J.; Smit, M.S.; Hugo, A.; Joseph, M. Acetate enhances citric acid production by *Yarrowia lipolytica* when grown on sunflower oil. *Syst. Appl. Microbiol.* **2004**, *27*, 135–138. [CrossRef] [PubMed]
47. Çelik, G.; Bahriye Uçar, F.; Akpınar, O.; Çorbacı, C. Production of citric and isocitric acid by *Yarrowia lipolytica* strains grown on different carbon sources. *Turk. J. Biochem.* **2014**, *39*, 285–290. [CrossRef]
48. Liu, X.; Lv, J.; Xu, J.; Xia, J.; He, A.; Zhang, T.; Xu, X.; Xu, J. Effects of osmotic pressure and pH on citric acid and erythritol production from waste cooking oil by *Yarrowia lipolytica*. *Eng. Life Sci.* **2018**, *18*, 344–352. [CrossRef] [PubMed]
49. Wan, S.; Liu, X.; Sun, W.; Lv, B.; Li, C. Current advances for omics-guided process optimization of microbial manufacturing. *Bioresour. Bioprocess.* **2023**, *10*, 30. [CrossRef] [PubMed]
50. Taiwo, A.E.; Madzimbamuto, T.N.; Ojumu, T.V. Optimization of process variables for acetoin production in a bioreactor using Taguchi orthogonal array design. *Heliyon* **2020**, *6*, 05103. [CrossRef] [PubMed]
51. Hesham, A.E.L.; Mostafa, Y.S.; AlSharqi, L.E.O. Optimization of citric acid production by immobilized cells of novel yeast isolates. *Mycobiology* **2020**, *48*, 122–132. [CrossRef]
52. Kamzolova, S.V.; Morgunov, I.G. Metabolic peculiarities of the citric acid overproduction from glucose in yeasts *Yarrowia lipolytica*. *Bioresour. Technol.* **2017**, *243*, 433–440. [CrossRef]
53. Alavi-Borazjani, S.A.; da Cruz Tarelho, L.A.; Capela, M.I. Parametric optimization of the dark fermentation process for enhanced biohydrogen production from the organic fraction of municipal solid waste using Taguchi method. *Int. J. Hydrogen Energy* **2021**, *46*, 21372–21382. [CrossRef]
54. Chenthamarakshan, A.; Parambayil, N.; Miziriya, N.; Soumya, P.S.; Lakshmi, M.K.; Ramgopal, A.; Dileep, A.; Nambisan, P. Optimization of laccase production from *Marasmiellus palmivorus* LA1 by Taguchi method of design of experiments. *BMC Biotechnol.* **2017**, *17*, 12. [CrossRef] [PubMed]
55. Kamil, F.H.; Salmiaton, A.; Hafriz, R.S.R.M.; Hussien, I.R.; Omar, R. Characterization and application of molten slag as catalyst in pyrolysis of waste cooking oil. *Bull. Chem. React. Eng. Catal.* **2020**, *15*, 119–127. [CrossRef]
56. Poiana, M.A.; Alexa, E.; Munteanu, M.F.; Gligor, R.; Moigradean, D.; Mateescu, C. Use of ATR-FTIR spectroscopy to detect the changes in extra virgin olive oil by adulteration with soybean oil and high temperature heat treatment. *Open Chem.* **2015**, *13*, 689–698. [CrossRef]
57. Agatonovic-Kustrin, S.; Ristivojevic, P.; Gegechkori, V.; Litvinova, T.M.; Morton, D.W. Essential Oil Quality and Purity Evaluation via FT-IR Spectroscopy and Pattern Recognition Techniques. *Appl. Sci.* **2020**, *10*, 7294. [CrossRef]
58. Vlachos, N.; Skopelitis, Y.; Psaroudaki, M.; Konstantinidou, V.; Chatzilazarou, A.; Tegou, E. Applications of Fourier transform-infrared spectroscopy to edible oils. *Anal. Chim. Acta.* **2006**, *573*, 459–465. [CrossRef] [PubMed]
59. Mousa, M.A.; Wang, Y.; Antora, S.A.; Al-Qurashi, A.D.; Ibrahim, O.H.; He, H.J.; Liu, S.; Kamruzzaman, M. An overview of recent advances and applications of FT-IR spectroscopy for quality, authenticity, and adulteration detection in edible oils. *Crit. Rev. Food Sci. Nutr.* **2022**, *62*, 8009–8027. [CrossRef]
60. Matwijczuk, A.; Zając, G.; Karcz, D.; Chruściel, E.; Matwijczuk, A.; Kachel-Jakubowska, M.; Łapczyńska-Kordon, B.; Gagoś, M. Spectroscopic studies of the quality of WCO (Waste Cooking Oil) fatty acid methyl esters. In *BIO Web of Conferences*; EDP Sciences: Paris, France, 2018; Volume 10, p. 02019.
61. Jović, O.; Smolić, T.; Jurišić, Z.; Meić, Z.; Hrenar, T. Chemometric analysis of croatian extra virgin olive oils from central Dalmatia region. *Croat. Chem. Acta* **2013**, *86*, 335–344. [CrossRef]
62. Guillén, M.D.; Cabo, N. Usefulness of the frequencies of some Fourier transform infrared spectroscopic bands for evaluating the composition of edible oil mixtures. *Lipid/Fett* **1999**, *101*, 71–76. [CrossRef]
63. Mores, S.; de Souza Vandenberghe, L.P.; Júnior, A.I.M.; de Carvalho, J.C.; de Mello, A.F.M.; Pandey, A.; Soccol, C.R. Citric acid bioproduction and downstream processing: Status, opportunities, and challenges. *Bioresour. Technol.* **2021**, *320*, 124426. [CrossRef]
64. Holz, M.; Förster, A.; Mauersberger, S.; Barth, G. Aconitase overexpression changes the product ratio of citric acid production by *Yarrowia lipolytica*. *Appl. Microbiol. Biotechnol.* **2009**, *81*, 1087–1096. [CrossRef] [PubMed]
65. Hapeta, P.; Rakicka-Pustułka, M.; Juszczyk, P.; Robak, M.; Rymowicz, W.; Lazar, Z. Overexpression of citrate synthase increases isocitric acid biosynthesis in the yeast *Yarrowia lipolytica*. *Sustainability* **2020**, *12*, 7364. [CrossRef]

66. Förster, A.; Jacobs, K.; Juretzek, T.; Mauersberger, S.; Barth, G. Overexpression of the *ICL1* gene changes the product ratio of citric acid production by *Yarrowia lipolytica*. *Appl. Microbiol. Biotechnol.* **2007**, *77*, 861–869. [CrossRef]
67. Yuzbasheva, E.Y.; Scarcia, P.; Yuzbashev, T.V.; Messina, E.; Kosikhina, I.M.; Palmieri, L.; Shutov, A.V.; Taratynova, M.O.; Amaro, R.L.; Palmieri, F.; et al. Engineering *Yarrowia lipolytica* for the selective and high-level production of isocitric acid through manipulation of mitochondrial dicarboxylate–tricarboxylate carriers. *Metab. Eng.* **2021**, *65*, 156–166. [CrossRef] [PubMed]
68. Finogenova, T.; Kamzolova, S.; Dedyukhina, E.; Shishkanova, N.; Il'Chenko, A.; Morgunov, I.; Chernyavskaya, O.; Sokolov, A. Biosynthesis of citric and isocitric acids from ethanol by mutant *Yarrowia lipolytica* N 1 under continuous cultivation. *Appl. Microbiol. Biotechnol.* **2002**, *59*, 493–500. [CrossRef]
69. Kamzolova, S.V.; Samoilenko, V.A.; Lunina, J.N.; Morgunov, I.G. Effects of medium components on isocitric acid production by *Yarrowia lipolytica* yeast. *Fermentation* **2020**, *6*, 112. [CrossRef]
70. Cavallo, E.; Charreau, H.; Cerrutti, P.; Foresti, M.L. *Yarrowia lipolytica*: A model yeast for citric acid production. *FEMS Yeast Res.* **2017**, *17*, fox084. [CrossRef] [PubMed]
71. Liu, X.; Yu, X.; Gao, S.; Dong, X.; Xia, J.; Xu, J.; He, A.; Hu, L.; Yan, Y.; Wang, Z. Enhancing the erythritol production by *Yarrowia lipolytica* from waste oil using loofah sponge as oil-in-water dispersant. *Biochem. Eng. J.* **2019**, *151*, 107302. [CrossRef]
72. Rakicka, M.; Rywinska, A.; Cybulski, K.; Rymowicz, W. Enhanced production of erythritol and mannitol by *Yarrowia lipolytica* in media containing surfactants. *Braz. J. Microbiol.* **2016**, *47*, 417–423. [CrossRef]
73. Mirbagheri, M.; Nahvi, I.; Emtiazi, G.; Darvishi, F. Enhanced production of citric acid in *Yarrowia lipolytica* by Triton X-100. *Appl. Biochem. Biotechnol.* **2011**, *165*, 1068–1074. [CrossRef]
74. Gao, Y.; Wang, F.; Li, X.; Mao, G.; Xie, H.; Song, A.; Santos, J.C.; Zhang, Z. Tailored production of citric acid and mannitol by *Yarrowia lipolytica* from corn stover pretreated by glycerol-assisted instant catapult steam explosion. *Ind. Crops Prod.* **2022**, *189*, 115820. [CrossRef]
75. Ping, L.; Yuan, X.; Zhang, M.; Chai, Y.; Shan, S. Improvement of extracellular lipase production by a newly isolated *Yarrowia lipolytica* mutant and its application in the biosynthesis of L-ascorbyl palmitate. *Int. J. Biol. Macromol.* **2018**, *106*, 302–311. [CrossRef] [PubMed]
76. Cavallo, E.; Nobile, M.; Cerrutti, P.; Foresti, M.L. Exploring the production of citric acid with *Yarrowia lipolytica* using corn wet milling products as alternative low-cost fermentation media. *Biochem. Eng. J.* **2020**, *155*, 107463. [CrossRef]
77. Panadare, D.C. Applications of waste cooking oil other than biodiesel: A review. *Iran. J. Chem. Eng.* **2015**, *12*, 55–76.

fermentation

MDPI

Article

Online Monitoring of the Temperature and Relative Humidity of Recycled Bedding for Dairy Cows on Dairy Farms

Yong Wei [1,†], Kun Liu [1,2,†], Yaao Li [2,†], Zhixing Li [1], Tianyu Zhao [2], Pengfei Zhao [3], Yayin Qi [3], Meiying Li [1,*] and Zongyuan Wang [1,2,*]

[1] Xinjiang Tianrun Dairy Co., Ltd., Urumqi 830063, China; trweiyong@outlook.com (Y.W.); liukun@stu.shzu.edu.cn (K.L.); trlizhixing@outlook.com (Z.L.)
[2] School of Chemistry and Chemical Engineering, State Key Laboratory Incubation Base for Green Processing of Chemical Engineering, Shihezi University, Shihezi 832003, China; liyaao@stu.shzu.edu.cn (Y.L.); zhaotianyu@stu.shzu.edu.cn (T.Z.)
[3] College of Animal Science and Technology, Shihezi University, Shihezi 832003, China; accelerator1908@outlook.com (P.Z.); qiyayin@163.com (Y.Q.)
* Correspondence: limeiying_tr@hotmail.com (M.L.); zywang@shzu.edu.cn (Z.W.)
† These authors contributed equally to this work.

Abstract: In large-scale dairy farming, the use of high-temperature-fermented dairy manure bedding instead of rice husk-based bedding and other commercial types of bedding is widely favored. Strip-stacking aerobic fermentation is the main production method of dairy manure bedding, but it has problems including unstable fermentation and the secondary breeding of pathogens. In this work, a multi-probe, integrated, online monitoring system for temperature and relative humidity was used for fermentation process optimization. The effects of the temporal and spatial distribution of fermentation temperature and relative humidity on the nutrient content curve and the moisture and ash content of manure bedding materials were systematically studied. The effect of the fermentation process on the retention rate of effective bedding materials (cellulose, hemicellulose, and lignin) was analyzed. The experiments proved that high-quality bedding material can be obtained through reasonable stacking fermentation. The fabricated bedding material has a total dry base content consisting of cellulose, hemicellulose, and lignin of 78%, an ash content of 6%, and a nutrient content of 17%. The obtained bedding material was produced to increase the bed rest rate and continuously inhibit the bedding bacteria content, keeping it at a low level for 5 days. This study proves that temperature and humidity monitoring can guide the optimization of the strip-stacking fermentation process of dairy manure and that it can be applied to large-scale farms to improve fermentation parameters.

Keywords: stacking fermentation; recycled bedding; temperature and relative humidity; online monitoring

1. Introduction

In recent years, with the rapid development of the economy, dairy farms have been scaled up, and the amount of dairy manure has become a great challenge for the farming sector [1,2]. Dairy manure places a great burden on the environment and resources [3]. One of the most commonly used methods of manure treatment is using it to fertilize the land. In dairy manure, there are abundant N, P, and S elements, which can also play a role in increasing soil fertility. However, cow manure is produced in large quantities, and the ability of the land to decompose it is limited. Excessive or inappropriate return of manure to the field can cause a number of problems, such as environmental degradation, climate change, resource depletion [4], acidification, and potential eutrophication [5]. Therefore, there is an urgent need for a green treatment method to relieve the pressure placed on the land by manure and improve its degradation process. The use of high-temperature-fermented dairy manure to produce recycled manure bedding materials instead of non-

renewable sand and biomass has been widely adopted in large-scale dairy cow farming. Recycled manure bedding could be used as a good alternative to bulk sawdust, wood chips, shavings, square harvesting straw, chopped straw, rice husks, peanut shells, corn cobs, and other commercial biomass bedding materials [6–12]. Not only can it save costs, but it can also reduce the risk of the introduction of pathogens carried by biomass [13].

Dairy cow mastitis is one of the most common diseases in dairy farming [14]. Pathogen infection is the main cause of mastitis in dairy cows and is closely related to the quality and use of the bedding materials. The pathogenic microorganisms most commonly detected in mastitis milk samples are *Escherichia coli* (*E. coli*) [15], *Streptococcus agalactiae* (*S. agalactiae*), and *Staphylococcus aureus* (*S. aureus*) [12,16,17]. The latter species is the most representative pathogen in milk [18]. The number of bacteria in the bedding material is positively correlated with the type of bacteria on the tip of the cow teat [7]. Cow teats are in direct contact with the bacteria in the bedding material [8,9,17]; therefore, the bedding material is the main source of the teats' exposure to environmental pathogens that cause mastitis. The improper use of bedding can lead to mastitis outbreaks, which can lead to huge financial losses [11,19].

With the expansion of the scale of automated farming, the demand for bedding material is increasing [10,20]. The methods of high-temperature aerobic fermentation mainly include strip-stacking fermentation, drum-type tank fermentation [20], and membrane fermentation [21]. Among them, strip-stacking composting has been widely used to treat dairy manure because of its high capacity for treatment and low cost [22]. However, the implementation process of the strip-stacking fermentation method makes it difficult to control the quality of the fermented products. Random factors such as the weather, the differences in ambient temperature between the farm and the pasture, and the amount of manual work involved in the process can all affect the final nature of the manure and the sterilization effect. Therefore, there are problems including bacterial regeneration and high-frequency replacement in recycled bedding prepared by strip-stacking fermentation. The climate and environment of every pasture are different in different seasons. Pastures need a long production practice cycle to form a stable aerobic fermentation process, and targeted adjustments need to be made in different seasons throughout the year. However, in actual pastures, it is difficult to flexibly adjust the fermentation process because there is a lack of indication signals. Therefore, it is of great significance to establish a rapid strip-stacking fermentation condition monitoring method to assess the influence of fermentation process parameters on the establishment and optimization of aerobic fermentation processes in large-scale pastures.

At present, the main factors influencing the fermentation process in strip-stacked aerobic compost include stack size, initial moisture content, fermentation time, air permeability, sunshine time, and ambient temperature. The influence of these factors has been widely studied. The evaluation of the quality of dairy manure bedding material mainly includes softness [23], dryness, cleanness, elasticity, and deformation resistance [24,25]. This is related to the dry matter content [15], moisture content [26], cellulose, hemicellulose, and lignin content, particle size [23], and other factors. Shane et al. found that bedding material with good physical structure and good water absorption (moisture content of less than 25% and particle size of less than 2.5 cm) is the best choice for breeding systems [27]. Robles et al. found that the type of bedding material is related to the rate of bacterial growth [28]. Moreover, bacterial growth is closely related to the usage process [15,23]. However, most existing studies only focus on the fermentation process, studying the use of bedding material separately. There are relatively few studies on the interaction between the two processes. Therefore, it is important to establish the relationship between the fermentation process and bedding quality and usage. To the best of our knowledge, there has been no systematic investigation on the use of automatic online equipment to monitor the actual use of strip-stacked bedding fermentation on large-scale dairy farms.

Therefore, in this study, an online detection system for the temporal and spatial distribution of stacking temperature and humidity was established. Long-term continuous

detection data of stacking temperature and humidity at different depths was obtained. Variations in the temperature and relative humidity of the stacking section with fermentation time, day and night alternation, and sunny and rainy seasons were analyzed. The pathogenic bacteria killing rate, the content of water and cellulose, and the nutrient particle size were evaluated. Meanwhile, the determination of the fermentation endpoint was realized by combining bacterial detection and online monitoring. It was found that the stacking fermentation process had a significant effect on comfort, bed rest rate, and bacterial reproduction rate.

2. Materials and Methods

2.1. Materials

The materials used in this study included LB nutrient agar (Shanghai Titan Scientific Co., Ltd., Shanghai, China), Staphylococcus aureus chromogenic medium (Shanghai Titan Scientific Co., Ltd.), KF streptococcus agar (Shanghai Titan Scientific Co., Ltd.), MacConkey agar medium (Shanghai Titan Scientific Co., Ltd.), agar powder (Solarbio Science & Technology, Beijing, China), and ethanol (C_2H_6O, $\geq$99.7%, Sigma-Aldrich, St Louis, MO, USA).

2.2. Strip Stacking Fermentation of Dairy Manure

The experiment was carried out on a large-scale ranch with 5000 cows in western China. The time chosen for this study was July to August during the high-temperature periods. The outdoor daytime temperature was maintained at an average of 30 °C. Dairy manure was scraped to the manure storage tank through the hanging manure board, transported to the dry and wet separation room by the manure pump, and then transported to the fermentation site by machinery after separation (Figure S1a). The fermentation process adopted the strip stack aerobic fermentation method, with a length of 16 m, a trapezoidal cross-section, a bottom width of 2 m, and a height of 1 m, so as to ensure the sufficient mass transfer of water and oxygen (Figure S1b). The whole fermentation process lasted for 15 days. The samples were collected at three different depths as follows: the surface layer (0.05 m depth), the middle layer (0.5 m depth), and the deep layer (1 m depth) for bacterial content and other characterization. Each sample was collected at three locations, and the test results were averaged. The stack was divided into two piles with different fermentation processes, as shown in Figure S2. The A group was spread out and mixed evenly on the 5th and 12th days and then stacked up to return to its original shape. The B group was kept unchanged for 15 days to make a comparison.

After the fermentation was over, the dairy manure of the A and B groups was spread out, dried under the sun, and turned three times a day. The final moisture content decreased to below 10%. The dairy manure bedding material was obtained, sprinkled with slaked lime, and stirred evenly before being used in the barn.

2.3. Temperature and Relative Humidity Online Monitoring

An online monitoring system was used for the detection of temperature and relative humidity, as shown in Figure S1c. The temperature and relative humidity probe contain a detection area with a total length of 0.9 m, and 10 sensors are evenly distributed in the detection area. The data is transmitted to the computer through the network. The detection interval is 30 s. The first sensor is exposed to the outside of the stack and is used to monitor the ambient temperature. Two probes were used for the A group and the B group, respectively. Data from the spreading, drying, and flip processes were discarded.

2.4. Composition Measurement

Moisture content was measured using a halogen moisture analyzer using the differential gravity method. The determination of lignocellulosic fibers (including cellulose, hemicellulose, and lignin) and ash content was measured using the Van Soest method

of the reported article [29]. The nutrient content was obtained by subtracting the above substances from the total weight.

2.5. Bacterial Content Measurement

The content of *E. coli*, *S. aureus*, *S. agalactiae*, and *Total Bacteria Counts* (*T. B. Cs*) was obtained by combining the solid medium coating plate counting method with the polymerase chain reaction (PCR). Typically, 40 g of LB nutrient agar, 35.04 g of Staphylococcus aureus chromogenic medium, 69.5 g of KF streptococcus agar, and 50 g of MacConkey agar medium were dissolved in 1000 mL of ultrapure water. Meanwhile, 2.4 g of agar powder was added to the above solution and heated at 121 °C for 15 min in an autoclave. After cooling, the medium was solidified, sealed with parafilm, and stored at 4 °C. LB nutrient agar was used to grow *T. B. Cs*; Staphylococcus aureus chromogenic medium (second generation) was used to grow *S. aureus*; KF Streptococcus agar (with TTC) was used to grow *S. agalactiae*; and MacConkey agar medium (containing crystal violet) was used to grow *E. coli* [30].

The bedding samples were thawed at room temperature, and 0.07 g of a sample was added into 7 g of sterile water. Then, the stock solution was fully shaken and filtered with a vortex mixer to create a 1:100 dilution. After the mixture stood at room temperature for 10 min, 100 μL of the supernatant was taken for further dilution ($1{:}10^2$, $1{:}10^3$, $1{:}10^4$, $1{:}10^5$, $1{:}10^6$, or $1{:}10^7$). The LB nutrient agar medium was inoculated onto a $1{:}10^7$ dilution; the *S. aureus* medium and *S. agalactiae* medium were inoculated onto a $1{:}10^3$ dilution; and the *E. coli* medium was inoculated onto a $1{:}10^4$ dilution. The dilution was evenly smeared on the disposable medium with a coating rod. After being fully absorbed by the medium, it was placed under aerobic conditions at 37 °C and cultured for 24 h. The number of bacteria was obtained by counting the plate, as shown in Figure S3, Supporting Information.

The polymerase chain reaction (PCR) was detected on a PCR machine (Zimmer Bonmei, Dover, OH, USA), which is used to determine the type of bacteria. Its model is the jy300C electrophoresis apparatus. All specific primers for PCR were designed using Beacon Designer 17.0 software based on the gene sequences available in GenBank [31]. The primer designs for different bacteria are shown in Table S1.

2.6. Bed Rest Rate Measurement

The bed rest rate of dairy cows was measured in a large lactating cow barn in the pasture, covering 500 adult lactating cows. Ten beds among the 200 beds in the barn were selected for collecting bedding samples. About 10 kg of fresh bedding material for each bed is supplemented every 3 days. Previous studies have shown that frequent addition or replacement of bedding material can reduce exposure to mastitis pathogens in the environment [32]. Supplementation of the bedding material was carried out during the milking time to avoid the process of manure throwing affecting the feeding and rest of the cows. The 10 beds were divided into two parts, with bedding materials for the A and B groups. The bedding was laid as shown in Figure S4. On the bed, the thickness of the dairy manure material under the head and the udder of the dairy cows was about 45 cm and 20 cm, respectively. The samples that were stepped on 2–5 cm below the breast were collected every 12 h and stored at −20 °C. The number of cows lying in 5 beds in the A or B group was recorded every 10 min for 120 h during 5 days. The rate of bed rest was based on the ratio of beds with lying cows. In the milking process, the cows were not in the barn, and the data were discarded.

3. Results and Discussion

3.1. Temporal and Spatial Distribution of Temperature

The time-temperature characteristic curve that was collected by the online monitor is shown in Figure 1a,b. For both the A and B groups, there was a periodic change in temperature between 16.4 °C and 45.8 °C at 0.05 m, which is assigned to the ambient temperature. The periodic changes reflected the alternating fluctuations in temperature

during the day and night. Therefore, the detection method in this work can also monitor the ambient temperature of a pasture in real time. The results showed that the average ambient temperature during the experiment was about 30 °C. The temperature curves from −0.05 m to −0.85 m showed the temperature at the corresponding depths in the stack. The temperature curves of the −0.05 m and −0.25 m depths synchronously fluctuated with the ambient temperature, indicating the superficial temperature of manure stacks was significantly affected by the ambient temperature. For the A group, the maximum temperature of superficial manure (−0.05 m) was 50.3 °C, which is too low to reach the temperature of complete sterilization. However, the lowest temperature at −0.25 m depth could reach 60 °C during the second to seventh day. The temperature change during the fermentation experiment is a fluctuation in the high-temperature range from 50 °C to 75 °C. Therefore, the temperature fluctuations in this range do not easily alter microbial populations, and the surviving microbial population is bacteria that are resistant to high temperatures. It has been reported in the literature that the minimum sterilization temperature for *E. coli* and *S. aureus* is 50 °C and 40 °C [30,33], respectively. Therefore, cow manure must undergo high-temperature sterilization at different depths by flipping over the stack.

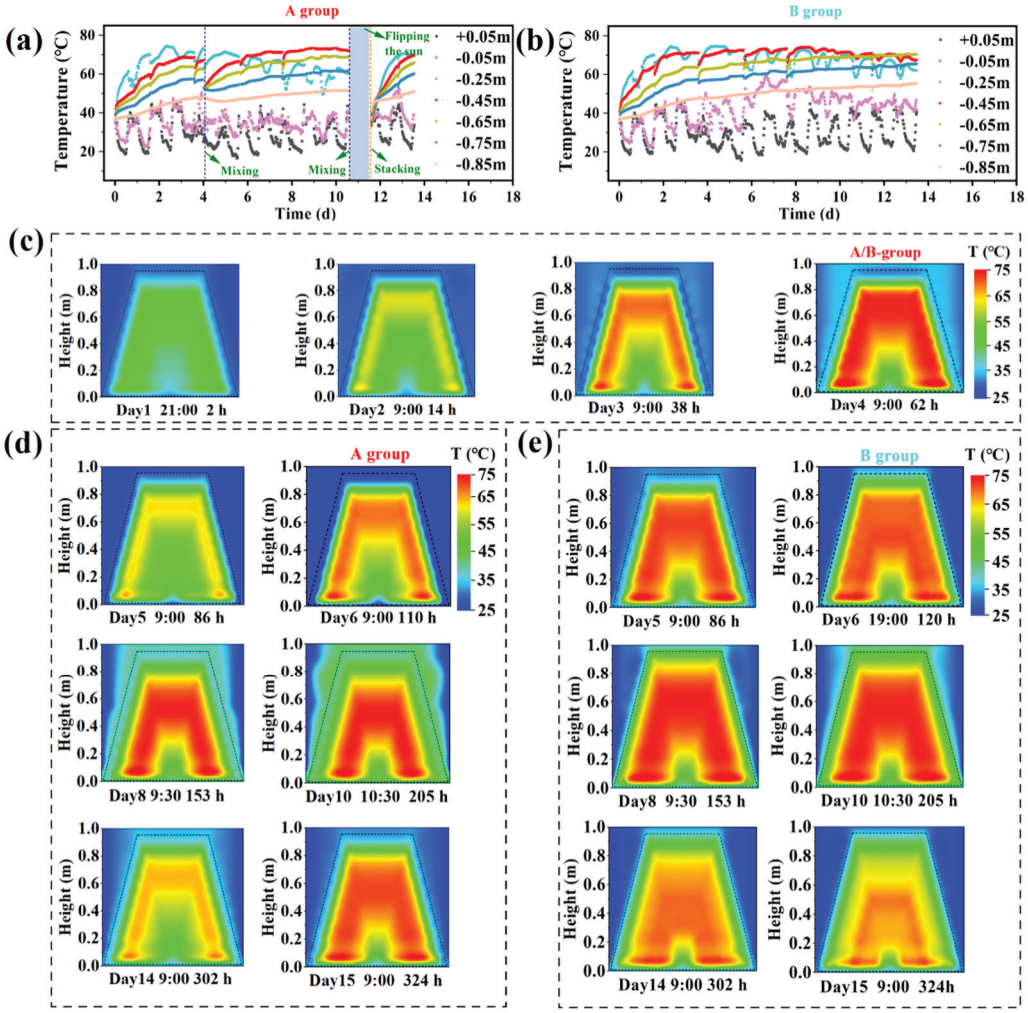

Figure 1. Temporal and spatial distribution of temperature during dairy manure fermentation. Time–temperature diagram showing the fermentation of dairy manure in the (**a**) A and (**b**) B groups; space–temperature diagram of fermentation during (**c**) 1–4 days and 5–15 days for the (**d**) A and (**e**) B groups.

The temperature curves were fitted with the stacking section to obtain the temperature distribution map of the stacking section, as shown in Figure 1c–e. A higher temperature (about 75 °C) was achieved at a depth of 0.3 m, about 3 days from the start of fermentation (Figure 1c). The high temperature gradually expanded to a depth range of 0.25~0.65 m on the fifth day. This result proves that temperature accumulation is raised from the outside to the inside, and only a shallow layer (<20 cm) of manure insulation is required. The temperature curves at the 0.45 m and 0.65 m depths exhibited the highest temperature (73.4 °C to 69.4 °C) without noticeable fluctuations, indicating the best fermentation and sterilization intervals. The temperature in this zone can be recovered within 35 h after the 5th and 12th days of flipping the stack. The temperature recovery on the 12th day was quicker than the 5th day because of more aerobic bacteria. Therefore, it is necessary to maintain the fermentation time for at least 5 days after each flipping of the stack to ensure a high-temperature environment.

Next, the difference in temperature distribution between the A and B groups was compared and shown in Figure 1d,e. The A group could quickly rise to a high temperature (~73.4 °C) after turning the stack, and the high temperature could be maintained until the end of the stacking. However, the B group showed an obvious decrease in temperature from the 10th day to the 15th day. After the nutrient depletion in the middle depth of the B group, the number of beneficial bacteria decreased, resulting in a decrease in temperature. Nutrients in other low-temperature areas of the B group may breed pathogens that are not killed.

3.2. Temporal and Spatial Distribution of Relative Humidity

Since bacterial growth is related to relative humidity (RH) [20], a time-relative humidity characteristic curve according to the monitoring data was investigated, as shown in Figure 2 and Figure S5. In the first 5 days (Figure 2c), the distribution of RH was closely correlated with temperature. The more active the bacteria, the higher the temperature and RH. The deepest relative humidity was more than 100%, which exceeded the upper limit of detection. Because of the compaction of the manure on the surface, it is difficult for moisture to diffuse outside, and excessive RH affects the diffusion of oxygen.

After flipping the stack, there was a significant difference in the RH distribution between the A (Figure 2c) and B (Figure S5b) groups. In the A group, areas with high RH were only found in the bottom area of the stack. Flipping the stack could effectively maintain the permeability of the stack with RH < 25% so that the moisture generated by bacterial activities could be emitted over time. In addition, the −0.85 m depth of the B group showed an increasing RH from 20% to 100% (Figure S5a), indicating the anaerobic fermentation in the deep area is the gradual accumulation of water. In the high-RH region at the bottom, the A group also had a smaller range than the B group, indicating a smaller anaerobic area. Therefore, the flipping of the stack is conducive to the diffusion and mass transfer of water and helps to reduce the distribution of anaerobic fermentation areas and the generation of stench, such as H_2S and NH_3 [34,35], while promoting aerobic fermentation.

3.3. Moisture Content Analysis

Next, changes in the water content of the stacks during the fermentation process were investigated. As shown in Figure 3, the moisture content was 65–75% in the first 2 days, which was similar to that reported by Black R.A et al. [28]. Bacterial growth is affected by moisture and will also affect water cumulation [20]. The moisture content reached its maximum on the third day because of bacterial metabolism, and the moisture content in the deep layers was as high as 75%. From the curves of the A and B groups, it can be seen that the moisture content of manure did not change during the fermentation process, regardless of whether the pile was turned over or not. The removal of water from bedding materials mainly depended on the drying process (after the 15th day). Therefore, the initial moisture of the manure before fermentation needs to be strictly controlled. Too much

moisture (>70%) will limit air permeability [36], and too low moisture (<30%) will affect the reproduction of beneficial bacteria [37].

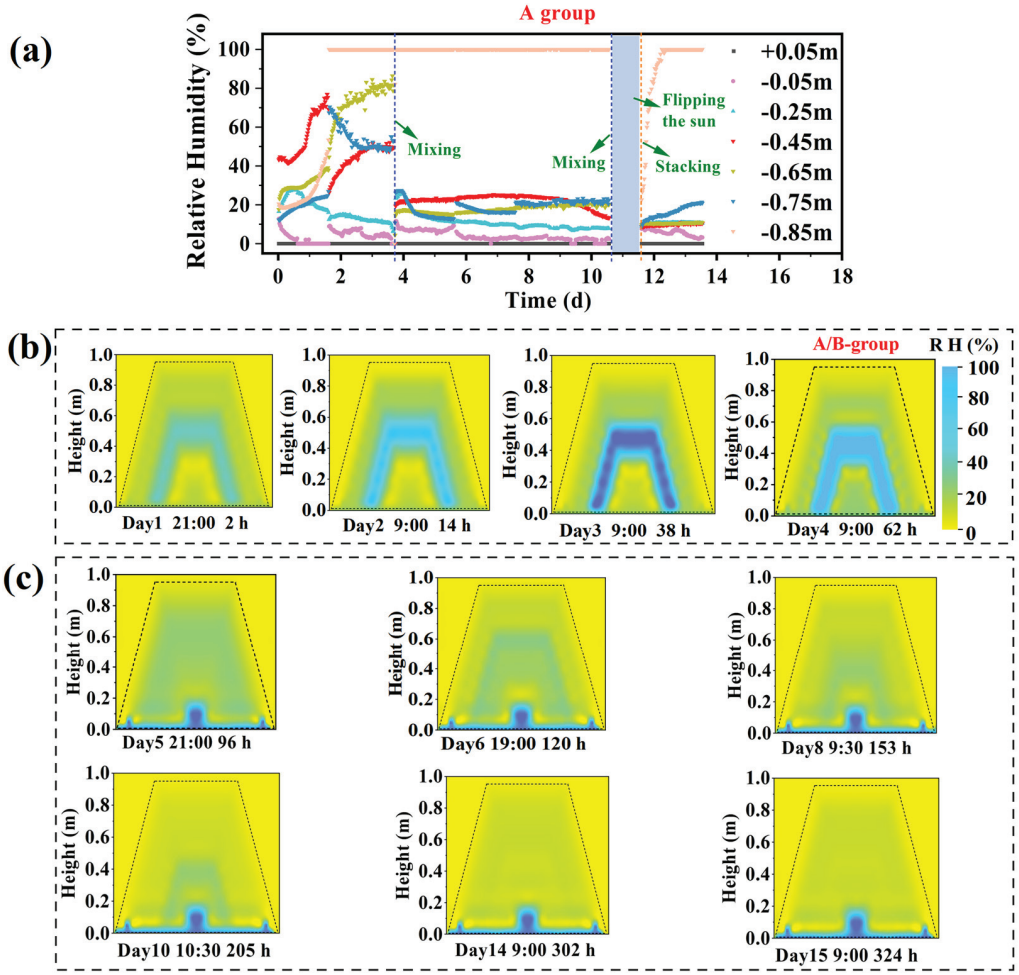

Figure 2. Temporal and spatial distribution of relative humidity (RH) during dairy manure fermentation. Time–RH diagram showing the fermentation of dairy manure in (**a**) the A group; space–RH diagram of fermentation during (**b**) 1–4 days and 5–15 days for (**c**) the A group.

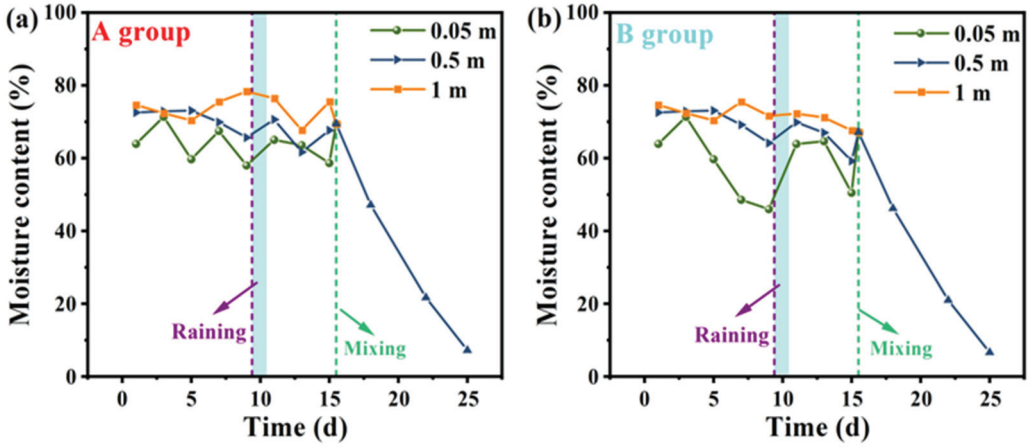

Figure 3. Moisture content distribution during fermentation. (**a**) Time–moisture content change diagram of dairy manure in the A group. (**b**) Time–moisture content change diagram of dairy manure in the B group.

The moisture content of the surface manure in the B group decreased on the third to ninth days. This process of water loss is the result of surface manure compaction. On the ninth day, because of rain, the moisture content of both groups increased in both the surface and middle layers, but the rain did not penetrate into the deep layer. Therefore, open-air fermentation is tolerant to general rain and snow weather, and the fermentation inside the stack is not easily affected by general rainfall. After the 15th day, the two groups of dairy manure were spread out and mixed evenly, and the moisture content decreased rapidly with an average rate of 4% per day.

3.4. Bactericidal Performance Evaluation

The number of bacteria in the recycled bedding produced by the A group was obtained by plate counting, as shown in Figure 4. As shown in Figure 4a, the number of *E. coli* at the beginning of fermentation was about 10^6 CFU/g, which is similar to the results of the work reported in [9]. *E. coli* was eradicated after 3 days at 0.5 m, quicker than that of 5 days at 0.05 m, and 7 days at 1 m, indicating that the middle layer had a better bactericidal effect. Llonch et al. reported the same result [32]. As shown in Figure 4b, the same change occurred in the superficial layer and middle layer of *S. agalactiae*, but the difference was that this species was eradicated on the fifth day in the deeper layer. *S. aureus* was not detected in the entire experiment (Figure 4c). The number of *T. B. C* was measured, as shown in Figure 4d. The number of *T. B. C* was about 10^9 CFU/g at the beginning, which is more than previously reported [9]. On the 12th day, the number of *T. B. C* sharply increased because of the breakdown and decay of cellulose to provide more nutrients. Therefore, 15 days of fermentation time is sufficient to achieve good sterilization. A fermentation time that is too long will make the manure rot, which is not conducive to improving bedding quality.

3.5. Composition Analysis

The composition analysis of lignocellulosic fibers, nutrients, and ash was carried out to compare the effect of the flip stack on bedding between the A and B groups. These lignocellulosic fibers are mainly composed of cellulose, hemicellulose, and lignin [38]. Lignocellulosic fibers are a measure of the indigestible plant material in livestock. Crude fiber is determined by acid and alkaline treatment of the sample to remove soluble carbohydrates, proteins, and ash, leaving the insoluble fiber fraction. It includes neutral detergent fiber (NDF) and acid detergent fiber (ADF) [39]. The composition analysis of the dry matter results of the A and B groups is shown in Figure 5. During fermentation, the nutrients decreased for both the A and B groups because of the gradual increase in the number of beneficial strains during the fermentation process, which coincides with the number of T. B. C. in Figure 4. Several beneficial bacteria in cow manure have been reported, such as *Firmicutes*, *Proteobacteria*, *Bacteroidetes*, and *Actinobacteria* [40]. These bacteria could degrade the nutrients in cow manure and produce a high temperature to kill the eggs of pathogenic bacteria. In the former 5 days, the nutrient content decreased from 21–27% to 10–17%, and the superficial layer and middle layer decreased significantly, by about 13%, showing a similar trend in the two groups. The deep decline is slow, by about 16–17%. Because oxygen and moisture can be diffused by mass transfer, aerobic fermentation dominated in the middle and upper layers. But the oxygen could not transfer into the deep layer, so anaerobic fermentation dominated. During anaerobic fermentation, short-chain fatty acids and dicarboxylic acids (such as fumaric acid) could be produced [41]. These short-chain fatty acids and dicarboxylic acids can provide nutrients to the bacteria but are not conducive to the long-term use of the litter. Therefore, anaerobic fermentation needs to be avoided as much as possible.

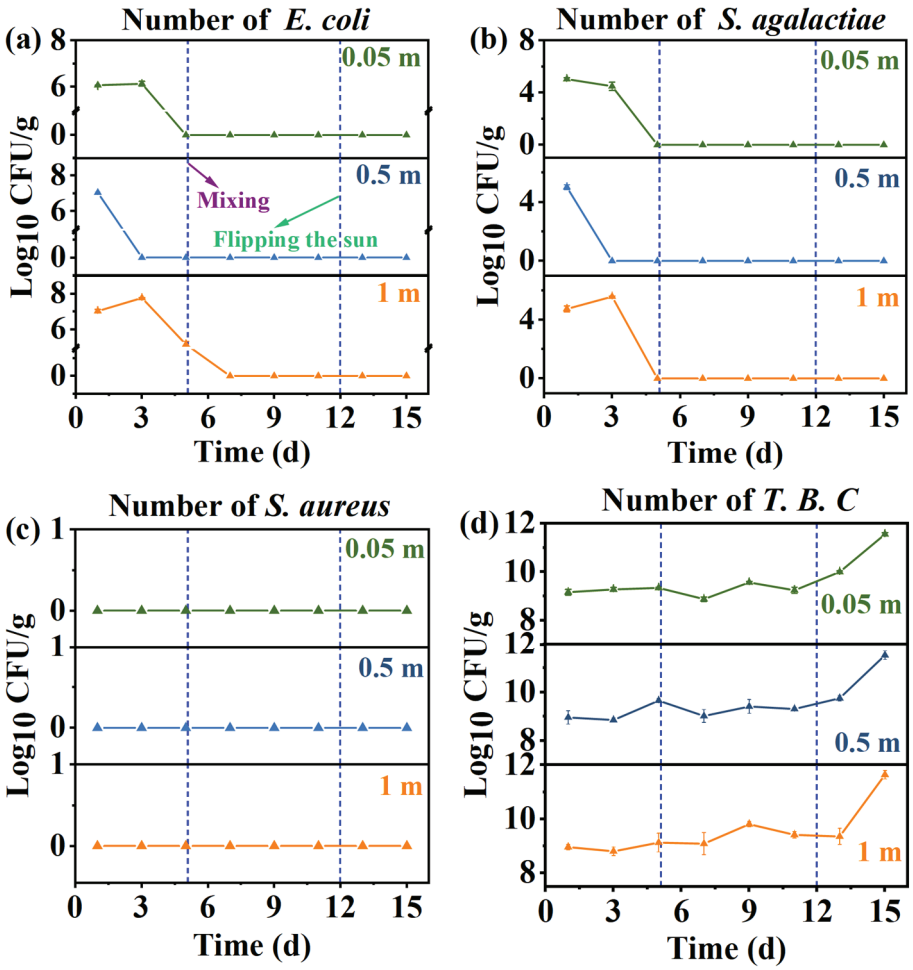

Figure 4. Bacterial changes during fermentation. Changes in the number of (**a**) *Escherichia coli* (*E. coli*), (**b**) *Streptococcus agalactiae* (*S. agalactiae*), (**c**) *Staphylococcus aureus* (*S. aureus*), and (**d**) *Total Bacteria Counts* (*T. B. Cs*).

Comparing the difference between the A and B groups, the rate of nutrient consumption in the A group was faster than that in the B group, indicating that flipping the stack increased the mass transfer of water and oxygen, promoting aerobic fermentation [42]. Flipping the stack is the switch between the A and B groups that regulates aerobic and anaerobic fermentation. In this work, the stack of the A group was flipped twice, while the B group was not flipped. The total contents of the lignocellulosic fiber, including cellulose, hemicellulose, and lignin, increased from 75% to 83% (0.05 m depth), 82% (0.5 m depth), and 78% (1.0 m depth). Mono-anaerobic digestion (AD) of dairy cow manure is constrained by ash [43]. Improving and retaining fibrous matter in dairy manure is an important reason why fermentation can make recycled bedding. The A group presented a higher lignocellulosic fiber content than the B group, indicating a better fermentation performance. It was also found that in the samples at the 1.0 m depth, the B group had a higher hemicellulose content of 26% than the A group (21%), while the cellulose content decreased from 33% (A) to 29% (B). This result indicates that there is excessive decomposition in the B group, which dissociates cellulose to form hemicellulose. The additional flipping of the stack in the A group can effectively reduce over-fermentation and decay.

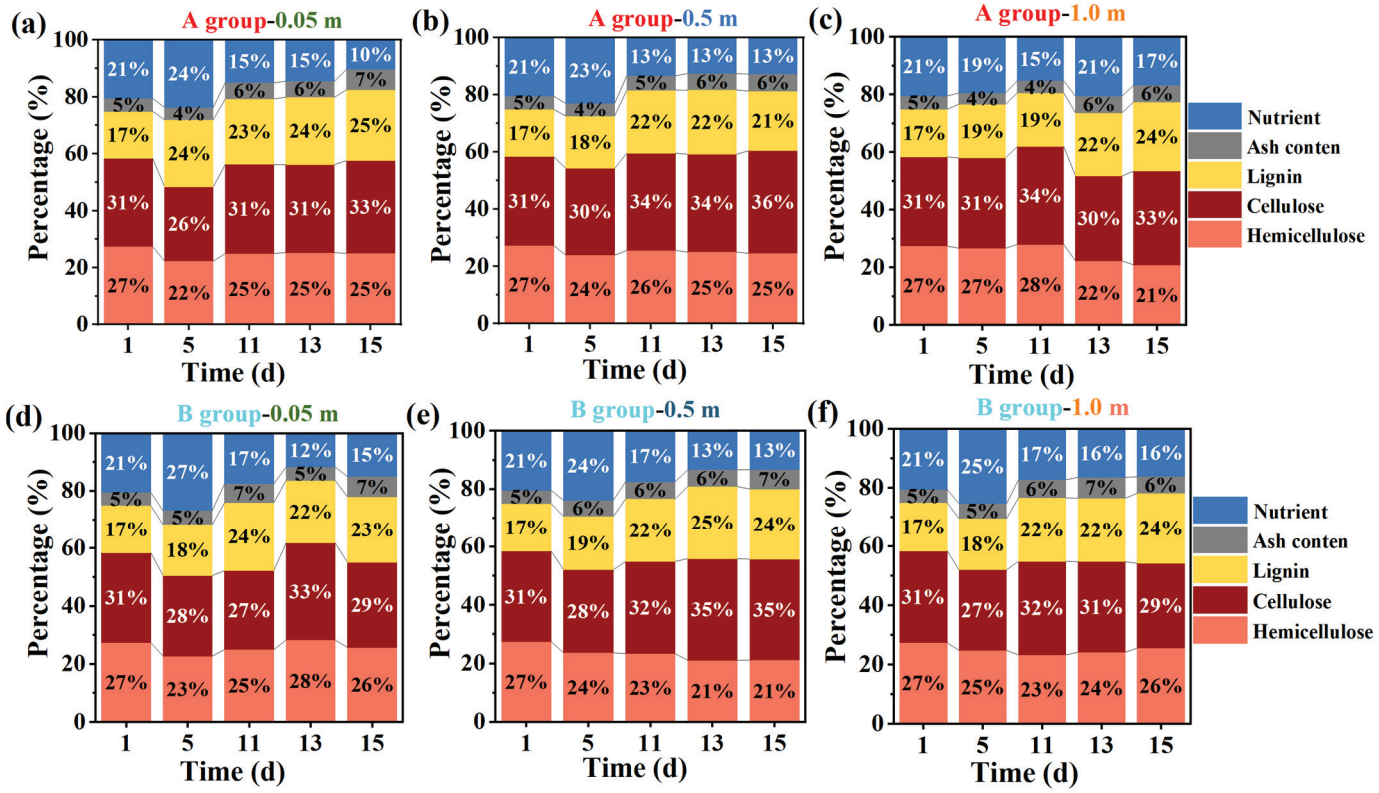

Figure 5. Changes in lignocellulosic fiber, nutrient, and ash content in the dry matter. A depth of 0.05 m for the A group (**a**) and the B group (**d**). A depth of 0.5 m for the A group (**b**) and the B group (**e**). A depth of 1.0 m for the A group (**c**) and the B group (**f**).

3.6. Bedding Bacteriostatic Performance

Before the actual application in the barn, the bacterial reproduction of the bedding materials with and without the influence of dairy cows was investigated. The A and B groups of recycled dairy manure bedding materials were mixed evenly with hydrated lime. The recycled manure bedding materials were placed in the barn environment (26.4 °C for daytime, 20.6 °C for night, and 56.2% of RH), and samples were taken regularly to observe changes in bacterial levels (Figure 6). *E. coli*, *S. agalactiae*, and *S. aureus* were not detected in the A group. But *E. coli* increased to about 2×10^6 CFU/g in the B group after 12 h. At 36 h and 96 h, adding new bedding material and hydrated lime according to the actual use process could slightly reduce the number of *E. coli*, but the effect was minimal. In the absence of dairy cows, the secondary growth of *E. coli* in the B group was delayed until 36 h, with an *E. coli* content of 5.5×10^5 CFU/g. Therefore, cleaning up manure timely will increase the cleanliness of bedding, thereby increasing milk production [20]. This comparison result proves that the recycled bedding material of the A group can effectively extend the service life and inhibit the secondary reproduction of pathogens because of its low nutrient content and complete sterilization of pathogens. In general, the dairy manure bedding material obtained by the group A method is used for no less than 5 days with dairy cows, so it is recommended to replenish with fresh litter every 3–5 days.

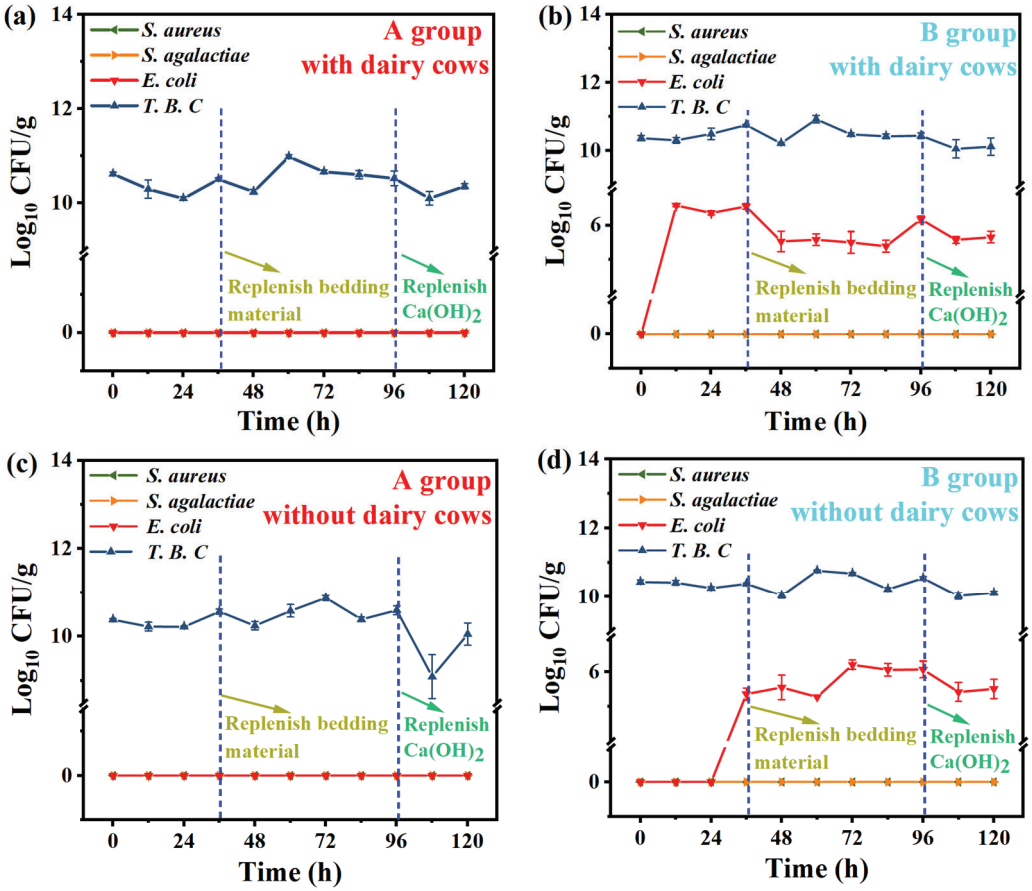

Figure 6. Changes in the number of *Escherichia coli* (*E. coli*), *Streptococcus agalactiae* (*S. agalactiae*), *Staphylococcus aureus* (*S. aureus*), and *Total Bacteria Count* (*T. B. C.*) with cow beds and without cow beds. (**a**) The A group dairy manure material in cow beds. (**b**) The B group dairy manure material in cow beds. (**c**) The A group dairy manure material without cow beds. (**d**) The B group dairy manure material without cow beds.

3.7. Bed Rest Rate Measurement

Adequate bed rest for dairy cows helps to increase milk production [44,45]. The average bed rest time of dairy cows is 8–16 h per day [46]. The bedding time of dairy cows depends on the type of dairy manure, and the bedding time of the cow will increase significantly when the bedding material is comfortable and relatively dry [46]. In this study, the A and B groups of recycled manure bedding materials were thrown onto the cow bed to count the number of cows lying in the bed (Figure 7a). During the experiment, the bedding needed to be 45 cm thick below the head and 20 cm below the udder, as shown in Figure 7b and Figure S4. Sufficient bedding materials can reduce lameness and some lesions [47]. The number of curves of cows lying in a bed according to the monitoring are shown in Figure 7c. It can be clearly seen that the bed rest rate of the A group is significantly higher than that of the B group, which proves that the fermentation mode of dairy manure in the A group brought better comfort than that of the B group.

To determine the reasons for the increase in comfort, particle size analysis was carried out (Figure 7d–f). A series of samples of different depths (0.05 m, 0.5 m, and 1.0 m) were collected on the first day (marked A-1 and B-1 for the A and B groups, respectively) and the 15th day (A-15 and B-15). The results prove the recycled bedding materials of the A group better retained their original granularity. The B group decreased the particle size because of decay, which was consistent with the composition test results of partial cellulose conversion to hemicellulose. Therefore, the statistical results of the bed rest rate and the

particle size test prove that the flipping of the stack could improve the comfort of recycled manure bedding materials.

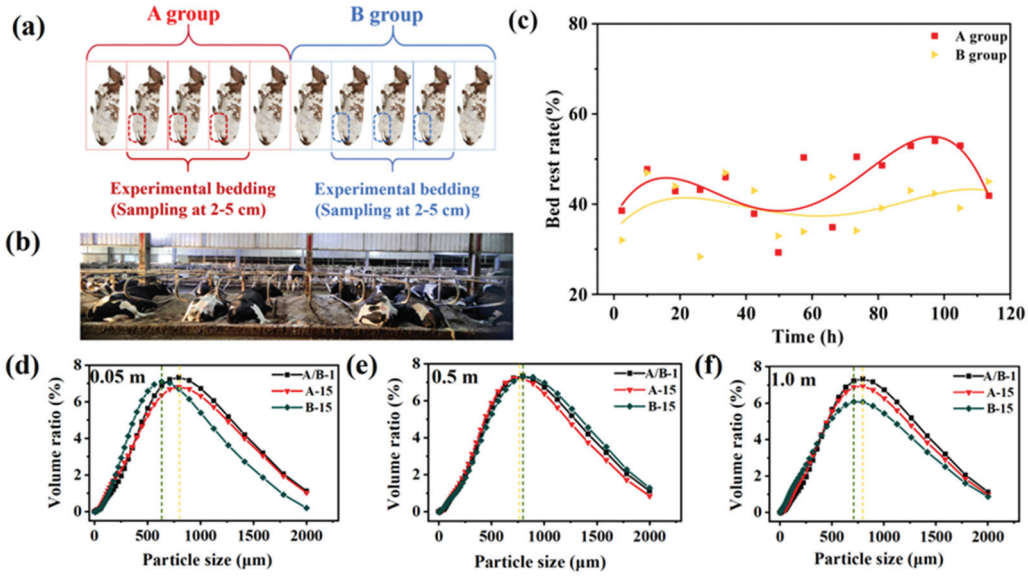

Figure 7. Bed rest rate and granularity statistics of the A and B groups of recycled dairy manure bedding materials. (**a**) Schematic diagram of the distribution of beds; (**b**) digital photos of dairy cows lying in beds; (**c**) bed rest rate of the A and B groups; (**d**) particle size changes at the different depths collected on (**e**) the 1st day and (**f**) the 15th day.

4. Conclusions

In this work, the spatial and temporal distribution characteristics of temperature and RH were drawn according to the online monitoring system. The changes in moisture content, number of bacteria, lignocellulosic fibers, and nutrient and ash content of recycled dairy manure bedding materials were detected during 15-day strip-stacked aerobic fermentation. The effects of flipping manure stacks on the bedding material composition, antibacterial properties, and bed rest rate were compared. The work proves flipping over manure stacks facilitates the diffusion of water and oxygen in the stack, retention of more cellulose, and improvement in bed rest. Within 48 h after flipping, the high stacking temperature will be recovered. The dairy manure shell formed by not flipping for a long time affected heat and mass transfer, which was not conducive to fermentation, leading to enhanced anaerobic fermentation and over-ripening. This work proves that in situ online temperature and RH monitoring combined with ex situ detection can effectively explore the rationality of large-scale pasture fermentation processes. This online monitoring system can better realize the automation of farm production and control. This monitoring method can be potentially applied in large dairy farms to optimize the process by designing the fermentation process and monitoring the daily bedding production process.

Supplementary Materials: The following supporting information can be downloaded at https://www.mdpi.com/article/10.3390/fermentation10070346/s1, Figure S1. Cow manure strip-stacking fermentation and the online monitoring system for temperature and relative humidity; Figure S2. The fermentation process of the A and B groups of dairy manure; Figure S3. Colony picture of *E. coli*, *S. agalactiae*, *S. agalactiae*, and *T. B. C*; Figure S4. Experimental bedding material distribution and sampling method; Figure S5. Temporal and spatial distribution of relative humidity during dairy manure fermentation of the B group; Table S1. Primer designs for different bacteria.

Author Contributions: Conceptualization, Z.W.; methodology, Y.W. and K.L.; software, Y.L.; formal analysis, Y.W. and K.L.; investigation, Y.W., K.L. and M.L.; resources, Y.W.; data curation, K.L., Y.L., T.Z. and P.Z.; writing—original draft preparation, Y.W., K.L. and Z.W.; writing—review and editing, M.L., Z.L. and Z.W.; supervision, M.L., Y.Q. and Z.W.; project administration, Y.W. and Z.W.;

funding acquisition, Y.W. and Z.W. All authors have read and agreed to the published version of the manuscript.

Funding: This research was funded by the Youth Science and Technology Top-notch Talent Project of Bingtuan, Major Scientific and Technological Projects of Bingtuan (SR202101), and the Tianchi Talent Program of Xinjiang.

Institutional Review Board Statement: Not applicable.

Informed Consent Statement: Not applicable.

Data Availability Statement: The data are contained within this article and the Supplementary Materials.

Conflicts of Interest: The authors declare no conflicts of interest.

References

1. Cui, X.; Guo, L.; Li, C.; Liu, M.; Wu, G.; Jiang, G. The total biomass nitrogen reservoir and its potential of replacing chemical fertilizers in China. *Renew. Sustain. Energy Rev.* **2021**, *135*, 110215. [CrossRef]
2. Li, Y.; Qi, C.; Zhang, Y.; Li, Y.; Wang, Y.; Li, G.; Luo, W. Anaerobic digestion of agricultural wastes from liquid to solid state: Performance and environ-economic comparison. *Bioresour. Technol.* **2021**, *332*, 125080. [CrossRef] [PubMed]
3. Bai, Z.; Lee, M.R.F.; Ma, L.; Ledgard, S.; Oenema, O.; Velthof, G.L.; Ma, W.; Guo, M.; Zhao, Z.; Wei, S.; et al. Global environmental costs of China's thirst for milk. *Glob. Chang. Biol.* **2018**, *24*, 2198–2211. [CrossRef] [PubMed]
4. Adghim, M.; Abdallah, M.; Saad, S.; Shanableh, A.; Sartaj, M.; El Mansouri, A.E. Comparative life cycle assessment of anaerobic co-digestion for dairy waste management in large-scale farms. *J. Clean. Prod.* **2020**, *256*, 120320. [CrossRef]
5. Wang, X.; Ledgard, S.; Luo, J.; Guo, Y.; Zhao, Z.; Guo, L.; Liu, S.; Zhang, N.; Duan, X.; Ma, L. Environmental impacts and resource use of milk production on the North China Plain, based on life cycle assessment. *Sci. Total Environ.* **2018**, *625*, 486–495. [CrossRef] [PubMed]
6. Tasistro, A.S.; Cabrera, M.L.; Ritz, C.W.; Kissel, D.E. Manipulating bedding materials and PLT^{TM} to reduce NH(3) emissions from broiler manure. *Bioresour. Technol.* **2008**, *99*, 1952–1960. [CrossRef] [PubMed]
7. Zigo, F.; Sasáková, N.; Gregová, G.; Výrostková, J.; Ondrašovičová, S. Effects of Using an Alternative Bedding Composition on the Levels of Indicator Microorganisms and Mammary Health in Dairy Farm Conditions. *Agriculture* **2020**, *10*, 245. [CrossRef]
8. Fernández, A.; Mainau, E.; Manteca, X.; Siurana, A.; Castillejos, L. Impacts of Compost Bedded Pack Barns on the Welfare and Comfort of Dairy Cows. *Animals* **2020**, *10*, 431. [CrossRef]
9. Fávero, S.; Portilho, F.V.R.; Oliveira, A.C.R.; Langoni, H.; Pantoja, J.C.F. Factors associated with mastitis epidemiologic indexes, animal hygiene, and bulk milk bacterial concentrations in dairy herds housed on compost bedding. *Livest. Sci.* **2015**, *181*, 220–230. [CrossRef]
10. Leso, L.; Barbari, M.; Lopes, M.A.; Damasceno, F.A.; Galama, P.; Taraba, J.L.; Kuipers, A. Invited review: Compost-bedded pack barns for dairy cows. *J. Dairy Sci.* **2020**, *103*, 1072–1099. [CrossRef]
11. Bertocchi, L.; Fusi, F.; Angelucci, A.; Bolzoni, L.; Pongolini, S.; Strano, R.M.; Ginestreti, J.; Riuzzi, G.; Moroni, P.; Lorenzi, V. Characterization of hazards, welfare promoters and animal-based measures for the welfare assessment of dairy cows: Elicitation of expert opinion. *Prev. Vet. Med.* **2018**, *150*, 8–18. [CrossRef] [PubMed]
12. Bradley, A.J.; Leach, K.A.; Green, M.J.; Gibbons, J.; Ohnstad, I.C.; Black, D.H.; Payne, B.; Prout, V.E.; Breen, J.E. The impact of dairy cows' bedding material and its microbial content on the quality and safety of milk—A cross sectional study of UK farms. *Int. J. Food Microbiol.* **2018**, *269*, 36–45. [CrossRef] [PubMed]
13. Šubová, E.; Sasáková, N.; Zigo, F.; Mindžáková, I.; Vargová, M.; Kachnič, J.; Laktičová, K.V. Amendment of Livestock Manure with Natural Zeolite-Clinoptilolite and Its Effect on Decomposition Processes during Composting. *Agriculture* **2021**, *11*, 980. [CrossRef]
14. Ferraz, P.F.P.; Ferraz, G.A.E.S.; Leso, L.; Klopcic, M.; Barbari, M.; Rossi, G. Properties of conventional and alternative bedding materials for dairy cattle. *J. Dairy Sci.* **2020**, *103*, 8661–8674. [CrossRef] [PubMed]
15. Kupczyński, R.; Bednarski, M.; Budny-Walczak, A.; Kociuba, W. Evaluation of Suitability of New Bedding Material Obtained after Straw Biogasification for Dairy Cows. *Animals* **2023**, *13*, 1905. [CrossRef] [PubMed]
16. Levison, L.J.; Miller-Cushon, E.K.; Tucker, A.L.; Bergeron, R.; Leslie, K.E.; Barkema, H.W.; DeVries, T.J. Incidence rate of pathogen-specific clinical mastitis on conventional and organic Canadian dairy farms. *J. Dairy Sci.* **2016**, *99*, 1341–1350. [CrossRef] [PubMed]
17. Li, H.; Wang, X.; Wu, Y.; Zhang, D.; Xu, H.; Xing, X.; Qi, Z. Relationships among bedding materials, bedding bacterial composition and lameness in dairy cows. *Anim. Biosci.* **2021**, *34*, 1559. [CrossRef] [PubMed]
18. Vargová, M.; Zigo, F.; Výrostková, J.; Farkašová, Z.; Rehan, I.F. Biofilm-Producing Ability of Staphylococcus aureus Obtained from Surfaces and Milk of Mastitic Cows. *Vet. Sci.* **2023**, *10*, 386. [CrossRef] [PubMed]
19. Seegers, H.; Fourichon, C.; Beaudeau, F.O. Production effects related to mastitis and mastitis economics in dairy cattle herds. *Vet. Res.* **2003**, *34*, 475–491. [CrossRef] [PubMed]

20. Yajima, A.; Owada, H.; Kobayashi, S.; Komatsu, N.; Takehara, K.; Ito, M.; Matsuda, K.; Sato, K.; Itabashi, H.; Sugimura, S.; et al. Cacao bean husk: An applicable bedding material in dairy free-stall barns. *Asian-Australas. J. Anim. Sci.* **2017**, *30*, 1048–1053. [CrossRef]
21. Yin, H.; Fang, C.; He, X.; Yu, H.; Liang, Y.; Han, L.; Huang, G. Safety production and application of dairy bedding by membrane-covered aerobic fermentation: Insight into the evolution of mastitis pathogens and harmful gas emissions. *J. Environ. Chem. Eng.* **2023**, *11*, 110002. [CrossRef]
22. Zeng, J.; Shen, X.; Sun, X.; Liu, N.; Han, L.; Huang, G. Spatial and temporal distribution of pore gas concentrations during mainstream large-scale trough composting in China. *Waste Manag.* **2018**, *75*, 297–304. [CrossRef] [PubMed]
23. Sobte, H.F.M.; Buijs, S. Impact of paper bedding on lying behaviour and welfare in lactating dairy cows. *Appl. Anim. Behav. Sci.* **2021**, *239*, 105321. [CrossRef]
24. Teixeira, D.L.; Villarroel, M.; María, G.A. Assessment of different organic beddings materials for fattening lamb. *Small Rumin. Res.* **2014**, *119*, 22–27. [CrossRef]
25. Dunlop, M.W.; Blackall, P.J.; Stuetz, R.M. Water addition, evaporation and water holding capacity of poultry litter. *Sci. Total Environ.* **2015**, *538*, 979–985. [CrossRef]
26. Fregonesi, J.A.; Veira, D.M.; von Keyserlingk, M.A.G.; Weary, D.M. Effects of Bedding Quality on Lying Behavior of Dairy Cows. *J. Dairy Sci.* **2007**, *90*, 5468–5472. [CrossRef]
27. Peltre, C.; Dignac, M.F.; Derenne, S.; Houot, S. Change of the chemical composition and biodegradability of the Van Soest soluble fraction during composting: A study using a novel extraction method. *Waste Manag.* **2010**, *30*, 2448–2460. [CrossRef]
28. Robles, I.; Kelton, D.F.; Barkema, H.W.; Keefe, G.P.; Roy, J.P.; von Keyserlingk, M.A.G.; DeVries, T.J. Bacterial concentrations in bedding and their association with dairy cow hygiene and milk quality. *Animal* **2020**, *14*, 1052–1066. [CrossRef]
29. Pabón-Pereira, C.P.; Hamelers, H.V.M.; Matilla, I.; van Lier, J.B. New Insights on the Estimation of the Anaerobic Biodegradability of Plant Material: Identifying Valuable Plants for Sustainable Energy Production. *Processes* **2020**, *8*, 806. [CrossRef]
30. Hossain, M.S.; Nik Norulaini, N.A.; Banana, A.A.; Mohd Zulkhairi, A.R.; Ahmad Naim, A.Y.; Mohd Omar, A.K. Modeling the supercritical carbon dioxide inactivation of Staphylococcus aureus, Escherichia coli and Bacillus subtilis in human body fluids clinical waste. *Chem. Eng. J.* **2016**, *296*, 173–181. [CrossRef]
31. Wang, J.; Lu, D.-Q.; Jiang, B.; Mo, X.-B.; Du, J.-J.; Li, A.-X. Influence of temperature on the vaccine efficacy against *Streptococcus agalactiae* in Nile tilapia (*Oreochromis niloticus*). *Aquaculture* **2020**, *521*, 734943. [CrossRef]
32. Hogan, J.S.; Smith, K.L.; Todhunter, D.A.; Schoenberger, P.S. Bacterial Counts Associated with Recycled Newspaper Bedding. *J. Dairy Sci.* **1990**, *73*, 1756–1761. [CrossRef] [PubMed]
33. Ohshima, T.; Okuyama, K.; Sato, M. Effect of culture temperature on high-voltage pulse sterilization of *Escherichia coli*. *J. Electrost.* **2002**, *55*, 227–235. [CrossRef]
34. Fu, Q.; Xu, Q.; Liu, Z.; Wang, D.; Liu, X.; He, D.; He, Y.; Li, Y.; Yang, J.; Duan, A. Insights into potassium permanganate reducing H_2S generation from anaerobic fermentation of sludge. *Chem. Eng. J.* **2022**, *430*, 133150. [CrossRef]
35. Amon, B.; Amon, T.; Boxberger, J.; Alt, C. Emissions of NH_3, N_2O and CH_4 from dairy cows housed in a farmyard manure tying stall (housing, manure storage, manure spreading). *Nutr. Cycl. Agroecosyst.* **2001**, *60*, 103–113. [CrossRef]
36. Das, K.; Keener, H.M. Moisture effect on compaction and permeability in composts. *J. Environ. Eng.* **1997**, *123*, 275–281. [CrossRef]
37. Giambra, I.J.; Jahan, Y.; Yin, T.; Engel, P.; Weimann, C.; Brügemann, K.; König, S. Identification of Thermophilic Aerobic Sporeformers in Bedding Material of Compost-Bedded Dairy Cows Using Microbial and Molecular Methods. *Animals* **2021**, *11*, 2890. [CrossRef]
38. Megiatto, J.D.; Silva, C.G.; Rosa, D.S.; Frollini, E. Sisal chemically modified with lignins: Correlation between fibers and phenolic composites properties. *Polym. Degrad. Stab.* **2008**, *93*, 1109–1121. [CrossRef]
39. Ikusika, O.O.; Akinmoladun, O.F.; Mpendulo, C.T. Enhancement of the Nutritional Composition and Antioxidant Activities of Fruit Pomaces and Agro-Industrial Byproducts through Solid-State Fermentation for Livestock Nutrition: A Review. *Fermentation* **2024**, *10*, 227. [CrossRef]
40. Tang, M.; Wu, Z.; Li, W.; Shoaib, M.; Aqib, A.I.; Shang, R.; Yang, Z.; Pu, W. Effects of different composting methods on antibiotic-resistant bacteria, antibiotic resistance genes, and microbial diversity in dairy cattle manures. *J. Dairy Sci.* **2023**, *106*, 257–273. [CrossRef]
41. Coban, H.B. Organic acids as antimicrobial food agents: Applications and microbial productions. *Bioprocess Biosyst. Eng.* **2020**, *43*, 569–591. [CrossRef] [PubMed]
42. Hall, C.W.; Mah, T.-F. Molecular mechanisms of biofilm-based antibiotic resistance and tolerance in pathogenic bacteria. *FEMS Microbiol. Rev.* **2017**, *41*, 276–301. [CrossRef] [PubMed]
43. Sutaryo, S.; Sempana, A.N.; Mulya, R.M.; Sulistyaningrum, D.; Ali, M.S.; Damarjati, R.I.; Purbowati, E.; Adiwinarti, R.; Purnomoadi, A. Methane Production of Pistia Stratiotes as a Single Substrate and as a Co-Substrate with Dairy Cow Manure. *Fermentation* **2022**, *8*, 736. [CrossRef]
44. Munksgaard, L.; Jensen, M.B.; Pedersen, L.J.; Hansen, S.W.; Matthews, L. Quantifying behavioural priorities—Effects of time constraints on behaviour of dairy cows, *Bos taurus*. *Appl. Anim. Behav. Sci.* **2005**, *92*, 3–14. [CrossRef]
45. Norring, M.; Manninen, E.; de Passillé, A.M.; Rushen, J.; Munksgaard, L.; Saloniemi, H. Effects of Sand and Straw Bedding on the Lying Behavior, Cleanliness, and Hoof and Hock Injuries of Dairy Cows. *J. Dairy Sci.* **2008**, *91*, 570–576. [CrossRef] [PubMed]

46. Tucker, C.B.; Weary, D.M.; von Keyserlingk, M.A.G.; Beauchemin, K.A. Cow comfort in tie-stalls: Increased depth of shavings or straw bedding increases lying time. *J. Dairy Sci.* **2009**, *92*, 2684–2690. [CrossRef]
47. Tucker, C.B.; Weary, D.M. Bedding on Geotextile Mattresses: How Much is Needed to Improve Cow Comfort? *J. Dairy Sci.* **2004**, *87*, 2889–2895. [CrossRef]

MDPI AG
Grosspeteranlage 5
4052 Basel
Switzerland
Tel.: +41 61 683 77 34

Fermentation Editorial Office
E-mail: fermentation@mdpi.com
www.mdpi.com/journal/fermentation

Academic Open
Access Publishing

mdpi.com

ISBN 978-3-7258-5112-6